THE GEOTHERMAL SYSTEM NEAR PAISLEY, OREGON: A TECTONOMAGMATIC FRAMEWORK FOR UNDERSTANDING THE GEOTHERMAL RESOURCE POTENTIAL OF SOUTHEASTERN OREGON

by

Kyle Aaron Makovsky

A thesis

submitted in partial fulfillment

of the requirements for the degree of

Master of Science in Geology

Boise State University

May 2013

BOISE STATE UNIVERSITY GRADUATE COLLEGE

DEFENSE COMMITTEE AND FINAL READING APPROVALS

of the thesis submitted by

Kyle Aaron Makovsky

Thesis Title: The Geothermal System near Paisley, Oregon: A Tectonomagmatic Framework for Understanding the Geothermal Resource Potential of Southeastern Oregon

Date of Final Oral Examination: 01 March 2013

The following individuals read and discussed the thesis submitted by student Kyle Aaron Makovsky, and they evaluated his presentation and response to questions during the final oral examination. They found that the student passed the final oral examination.

Walter S. Snyder, Ph.D.	Chair, Supervisory Committee
Clyde J. Northrup, Ph.D.	Member, Supervisory Committee
Craig White, Ph.D.	Member, Supervisory Committee

The final reading approval of the thesis was granted Walter S. Snyder, Ph.D., Chair of the Supervisory Committee. The thesis was approved for the Graduate College by John R. Pelton, Ph.D., Dean of the Graduate College.

DEDICATION

For Mom and Dad

ACKNOWLEDEMENTS

Many people have helped me over the years; without them, I would not be where I am today. Of course, I cannot thank my parents, Terry and Leslie, enough for raising me with the proper skills to be successful in life and for showing me how to treat people with respect. Thank you for sticking with me even when things looked grim. I would like to thank my brother, Ryan, for always encouraging me to keep on truckin' towards the end, and for many much needed conversations regarding mom and dad. I want to thank my faithful companion, Kayla, for being such a good friend the last few years and for putting up with me when I was disgruntled over research and writing. Finally, I want to thank my two best friends Penny Lane and Grizzly Bear, my two favorite dogs.

I would like to thank my friends everywhere who have been such an inspiration to me and for their undying encouragement. Thank you to my friends and colleagues here at Boise State University for everything, but especially for helping me get through the research woes. Thank you to Bryant Ware and Reggie Walters for making my dream of playing in a bluegrass band possible, and to all of Sunnyvale Stringband's fans for their support.

I want to thank the faculty and staff at Minnesota State University, Mankato for giving me the education required to be successful in my graduate studies here at Boise State. I also want to thank faculty and staff at Boise State University for all of your help during this amazing experience. Thank you, Debbie Pierce, Dave Wilkins, Lejo Flores,

Shawn Benner, Jim McNamara, Mark Schmitz, Karen Viskupic, Matt Kohn, Sam Evans, Paul Olin, Cheri Folkner, Liz Johansen, and Teresa Lobb. Help and stimulating conversations with Silvio Pezzopane, Roy Mink, Bob Beckwith, and Surprise Valley Electrification were much appreciated. Last, but certainly not least, thank you to my committee, Dr. Craig White, Dr. CJ Northrup, and of course, Dr. Walt Snyder, for being so patient with me over the last 3 years. Lastly, I want to show my appreciation to Walt for giving me the opportunity to study here at Boise State. I respect you because I know I didn't look especially appealing on paper, but you gave me a chance when many others did not, and for that I cannot thank you enough.

ABSTRACT

The tectonic and magmatic framework of southeast Oregon provides the conditions necessary for the existence of geothermal energy resources. However, few detailed studies of geothermal systems in this part of the Basin and Range have been conducted. Young bimodal magmatism and faulting associated with the High Lava Plains coupled with the encroachment of the Basin and Range tectonic province and potentially the Walker Lane have created the structural configuration, heat source, and secondary permeability necessary for geothermal systems in southeast Oregon. The relative contribution of these provinces to the overall tectonomagmatic framework is less well understood. In this study, the geothermal system near Paisley, Oregon has been characterized by a detailed regional heat flow study, geologic mapping, aqueous geochemical analysis, a gravity survey, and a X-ray diffraction analysis of secondary alteration minerals.

Based on these analyses, the Paisley geothermal system shares many aspects similar to Basin and Range geothermal systems. Geologic mapping has revealed a sequence of rocks with ages spanning from the mid Eocene-Present as well as structures related to the Basin and Range Province. A structural transfer zone connects two en-echelon normal faults in Summer Lake Basin, which controls the upwelling of thermal waters. The fault controlling fluid flow in the Paisley geothermal system was imaged using a gravity survey. Thermal water in the Paisley geothermal system has been

determined to be of meteoric source, and is interpreted to be of Pleistocene age based on stable isotopes having average values of -119.59‰ and -14.18‰ for δD and $\delta^{18}O$, respectively. Recharge to the thermal aquifer is driven dominantly by topographic flow, with residence times on the order of 1000s of years. Aqueous geochemistry was used to determine that the Paisley geothermal system is not magmatic in origin, with low values of magmatic SO_4, As, B, and high values of HCO_3 and Na. Geothermometers were used to calculate reservoir temperatures between 95 °C – 166 °C. These results were independently checked by X-ray diffraction studies of alteration mineral assemblages in reservoir rocks from two production wells drilled by Surprise Valley Electrification, which revealed similar temperatures for the stability field of mineral assemblages present in the wells.

Because it has been determined that the Paisley geothermal fluids are not influenced by recent magmatism, the role of bimodal magmatism associated with the High Lava Plains on geothermal systems in southeastern Oregon appears to be minimal. However, in areas where magmatism is younger than 2 million years, this may not be true. Like the geothermal systems of the western Great Basin, the location of geothermal systems in southeast Oregon is highly dependent on the regional structural architecture. Also similar to some geothermal systems of the Basin and Range, the source of water is not modern meteoric water, but is "fossil" water, which implies that production must be managed carefully to create a sustainable resource.

TABLE OF CONTENTS

LIST OF TABLES

LIST OF FIGURES

CHAPTER ONE: INTRODUCTION

The Northern Basin and Range Province of the western United States is host to a vast number of known and unknown geothermal resources (Muffler and Guffanti, 1978; Williams et al., 2008). The majority of research has focused on geothermal resources in California, Utah, and especially Nevada. Detailed geologic, geochemical, and geophysical studies have provided considerable insight into the behavior of these systems. In contrast, little work has been done on known or potential geothermal resources in Oregon, in particular, southeast Oregon. This thesis aims to provide a detailed geologic description of the geothermal system near Paisley, Oregon and to place it into a broader tectonomagmatic framework that is built upon a detailed summary of the geologic history of the Northern Basin and Range Province and review of geothermal systems in the Great Basin.

For most geothermal projects in the western United States, development of the resource is usually preceded by exploration. In Paisley, the opposite is true, the resource had already been discovered; therefore, the need was to characterize the system prior to drilling development wells. It is hoped that a greater understanding of the geologic framework for geothermal systems of southeast Oregon will be obtained by studying the Paisley system. The overall goal of this research is to provide a case study for the geothermal systems in southeastern Oregon, placing them within their larger tectonmagmatic framework, and thus to facilitate the discovery and expanded use of these renewable resources.

Project Background

Hot water near Paisley, Oregon was discovered in the 1960s by a local rancher while drilling an irrigation well. During the drilling of this well, water of ~240 °F (115 °C) was discovered. This well water has been pumped into a cooling pond, and after a short time the cooled water is pumped to irrigation pivots.

Around 2005, the local power cooperative, Surprise Valley Electrification Corporation, based in Alturas, California, was awarded a cooperative agreement by the United States Department of Energy, to drill a geothermal well to support a small power generation system that could produce 3 Megawatts of electricity. Currently, three wells have been drilled and power production is proposed to commence in mid-2013.

Location

Paisley, Oregon is in south-central Oregon on Highway 31 about 45 miles north of Lakeview, Oregon (Fig. 1.1). It lies between Fremont National Forest to the west and the High Desert of eastern Oregon to the east. The Chewaucan River flows out from the Paisley Hills through Paisley into Summer Lake Basin and then continues to flow south into Abert Lake. The Chewaucan Basin is subdivided into for sub-basins: Summer Lake Basin to the North, in which Summer Lake resides, the Upper and Lower Chewaucan Marsh, and Abert Lake (Allison, 1982). Paisley lies on the boundary between the southern part of Summer Lake Basin and the northern part of the Upper Chewaucan Marsh. The basin is terminated to the west near Paisley by the Paisley Hills and on the eastern side by the Coglan Hills.

One special characteristic of Paisley is its location at the intersection of several geologic provinces and the lack of discussion of this in the literature. For example, the

Cascades lie only 120 km to the west. Paisley is also in the Basin and Range Province, the boundary of which is shown in Figure 2.1 after Egger and Miller (2011). Paisley also lies near the High Lava Plains of central Oregon. The fact that Paisley lies near the boundary of these geologic provinces makes the geology very complex and conducive to geothermal resources. Understanding the inter-relations of these provinces will be necessary to correctly characterize the geothermal system at Paisley.

The climate in this area is classified as semi-arid due to the fact that it lies within the rain shadow of the Cascade Range to the west, receiving around 28 cm of precipitation per year (2010 total, National Climate Data Center). Most of the precipitation in Paisley falls in the winter and spring months. The summer and fall months are hot and dry. As a result, a Sagebrush Steppe ecosystem dominates.

The topography of the Paisley area is mountainous adjoining with flat basins. The Chewaucan River carves a steep NE trending V-shaped valley that terminates once it enters Summer Lake Basin. The elevation ranges from 1341 meters in the basin to 2072 meters in both the Coglan and Paisley Hills. On either side of the basin, Pleistocene age shorelines are present, created by ancient Lake Chewaucan. At its high stand around 12,000 ^{14}C years ago, Lake Chewaucan was 114 meters deep and reached a maximum elevation of 1387 meters (Licciardi, 2001).

Methodology

Geologic mapping, hydrochemistry studies, a gravity survey, and lithologic well log analyses were conducted to characterize this geothermal system. Collectively, these techniques provide information required for creating a conceptual model of the Paisley geothermal system.

Geologic mapping was carried out at 1:48,000 scale in the vicinity of Paisley. Such detailed mapping was required to properly delineate and characterize the geologic units that presumably also occur in the subsurface and host the geothermal aquifer. Global Positioning System was used in conjunction with ESRI's ArcInfo software suite to create the geologic map (Plate 1).

Water samples from regional wells and springs had been gathered by previous workers on the Paisley project and were analyzed using Inductively Coupled Plasma-Atomic Emission Spectrometry (EPA 200.7) for chemical constituents. Based on the concentration of certain chemical constituents, an estimated temperature in the reservoir was calculated. Also from this information, the potential effect of fluid mixing models can be evaluated. Samples from the production well (SVEC-1) and from the injection well (SVEC-2) were collected by Lynn Culp and samples from the Chewaucan River were collected by the author for stable isotope analysis. All of these results will be presented in Chapter Four.

The gravity survey was designed by the author and was carried out in January of 2011 with the help of Silvio Pezzopane. A Worden Gravimeter was used for this survey. This gravimeter uses an object with a small mass suspended from a zero-length quartz spring contained in a vacuum chamber. These gravimeters are sensitive to changes in gravity of 1 unit in 100,000,000 and, if reduction procedures are calculated correctly, a precision of 0.01 mGal can be achieved (Burger et al., 2006). A total of 53 sites were occupied, 3 of which were base stations. A base station was reoccupied every 4 stations or 3 hours, whichever came first in order to correct for tidal variations and meter drift. A

MATLAB© code was written to reduce the data and will be discussed in further detail in Chapter Four.

Well cuttings were gathered at the time of drilling by Silvio Pezzopane, Leland "Roy" Mink, and the author for well SVEC-1 and were used to create the lithologic log. Well cuttings for SVEC-2 were gathered by Silvio Pezzopane and Leland "Roy" Mink at the time of drilling and were also used to create the lithologic logs for this well. Four samples of drill cuttings from well SVEC-1 from depths of 895, 995, 1095, and 1197 feet were gathered, cleaned, and powdered for X-Ray Diffraction (XRD) analysis to identify alteration minerals present. Petrographic thin-sections were also made from samples at these depths to aid in the identification of alteration minerals. Four samples from well SVEC-2 at depths of 770, 870, 970, and 1065 feet were also gathered and prepared for XRD and petrographic thin section analysis. The results of these analyses will be discussed in Chapter 4.

Previous Studies

The first to geologically map southeast Oregon was Russell (1884), who conducted a reconnaissance-level mapping project of the region. Donath (1962) and Donath and Kuo (1962) were the first to discuss in detail the geometry of faulting within Summer Lake Basin. Walker (1963, 1977) produced maps at 1:250,000 scale with detailed descriptions of the geologic units in this area. Pezzopane and Weldon (1993) mapped several faults along Winter Ridge and Slide Mountain, determining they have been active in the Quaternary. Crider (2001) did a structural analysis of the geometry of faulting northeast of Summer Lake. Most recently, Scarberry et al. (2010) concluded that the emplacement of basaltic dikes near Abert Rim (approximately 30 km east of Paisley;

Fig. 1.1) was related to the onset of Basin and Range extension in the late-Miocene early-Pliocene. Travis (1977) described some geologic units in the northern part of Summer Lake Basin and also conducted a regional-scale gravity survey to try and understand the geometry of faulting northeast of Summer Lake. Blank (1973) conducted a gravity survey and an aeromagnetic survey in the Summer Lake basin. Appling (1950), Muntzert and Field (1968), and Muntzert (1969) describe the geology and mineral deposits in the Paisley Hills. Peterson and McIntyre (1970) describe rocks of Eocene-Oligocene age in the Paisley Hills. To date, no paper has been published on the greater tectonic framework of the Paisley area and how it may affect the geothermal system there.

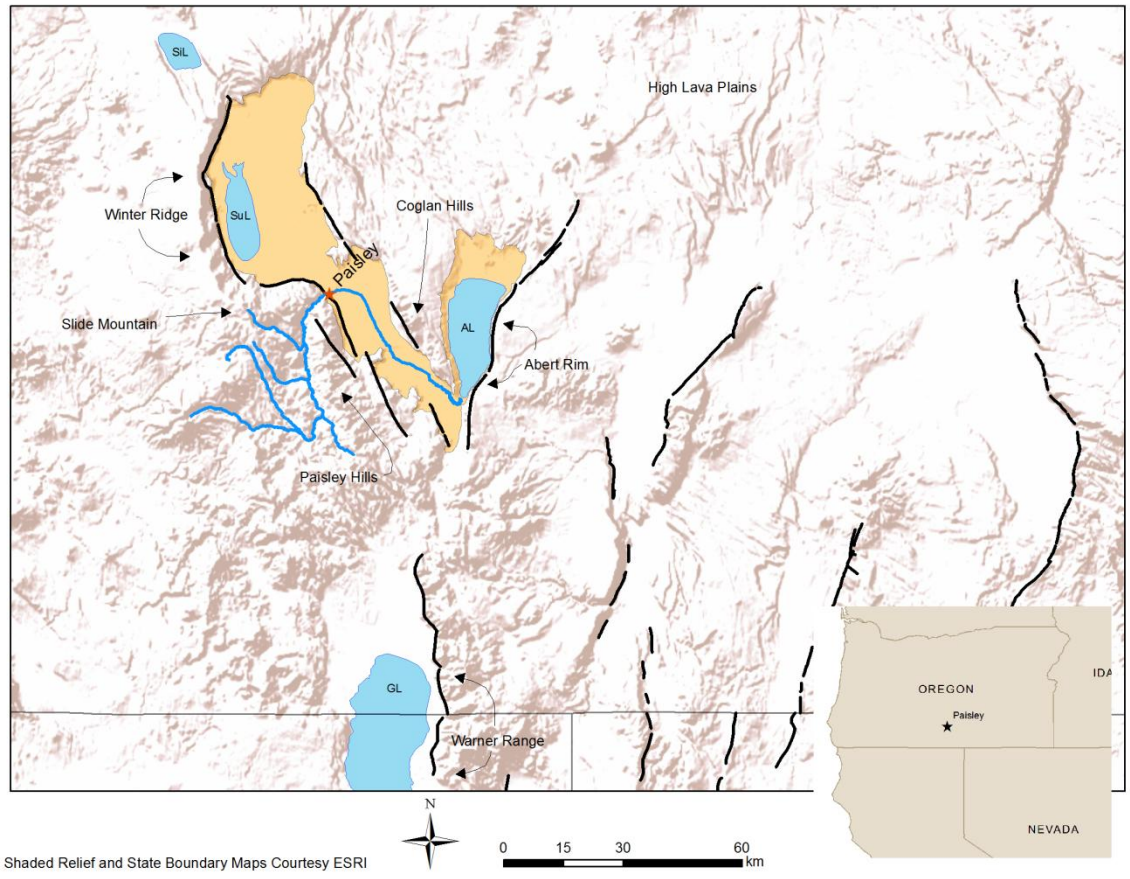

Figure 1.1. Map showing location of Paisley and regional features that will be discussed in text. Major faults in the area are represented by thick black lines.

Thinner lines represent state boundaries. Shaded area outlines boundary of Ancient Lake Chewaucan's High Stand at the 1387 m contour and the portion other than Abert Lake is that of Summer Lake Basin. Blue line represents the Chewaucan River and major tributaries. SiL- Silver Lake, SuL- Summer Lake, AL- Abert Lake, GL- Goose Lake. Fault data from USGS; river data from Oregon Explorer.

References Cited

Allison, I.S. 1982. Geology of Pluvial Lake Chewaucan, Lake County, Oregon. Oregon State Monographs. Studies in Geology No. 11. Oregon State University Press. Corvallis. 79 p.

Appling., R.N. 1950. Economic Geology of the Brattain mining area, Paisley, Oregon. Master's Thesis. University of Oregon. Eugene, Oregon. 74 p.

Blank., H.R. 1973. Geothermal Investigations in Eastern Oregon: A report on work carried out on behalf of Eugene Water and Electric Board. 49 p.

Burger, R.H., Sheehan, A.F., Jones, C.H. 2006. Introduction to Applied Geophysics: Exploring the Shallow Subsurface. W.W. Norton & Company. 600 p.

Crider, J.G. 2001. Oblique Slip and the Geometry of Normal –Fault Linkage: Mechanics and a Case Study from the Basin and Range in Oregon. Journal of Structural Geology. v. 23. p. 1997-2009.

Donath, F.A., Kuo, J.T. 1962. Seismic-Refraction Study of Block Faulting, South-Central Oregon. Geological Society of America Bulletin. v. 73. p. 429-434. DOI: 10.1130/0016-7606(1962)73[429:SSOBFS]2.0.CO;2.

Donath, F.A. 1962. Analysis of Basin-Range Structure, South-Central Oregon. Geological Society of America Bulletin. v. 73. p. 1-16. DOI: 10.1130/0016-7606(1962)73[1:AOBSSO]2.0.CO;2.

Egger, A.E., Miller, E.L. 2011. Evolution of the Northwest Margin of the Basin and Range: The Geology and Extensional History of the Warner Range and Environs, Northeastern California. Geosphere. v. 7. p. 756-773. DOI: 10.1130/GES00620.1.

Licciardi, J.M. 2001. Chronology of the latest Pleistocene Lake Level Fluctuations in the Pluvial Lake Chewaucan Basin, Oregon, USA. Journal of Quaternary Science. v. 16, no. 6. p. 545-553. DOI: 10.1002/jqs.619.

Muffler, L.P., Guffanti, M. 1978. Assessment of Geothermal Resources of the United States-1978. United States Geological Survey Circular 790. Boulder, CO.

Muntzert, J.K., Field, C.W. 1969. Geology and Mineral Deposits of the Brattain District, Lake County, Oregon. Geological Society of America Abstracts. p. 616-617.

Muntzert, J.K. 1969. Geology and Mineral Deposits of the Brattain District, Lake County, Oregon. Master's Thesis. Oregon State University. 70 p.

Peterson, N.V., McIntyre, J.R. 1970. The Reconnaissance Geology and Mineral Resources of Eastern Klamath County and Western Lake County, Oregon. Oregon Department of Geology and Mineral Industries Bulletin 66. 70 p.

Pezzopane, S.K., Weldon, R.J. 1993. Tectonic Role of Active Faulting in Central Oregon. Tectonics. v. 12, no. 5. p. 1140-1169.

Russell, I.C. 1884. A Geological Reconnaissance in Southern Oregon. United States Geological Survey Annual Report. Boulder, CO. v. 4. p. 431-464

Scarberry, K.C., Meigs, A.J., Grunder, A.L. 2010. Faulting in a Propagating Continental Rift: Insight from the late Miocene Structural Development of the Abert Rim Fault, Southern Oregon, USA. Tectonophysics. v. 488. p. 71-86. DOI: 10.1016/j.tecto.2009.09.025.

Travis, P.L. 1977. Geology of the Area near the North End of Summer Lake, Lake County, Oregon. Master's Thesis. University of Oregon. Corvallis, OR. 95 p.

Walker, G. 1963. Reconnaissance Geologic Map of the Eastern Half of the Klamath Falls (AMS) Quadrangle, Lake and Klamath Counties, Oregon. United States Geological Survey Miscellaneous Field Studies Map MF-260. 1:250 000 scale. 1 sheet. Reston, VA.

Walker, G. 1977. Geologic Map of Oregon east of the 121st Meridian. United States Geological Survey Miscellaneous Investigation Series Map I-902. 1:500 000 scale. 2 sheets. Reston, VA.

Williams, C.F., Reed, M.J., Mariner, R.H. 2008. A Review of Method Applied by the U.S. Geological Survey in the Assessment of Identified Geothermal Resources. USGS Open-File Report 2008-1296. Reston, VA. 27 p. http://pubs.usgs.gov/of/2008/1296/.

CHAPTER TWO: CENOZOIC TECTONOMAGMATIC HISTORY OF THE NORTHERN BASIN AND RANGE AND SOUTHEASTERN OREGON

Introduction

Southeast Oregon has a complex tectonic history because it lies at the juncture of the Northern Basin and Range, Walker Lane, Cascades, Columbia Plateau, and the High Lava Plains (Fig. 2.1). The juncture of these provinces and the resultant tectonomagmatic architecture reflects a complex succession of regional events that mark the late-Mesozoic and Cenozoic history of the western United States. These events are summarized in Figure 2.2, which forms the basis for the following discussions for events happening from 55 to 0 Ma; these figures demonstrate the spatial and temporal relationships that characterize the Northern Basin and Range.

The purpose of this chapter is to provide an overview of the tectonic development of the Northern Basin and Range and summarize why these developments are important to understanding geothermal resources within the Great Basin. Topics covered in this chapter include the Laramide Orogeny, the development of the Cascade Arc, the mid-Tertiary Ignimbrite Flare-Up, Yellowstone Hotspot, the High Lava Plains, the development of the Northern Basin and Range, and the Walker Lane. Each of these events is potentially important to understanding the creation and geospatial distribution of geothermal resources in both the Great Basin and southeastern Oregon. How these events are related to one another in time and space will be the focus of this chapter. This

overview thus provides a framework for discussion of the geothermal systems in southeast Oregon and their relationship to geothermal systems in the Great Basin.

Late-Cretaceous to Mid-Eocene

The late Mesozoic to early Cenozoic (75 to 40 Ma) history of the central portion of the western U.S. Cordillera was dominated by terrane accretion, calc-alkaline continental arc magmatism, and crustal shortening related to the Sevier and Laramide orogenies (Burchfiel et al., 1992; Dickinson, 2004; Fig. 2.3). Arc magmatism ceased between the latitudes of 44°N and 34°N (Fig. 2.3), but calc-alkaline magmatism continued in the Challis-Kamloops belt in Idaho (Verplanck and Duncan, 1987; Breitsprecher et al., 2003; Gaschnig et al., 2009; Schmandt and Humphreys, 2011). Around 55 Ma, the accretion of the Siletzia terrain in Oregon resulted in a shift of the loci of magmatism to the Western Cascades (du Bray and John, 2011; Schmandt and Humphreys, 2011). The Clarno Formation of central and eastern Oregon and Washington (?) is an intermediate phase of intracontinental volcanism from the cessation of the Challis-Kamloops volcanic center to the beginning of the Western Cascades, both geographically and temporally.

The Laramide Orogeny

In the late-Cretaceous to mid-Eocene, the Laramide Orogeny commenced in the western Cordillera (Burchfiel et al., 1992; Dickinson, 2002; English and Johnston, 2004; Scarberry et al., 2010). Figure 2.3 shows that the magmatic belt associated with this orogeny stretched from northern Idaho southeastward into central New Mexico. Behind this magmatic front there was a magmatic gap. This zone of amagmatism characterizes a

unique property of the type of deformation associated with the Laramide Orogeny, which is flat slab subduction of the Kula-Farallon plates underneath the North American Plate south of 49°N latitude (Ewing, 1980).

The geometry of the down-going slab during this time is an important precursor to later events that have direct impacts on geothermal resources. The removal of the subducted slab from the base of the lithosphere allowed for renewed interaction of asthenosphere with the lower crust. The removal of this slab and its implications for the development of other important geologic events (and their bearing on geothermal resources) will be discussed later in this chapter.

Eocene Magmatism in Eastern Oregon, Washington and Idaho

Challis-Kamloops Magmatism

Challis-Kamloops magmatism is an important syn-Laramide feature stretching from Idaho northwards into Canada (Breitsprecher et al., 2003). This event is an important precursor to the space-time patterns of calc-alkaline magmatism in the Northern Basin and Range during the Oligocene and Miocene. The events this magmatism led to have direct implications for the development of geothermal resources (via Basin and Range); therefore, understanding the origins of these events is important.

Rocks constituting the Idaho portion of the Challis-Kamloops magmatic belt were formed in a complex tectonomagmatic environment. The subalkaline to alkaline nature of the lavas erupted through central Idaho is consistent with a back-arc or intra continental setting. Another hypothesis is that they were erupted in an intraplate setting (Morris et al., 2000). Yet another hypothesis is that subduction of the Farallon-Kula spreading ridge and resultant slab window formed these rocks, supported by geochemical

work done by Breitsprecher et al. (2003). If the latter case is true, and the slab window was oriented east west, then it is easy to imagine that the edge of the Farallon plate, not being "attached" to another plate, was in a position where it could retreat into the mantle in a southwesterly direction (see Fig. 1E in Breitsprecher et al., 2003), and thus, its relationship to the Ignimbrite Flare-Up in the Northern Basin and Range.

Siletzia Accretion and Westward Migration in Arc Magmatism

An important event in reconstructing the history of the Cascade arc is that of the accretion of the Siletzia terrain in early to mid-Eocene. The accretion of Siletzia allowed for the westward migration in arc-type magmatism from the Challis-Kamloops magmatic center to the Western Cascades, in which the Clarno Formation of central Oregon could represent a transitional phase of volcanism between these two entities. The Siletzia terrain has been characterized as an oceanic island seamount chain, probably created by intraplate hotspot volcanism within the Farallon plate (Duncan, 1982; Christiansen and Yeats, 1992; Dickinson, 2004). The accretion of Siletzia terrain most likely stalled subduction for a period of 5-10 million years. When subduction resumed, the trend of the ancestral Cascade arc was established farther west than the previous locus of volcanism (Schmandt and Humphreys, 2011). Tholeiitic magmatism dominated from about 45-18 Ma followed by Calc-alkaline magmatism until about 5 Ma (du Bray and John, 2011).

The earliest magmatic systems in central Oregon, including the Paisley area, are of mid- to late-Eocene age. Prior to this, magmatism as young as mid-Eocene continued north of the Laramide amagmatic zone in Idaho and Montana (Christiansen and Yeats, 1992; Breitsprecher et al., 2003; Madsen et al., 2006). The chemistry suggests that calc-alkaline volcanism was dominant in Oregon, whereas slab window volcanism is

responsible for the alkaline and siliceous rocks of the Challis-Kamloops magmatic center (Breitsprecher et al., 2003; Madsen et al., 2006).

The Clarno Formation of Central Oregon

Late-middle to late-Eocene volcanism (54-33(?) Ma) along the continental margin in Oregon is evidenced by the intra-arc volcanic and volcaniclastic Clarno Formation (Evernden and James, 1964; Swanson and Robinson, 1968; Rogers and Novinsky-Evans, 1977; Christiansen and Yeats, 1992; White and Robinson, 1992; Urbanczyk, 1994). Figure 2.4 shows the distribution of the Clarno Formation based on outcrop patterns in Oregon (Christiansen and Yeats, 1992).

The distribution of calc-alkaline volcanic centers in central Oregon during the Eocene (54-40 Ma) was widespread, possibly near 200 km wide (McBirney and White, 1982; Christiansen and Yeats, 1992). A shallow dip angle of the subducting slab would produce a large lateral distribution of volcanic centers normal to the trench. This scenario is feasible for describing this type of volcanism in central Oregon because around 50 Ma, the rate of subduction of the Farallon plate was 125 mm/yr, which is relatively fast and promotes a shallower dip angle (Fig. 2.5, Schmid et al., 2002). However, by about 39 Ma, the location of volcanic centers became more centralized with the development of the Western Cascades. This was most likely a result of steepening of the subducting slab, which is in part due to the declining rate of subduction concomitant with increasing obliquity of subduction (Verplanck and Duncan, 1987; Schmid et al., 2002; du Bray and John, 2011, Fig 2.5). As the slab steepens, the zone of melting in the subducting plate becomes narrower and will shift volcanism towards the trench. Another explanation is that clockwise rotation has distributed the outcrops representing these

volcanic centers and their depositional products throughout central and southern Oregon, in part due to extension in the mid-late Miocene to present (e.g., Wells and Simpson, 2001; Trench et al., 2012).

The Clarno Formation consists mostly of andesitic breccias, mudflows, lahars, hypabyssal intrusions, and minor basalt flows in the lower part of the sequence (White and Robinson, 1992). Chemically, the Clarno Formation is characterized as calc-alkaline, similar to most subduction related circum-Pacific magmatism. High K/Rb ratios of 200-400 are reported by Rogers and Novinsky-Evans (1977), which provides some support for these rocks being erupted through continental crust. Other evidence for volcanism on a continental margin comes from the preponderance of fossil floras and abundant paleosols (Retallack et al., 2000). However, based on other parameters such as low Sr concentrations in andesites and pyroxene instead of hornblende in basalts and basaltic andesites, eruption through oceanic crust is also possible (Rogers and Novinsky-Evans, 1977). Locally, volcaniclastic sedimentary rocks are also found in the Clarno Formation, representing deposition at the flanks of large stratovolcanoes (White and Robinson, 1992).

Late-Eocene to Early-Miocene

Two important tectonomagmatic events happened during the late-Eocene through early-Miocene (39 to 20 Ma): the southward sweeping calc-alkaline magmatism of the Ignimbrite Flare-Up (IFU) in the Northern Basin and Range, and development of the Western Cascade volcanic arc. The IFU is an important precursor to the structural development of the Basin and Range Province because of the thermal weakening it imposed on the upper and middle crust. In the Pacific Northwest, and more specifically

southeast and central Oregon, the locus of volcanism shifted to the Western Cascades and created rocks of the John Day Formation in the back-arc region (Walker and MacLeod, 1991; Smith et al., 1998). Rocks equivalent to the John Day Formation crop out in Paisley; therefore, it is important to discuss the origins of this unit.

Mid-Tertiary Ignimbrite Flare-Up

A change in the location of major magmatic activity from the Challis-Kamloops belt to a southward migrating, east-west oriented (Fig. 2.6) belt of intermediate to silicic volcanism took place around 45 to 20 Ma and is often referred to as the middle-Tertiary Ignimbrite Flare-up (Snyder et al., 1976; Cross and Pilger, 1978; Armstrong and Ward, 1991; Lipman and Glazner, 1991; Dickinson, 2006; Schmandt and Humphreys, 2011). Volcanism associated with this event occurred in the zone previously delineated by the Laramide amagmatic zone. Hence, it is directly related to conditions of the subducted oceanic lithosphere of the Laramide Orogen. As the plate decoupled from the base of the North American lithosphere, magmatism resulted from the rejuvenated interaction of the lower crust and aesthnospheric mantle. Large amounts of volatiles had been stored at the base of the lithosphere so when the mantle wedge once again began to interact with the base of the lithosphere, volatile flux melting restarted. The southward migration of this magmatic front tracks the plate as it fell deeper into the mantle (Humphreys, 1995; Liu, 2001).

As much as 500,000 km^3 of silicic magma was erupted over a period of ~25 million years in the western United States (Johnson, 1991; Askren et al., 1997). Best et al. (2009) postulated that the large volume of rhyolitic and dacitic lavas is the result of

the melting of an overthickened crust that was produced during the early Tertiary; as a result, rocks in the lower crust were already near solidus conditions.

The John Day Formation of Central Oregon

The late-Eocene early-Miocene (~39-22 Ma) John Day formation of central Oregon consists of welded and non-welded ignimbrite sheets, volcanic sediments, and also includes local basalt and rhyolite flows. This formation is the product of the Western Cascade magmatic episode and is the result of the localization of magmatic centers in Oregon after the accretion of the Siletzia terrain. The Oligocene section of the John Day formation is coeval with the voluminous eruptions associated with Ignimbrite Flare-Up in the Northern Basin and Range. Figure 2.7 provides a map from Christiansen and Yeats (1992) showing the extent of the John Day Formation and Western Cascade volcanics based on known outcrop patterns across Oregon.

In some areas, the John Day Formation is conformable with the underlying Clarno Formation and is everywhere unconformably overlain by basalts of the Columbia River Group (Woodburne and Robinson, 1977). The base of the John Day Formation in the Horse Heaven Mining District near Grizzly, Oregon is a welded ignimbrite dated at about 36.4 Ma old (Swanson and Robinson, 1968). Regionally, the base of the John Day has been assigned to ash-flow A, which has been $^{40}Ar/^{39}Ar$ dated to about ~39 ± 0.15 Ma near Painted Hills, Clarno, and Ashwood, Oregon (McClaughry et al., 2009; Bestland and Rettalack, 1994a, b; Smith et al., 1998; Retallack et al., 2000). Other major ignimbrites in the John Day Formation (from stratigraphically lowest to highest) include ash flow members E, F, G, H (Picture Gorge Ignimbrite), and I (Evernden et al., 1964; Peck, 1964;

Woodburne and Robinson, 1977; Robinson et al., 1990; McClaughry et al., 2009; Fig. 2.8).

The general interpretation of the John Day Formation is that it represents distal ash fall products of the Western Cascades arc (Fig. 2.7). The idea is that the axis of the arc migrated westward from the trend of the Clarno Formation and related magmatic centers to the Western Cascades (White and Robinson, 1992; Christiansen and Yeats, 1992). The welded ignimbrite sheets also were probably sourced from calderas further to the west, while basaltic to rhyolitic lava flows were of local origin (Robinson et al., 1984). The presence of locally sourced lava flows of alkali basalt and rhyolite suggest a back-arc setting for the John Day Basin (Smith et al., 1998). Further evidence comes from the volcaniclastic sediments. Deposition of sedimentary units requires adequate accommodation space for the sediments; hence, this space was most likely created by subsidence due to normal faulting (Walker and MacLeod, 1991; Smith et al., 1998).

Recent studies (e.g., McClaughry et al., 2009) have documented silicic calderas further east than previously known, such as the Wildcat Mountain caldera (43-36 Ma), located near Prineville, Oregon. Large silicic caldera forming eruptions associated with the Ignimbrite Flare-Up were happening concomitant to eruptions of the Wildcat Mountain caldera (McClaughry et al., 2009; Stewart and Carlson, 1976; Christiansen and Yeats, 1992; Ludington et al., 1996; Honn and Smith, 2007). This suggests then that they may be related to the same tectonic event. However, at this time (~40 Ma), the main locus of magmatism associated with the Ignimbrite Flare-Up was in northern Nevada. There is a window of 3 million years for these two events to be connected geographically, but to the author's knowledge no rocks of this age have been mapped in Oregon between

these, the Wildcat Mountain Caldera and the Oligocene-Miocene, calderas of northern Oregon. Indeed, this does not preclude their existence but could merely reflect a dearth in, or complete absence of, outcrops of rocks this age.

Mid-Miocene to Present

The Miocene (20 Ma to present) is the single most important time period for both the Great Basin and southeast Oregon with respect to geothermal resource development. In this period, the development of the Northern Basin and Range Province in both the Great Basin and southeast Oregon provides the main control on the development of geothermal systems in the region. Voluminous outpourings of basalt magma occurred in eastern Oregon and Washington and are evidenced by the Steens and Columbia River Basalts, respectively. A distinct package of bimodal basalt and rhyolite lavas defines magmatism on the High Lava Plains of Oregon. The silicic volcanics of the High Lava Plains youngs to the northwest, terminating at Newberry Caldera. Also important to geothermal resources in the Great Basin in western Nevada and eastern California (and potentially southeast Oregon) is the Walker Lane, a zone of Miocene-present faults accommodating strain from relative plate motions between the Pacific and North American plates. The coexistence of faulting associated with the Walker Lane with pre-existing structures of the Basin and Range provide the structural controls for fluid flow in geothermal systems of the Great Basin and southeast Oregon. This is facilitated by the creation of fault intersections and high strain rates in the Walker Lane Belt.

The Northern Basin and Range Province

The Northern Basin and Range, with its characteristic high heat flow, magmatism and faulting is widely appreciated as the single most important tectonic development that led to the creation of important geothermal resources within the Great Basin and by extrapolation in southeast Oregon. Deformation in this region is characterized by a mixture of block faulting along listric normal faults that terminate at a lower detachment fault and traditional horst and graben structures. Within the Northern Basin and Range, changes in fault block dip-direction oscillates from east-west, with fault-bounded basins and ranges separated by transfer or accommodation zones, which usually exhibit strike-slip motion parallel to the extension direction (Stewart, 1978, 1980; Faulds and Varga, 1998; Fig. 2.9). Low-angle normal faults associated with older, Eocene metamorphic core complexes may have been reactivated during the initial pulse of Basin and Range extension (Dickinson, 2002).

The initiation of Basin and Range style faulting has been constrained in the Great Basin of Nevada by numerous studies (e.g., Miller et al., 1999; Stockli et al., 2002; McQuarrie and Wernicke, 2005; Colgan et al., 2006a, b, 2008). Most of these studies use thermochronology (i.e., the (U-Th)/He system) or fission track methods to constrain ages. Dates from major range bounding normal faults in Nevada range from 17 Ma in the Snake Range (Miller et al., 1999) to 15 Ma in the Wassuk Range (Stockli et al., 2002) to 16 Ma in the Shoshone and Toiyabe Ranges (Colgan et al., 2008). In general, the initiation of faulting in the Great Basin was concentrated in the central part of the province (McQuarrie and Wernicke, 2005). However, most faulting ongoing in the Basin and Range is concentrated at the margins of the province.

A much younger pulse of faulting occurred in the Basin and Range and was concentrated along the margins of the province. In the Pine Forest Range in northern Nevada, faulting most likely began around 13-11 Ma, much younger than the main pulse of faulting in central Nevada (Colgan et al., 2006a,b). Normal faulting in the Warner Range of California records a pulse of Basin and Range related extension in the late-Miocene (Egger and Miller, 2011). Young faulting concentrated at the margins of the Basin and Range province is attributed to the transfer of strain into relatively unextended terrains.

The amount of extension in the Great Basin varies from 10% at the margins to greater than 110% in the center (Colgan et al., 2008; Egger and Miller, 2011). Stewart (1980) reports that fault blocks tilted 15°-20° in Nevada and Utah correspond to 20%-30% extension across the Great Basin. Other areas have experienced much more extension than the 20%-30% reported above and this extension most likely represents reactivation of older structures.

Structures of Miocene age in the Great Basin record two main extension directions. The first set of structures were predominately oriented NNW-NW, the result of an extension direction of ENE-NE. A change in fault strike occurred in late mid-Miocene (~10 Ma) to NNE-NE, creating the structures that presently define topographic high and lows (Zoback et al., 1981). Geodetic studies show that the major direction of extension in the Great Basin is still oriented W-WNW (Bennett et al., 2003; Hammond and Thatcher, 2005; Payne et al., 2008). Extension behind the active arc in the early-mid-Miocene followed by oblique extension brought upon by changes in plate boundary

conditions around ~17 Ma may describe the change in deformation observed in Northern Basin and Range (e.g., Stewart, 1978; Zoback et al., 1981; Wernicke et al., 1988).

Southeast Oregon

Several studies in southeast Oregon have included this region as part of the Basin and Range province (e.g., Donath, 1962; Donath and Kuo, 1962; Lawrence, 1976). Much of the work done recently (e.g., Jordan et al., 2004; Scarberry et al., 2010; Egger and Miller, 2011) is in agreement that southeast Oregon is in the northwestern-most part of the Basin and Range Province. If this is justified, then the age of initiation of extension in south-central Oregon is much younger than that of the rest of the Northern Basin and Range, perhaps as young as late-Miocene earliest-Pliocene (~16 to 6 Ma). Scarberry et al. (2010) has dated the initiation of faulting on the Abert Rim Fault (Fig. 1.1) in southern Oregon to have begun <7.5 Ma based on minimum age requirements from cross-cutting relationships. Similarly, Pezzopane and Weldon (1993) determined that the Winter Ridge fault initiated ~6.5 m.y. ago (Fig. 1.1).

Faults in southeast Oregon occur in two main orientations, NE-SW and NW-SE (Fig. 4.11). The NW-SE trending ones are typically oblique-slip faults and are associated with the Brothers and Eugene-Denio Fault Zones and exhibit oblique to strike-slip motion and have relatively little vertical displacement (0.004 %, Trench et al., 2012 and 1.5%-4%, Scarberry et al., 2010). The NNE trending ones are extensional normal faults and are related to Basin and Range tectonics. It has been estimated that they exhibit only 3.8% extension (Donath, 1962; Scarberry et al., 2010). Slip on both fault orientations in southeast Oregon are thought to be coeval (Donath, 1962). The initiation of NE-SW faults slightly preceded those of NW-SE orientation (Scarberry et al., 2010). Donath

(1962) interpreted these two faults sets to be related to north-south directed compression, but given the geologic setting of southeast Oregon (specifically Summer Lake), it is unlikely that this is the case because of the undisputed extension ongoing since 7 Ma.

The Walker Lane Belt

A series of northwest trending strike-slip and oblique-slip faults are present in the western Great Basin and eastern Sierra Nevada and constitute the Walker Lane (Fig. 2.10). These faults have been identified as producing favorable conditions for geothermal systems (e.g., Faulds et al., 2006, 2010), and perhaps can be considered as a subset of Basin and Range-type geothermal systems.

The Walker Lane Belt is a zone of dextral shear that accommodates nearly 15%-20% of the Pacific-North American plate motions (Thatcher et al., 1999; Bennett et al., 2003; Faulds et al., 2005; Egger and Miller, 2011). The Walker Lane Belt (WLB) encompasses the Eastern California Shear Zone (ECSZ), which makes up the southern part of the Walker Lane Belt (Fig. 2.10). Relative crustal motion within the Walker Lane Belt is usually described in terms of the Sierra Nevada block (or microplate) with respect to stable North America or the Colorado Plateau and in this reference frame is translating northwestward (Oldow et al., 2001; McQuarrie and Wernicke, 2005). Deformation in the southern Walker Lane and northern ECSZ started at ~16 Ma and has slowly migrated northwards, where the northern boundary is typically delineated where it meets the Modoc Plateau, where deformation is as young as 3 Ma (Cashman and Fontaine, 2000; Bennett et al., 2003; Faulds et al., 2005; Faulds and Henry, 2008). Total dextral offset in the Walker Lane consequently decreases to the north. This northward younging may possibly be coupled with the northward migration of the Mendocino Triple Junction, or it

reflects increased influence of clockwise rotation of the Pacific Northwest (Cashman and Fontaine, 2000; Wells and Simpson, 2001; Faulds and Henry, 2008; Trench et al., 2012).

Magmatism in the Northwest Northern Basin and Range

Basaltic and rhyolitic lavas in the northwestern Northern Basin and Range span from the mid-Miocene to present (~17-0 Ma). Most of this volcanism has been concentrated along the edges of the province (Smith and Luedke, 1984; Christiansen and Lipman, 1992), though local volcanic centers in the Central Nevada Seismic Belt (Fig. 2.10) area of the Basin and Range are abundant (Colgan and Henry, 2009). It appears that most of the volcanism in the Northern Basin and Range was synchronous with extension (Christiansen and Lipman, 1992).

Steens Basalt and Columbia River Basalts

A major outpouring of basalt magma in southeast Oregon led to the wide distribution of Steens Basalt (SB) (Fuller, 1931; Hooper et al., 2002; Camp and Ross, 2004; Brueseke et al., 2007). The upper SB and lower CRBs have been correlated stratigraphically by the Malheur Gorge Basalt (e.g., Camp et al., 2003). Basalts mapped in Paisley are slightly younger than the SB and are correlated to the Saddle Mountain member of the CRB group (Walker and MacLeod, 1991; Camp and Ross, 2004).

Several hypotheses have been presented to explain the origin of the SB and CRB. The most widely accepted hypothesis is that they were formed by the impingement of the Yellowstone Hotspot, made apparent by their tholeiitic nature and association to dike swarms (Pierce and Morgan, 1992; Hooper et al., 2002; Camp and Ross, 2004; Brueseke et al., 2007 and references therein, Ponce and Glen, 2008). Evidence for this comes from

stratigraphic relationships and $^{40}Ar/^{39}Ar$ dating. The SB were first described by Fuller (1931) and summarized by Gunn and Watkins (1970) as being about 1000 m thick. The entire volume of the Steens Mountain basalts could have erupted in as little as 1 million years as constrained by $^{40}Ar/^{39}Ar$ studies of Brueseke et al. (2007), initiated around 16.6 Ma based on $^{40}Ar/^{39}Ar$ dates determined by Hooper et al. (2002). In addition to voluminous basaltic magmatism, voluminous silicic magmatism created by secondary melting of the crust over this hot spot is widespread (Jordan et al., 2004; Brueseke et al., 2007).

An alternative to the mantle plume hypothesis is that the SBs were formed by back-arc extension during mid-Miocene (Carlson and Hart, 1987). Basalt produced in this setting is typically recognized by a bimodal basalt-rhyolite assemblage and in the generally alkalic chemistry of basalts. Camp et al. (2003) present the chemistry of the lowermost flows of the SB, and note that they are mostly tholeiitic. However, they also note that the upper flows are actually calc-alkaline in nature; but since most are tholeiitic, the hypothesis that they were erupted in an extensional stress regime seems satisfactory. To explain this chemistry, Hooper et al. (1995, 2002) suggest that the early pulses of SB and CRB magmatism are an interlude of tholeiitic magmatism between prior and post calc-alkaline magmatism. The rocks became more calc-alkalic through time because they were emplaced (and presumably entrained) through rocks of this type.

Newberry Trend of Bimodal Magmatism

It was discovered by MacLeod et al. (1976) that rhyolitic volcanic centers in the HLP young to the northwest along two distinct trends. The southern arm extends from Beaty's Butte (10.4 Ma) to Newberry Crater whereas the northern arm extends from

Duck Butte (10 Ma), also terminating at Newberry Crater. Further work by Jordan et al. (2004) confirmed these trends. The reason for the northwest younging trend in silicic volcanic centers is a subject of much controversy. Crustal melting induced by westward mantle flow is the best explanation for the observed trend. An experiment by Druken et al. (2011) shows that slab rollback induced flow in the mantle is happening in Oregon. This is supported by the geochemical signature of basalts associated with the bimodal assemblage. For example, they have been shown to be primitive by both major and trace elements by several authors (e.g., Hart et al., 1984; Draper, 1991; Jordan et al., 2004; Carmichael et al., 2006; Ford, 2011) and by recent work with helium isotopes (e.g., Graham et al., 2009).

The origin of High Lava Plains (HLP) basalts is controversial; they could be created from mantle melting associated with subduction-induced mantle convection (Christy Till, personal communication, 2012) or from the interaction of a plume-head with the base of the lithosphere (Jordan et al., 2004; Ford, 2011). Crustal structure plays a large role in the type (i.e., basalt vs rhyolite) and in the chemistry (i.e., high vs low silica rhyolites and tholeiitic vs calc-alkaline basalts) of magmas formed in this region. Beneath the Tertiary volcanic cover, it has been hypothesized that there exists large amounts of mafic rocks accreted to North America during the Mesozoic (Ford, 2011). The interaction between rising mafic magma with pre-existing mafic crust produces the bimodality in the rocks of southeastern Oregon. Melting of mafic crust is one way to produce the low silica rhyolites found in the HLPs, as melts of rhyolitic composition will be produced first from this melting. Crystal fractionation after separation of rhyolitic melt can produce the high silica rhyolites that are found on the HLP (Ford, 2011).

Basalt magmatism in the HLP is distinct in its distribution from its rhyolitic counterpart. Unlike the rhyolites of the HLP, basalts do not show a distinctive younging to the northwest trend; the ages of basalt are instead widely distributed across the province. This relationship is similar to that found in the Snake River Plain of Idaho, where a distinct younging trend is identified in rhyolitic rocks and no definitive pattern of basalt magmatism exists (Christiansen et al., 2002; Camp and Ross, 2004).

Geochemistry of the HLP basalts has distinguished them from SB and CRB. Hart et al. (1984) have identified the primitive nature of the HLP basalts based on high concentrations of aluminum, high MgO/FeO, and low incompatible trace element concentrations. These traits of HLP basalts are generally more primitive than the SB and CRB. Therefore, the CRB and SB are probably related to a mantle plume whereas the HLP basalts are probably related to back-arc mantle convection.

Modoc Plateau

Work done by previous authors shows that the Miocene-present (10 to 0 Ma) volcanic rocks in the Modoc Plateau region of southern Oregon and northern California area have a bimodal signature, with the majority of them being basalts (Cater, 1982; McKee et al., 1983; Draper, 1991; Macdonald et al., 1992; Streck and Grunder, 1997; Jordan et al., 2002; Jordan et al., 2004; Carmichael et al., 2006). Latest Miocene-Quaternary basalts have been described by Bacon (1989) and Hart et al. (1984) as low-K high alumina olivine tholeiites (HAOT) and have chemical signatures typical of intraoceanic arc or back-arc extensional settings (Pearce and Cann, 1977; Hart et al., 1984).

The age and chemistry of the High Alumina Olivine Tholeiites (HOATs) on the Modoc Plateau is similar to those of the HLP suggesting possible genetic connections (Hart et al., 1984; Jordan et al., 2004; Carmichael et al., 2006). The interpretation for the tectonic setting is hence similar, as Hart et al. (1984) interpret that the Modoc Plateau basalts as having formed in a back-arc setting, similar to that of the High Lava Plains.

Summary and Discussion

The Cenozoic geologic history of the Northern Basin and Range provides the structure, magmatism, and high heat flow necessary to produce geothermal systems. Events that led to the development of geothermal resources in the Great Basin can be traced all the way back to The Laramide Orogeny. The Laramide Orogeny is interpreted to reflect thick-skinned tectonics in which sub-horizontal subduction of a young, warm oceanic plate produces a magmatic arc, behind which is a zone of magmatic quiescence. The post-Laramide Ignimbrite Flare-Up (IFU) set the stage for later deformation associated with the Basin and Range. The IFU is marked by a general southward younging of voluminous ash-flow tuffs and calc-alkaline volcanism from Washington and Idaho at~50-45 Ma to southern Nevada by ~20 Ma. The IFU was important because of the thermal weakening it imposed on crustal rocks, setting the stage for later Basin and Range deformation. Extension becomes the dominant deformation style in the Great Basin in the early-Miocene (17 Ma) and persists until today. Extension is defined by two fault orientations. The older of these two is oriented NW-SE followed by modern Basin and Range faults oriented NE-SW, developed by changing stress conditions behind the plate boundary at about 10 Ma. Basin and Range structures are extremely important fluid transport pathways for geothermal systems, and the complex nature of the faulting allows

for increased zones of secondary permeability. These topics will be elaborated upon further in Chapter Three.

Dextral shear in the Walker Lane Belt of western Nevada and eastern California also coincides with the northward migration of the Mendocino Triple Junction. This zone of faulting apparently terminates at the Modoc Plateau; however, dextral oblique-slip faults occur in southeastern Oregon and may imply that the same dextral strain is overprinted in the Paisley area.

Volcanism in central and eastern Oregon during the mid-Eocene is represented by the Clarno Formation. This formation represents a phase of volcanism that changed geographic position from the continental interior (i.e., Challis Volcanics, ~55 Ma) to that of the Western Cascades (~45 to 40 Ma). Volcanism in Oregon eventually became more localized in mid-Oligocene and early-Miocene. The John Day Formation of central Oregon is record of this westward shift in magmatism related to the early Western Cascades. The back-arc setting and related structures of the John Day Basin (in which the John Day Formation was deposited; see Fig. 2.7) is important to geothermal resources because later faulting in the Miocene-present may be reactivating these structures, thereby promoting fluid transport pathways (i.e., permeability). An idea for the formation of calderas that produced ignimbrites of the John Day Formation in central Oregon in the Oligocene is that of a northern expression of the Ignimbrite Flare-Up, though a gap of 3 million years and large horizontal distance separate similar events in Nevada. Early workers proposed that the John Day Formation was exclusively the product of Cascades volcanism but new work suggests that it is most likely a combination of Cascade volcanism and volcanism associated with the IFU.

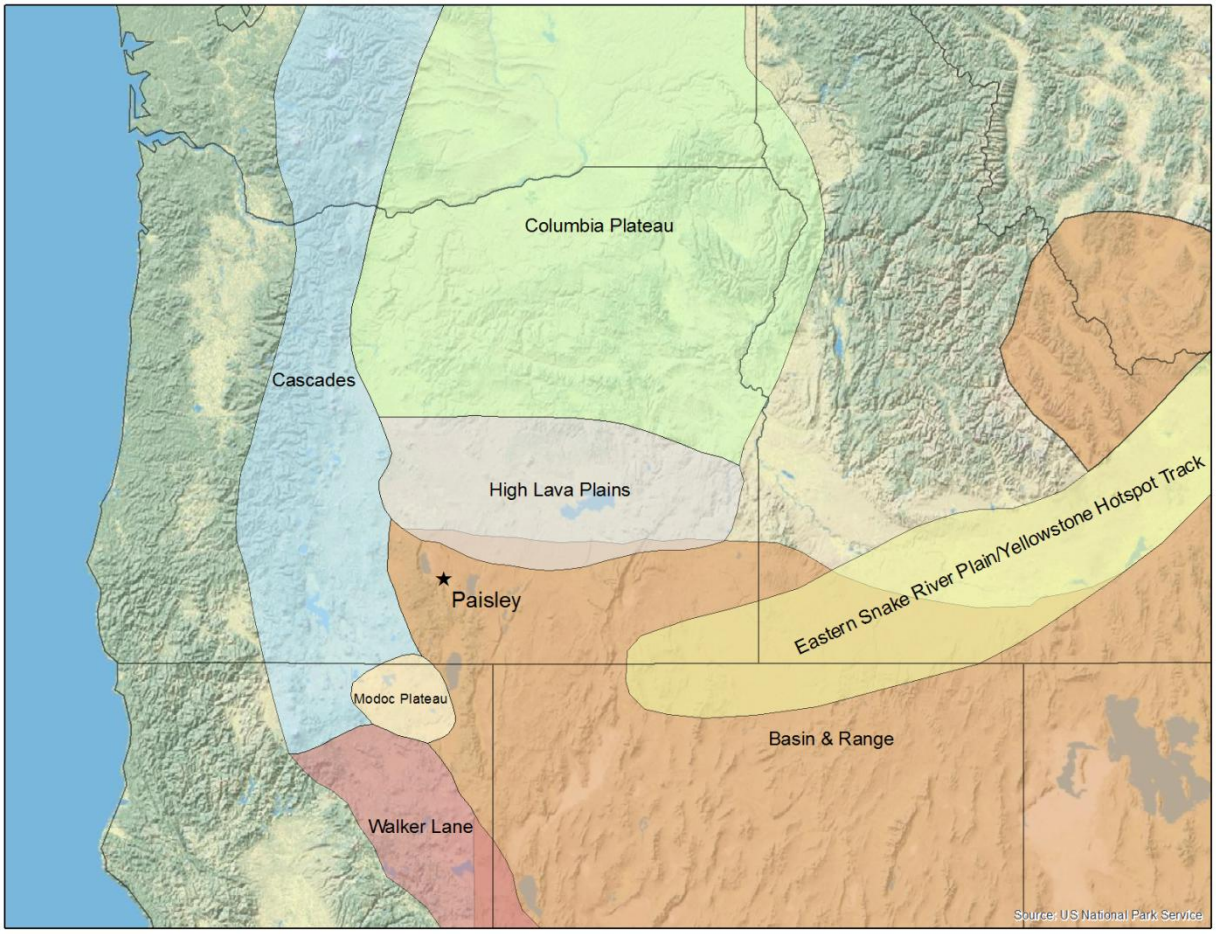

Figure 2.1. Map of major geologic provinces discussed in text. Boundary of Basin and Range after Egger and Miller (2011). Boundary of Walker Lane after Putirka and Busby (2011).

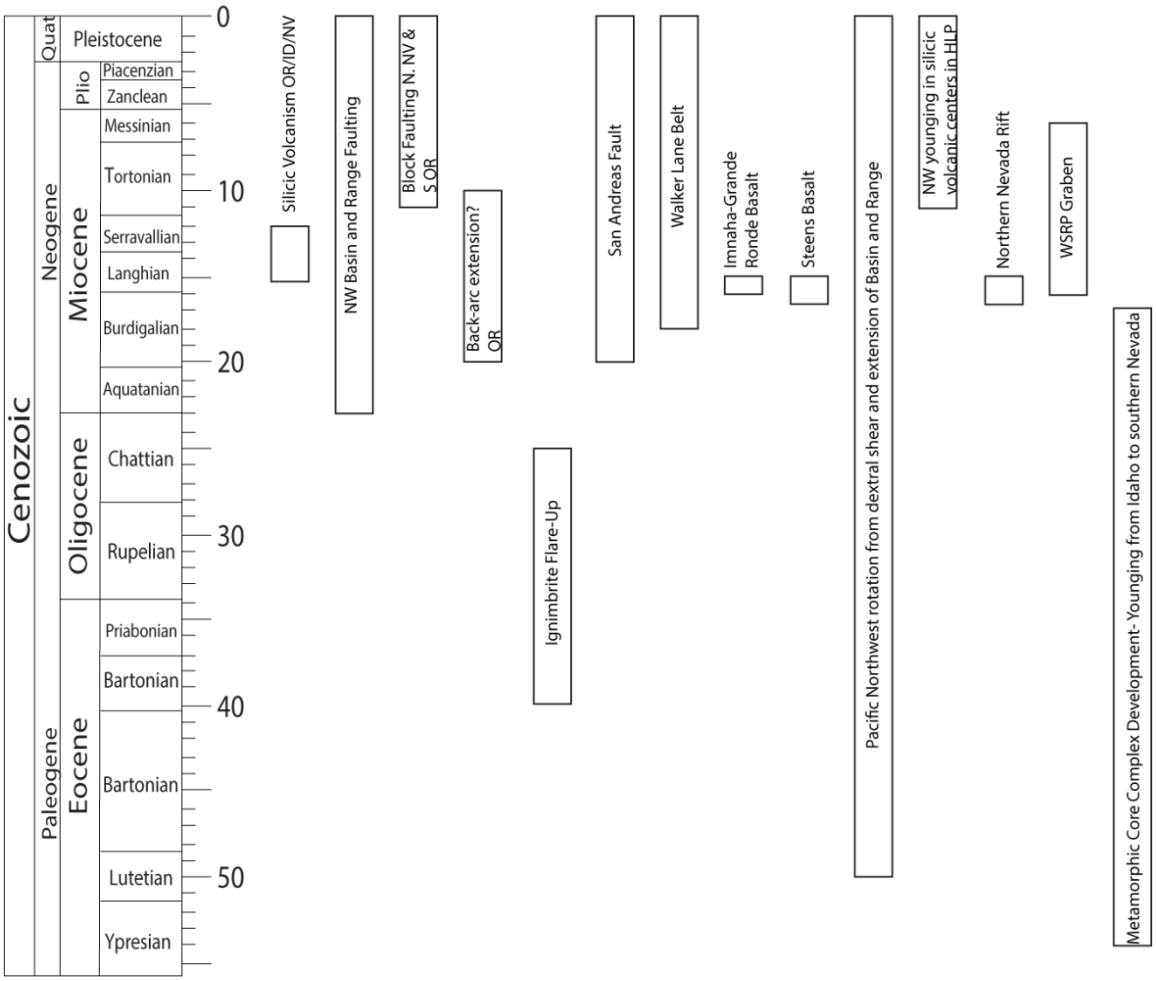

Figure 2.2. Major tectonic events in the northwestern Great Basin from 55-0 Ma using the 2009 Geological Time Scale. Most topics shown here will be discussed in the text.

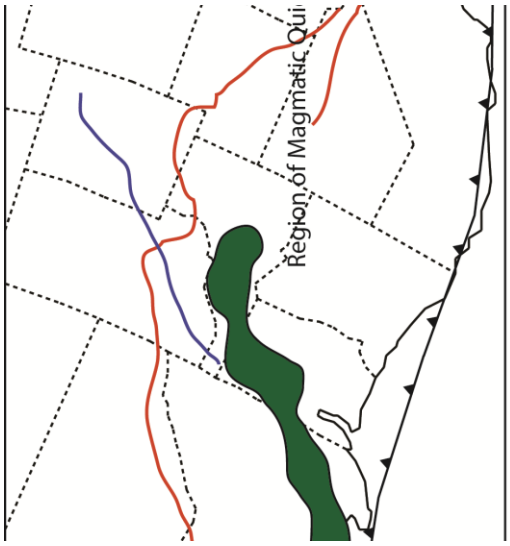

Figure 2.3. Tectonic reconstruction of late-Cretaceous mid-Eocene western United States. Blue line represents eastern extent of Laramide deformation. Orange line represents the eastern extent of major Sevier, thin-skinned deformation. Green strip represents magmatic belt, the northern arm of which stretched from Idaho to Alaska and constitutes the Challis-Kamloops magmatic belt. Modified from Dickinson (2004).

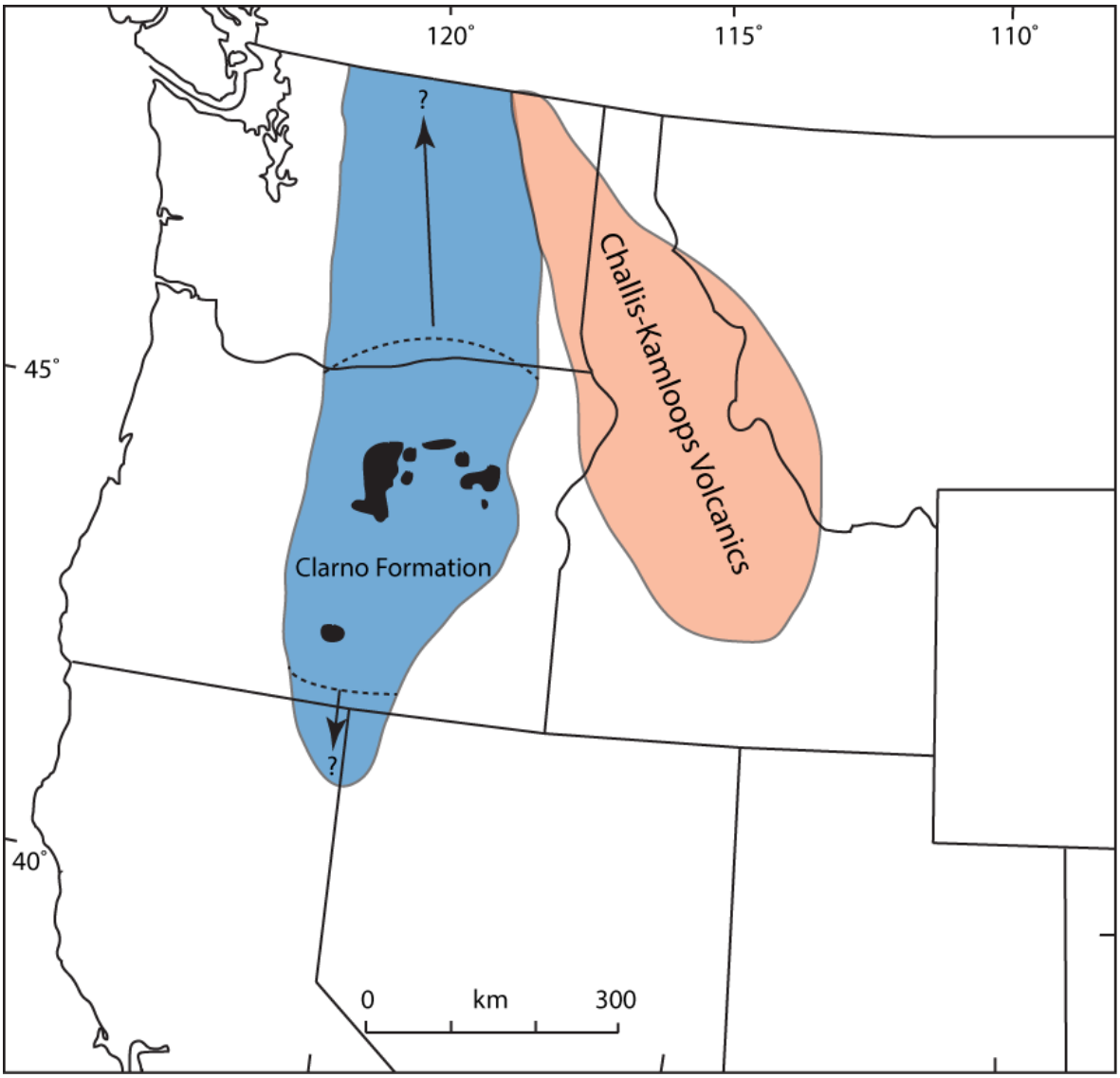

Figure 2.4. Map showing the distribution of the Clarno Formation of Central Oregon. The southern extent of Clarno type deposits as shown here are based on outcrops in the Warner Mountains in northern California and south-central Oregon. It should be noted that these units are similar in chemistry but are distinctly younger, around 31 Ma (Carmichael et al., 2006) whereas typical ages on Clarno Formation are 44-39 Ma but as old as 54 Ma. It is believed that similar rocks which outcrop near Paisley of Clarno type would fall between these two ages. Peach colored area represents extent of older Challis-Kamloops magmatic center. Modified from Christiansen and Yeats (1992).

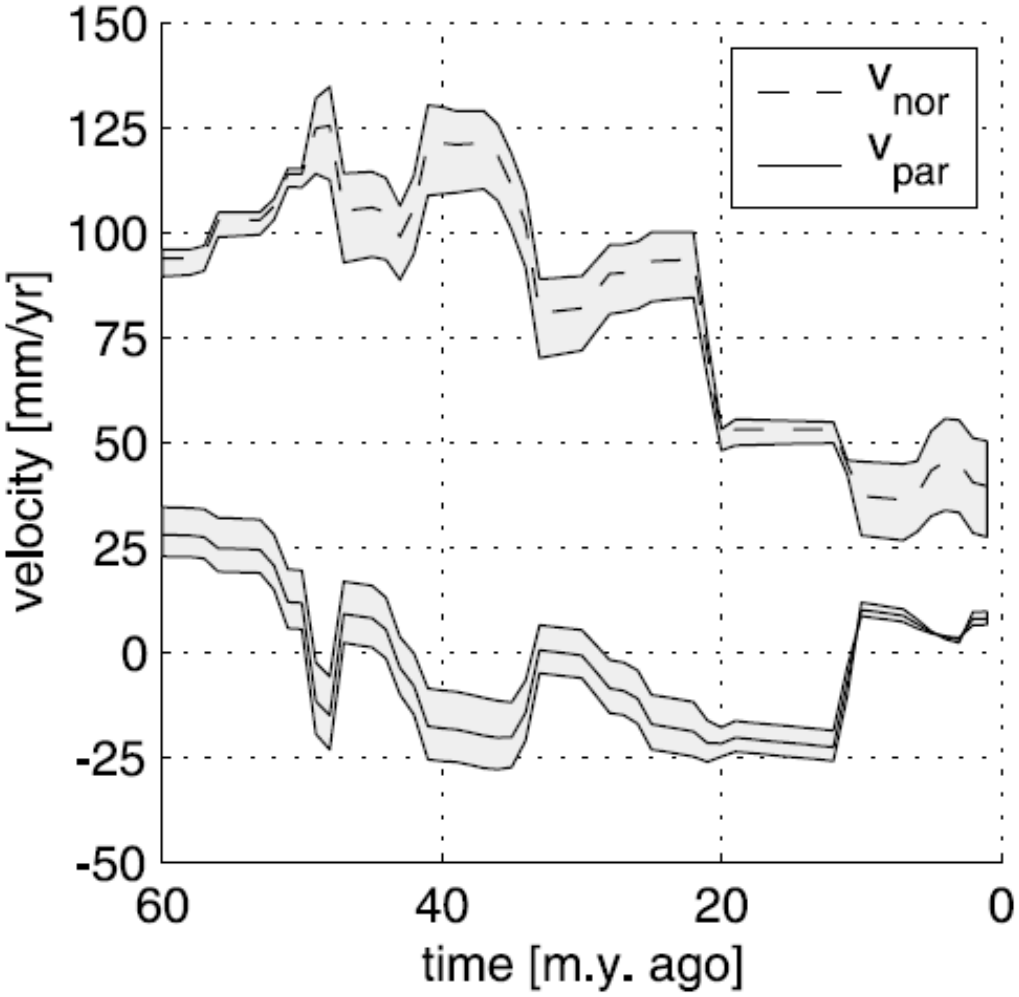

Figure 2.5. Velocity vs time chart for subduction of the Farallon (and subsequently the Juan de Fuca plate) plate from 60-0 Ma. Upper dashed line represents the average velocity perpendicular to the subduction zone, upper and lower lines represents error. Lower line represents velocity parallel to the trench. Velocity in the Paleogene was consistently faster than in the Neogene. Around 10 Ma, the obliquity of subduction increases, evidenced by a greater velocity parallel to the trench. From Schmid et al. (2002).

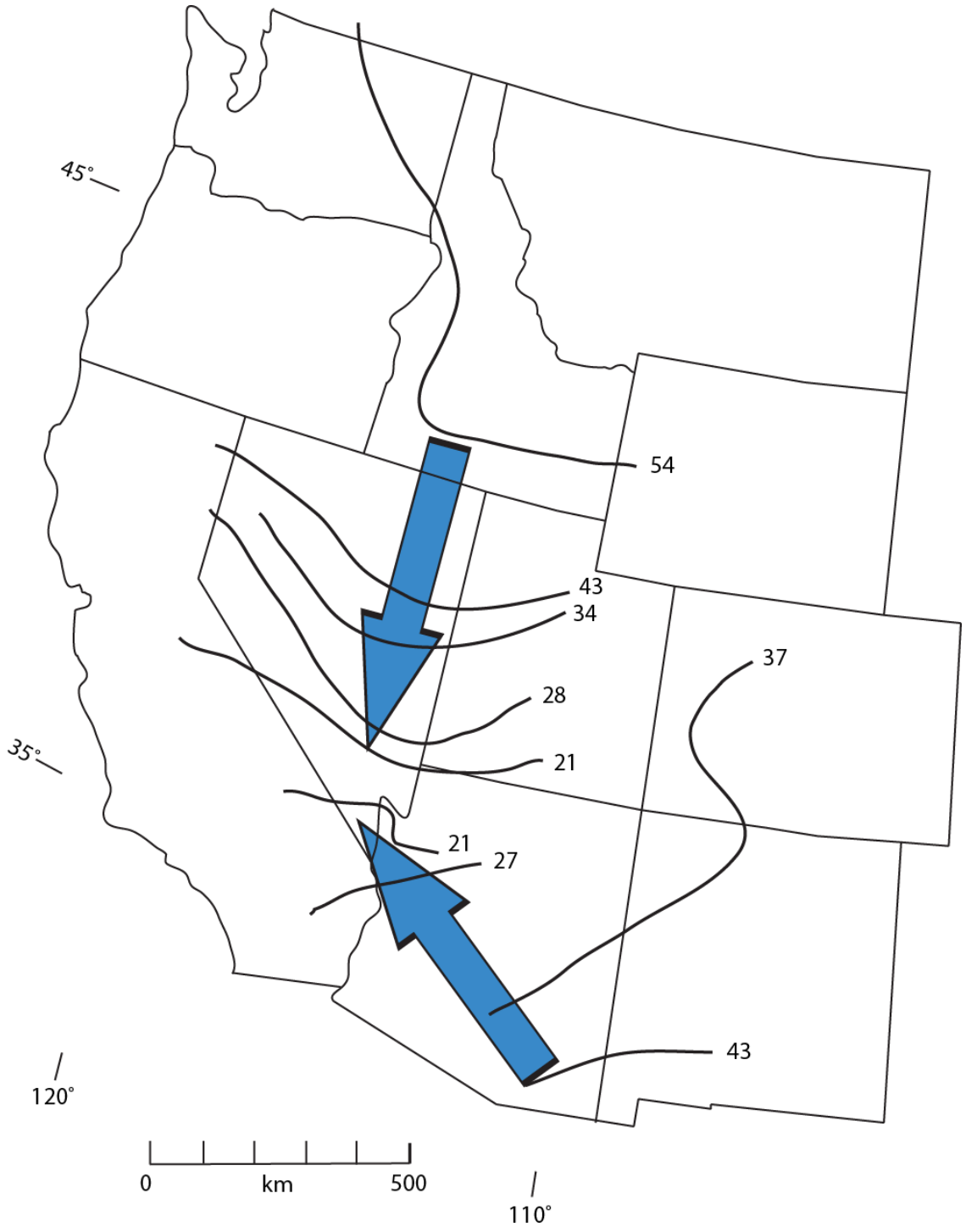

Figure 2.6. Map showing the northward and southward sweeping magmatism in the Oligocene and early Miocene of the Ignimbrite Flare-Up. This event is important for the development of the Basin and Range Province, see text for further discussion. Radiometric dates from rocks converge at 20 Ma in southern Nevada. Numbers on diagram are in millions of years (Ma). Modified from Humphreys (1995).

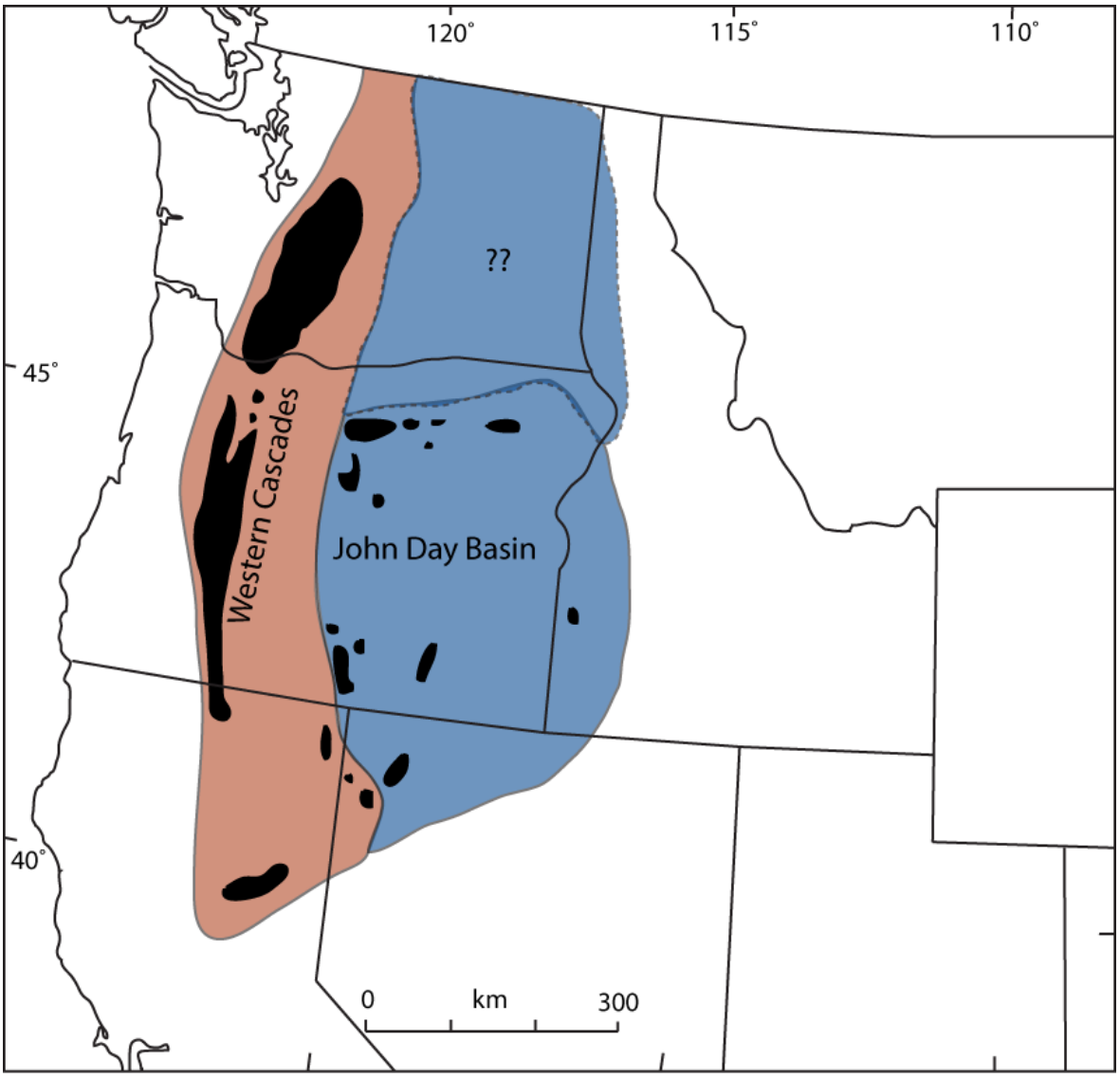

Figure 2.7. Aerial distribution of John Day back-arc basin and Western Cascades in Oligocene early-Miocene. Modified from Christiansen and Yeats (1992).

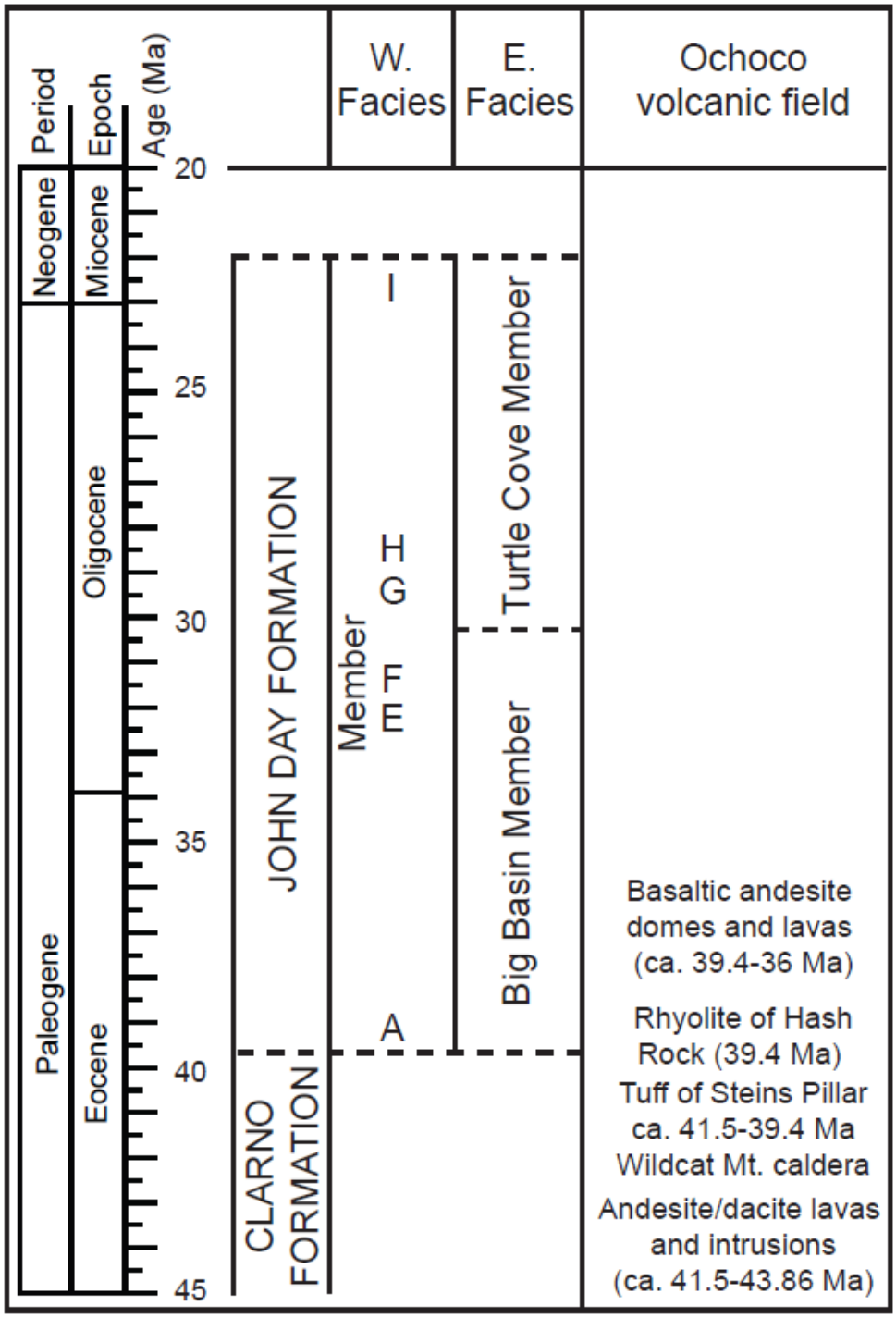

Figure 2.8. Stratigraphy of Central Oregon from Upper Eocene through Lower Miocene. Regional boundary between the Clarno Formation and the John Day Formation is represented by ash flow A at 39 Ma. Taken from McClaughry et al. (2009).

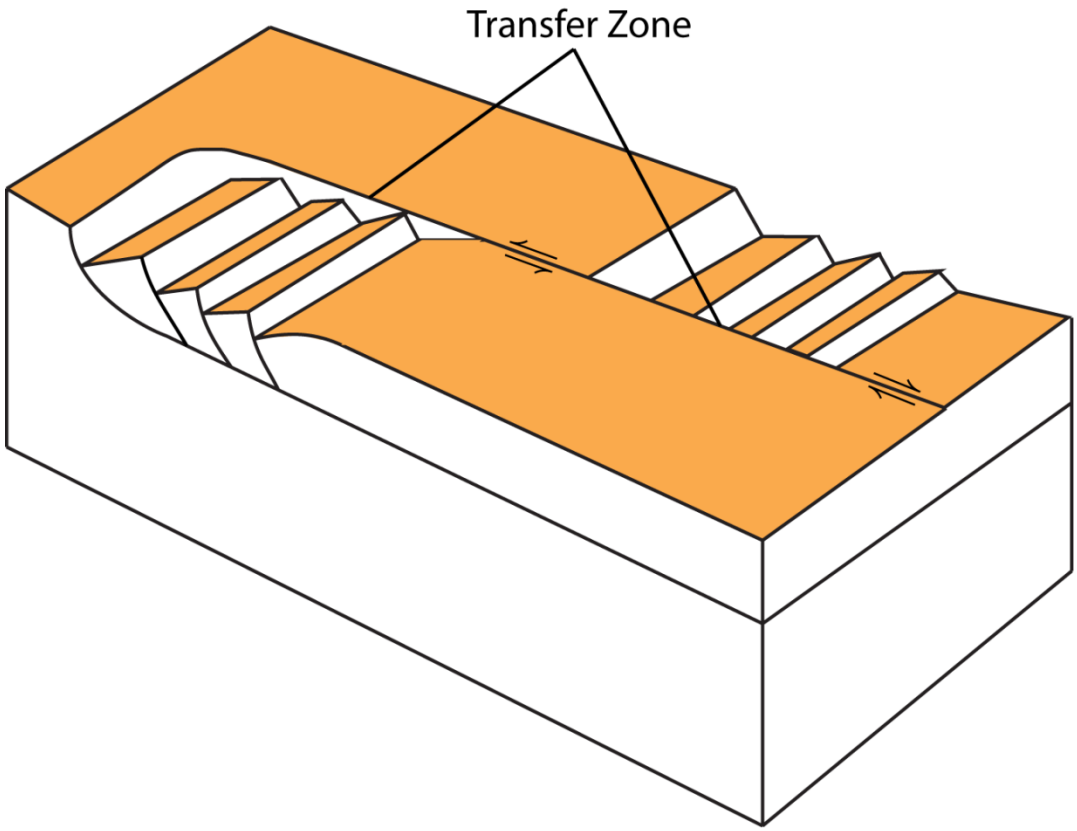

Figure 2.9. Schematic diagram depicting how strain is transferred between two, or sets of, en echelon normal faults via a transfer fault. The transfer fault is typically parallel or oblique to the direction of extension. Modified from Faulds and Varga (1998).

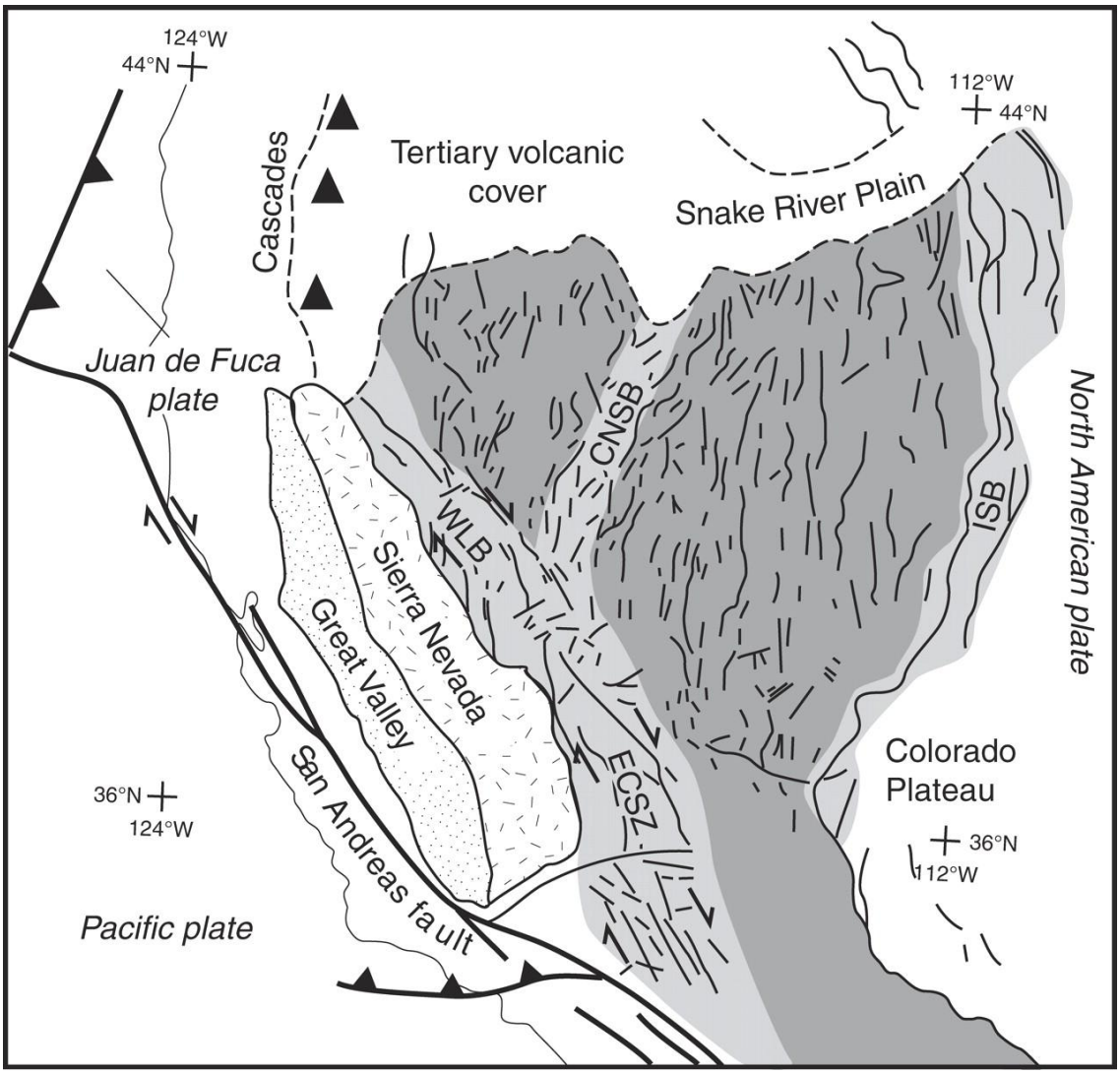

Figure 2.10. Map showing extent of the Walker Lane and Eastern California Shear Zone. This is a zone of dextral shear due to northwestward translation of the Sierra Nevada Crustal Block. WLB- Walker Lane Belt; CNSB- Central Nevada Seismic Belt; ISB- Intermountain Seismic Belt; ECSZ- Eastern California Shear Zone. Taken from Lee et al. (2009).

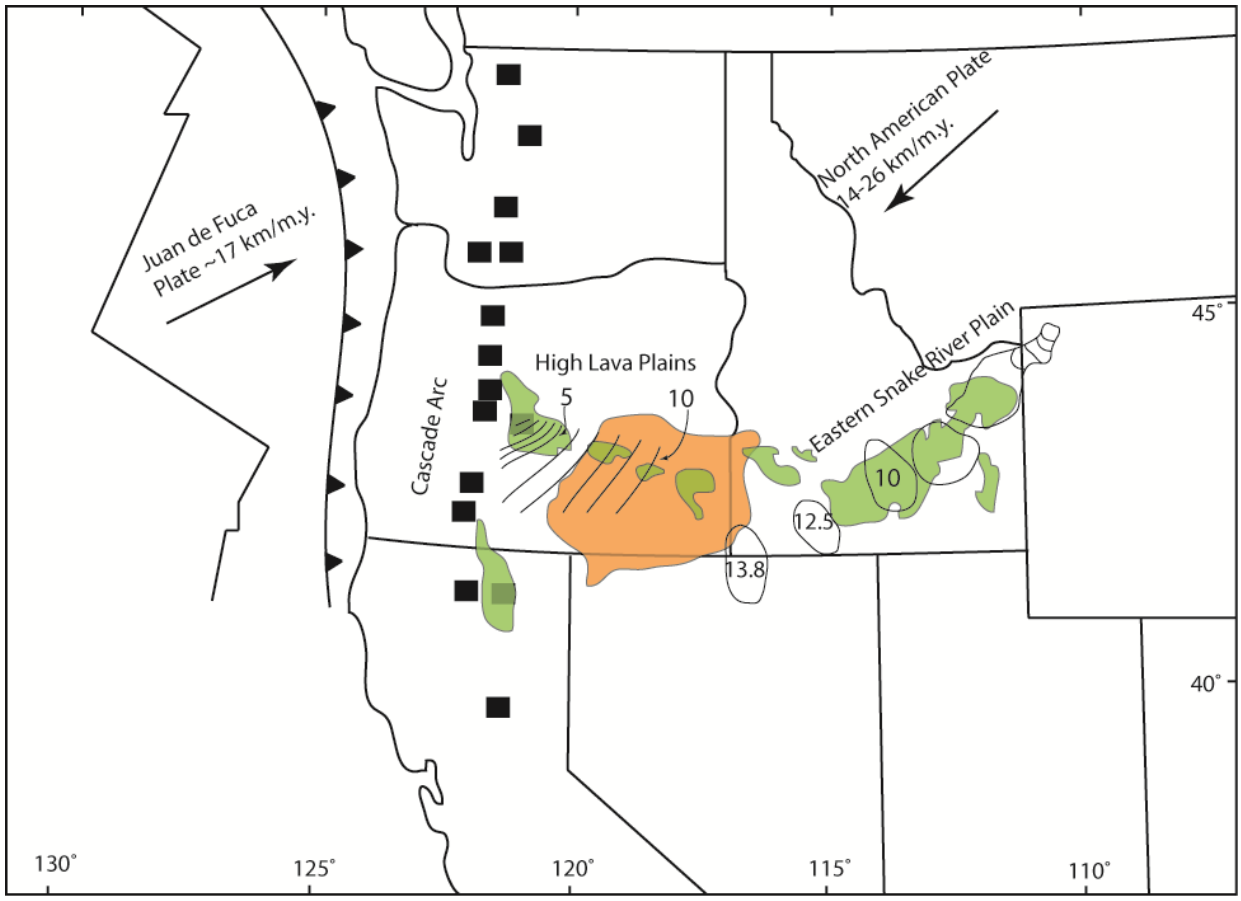

Figure 2.11. Map showing distribution of bimodal magmatism on the High Lava Plains (HLP) and Eastern Snake River Plain (ESRP)/Yellowstone Hot Spot tracks. Circles and solid lines with numbers indicate eastward/westward age-progressive silicic volcanism on the ESRP and HLP tracks, respectively. Black boxes represent major volcanic centers associated with the modern Cascade Range. Green areas indicate Pliocene and younger basalts from Jordan et al. (2004). Orange area delineates extent of Steen Mountain Basalt after Camp and Ross (2004). ESRP volcanic centers after Pierce and Morgan (1992). Modified from Jordan et al. (2004).

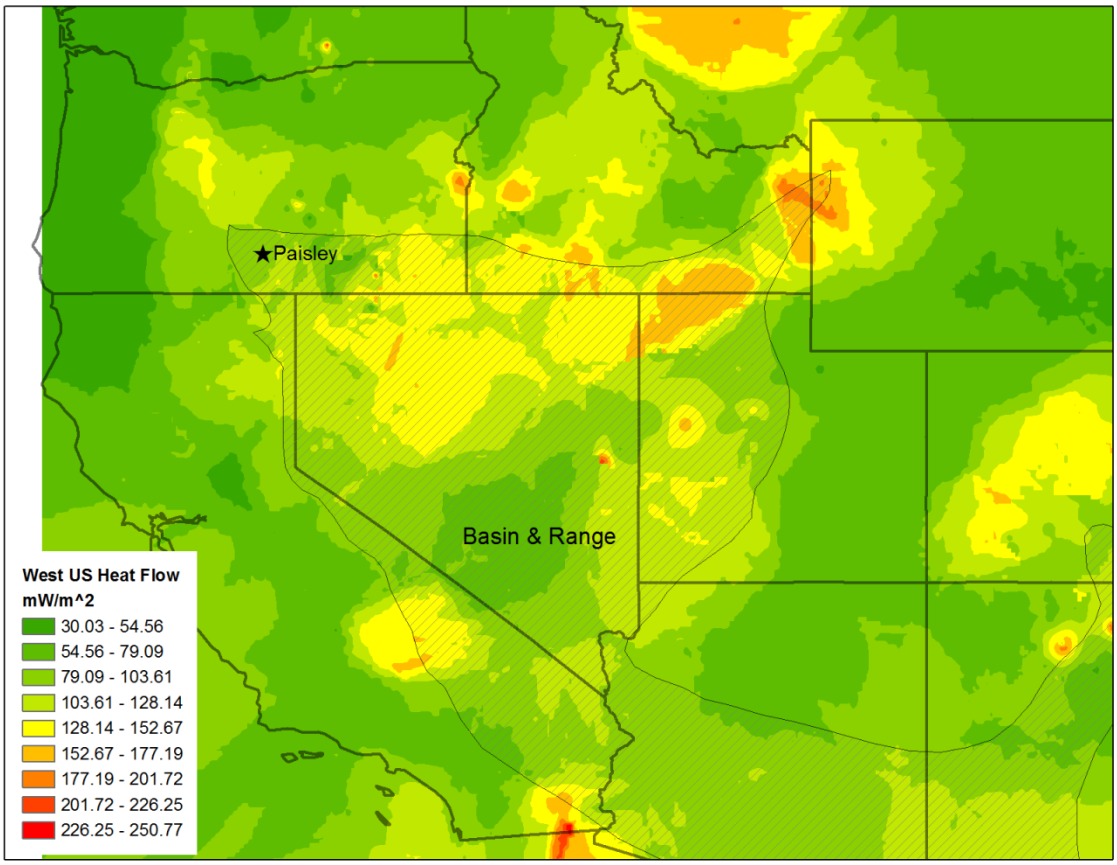

Figure 2.12. Map showing surface heat flow of the western United States with data from the University of North Dakota Heat Flow Database. See text for further discussion. Units are in mW/m^2.

References Cited

Armstrong, R.L., Ward, P. 1991. Evolving Geographic Patterns of Cenozoic Magmatism in the North American Cordillera: The Temporal and Spatial Association of Magmatism and Metamorphic Core Complexes. Journal of Geophysical Research. v. 96, no. 8. p. 13201-13224.

Askren, D.R., Roden, M.F., Whitney, J.A. 1997. Petrogenesis of Tertiary Andesite Lava Flows Interlayered with Large-Volume Felsic Ash-Flow Tuffs of the Western US. Journal of Petrology. v. 38, no. 8. p. 1021-1046.

Bacon, C.R. 1989. Calc-alkaline, Shoshonitic, and Primitive Tholeiitic Lavas from Monogenetic Volcanoes near Crater Lake, Oregon. Journal of Petrology. v. 31, Part 1. p. 135-166.

Bennett, R.A., Wernicke, B.P., Niemi, N.A., Fridrich, A.M. 2003. Contemporary strain rates in the northern Basin and Range province from GPS data. Tectonics. v. 22, no. 2. DOI: 10.1029/2001TC001355.

Best, M.G., Barr, D.B., Christiansen, E.H., Gromme, S., Deino, A.L., Tingey, D.G. 2009. The Great Basin Altiplano During the Middle Cenozoic Ignimbrite Flareup: Insights from Volcanic Rocks. International Geology Review. v. 51, no. 7-8. p. 589-633. DOI: 10.180/00206810902867690.

Bestland, E.A., Rettalack, G.J. 1994a. Geology and Paleoenvironments of the Clarno Unit, John Day Fossil Beds National Monument, Oregon. US National Park Service Open-File Report. 160 p.

Bestland, E.A., Rettalack, G.J. 1994b. Geology and Paleoenvironments of the Clarno Unit, John Day Fossil Beds National Monument, Oregon. US National Park Service Open-File Report. 211 p.

Breitsprecher, K., Thorkelson, D.J., Groome, W.G., Dostal, J. 2003. Geochemical Confirmation of the Kula-Farallon Slab Window Beneath the Pacific Northwest in Eocene Time. Geology. v. 31, no. 4. p. 351-354.

Brueseke, M.E., Hart, W.K., Heizler, M.T. 2007. Diverse mid-Miocene silicic volcanism associated with the Yellowstone–Newberry thermal anomaly. Bulletin of Volcanology. v. 70, no. 3. p. 343–360. DOI: 10.1007/s00445-007-0142-5.

Burchfiel, B.C., Cowan, D.S., Davis, G.A. 1992. Tectonic Overview of the Cordilleran Orogen in the Western United States. *In* The Cordilleran Orogen: Conterminous U.S. Burchfiel, B.C., Lipman, P.W., Zoback, M.L. (eds). Geological Society of America, The Geology of North America. v. G3. 724 p.

Camp, V.E., Ross, M.E. 2004. Mantle Dynamics and Genesis of Mafic Magmatism in the Intermontane Pacific Northwest. Journal of Geophysical Research. v. 109. DOI: 10.1029/2003JB002838.

Camp, V.E., Ross, M.E., Hanson, W.E. 2003. Genesis of Flood Basalts and Basin and Range Volcanic Rocks from Steens Mountain to Malheur River Gorge, Oregon. Geological Society of America Bulletin. v. 115, no. 1. p. 105-128. DOI: 10.1130/0016-7606(2003)115<0105:GOFBAB>2.0.CO;2.

Carlson, P.I., Hart, K. 1987. Crustal Genesis on the Oregon Plateau. Journal of Geophysical Research. v. 92, no. B7. p. 6191–6206.

Carmichael, I.S.E., Lange, R.A., Hall, C.M., Renne, P.R. 2006. Faulted and tilted Pliocene olivine-tholeiite lavas near Alturas, NE California, and their bearing on the uplift of the Warner Range. Geological Society of America Bulletin. v. 118, no. 9/10. p. 1196–1211. DOI: 10.1130/B25918.1.

Cashman, P.H., Fontaine, S.A. 2000. Strain partitioning in the northern Walker Lane, western Nevada and northeastern California. Tectonophysics. v. 326, no. 1/2. p. 111–130. DOI: 10.1016/S0040-1951(00)00149-9.

Cater, F.W. 1982. Intrusive Rocks of the Holden and Lucerne Quadrangles, Washington: The Relation of Depth Zones, Composition, Textures, and Emplacement of Plutons. United States Geological Survey Professional Paper 1220. 108 p.

Christiansen, R.L., Lipman, P.W. 1992. Cenozoic Volcanism and Plate-Tectonic Evolution of the Western United States II- Late Cenozoic. Philosophical Transactions of the Royal Society of London. Series A, Mathematical and Physical Sciences. v. 271, no. 1213, A Discussion on Volcanism and the Structure of the Earth. p. 249-284.

Christiansen, R.L., Yeats, R.S. 1992. Post-Laramide Geology of the U.S. Cordilleran Region. *In* The Cordilleran Orogen: Conterminous U.S. Burchfiel, B.C., Lipman, P.W., Zoback, M.L. (eds). Geological Society of America, The Geology of North America. v. G3. 724 p.

Christiansen, R.L., Foulger, G.R., Evans, J.R. 2002. Upper-Mantle Origin of the Yellowstone Hotspot. Geological Society of America Bulletin. v. 114, no. 10. p. 1245-1256. DOI: 10.1130/0016-7606(2002)114<1245:UMOOTY>2.0.CO;2.

Colgan, J.P., Henry, C.D. 2009. Rapid Middle Miocene Collapse of the Mesozoic Orogenic Plateau in North-Central Nevada. International Geology Review. v. 51, no. 9-11. p. 920-961. DOI: 10.1080/00206810903056731.

Colgan, J.P., Dumitru, T.A., McWilliams, M., Miller, E.L. 2006a. Timing of Cenozoic Volcanism and Basin and Range extension in the northwestern Nevada: New constraints from the northern Pine Forest Range. Geological Society of America Bulletin. v. 118, no. 1/2. p. 126-239. DOI: 10.1130/B25681.1.

Colgan, J.P., Dumitru, T.A., Reiners, P.W., Wooden, J.L., Miller, E.L. 2006b. Cenozoic Tectonic Evolution of the Basin and Range Province in Northwestern Nevada. American Journal of Science. v. 306. p. 616-654. DOI: 10.2475/08.2006.02.

Colgan, J.P., John, D.A., Henry, C.D., Fleck, R.J. 2008. Large-Magnitude Miocene Extension of the Eocene Caetano Caldera, Shoshone and Toiyabe Ranges, Nevada. Geosphere. v. 4, no. 1. p. 107-130. DOI: 10.1130/GES00115.1.

Cross, T.A., Pilger Jr., R.H. 1978. Constraints on Absolute Motion and Plate Interaction Inferred from Cenozoic Igneous Activity in the Western United States. American Journal of Science. v. 278. p. 865-902.

Dickinson, W.R. 2002. The Basin and Range Province as a Composite Extensional Domain. International Geology Review. v. 44. p. 1-38.

Dickinson, W.R. 2004. Evolution of the North American Cordillera. Annual Review of Earth and Planetary Science Letters. v. 32. p. 13-45. DOI: 10.1146/annurev.earth.32.101802.120257.

Dickinson, W.R. 2006. Geotectonic Evolution of the Great Basin. Geosphere. v. 2, no. 7. p. 353-368. DOI: 10.1130/GES00054.1.

Donath, F.A., Kuo, J.T. 1962. Seismic-Refraction Study of Block Faulting, South-Central Oregon. Geological Society of America Bulletin. v. 73. p. 429-434. DOI: 10.1130/0016-7606(1962)73[429:SSOBFS]2.0.CO;2.

Donath, F.A. 1962. Analysis of Basin-Range Structure, South-Central Oregon. Geological Society of America Bulletin. v. 73. p. 1-16. DOI: 10.1130/0016-7606(1962)73[1:AOBSSO]2.0.CO;2.

Draper, D.S. 1991. Late Cenozoic Bimodal Magmatism in the Northern Basin and Range Province of Southeastern Oregon. Journal of Volcanology and Geothermal Research. v. 47. p. 299-328.

Druken, K.A., Long, M.D., Kincaid, C. 2011. Patterns in seismic anisotropy driven by rollback subduction beneath the High Lava Plains. Geophysical Research Letters. v. 38. p. L13310. 6 p. DOI: 10.1029/2011GL047541.

du Bray, E.A., John, D.A. 2011. Petrologic, Tectonic, and Metallogenic Evolution of the Ancestral Cascades Magmatic Arc, Washington, Oregon, and northern California. Geosphere. v. 7, no. 5. p. 1102-1133. DOI: 10.1130/GES00669.1.

Duncan, R.A. 1982. A Captured Island Chain in the Coast Range of Oregon and Washington. Journal of Geophysical Research. v. 87, no. B13. p. 10827-10837.

Egger, A.E., Miller, E.L. 2011. Evolution of the Northwest Margin of the Basin and Range: The Geology and Extensional History of the Warner Range and Environs, Northeastern California. Geosphere. v. 7. p. 756-773. DOI: 10.1130/GES00620.1.

English, J.M., Johnston, S.T. 2004. The Laramide Orogeny: What Were the Driving Forces?. International Geology Review. v. 46, no. 9. p. 833-838. DOI: 10.2747/0020-6814.46.9.833.

Evernden, J.F., James, G.T. 1964. Potassium-Argon Dates and the Tertiary Floras of North America. American Journal of Science. v. 262. p. 945-974.

Evernden, J.F., Savage, D.E., Curtis, G.H., James, G.T. 1964. Potassium-Argon Dates and the Cenozoic Mammalian Chronology of North America. American Journal of Science. v. 262. p. 145-198.

Ewing, T.E. 1980. Paleogene Evolution of the Pacific Northwest. The Journal of Geology. v. 88, no. 6. p. 619-638.

Faulds, J.E., Henry, C.D. 2008. Tectonic Influences on the Spatial and Temporal Evolution of the Walker Lane: An Incipient Transform Fault Along the Evolving Pacific-North American Plate Boundary. *In* Ores and Orogenesis: Circum-Pacific tectonics, geologic evolution, and ore deposits. Spencer, J.E., Titley, S.R., (eds). Arizona Geological Society Digest 22. p. 437-470.

Faulds, J.E., Varga, R.J. 1998. The Role of Accommodation Zones and Transfer Zones in the Regional Segmentation of Extended Terranes. *In* Accommodation and Transfer Zones: The Regional Segmentation of the Basin and Range Province. Faulds, J.E., Stewart, J.H. (eds). Geological Society of America Special Paper 323. Boulder, CO.

Faulds, J.E., Henry, C.D., Hinz, N.H. 2005. Kinematics of the Northern Walker Lane: An Incipient Transform Fault Along the Pacific-North American Plate Boundary. Geology. v. 33, no. 6. p. 505-508. DOI: 10.1130/G21274.1.

Faulds, J.E., Coolbaugh, M.F., Vice, G.S., Edwards, M.L. 2006. Characterizing Structural Controls of Geothermal Fields in the Northwestern Great Basin: A Progress Report. Geothermal Resources Council Transactions. v. 30. p. 69-76.

Faulds, J.E., Coolbaugh, M.F., Benoit, D., Oppliger, G., Perkins, M., Moeck, I., Drakos, P. 2010. Structural Controls of Geothermal Activity in the Northern Hot Springs Mountains, Western Nevada: The Tale of Three Geothermal Systems (Brady's, Desert Peak, and Desert Queen). Geothermal Resources Council Transactions. v. 34. p. 675-684.

Ford, M.T. 2011. Rhyolitic Magmatism of the High Lava Plains and Adjacent Northwest Basin and Range, Oregon: Implications for the Evolution of Continental Crust. Ph.D Dissertation. Oregon State University. Corvallis, OR.

Fuller, R.E. 1931. The Geomorphology and Volcanic Sequence of Steens Mountain in Southeastern Oregon. Washington University Publications in Geology. v. 3, no. 1. 130 p.

Gaschnig, R.M., Vervoort, J.D., Lewis, R.S., McClelland, W.C. 2009. Migrating Magmatism in the Northern United States Cordillera: in situ U-Pb Geochronology of the Idaho Batholith. Contributions to Mineral Petrology. v. 159. p. 863-883. DOI: 10.1007/s00410-009-0459-5.

Graham, D.W., Reid, M.R., Jordan, B.T., Grunder, A.L., Leeman, W.P., Lupton, J.E. 2009. Mantle Source Provinces Beneath the Northwestern USA Delimited by Helium Isotopes in Young Basalts. Journal of Volcanology and Geothermal Research. v. 188. p. 128-140. DOI: 10.1016/j.jvolgeores.2008.12.004

Gunn, B.M., Watkins, N.D. 1970. Geochemistry of the Steens Mountain Basalts, Oregon. Geological Society of America Bulletin. v. 81. p. 1497-1516.

Hammond, W.C., Thatcher, W. 2005. Northwest Basin and Range Tectonic Deformation Observed with the Global Positioning System, 1999-2003. Journal of Geophysical Research. v. 110. DOI: 10.1029/2005JB003678.

Hart, W.K., Aronson, J.L., Mertzman, S.A. 1984. Areal Distribution and Age of Low-K, High-Alumina Olivine Tholeiite Magmatism in the Northwestern Great Basin. Geological Society of America Bulletin. v. 95. p. 186-195.

Honn, D.K., Smith, E.I. 2007. Nested Calderas in the Northern Kawich Range, Central Nevada: Termination of the Ignimbrite Flare-Up in the Great Basin. American Geophysical Union, Fall Meeting 2007. Abstract # V41A-10.

Hooper, P.R., Binger, G.B., Lees, K.R. 2002. Ages of the Steens and Columbia River Flood Basalts and their Relationship to Extension-Related Calc-Alkalic Volcanism in Eastern Oregon. Geological Society of America Bulletin. v. 114, no. 1. p. 43-50.

Hooper, P.R., Bailey, D.G., McCarley Holder, G.A. 1995. Tertiary Calc-Alkaline Magmatism Associated with Lithosphere Extension in the Pacific Northwest. Journal of Geophysical Research. v. 100, no. B7. p. 10303-10319.

Humphreys, E.D. 1995. Post-Laramide Removal of the Farallon Slab, Western United States. Geology. v. 23. p. 987-990. DOI: 10.1130/0091-7613(1995)023<0987:PLROTF>2.3.CO;2.

Johnson, C.M. 1991. Large-Scale Crust Formation and Lithosphere Modification Beneath Middle to Late Cenozoic Calderas and Volcanic Fields, Western North America. Journal of Geophysical Research. v. 96, no. B8. p. 13485-13507.

Jordan, B.T., Streck, M.J., Grunder, A.L. 2002. Bimodal Volcanism and Tectonism of the High Lava Plains, Oregon. *In* Field Guide to Geologic Processes in Cascadia. Oregon Department of Geology and Mineral Industries Special Paper. p. 23-46.

Jordan, B.T., Grunder, A.L., Duncan, R.A., Deino, A.L. 2004. Geochronology of Age-Progressive Volcanism of the Oregon High Lava Plains: Implications for the Plume Interpretation of Yellowstone. Journal of Geophysical Research. v. 109. DOI: 10.1029/2003JB002776.

Lawrence, R.D. 1976. Strike-Slip Faulting Terminates the Basin and Range Province in Oregon. Geological Society of America Bulletin. v. 87, no. 6. p. 846-850. DOI: 10.1130/0016-7606(1976)87<846:SFTTBA>2.0.CO;2.

Lee, J., Garwood, J., Stockli, D.F., Gosse, J. 2009. Quaternary Faulting in Queen Valley, California-Nevada: Implications for Kinematic of Fault-Slip Transfer in the Eastern California Shear Zone- Walker Lane Belt. Geological Society of America Bulletin. v. 121, no. 3/4. p. 599-614. DOI: 10.1130/B26352.1.

Lipman, P.W., Glazner, A.F. 1991. Introduction to Middle Tertiary Cordilleran Volcanism: Magma Sources and Relations to Regional Tectonics. Journal of Geophysical Research. v. 96, no. B8. p. 13193-13199.

Liu, M. 2001. Cenozoic Extension and Magmatism in the North American Cordillera: The Role of Gravitational Collapse. Tectonophysics. v. 342. p. 407-433.

Ludington, S., Cox, D.P., Leonard, K.W., Moring, B.C. 1996. Cenozoic Volcanic Geology of Nevada. *In* An analysis of Nevada's metal-bearing Mineral Resources. Singer, D.A., (ed). Nevada Bureau of Mines and Geology Open-File Report 96-2. 1:1 000 000 scale.

Macdonald, R., Smith, R.L., Thomas, J.E. 1992. Chemistry of the Subalkalic Silicic Obsidians. United States Geological Survey Professional Paper 1523. Denver, CO.

MacLeod, N.S., Walker, G.W., McKee, E.H. 1976. Geothermal Significance of Eastward Increase in Age of Upper Cenozoic Rhyolitic Domes in Southeastern Oregon. Proceedings, Second United Nations Symposium on the Development and Use of Geothermal Resources, San Fransisco, 1975. v. 1. 10 p.

Madsen, J.K., Thorkelson, D.J., Friedman, R.M., Marshall, D.D. 2006. Cenozoic to Recent Plate Configurations in the Pacific Basin: Ridge Subduction and Slab Window Magmatism in Western North America. Geosphere. v. 2, no. 1. p. 11-34. DOI: 10.1130/GES00020.1.

McBirney, A.R., White, C.M. 1982. The Cascade Province. *In* Andesites: Orogenic Andesites and Related Rocks. Thorpe, R.S. (ed). John Wiley and Sons New York. 724 p.

McClaughry, J.D., Gordon, C.L., Ferns, M.L. 2009. Field Trip Guide to the Middle Eocene Wildcat Mountain Caldera, Ochoco National Forest, Crook County, Oregon. Oregon Geology. v. 69, no. 1. p. 5-24.

McKee, E.H., Duffield, W.A., Stern, R.J. 1983. Late Miocene and Early Pliocene Basaltic Rocks and Their Implications for Crustal Structure, Northeastern California and South-Central Oregon. Geological Society of America Bulletin. v. 94. p. 292-304. DOI: 10.1130/0016-7606(1983)94<292:LMAEPB>2.0.CO;2.

McQuarrie, N., Wernicke, B. P. 2005. An animated tectonic reconstruction of southwestern North America since 36 Ma. v. 3. P. 147–172. DOI:10.1130/GES00016.1.

Miller, E.L., Dumitru, T.A., Brown, R.W., Gans, P.B. 1999. Rapid Miocene Slip on the Snake Range-Deep Creek Range Fault System, East-Central Nevada. Geological Society of America Bulletin. v. 111, no. 6. p. 886-905.

Morris, G.A., Larson, P.B., Hooper, P.R. 2000. 'Subduction Style' Magmatism in a Non-subduction Setting: The Colville Igneous Complex, NE Washington State, USA. Journal of Petrology. v. 41, no. 1. p. 43-67

Oldow, J.S., Aiken, C.V., Hare, J.L., Ferguson, J.F., Hardyman, R.F. 2001. Active Displacement Transfer and Differential Block Motion Within the Central Walker Lane, Western Great Basin. Geology. v. 29, no. 1. p. 19-22.

Payne, S.J., McCaffrey, R., King, R.W. 2008. Strain Rates and Contemporary Deformation in the Snake River Plain and Surrounding Basin and Range from GPS and Seismicity. Geology. v. 36. p. 647-650. DOI: 10.1130/G25039A.1.

Pearce, J.A., Cann, J.R. 1977. Tectonic Setting of Basic Volcanic Rocks Determined Using Trace Element Analyses. Earth and Planetary Science Letters. v. 19. p. 290-300.

Peck, D. 1964. Geologic Reconnaissance of the Antelope-Ashwood Area of North-Central Oregon, with an Emphasis on the John Day Formation of late Oligocene and early Miocene Age. United States Geological Survey Bulletin 1161-D. 26 p.

Pezzopane, S.K., Weldon, R.J. 1993. Tectonic Role of Active Faulting in Central Oregon. Tectonics. v. 12, no. 5. p. 1140-1169.

Pierce, K.L., Morgan, L.A. 1992. The Track of the Yellowstone Hot Spot: Volcanism, Faulting, and Uplift. *In* Regional Geology of Eastern Idaho and Western Wyoming. Link, P.K., Kuntz, M.A., Platt, I.B. (eds). Geological Society of America Memoir 179. p. 1-52.

Ponce, D.A., Glen, J.M. 2008. A Prominent Geophysical Feature Along the Northern Nevada Rift and its Geologic Implications, North-Central Nevada. Geosphere. v. 4, no. 1. p. 207-217. DOI: 10.1130/GES00117.1.

Putirka, K.D., Busby, C.J. 2011. Introduction: Origin and Evolution of the Sierra Nevada and Walker Lane. Geosphere. v. 7. p. 1269-1272. DOI: 10.1130/GES00761.1.

Retallack, G.J., Bestland, E.A., Fremd, T.J. 2000. Eocene and Oligocene Paleosols of Central Oregon. In Eocene and Oligocene Paleosols of Central Oregon. Retallack, G.J., Bestland, E.A., Fremd, T.J. (eds). Geological Society of America Special Paper 344. Boulder, CO. 192 p.

Robinson, P.T., Brem, G.F., McKee, E.H. 1984. John Day Formation of Oregon: A Distal Record of Early Cascade Volcanism. Geology. v. 12. p. 229-232. DOI: 10.1130/0091-7613(1984)12<229:JDFOOA>2.0.CO;2.

Robinson, P.T., Walker, G.W., McKee, E.H. 1990. Eocene(?), Oligocene, and Lower Miocene Rocks of the Blue Mountains Region. *In* Geology of the Blue Mountains Region of Oregon, Idaho, and Washington: Cenozoic Geology of the Blue Mountains Region. Walker, G.W. (ed). United States Geological Survey Professional Paper 1437. Denver, CO. p. 29-62.

Rogers, J.W., Novinsky-Evans, J.M. 1977. The Clarno Formation of Central Oregon USA- Volcanism on a Thin Continental Margin. Earth and Planetary Science Letters. v. 34. p. 56-66.

Scarberry, K.C., Meigs, A.J., Grunder, A.L. 2010. Faulting in a Propagating Continental Rift: Insight from the late Miocene Structural Development of the Abert Rim Fault, Southern Oregon, USA. Tectonophysics. v. 488. p. 71-86. DOI: 10.1016/j.tecto.2009.09.025.

Schmandt, B., Humphreys, E. 2011. Seismically Imaged Relict Slab from the 55 Ma Siletzia Accretion to the Northwest United States. Geology. v. 39. p. 175-178. DOI: 10.1130/G31558.1.

Schmid, C., Goes, S., van der Lee, S., Giardini, D. 2002. Fate of Cenozoic Farallon Slab from a Comparison of Kinematic Thermal Modeling with Tomographic Images. Earth and Planetary Science Letters. v. 204. p. 17-32.

Smith, R.L., Luedke, R.G. 1984. Potentially Active Volcanic Lineaments and Loci in Western Conterminous United States. *In* Explosive Volcanism: Inception, Evolution, and Hazards. Geophysics Research Forum, Geophysics Study Committee. 176 p.

Smith, G.A., Manchester, S.R., Ashwil, M., McIntosh, W.C., Conrey, R.M. 1998. Late Eocene-Early Oligocene Tectonism, Volcanism, and Floristic Change near Gray Butte, Central Oregon. Geological Society of America Bulletin. v. 110, no. 6. p. 759-778.

Snyder, W.S., Dickinson, W.R., Silberman, M.L. 1976. Tectonic Implications of Space-Time Patterns of Cenozoic Magmatism in the Western United States. Earth and Planetary Science Letters. v. 32. p. 91-106.

Stewart, J.H., Carlson, J.E. 1976. Cenozoic Rocks of Nevada- Four Maps and a Brief Description of Distribution, Lithology, Age, and Centers of Volcanism. Nevada Bureau of Mines and Geology Map 52. 1:1 000 000 scale.

Stewart, J.H. 1978. Basin-Range Structure in Western North America: A Review. *In* Cenozoic Tectonics and Regional Geophysics of the Western Cordillera. Smith, R.B., Eaton, G.P. (eds). Geological Society of America Memoir 152. p. 1-31.

Stewart, J.H. 1980. Regional Tilt Patterns of Late Cenozoic Basin and Range Fault Blocks, Western United States. Geological Society of America Bulletin. v. 91, no. 8. p. 460-464. DOI: 10.1130/0016-7606(1980)91<460:RTPOLC>2.0.CO;2.

Stockli, D.F., Surpless, B.E., Dumitru, T.A. 2002. Thermochronological Constraints on the Timing and Magnitude of Miocene and Pliocene Extension in the Central Wassuk Range, Western Nevada. Tectonics. v. 21, no. 4. 19 p. DOI: 10.1029/2001TC001295.

Streck, M.J., Grunder, A.L. 1997. Compositional Gradients and Gaps in High-Silica Rhyolites of the Rattlesnake Tuff, Oregon. Journal of Petrology. v. 38, no. 1. p. 133-163.

Swanson, D.A., Robinson, P.T. 1968. Base of the John Day Formation in and near the Horse Heaven Mining District, North-Central Oregon. United States Geological Survey Professional Paper 600-D. p. D154-D161.

Thatcher, W., Foulger, G.R., Julian, B.R., Svarc, J., Quilty, E., Bawden, G.W. 1999. Present-Day Deformation Across the Basin and Range Province, Western United States. Science. v. 283, no. 5408. p. 1714-1718.

Trench, D., Meigs, A., Grunder, A. 2012. Termination of the Northwestern Basin and Range Province into a Clockwise Rotating Region of Transtension and Volcanism, Southeast Oregon. Journal of Structural Geology. v. 39. p. 52-65. DOI: 10.1016/j.jsg.2012.03.007.

Urbanczyk, K.M. 1994. Geology of the Eastern Part of the Clarno Formation, Northeast Oregon. Ph.D. Dissertation. Washington State University. Pullman, WA. 230 p.

Verplanck, E.P., Duncan, R.A. 1987. Temporal Variations in Plate Convergence and Eruption Rates in the Western Cascades, Oregon. Tectonics. v. 6, no. 2. p. 197-209.

Walker, G.W., MacLeod, N.S. 1991. Geologic Map of Oregon. United States Geological Survey. 1:500 000 scale. 2 sheets.

Wells, R.E., Simpson, R.W. 2001. Northward Migration of the Cascadia Forearc in the Northwestern US and Implications for Subduction Deformation. Earth Planets Space. v. 53. p. 275-283.

Wernicke, B., Axen, G.J., Snow, J.K. 1988. Basin and Range Extensional Tectonics at the Latitude of Las Vegas, Nevada. Geological Society of America Bulletin. v. 100. p. 1738-1757.

White, J., Robinson, P.T. 1992. Intra-arc Sedimentation in a Low-Lying Marginal Arc, Eocene Clarno Formation, Central Oregon. Sedimentary Geology. v. 80. p. 89-114.

Woodburne, M.O., Robinson, P.T. 1977. A New Late Hemingfordian Mammal Fauna From the John Day Formation, Oregon, and Its Stratigraphic Implications. Journal of Paleontology. v. 51, no. 4. p. 750-757.

Zoback, M.L., Anderson, R.E., Thompson, G.A. 1981. Cainozoic Evolution of the State of Stress and Style of Tectonism of the Basin and Range Province of the Western United States. Philosophical Transactions of the Royal Society of London. Series A, Mathematical and Physical Sciences. v. 300, no. 1454, Extensional Tectonics Associated with Convergent Plate Boundaries. p. 407-434.

CHAPTER THREE: GEOTHERMAL RESOURCES OF THE NORTHERN BASIN AND RANGE

Introduction

Geothermal systems in the western United States are widespread (Fig. 3.3) and reflect the complex Cenozoic geologic history of this area. The utilization of geothermal energy as a viable resource for power production hinges on our ability to understand the full spectrum of system characteristics. From this knowledge, our ability to sustain and possibly expand existing resources and the ability to identify new systems as targets for development greatly increases. This chapter serves as a summary drawn primarily from the literature and is not intended to serve as a critical assessment of the concepts and data presented by cited authors, rather this chapter is intended to provide the overall geothermal framework for assessing the resources near Paisley.

For the western United States, two types of geothermal systems predominate: 1) those associated with mostly amagmatic crustal extension, faults, and high heat flow (Basin and Range-type), and 2) those related to recent magmatism (Coolbaugh et al., 2005). The focus of this chapter will be on the extensional or Basin and Range type of geothermal systems. However, examples of both types will be examined to better construct a framework for discussing the Paisley resource, which plausibly is a mixed magmatic Basin and Range resource.

Fundamental to geothermal system characterization is heat provenance and source(s) of water. This chapter presents a brief summary on both of these topics, emphasizing their importance in evaluating Basin and Range-type geothermal systems as well as the Paisley geothermal system. Methodologies used in geothermometers, aqueous geochemistry, and stable isotopes of water in fingerprinting sources of water are presented because of their importance in the evaluation of Basin and Range-type systems. Understanding the source of water is important for managing the resource and becomes important when discussing the Paisley system.

Faults and fractures create the pathways for fluid movement both toward and away from the heat source and create the reservoirs for geothermal systems. The importance of regional and local structural features and their role in creating permeability is summarized by examining studies done on known geothermal resources within the Great Basin. Permeability tends to be greatest in areas of fault intersections, transfer zones, and in zones of en echelon normal faults. The creation of permeability is crucial because the production of geothermal fluids can occur in rocks with poor primary permeability. The Northern Basin and Range has structures at several scales that help to create the permeability in geothermal systems. For example, structures can be related at the province scale (e.g., Northern Basin and Range Province), regional scale (e.g., Central Nevada Seismic Belt), and local scales (e.g., intersection of two individual fault strands).

The Great Basin of the western United States encompasses nearly 22,000 km^2 located in 6 states. Within this region lies the Northern Basin and Range tectonic province. For the purposes of this thesis, the term Great Basin will only be applied to a

geographic area and does not imply any genetic relation to geologic processes happening therein. Rather, the term Northern Basin and Range will be applied when discussing geologic entities associated with this geologic province. Note, however, that the term Northern Basin and Range does include other smaller, regional provinces, but when these are discussed it will be explicitly stated (i.e., the term Northern Basin and Range geographically includes entities such as the Walker Lane Belt and the Central Nevada Seismic Belt); however, no genetic relation is thereby implied.

Geothermal Systems of the Western U.S.

Geologically, geothermal systems in the western U.S. have been combined into two general groups: 1) Magmatic, or 2) Extension related (amagmatic) (e.g., Sass and Lachenbruch, 1978; Smith and Shaw, 1978). These two types of systems have similarities with respect to sources of water but differ in heat source (e.g., Coolbaugh et al., 2005). This section briefly describes general characteristics of each type and includes a subdivision or expansion of the Basin and Range-type geothermal system.

Magmatic Geothermal Systems

Globally, the most common and extensively studied geothermal systems are those associated with active magmatic systems, for example, systems in Iceland, Italy, New Zealand, Mexico, East Africa, and the United States. The model for these systems is relatively straightforward; meteoric water is heated by an active magma body or from a cooling pluton. The heated water then either moves upward via faults to the surface or is contained in a thermal reservoir where drilling can tap the resource. The contribution of magmatic heat to these systems can then easily be fingerprinted by geochemical methods

(Fig. 3.1). Geothermal waters contaminated by magmatic systems tend to include significant concentrations of: As, H_2S, SO_4, Cl, B, F, and elevated $^3He/^4He$ ratios (Giggenbach, 1988; Arehart et al., 2007; Kennedy and van Soest, 2007, Fig. 3.1). Faults may be required for the upward movement of thermal waters in magmatic systems but are not the dominant feature of these magmatic-related systems.

It is worth noting that in the U.S. magmatic systems are the highest producing (with respect to power) geothermal systems, accounting for nearly 78% of the geothermal power produced (Geothermal Energy Association, 2012). It is more difficult to ascertain the relative contribution of magmatic systems globally to the total amount being produced, but based on figures from the Geothermal Energy Association's International Market Overview Report, an estimated 80% comes from magmatic systems. In the U.S. for example, the Geysers Geothermal Field in northern California is the world's largest producing geothermal system, producing an estimated 35 MW per annum since 1955 (Barker et al., 1992; Moore et al., 2001; Schmitt et al., 2003b). The heat source for this system is from an active magma body of the Clear Lake volcanic field. This active magmatism is related to the northward migration of the Mendocino Triple Junction and slab window tectonism in the northern California Coast Range (e.g., Schmitt et al., 2003a and references therein). The Geysers lie outside the boundaries of the Basin and Range and therefore the geologic setting is much different from those related to the Northern Basin and Range but is nonetheless a prime example of a magmatic geothermal system. However, Cove Fort and Roosevelt Hot Springs in western Utah are examples of magmatic geothermal systems that lie within the Northern Basin and Range (Ross et al., 1982; Chiasson, 2004). These systems, in the eastern Northern Basin and Range,

probably represent a hybrid of the two end-member types of geothermal systems, given the geologic setting of these systems. These systems have both been found to be heated primarily by Quaternary magmatism (e.g., Ross et al., 1982; Chiasson, 2004) yet both lie at range bounding normal faults produced by Basin and Range tectonism. Hence, it is envisaged that they lie somewhere along a continuum of the end-member types of geothermal systems previously defined.

Basin and Range-Type Geothermal Systems

The most common type of geothermal system in the western U.S. are those related to extensional tectonics (e.g., the Basin and Range type). Similar to magmatic systems, geothermal systems related to extension require heating of meteoric water (Giggenbach and Soto, 1992; Person et al., 2008). However, unlike magmatic systems, the heat source for extension-related geothermal systems comes from high heat flow created from the extension process. This extension elevates the geothermal gradient by bringing the mantle closer to the surface (e.g., Blackwell, 1971; Stewart, 1978). The distribution of heat flow in the Great Basin is complex and is either accentuated or masked by other geologic or hydrologic factors. Possible reasons for the concentration of higher heat flow values are discussed later in this chapter.

The faults and fractures created by Basin and Range extension are critical for the development of geothermal systems as they provide secondary permeability that is essential to the economic feasibility of a geothermal system. Fault patterns across the Northern Basin and Range are complex and the result of an equally complex geologic history. It has long been observed that extension-related geothermal systems are closely associated with recent seismicity (Bennett, 2011). A review of the dominant trends of

faulting in the Northern Basin and Range and their importance to geothermal systems is discussed later in the chapter.

As was mentioned above, some geothermal systems within the Great Basin (and presumably world-wide) lie along a continuum between two end-member types. This could become extremely important when trying to assess the characteristics and origins of a geothermal system. For example, an interesting question that has yet to be considered is at what point will a magma body or pluton's geochemical influence on the thermal fluids within a geothermal system become undetectable in such a way that the geochemical signature would lead one to conclude it is not heated by said magmatic body? What implications would this have on regional correlations to other geothermal systems? Important questions like these need to be asked because undoubtedly there is a need to characterize hybrid geothermal systems. These questions are important to the Paisley resource because it lies in an area with Quaternary volcanism but is still within the margins of the Northern Basin and Range (Fig. 2.1).

Tectonic Framework of the Northern Basin and Range

Geothermal systems of the Northern Basin and Range and specifically those in Nevada have been extensively studied (e.g., McKenna and Blackwell, 2004; Coolbaugh et al., 2005; Faulds et al., 2006; Person et al., 2008). All of these systems lie within the Northern Basin and Range and are a direct result of recent tectonics. The development of the Basin and Range has produced both the structural framework and high heat flow characteristic of Basin and Range type geothermal systems.

Tectonic History

The Ignimbrite Flare-Up (IFU) of the mid-Miocene is one of the major tectonic events that played an important role in the development of the Basin and Range province. Many theories exist that try to explain the driver for the IFU; but, regardless of the driver, the IFU is evidenced by two sweeps of intermediate to felsic magmatism (Snyder et al., 1976; Dickinson, 2006). In the Northern Basin and Range, a southward and westward sweep in magmatism emanated from central Idaho. The beginning of the western sweep is evidenced by the Clarno Formation of Oregon during Ypresian time (Bestland et al., 1999). Volcanism at this time was diffuse across central Oregon and Washington (McBirney and White, 1982). The western sweep would eventually become more localized and by approximately 45 Ma established the Western Cascades (du Bray and John, 2011). The southern arm swept southwards through Nevada, eventually terminating in southern Nevada near 20 Ma (e.g., Snyder et al., 1976; Humphreys, 1995). Volcanism in the Great Basin since this time has been concentrated at the margins and is dominated by basalt lavas (e.g., Johnson, 1991). The IFU is thought to have helped prepare the crust for later deformation because of the thermal weakening imposed by voluminous volcanism (Liu, 2001).

Two extension directions are recorded by normal faults in the Northern Basin and Range, an older NW-SE striking set of faults and a younger NE-SW set. The first set of faults were created behind an active volcanic arc, though extension is not genetically related to this arc (i.e., it may not be “back-arc extension” per se) and was coeval with the IFU in Nevada (e.g., Lipman et al., 1972; Zoback et al., 1981; Wernicke et al., 1988). This event is manifested by NW-SE striking normal faults. In the mid-Miocene at about

10 Ma, the continued development of the San Andreas Fault system is concomitant with wholesale extension inboard of the plate boundary (Dickinson and Snyder, 1979; Atwater and Stock, 1998). The direction of least principle stress shifted from NE-SW to NW-SE as a result of this change in plate boundary type (Zoback et al., 1981). Extension has held consistent in this general direction to the present (Bennett et al., 2003).

In the western-most Northern Basin and Range of east-northeast California and western Nevada, a younger set of NW striking, oblique to dextral strike-slip faults, and NE striking, sinistral oblique to strike-slip faults occur that are associated with the Walker Lane Belt (Fig. 2.1). These faults are the result of the northwestern translation of the Sierra Nevada block relative to the Colorado Plateau and accommodate 15%-20% of motion between the Pacific and North American Plates (Bennett et al., 2003; Faulds et al., 2005). Walker Lane structures began developing around 10 m.y. ago at its southern terminus in southeast California (Wesnousky, 2005). The initiation of Walker Lane structures youngs northward (Faulds et al., 2005). This northward younging is concurrent with the northward migration of the Mendocino Triple Junction (Stewart, 1988; Oldow et al., 2008). Strain partitioning in the western Northern Basin and Range is extremely complex because in this region the Walker Lane and Basin and Range tectonic provinces overlap in spatial extent. It is important to note that one should not consider the Walker Lane as a sub-province to the Northern Basin and Range because they differ greatly in deformation styles, which is how each is defined. However, the coexistence of Walker Lane structures with Basin and Range structures, as well as simultaneous movement within both domains, increases the geothermal resource potential of this region.

The Northern Basin and Range is an area of abnormally high heat flow, a result of tectonomagmatic events occurring from the mid-Miocene to Present (Sass et al., 1971; Lachenbruch, 1979; Wisian et al., 1999; Coolbaugh et al., 2005) and perhaps as far back as the Oligocene. Regional heat flow highs occur within the Northern Basin and Range (Sass et al., 1971; Blackwell, 1983; Person et al., 2008), and basin-scale heat flow patterns exist that are key to understanding individual geothermal systems (Thakur et al., 2012).

Factors That Influence Localization of Basin and Range Geothermal Systems

High heat flow is characteristic of the entire Basin and Range Province; however, the key to understanding geothermal systems lies in the regional and local heat flow patterns and structures. These topics will be briefly mentioned in this section, and do not serve as a comprehensive examination of these subjects.

Heat Flow

High heat flow in the western U.S. Cordillera is attributed to extension and volcanism in the Tertiary and Quaternary (e.g., Blackwell, 1983). Figure 2.13 is a map showing the surface heat flow values for the western United States from data taken from boreholes with a maximum depth of 2 km (Blackwell and Richards, 2004). In general, the western U.S. has high heat flow values ranging from 50-150 mW/m^2 (Blackwell and Richards, 2004) but can exceed values of 1000-2000 mW/m^2 locally (Banerjee et al., 2011 and references therein). In eastern Nevada and western Utah, an area of high heat flow marks the edge of the Basin and Range province and a location where both extensional and magmatic geothermal systems exist (Joe Moore, personal

communication, 2012). From southern Nevada to Arizona and New Mexico, high heat flow is associated with the Rio Grande Rift. The Colorado Plateau is an area of anomalously low heat flow, probably a result of little volcanism in the last 20 Ma and virtually no extension since the initiation of the Basin and Range. The Eastern Snake River Plain in Idaho is an area of extremely high heat flow (100-150 mW/m^2) associated with the eastward trend of the Yellowstone Hotspot. High heat flow values in central Idaho are most likely related to high heat production due to radioactive decay of U, Th, and K of the Idaho Batholith (Swanberg and Blackwell, 1973). High heat flow in the area around southeastern California and western Nevada is most likely attributed to active dextral shear associated with the Eastern California Shear Zone and Walker Lane Belt. The Cascades also show a narrow but long zone of high heat flow, most likely attributed to active volcanism.

A regional heat flow high occurs in northwestern Nevada into the Oregon High Lava Plains and the Snake River Plain in Idaho (Fig. 3.2) (Sass et al., 1971; Brott et al., 1978, 1981; Blackwell, 1983; Williams et al., 1997). This so-called Battle Mountain heat flow high is characterized by mean heat flow values of greater than 100 mW/m^2 (Blackwell, 1983; Wisian et al., 1999). High values in this region are attributed to the late-Miocene to Recent volcanism and crustal extension. This area was thought to have been the greatest region of heat loss (e.g., Sass et al., 1971) in the Northern Basin and Range until Blackwell (1978) argued that the boundaries of the Basin and Range Province is where the highest amount of heat loss occurs, evidenced by high heat flow values. The edges of the Northern Basin and Range are areas in which the greatest amount of historic seismicity occurs and where some of the youngest volcanism exists;

but, even though the Battle Mountain heat flow high is not at the margin of the province, it nonetheless remains an area of abnormally high heat flow. The Battle Mountain heat flow high also crosses the Central Nevada Seismic Belt (e.g., Lee et al., 2009, Fig. 2.10) and the Humboldt Structural Zone of Coolbaugh et al. (2005) and Faulds et al. (2006) (Fig. 3.3). However, it is important to note that high heat flow is not directly created by geologic structures and active seismicity, but all are related in the sense that they can occur in areas where there is active extension.

The Eureka Heat Flow Low (Fig. 3.2) is an area of low heat flow north of Mercury, NV and south of Eureka, NV (Sass et al., 1971; Blackwell, 1983). Heat flow values in this trend average 60 mW/m^2 (Blackwell, 1983). This low is attributed to the regional hydrogeologic framework. A thick sequence of Paleozoic carbonates and siliciclastic rocks comprise the deep aquifer in this part of the Great Basin (Harril and Prudic, 1998) and meteoric recharge to these aquifers apparently plays a large role in dampening the heat flow signature. Additionally, meteoric water would have to be rapidly circulated through this aquifer if it were to have a significant effect on heat flow dampening. Sass et al. (1971) and Person et al. (2008) support this idea as they have delineated areas that have interbasin groundwater flow with rapid vertical velocities to depths of around 3 km. If this is true, then the interconnectedness of these aquifers must be significant; however, this begs the question, how do faults affect this interconnectedness? That faults act as rapid transport pathways for vertically moving fluids is not disputed; however, the role they play in lateral movement of water from basin to basin must be better constrained to allow for the conclusion that this movement is significant enough to dampen the high heat flow signature.

Overall, several factors play a role in the regional distribution of areas with relatively high and low heat flow. For example, variation in crustal thickness and its relationship to regional trends in heat flow are unknown but are conceivably important. Crustal thickness variations and its relationship to the heat flow regions discussed above can be seen in Figure 3.2 (Gilbert, 2012). Another factor is regional groundwater flow patterns (i.e., can water really move from basin to basin in a manner that dampens heat flow; is there a threshold velocity in which water moving from basin to basin will dampen the heat flow signature as opposed to transferring that heat?). This also raises issues with how faults control the lateral movement of this water. Regional variations in extension also play a role in heat flow, as areas that have been thinned to a greater degree would theoretically have higher heat flow values. Also, regional trends in the radioactivity of crustal rocks surely play a role in regional trends in heat flow (e.g., Swanberg and Blackwell, 1973).

Basin Scale Heat Flow

Heat flow on this scale is very complex. Typically, heat flow is distributed unevenly between alluvial valleys and adjacent mountain ranges. This is because heat flow is a function of a material's thermal conductivity (which varies by lithology), near-surface ground water circulation, and geologic structure (in particular faults), and permeability gradients between the fault zone and country rock (e.g., Lopez and Smith, 1995). Unconsolidated sedimentary units have lower thermal conductivities than "basement" rock, and similarly, the conductivities of various rock types can vary greatly. Therefore, heat flow is usually higher in mountain ranges adjacent to sedimentary basins in the Basin and Range (Thakur et al., 2012). Also, local and regional groundwater flow

regimes may affect the transport of heat in deep reservoirs from basin to basin and within a basin.

In addition, the unconsolidated basin fills tend to refract heat flow towards their margins. As heat flows to the surface from the interior of the Earth, it will preferentially flow in places where there is high conductivity (i.e., low resistivity). Hence, like electromagnetic waves, heat can be refracted. For example, if a 1 km-2 km thick package of unconsolidated sediments overlies igneous basement rock with relatively higher conductivity, heat travelling upwards will be refracted at the interface of these two materials (Thakur et al., 2012). The refracted heat will then be focused towards the edges of the basin, where the sedimentary fill presumably becomes less thick.

Fault Patterns

The crustal thinning and associated magmatism of extensional provinces produces the high heat flow conducive to the generation of geothermal systems. In addition, the faults generated by these extensional processes provide pathways for the upward flow of geothermal waters and the structural permeability that can help create geothermal reservoirs of sufficient size for exploitation. On a regional scale, stress, strain, and associated seismicity are all important for the development and exploration for geothermal resources. On the local scale, factors such as fault intersections and along-strike geometry (e.g., en echelon) of normal faults are important to identifying the structural controls of an individual geothermal system.

Structures created during the Oligocene and early-Miocene in the Great Basin are oriented NW-SE (e.g., Zoback et al., 1981). The importance of these older structures becomes apparent when determining the structural framework of geothermal systems.

The development of these structures in the Northern Basin and Range seems to coincide with the timing of southward migrating volcanism of the IFU (Stewart, 1988). Deformation during this time is exemplified by numerous low-angle normal faults accommodating 10% - 150% extension (Stewart, 1978, 1980; Zoback et al., 1981; Wernicke et al., 1988).

Current fault patterns across the Northern Basin and Range are the result of a complex province-wide strain field. In central Nevada, it has been determined by GPS that this part of the Basin and Range is extending in an E-W direction with respect to stable North America, corresponding to N-NNE trending normal faults (Bennett et al., 2003) (Fig. 3.4). In the western-most Great Basin, the strain field becomes much more complex. As one approaches the Sierra Nevada from the east, the GPS vectors change in both direction and magnitude (e.g., Bennett et al., 2003; Oldow, 2003; Hammond and Thatcher, 2005; Kreemer et al., 2009). The change in magnitude and direction of GPS vectors reflects how the San Andreas Fault system (including the Walker Lane) and the Northern Basin and Range respond differently to plate interactions. In the northern-most Northern Basin and Range (i.e., southeastern Oregon), the change in GPS vectors is created by clockwise rotation of the Cascadia fore-arc, which results in clockwise strain patterns in the back-arc (Wells and Simpson, 2001; Hammond and Thatcher, 2005; Trench et al., 2012).

Crustal deformation from 10 Ma to Present within the Northern Basin and Range seems to be the major control on the current distribution of geothermal systems in the Great Basin (Faulds et al., 2010). Figure 3.3 (Faulds et al., 2010) shows the distribution of geothermal systems across the Great Basin with respect to arbitrarily defined structural

zones. As it can be seen, most of the identified geothermal resources lie within the regions demarcated by this figure. But, it is interesting to note that several geothermal systems do not fit in this convenient characterization; for example, the Paisley resource lies just north of the Surprise Valley lineament identified in Figure 3.3. Geothermal resources in southeastern Oregon may not fit the classification presented in Figure 3.3. The structural zones demarcated by this figure are the result of tectonic forces whose relationship to structures in southeast Oregon is not well understood. Either this figure needs to be updated to include the Paisley resource or perhaps another classification scheme needs to be developed for geothermal systems in southeastern Oregon.

Active geothermal systems across the Northern Basin and Range are correlated to areas that have experienced recent seismicity. Notable regions with high Quaternary faulting and historic seismicity can be seen in Figure 3.5. Seismic events plotted on this diagram are greater than Magnitude 4.0 and are concentrated within the Walker Lane Belt and the Central Nevada Seismic Belt. In southern Nevada, an east-west trend in seismic events is associated with the Las Vegas Shear Zone (e.g., Duebendorfer and Black, 1992). These areas correspond to high strain rates seen in Figure 3.4.

The structural controls of an individual geothermal system reflect the local structural architecture. In the Northern Basin and Range, a feature common to several geothermal systems is major range bounding normal faults (i.e., Dixie Valley, Coso Hot Springs, Desert Queen, etc.). Blind faults (or faults with minimal offset) located within basins have also been identified as important faults controlling thermal fluids (e.g., Smith et al., 2001; Faulds et al., 2006; Hinz et al., 2010). Also, other common structural

controls on Basin and Range geothermal systems are en echelon faults, transfer zones, and fault intersections.

Transfer zones are prominent features of extensional provinces, including the Basin and Range. The exchange of strain from one en echelon fault to the next left or right stepping, overlapping fault occurs across a transfer fault. The specific type of fault(s) depends on whether or not it separates two normal faults that dip in the same or opposite direction (e.g., Faulds and Varga, 1998). For the purpose of this paper, it will be referred to as a transfer fault, or if several faults exist, a transfer zone, as it simply transfers strain from one fault to another. Transfer zones are extremely important to geothermal resources in general but are important specifically to the Paisley resource because it occurs near a step-over in normal faults (discussed more in Chapter Four).

Transfer zones may develop due to faults with en echelon geometries. The transfer zone is usually evidenced by a strike to oblique slip fault(s) between two or more normal faults (Fig. 2.9). The strike-slip fault(s) is oriented parallel to the extension direction and allows for the transfer of strain between two or more normal faults in an extensional regime (Faulds and Varga, 1998). The transfer zone can induce secondary permeability and allow for strain localization, which allows for fluids to flow through, and even stored in, rocks that typically would not have large rates of permeability or storativity.

Fault intersections are perhaps the most important structural feature controlling fluid flow in geothermal systems (Faulds et al., 2006; Cashman et al., 2012). Almost every geothermal system that has been studied in detail has fault intersections (e.g., Faulds et al., 2006; Blackwell et al., 2009; Waibel, 2011; Cashman et al., 2012). This

becomes important when discussing the Paisley resource because, as it was mentioned previously, southeastern Oregon is dominated by two trends in faulting, and intersections between these two trends occur in the Paisley area.

The Brady's, Desert Peak, and Desert Queen geothermal systems in northwest Churchill County, Nevada are examples of systems in which en echelon normal faults are the dominant structural control on fluid flow (Benoit et al., 1983; Faulds et al., 2003; Wesnousky et al., 2005). Also important to these systems is the intersection with these en echelon normal faults with NW-oriented faults associated with the Walker Lane Belt (Figure 3.6).

Perhaps one of the most highly studied geothermal systems in the Great Basin is the Dixie Valley Geothermal System in north-central Nevada (Fig 3.7). This system lies within the Northern Basin and Range and has been the classic example of Basin and Range geothermal systems (Waibel, 2011; Thakur et al., 2012). The structural controls of fluid flow in this system are complex, but a combination of fault intersections and en echelon normal faults has created the structural framework for this geothermal system. Here, the intersection of faults has created rhombohedral crustal blocks bounded by both normal and strike-slip faults, creating a complex distribution of strain (Fig. 3.7). A similar fault pattern was noted by Donath (1962) in the area east of Summer Lake, Oregon near Paisley. These two systems could be similar in the fact that faults intersecting at oblique angles to one another allow for the rise of thermal waters, and that the location of this upwelling is systematic and not random. In fact, Faulds et al. (2010) have stressed the importance of fault intersections as great exploration targets.

Areas of transtension can create several subsidiary structures important to geothermal resource development. In the western Great Basin, the Northern Basin and Range and the transtension of the Walker Lane Belt overlap to create extremely complex structural patterns. The complexity of these two systems together allows for much higher geothermal potential (e.g., Bennett, 2011). In addition to the overprinting and intersecting faults, the Walker Lane Belt also exhibits high strain rates, which seem to be conducive to fluid flows. The transtensional structures of the Walker Lane, the pull-apart basins, rotation of crustal blocks, and related faults and fractures can create sufficient secondary porosity to allow geothermal fluids to circulate to depths where they become heated and then return to the shallow subsurface (< 2 km) where they can be extracted for development.

Geothermal Water

The Basin and Range province clearly provides the heat flow and structural framework conducive to the generation of geothermal systems, but another key factor in not only finding but assessing the viability of these systems, is in the nature of the geothermal waters, in particular their volume, temperature, and composition. This also leads to questions of the source(s) of the waters for each system, whether it is modern meteoric water or older Plio-Pleistocene waters. This latter issue is critical for assessing the volume of available water and production rates.

The Great Basin is an arid region, and thus a finite amount of water is available for recharge of groundwater, and hence geothermal aquifers. Most water in geothermal systems of the Great Basin reflects the deep circulation of meteoric waters driven by topographic flow or from convective flow (Lopez and Smith, 1995; Person et al., 2008;

Ferguson et al., 2009). These two processes differ in the force that drives them. Topographic flow can simply be expressed as being created by hydraulic head created by recharge from topographically high areas whereas convective flow is driven by convections cells of thermal waters, typically within a basin.

Deep Circulation of Meteoric Water

Most geothermal systems in the Northern Basin and Range are at least partly recharged by meteoric water (Taylor, 1974; Person et al., 2008). Water enters the groundwater system via faults and fractures in topographically high areas, or by losing streams in alluvial basins (Gillespie et al., 2012). Once in the ground, water can flow laterally for hundreds of kilometers from basin to basin or it can be confined to flow within a basin (e.g., Sweetkind et al., 2007). Within this context, water will flow either by topographic flow or convective flow induced by thermal gradients (Lopez and Smith, 1995; Person et al., 2008).

Distribution of Groundwater in the Great Basin

The distribution of groundwater in the Great Basin is affected by subsurface stratigraphy and structure, in particular, faults and fractures. Groundwater distribution and flow patterns also affect the regional distribution of heat flow. Paleozoic and Mesozoic sedimentary rocks, chiefly carbonates at depths of 2-4 km (Harril and Prudic, 1998), underlie most of the eastern Great Basin. These rocks are the major aquifers in the Great Basin at the regional scale and constitute the major aquifers for interbasin flow (Harril and Prudic, 1998; Sweetkind et al., 2007; Gillespie et al., 2012). Local groundwater is usually held in alluvial sediment-filled basins. These local aquifers

typically do not exceed a depth of 2 km. The connectedness between local and regional groundwater aquifers depends on the rock type at the contact between alluvial fill and basement rock and also on the existence of faults or fractures that connect otherwise unconnected hydrologic units.

Interbasin flow of groundwater is variable within the Great Basin. The rocks that facilitate this supposed interbasin flow are normally given homogenous hydrologic properties, which is necessary to conceptualize studies of interbasin flow. However, these assumptions may not hold true at the regional, interbasin scale, or even at the local scale, as heterogeneities in the rock undoubtedly affect the hydrologic properties at all scales. These issues are beyond the scope of this thesis but are serious issues that must be addressed when developing a province-wide geothermal resource assessment or even a local assessment on the viability of a geothermal system. Also, a critical assessment of across-fault transport of fluids on regional and local scales is important to understanding the localization of geothermal systems on these scales. These two components combined severely complicate the simple notion that water is free to move from basin to basin solely based on a large carbonate aquifer, but does not preclude this from happening.

Interbasinal flow of groundwater in southeast Oregon is unknown. To complicate the problem, basement rock is not exposed anywhere in southeastern Oregon. However, it may be possible to assume that underneath the Tertiary volcanic cover, southeastern Oregon is underlain by the same types of Mesozoic accretionary sediments and mafic volcanics found in the Blue Mountains in northeastern Oregon and the Klamath Mountains in southwestern Oregon (Walker and MacLeod, 1991). If this is the case, and if the water in the Paisley resource reaches similar depths to that in the Great

Basin, then the chemistry of the water should be much different than those hosted in carbonate reservoirs.

Topographic and Convective Flow

Water can be driven to deep aquifers (> 2 km) by two processes, either topographic or convective flow (Lopez and Smith, 1995; Person et al., 2008). Topographic flow is driven by recharge in a topographically high region such as a mountain range adjacent to valleys, typical of Basin and Range topography. Water enters the ground at these elevations and is driven downward by gravity (Fig. 3.8). Water is then able to become heated by the regional and local high heat flow. The water eventually reaches a fault(s) where it will then rise rapidly because of increased buoyancy. However, cool unheated water can still rise along faults in topographic flow because these areas are below the site of recharge; therefore, upward flow can be created simply by hydraulic head.

Convective flow is more complex than topographic flow (Person et al., 2008). Water is brought to the basin via streams from topographically higher places, from topographic groundwater recharge (i.e., topographic flow), and directly by precipitation over the valley floor. Recharge of the groundwater aquifer can also occur via faults and fractures within and adjacent to the valley, or from other basins. In the Great Basin, thermal water could be rising from deep aquifers flowing through carbonate rocks across several basins. Fault-bounded graben structures can have a fault on one side of the valley in which cool, meteoric water flows down and another fault on the other side of the valley will have thermal upwelling water. The combination of cool water descending along one fault and hot water rising along another sets up vertical and horizontal thermal

gradients across the basin, which will induce convective flow of water (e.g., Lopez and Smith, 1995).

Faults and Permeability

It is well known that faults create permeability (Lopez and Smith, 1995; Fairley and Hinds, 2004) and that this permeability is required for upward moving thermal water. The idea is that meteoric water encounters a fault zone where flow then becomes concentrated within the fault zone because of higher permeability (Wisian and Blackwell, 2004; Ferguson et al., 2009). This water can become heated and rise to the surface along another fault, driven by convective or topographic flow (Banerjee et al., 2011). In order for the water to reach economically feasible temperatures, the fault must be of crustal scale (i.e., it extends at least 2-6 km into the crust). This brings the idea of deep circulation of meteoric water through the interplay of faults and permeable hydrologic units to the forefront of geothermal system conceptualization. High heat flow creates elevated geothermal gradients and meteoric water has long flow paths because of deep seated faults; these two processes together are characteristic of Basin and Range-type geothermal systems.

The velocity in which thermal waters can rise to the surface is a function of the permeability of the fracture or fault system in which it flows. Furthermore, the rate at which it rises could potentially be affected by the ambient temperatures of the rocks. Wisian and Blackwell (2004) suggest minimum permeabilities in the fault zone of 10^{-15} m^2 to 10^{-16} m^2 are needed to retain entrained heat in thermal waters rising to the surface (Fig. 3.9). If permeability is lower than this, temperatures within the fault rapidly decrease by conduction of heat to the country rock (Wisian et al., 1999; McKenna and

Blackwell, 2004; Wisian and Blackwell, 2004). Heat loss can occur along the fault zone if permeability in near surface sediments is high, as this increases the chance of mixing with cool surface meteoric water. This becomes important for all geothermal systems including the Paisley resource because it is essential to account for mixing of cool and hot waters to make the resource economic.

Geothermometry

The geochemistry of thermal waters is used as tracers to help understand the heat source(s) of the thermal fluid and to predict subsurface temperatures. The differentiation between types of waters becomes important in selecting, and possibly rejecting the use of certain types of geothermometers. As groundwater flows through the ground and into geothermal systems, they react with the aquifer and reservoir rocks. These water-rock interactions change the chemistry of the water, which provides the basis for classifying types of geothermal waters. The processes that lead to the different types of geothermal waters are extremely complex. To a first order, the evolution of a thermal fluid depends on its original chemistry and the type of rock in which it interacts. Within that context, the evolution of a thermal fluid also depends on its residence time within the reservoir and the temperature of the system because the kinetics (i.e., rate of reactions) of a system is elevated in a higher temperature system. The chemistry of the geothermal water is important for evaluating the validity of the geothermometers. Ellis and Mahon (1977) have suggested that there are four main types of geothermal waters:

- Alkali Chloride
- Acid Sulphate
- Acid Sulfate-Chloride

- Bicarbonate

Alkali-chloride waters have a pH of 4-11 (Armannsson and Fridriksson, 2009). These waters also have been described as sodium and potassium chloride waters by Armannsson and Fridriksson (2009). Acid sulphate waters form from the oxidation of magmatic H_2S to SO_4^{2-}, where the H_2S is most likely coming from a degassing magma body. In addition, most of the waters' chemical constituents come from dissolution of igneous rocks near the surface; therefore, this type of water is not useful in describing subsurface characteristics because its chemistry is dependent on near-surface reactions (Armansson and Fridriksson, 2009). Sulphate-chloride waters are not necessarily acidic and reflect very well the subsurface equilibria, and are therefore very useful in prediction of subsurface characteristics (Armannsson and Fridriksson, 2009). Acid sulphate-chloride water is a mixture of alkali-chloride water and acid sulphate water (Armansson and Fridriksson, 2009). Finally, bicarbonate waters may be derived from CO_2 rich steam condensing or mixing with water, is common in old geothermal waters, and is useful in determining subsurface properties (Armannsson and Fridriksson, 2009).

Geothermometry has become a mainstay in geothermal exploration because of its relative low cost, and overall efficiency (Williams et al., 2008). However, most of the geothermometers in use today were derived for magmatic geothermal systems having Cl dominated water, assumed to be chemically mature (Giggenbach, 1988). This is not the case in the Basin and Range-type geothermal system, where both the rocks and fluids have different chemistries (e.g., Zehner et al., 2006). Therefore, extreme caution must be used in the employment of geothermometers. Despite the limitations to geothermometry, it is still commonly used throughout the Great Basin. For the Paisley resource, the

geothermometer results were compared with temperatures obtained by alteration mineral assemblages because of uncertainties in the quality of water for geothermometry. The derivation of the commonly used geothermometer systems: Na/K, Na-K-Mg, Na-K-Ca-Mg, and silica geothermometers can be found in Appendix A.

The validity of geothermometers is dependent on several assumptions about the hydrothermal system. Five assumptions have been identified by White (1970) and are listed in Krahmer (1995):

- The concentration of the chemical species used in the geothermometer is controlled only by a temperature dependent mineral-fluid reaction.
- There is an adequate supply of the mineral and/or dissolved species in the rock-fluid system for the reaction to occur.
- The reactions attain equilibrium in the reservoir.
- There is rapid flow to the surface with no re-equilibration after the fluid leaves the reservoir.
- There is no mixing or dilution of the reservoir fluid.

It is unrealistic that all five of these cases will be met in nature and therefore caution must be exercised when using geothermometers (Joe Moore, pers. comm. 2012). Waters sampled from surface hot springs violate almost every one of the above stipulations; hence, it is recommended to evaluate the conditions of the individual hot spring to determine its validity in geothermometry applications. However, most samples taken from boreholes meet these criteria and are therefore considered valid samples to use for geothermometry.

Cation Geothermometers

One set of geothermometers that are widely used to evaluate geothermal systems are the cation geothermometers consisting of the Na/K, K/Mg, Na-K-Mg, and Na-K-Ca-Mg types. Each of these geothermometers was derived for the use in geothermal systems that had a magmatic heat source (e.g., Giggenbach, 1988; Nicholson, 1993). However, if the right reservoir rocks are present (i.e., basalt or tuff), then the cation geothermometers may be used with some confidence, as they depend on the dissolution of Ca, Na, and K feldspars. Hence, it is important to understand the geologic setting of the geothermal system in order to determine if the use of cation geothermometers are appropriate.

Several studies have used the cation geothermometers to predict subsurface reservoir temperatures successfully in areas that do not have a magmatic component (e.g., Sladek et al., 2004; Hantelmann, 2006; Casteel et al., 2010). The temperatures calculated from geothermometers were confirmed in all situations by measured temperatures of borehole fluids. This suggests that the fluids used for geothermometry are representative of the reservoir fluid and that the fluid has reached chemical equilibrium with the host rock. Several wells and springs were sampled from Paisley for similar chemical constituents, the results of which will be discussed in Chapter Four.

Silica Geothermometers

The other set of widely used geothermometers are the silica geothermometers. The concentration of silica in geothermal systems is controlled by the solubility of several silica minerals such as: quartz, chalcedony, and amorphous silica. An advantage to silica geothermometers is that they are relatively insensitive to the addition of salts and pressure below 300°C; however, above 300°C, the addition of salts and pressure becomes

extremely important (Fournier, 1989). The solubility of silica dramatically decreases with increasing temperature; therefore, processes like adiabatic cooling and conductive cooling if not accounted for can result in an estimation that is lower than actual reservoir temperatures (Fournier, 1989). Adiabatic cooling can have adverse effects on the silica geothermometer. As a fluid boils, CO_2 is partitioned into the resulting vapor thereby increasing the pH of the remaining liquid. An increased pH allows for more dissolution of silica. If this happens, the silica in solution hydrolyzes to form silicic acid:

$$H_4SiO_4 = H^+ + H_3SiO_4^-$$

An increase in dissolved silica during adiabatic cooling can result in an overestimation of reservoir temperatures, as equilibrium is usually attained in the reservoir at pH ranges of 5-7 (Fournier, 1992).

Use of Geothermometers

The accuracy of the calculated temperature is only as good as the choice in waters sampled and in the analytical certainty of the analysis; this led Reed and Mariner (1991) to develop a method to determine the analytical robustness of water samples submitted. This method was primarily intended for critical evaluation of charge balance in water samples because of assumptions made in calculating temperature from cation geothermometry. The Na-K-Ca geothermometer derived by Fournier and Truesdell (1973) has limitations in its robustness because of its derivation by empirical methods. The beta term in their equation used to shift the slope of the line to match observed data is sensitive to temperature, begging the question of the validity in doing this (see Appendix A). For the Na-K-Mg and Na-K-Ca-Mg geothermometers, the concentration of Ca and Mg is important in correcting the temperatures for variations these

concentrations have on the solubility of Na and K (Fournier, 1992). Mineral species commonly in geothermal environments, such as clays and zeolites, which contain Mg, Ca, and other cations, is relatively well-known. However, the effects these minerals have on the solubility of Na and K is less well-known.

Despite the seemingly long list of reasons not to use geothermometers, they have proved to be fairly robust in their application throughout the Basin and Range. It is recommended that if used on types of water not intended for the application of geothermometers, an independent means of predicting temperatures is used (i.e., stable isotopes of oxygen in the SO_4-H_2O system, or from assemblages of alteration minerals), which was done with the Paisley resource.

Sources of Water

Determining the source of fluid in a geothermal system is obviously extremely important for both characterizing and managing the resource. Several methods have been developed that elucidate these problems. This section introduces a few of these methods that have been useful in both magmatic and Basin and Range type geothermal systems.

Two ternary diagrams have proved useful for tracing the origin of geothermal fluids (Giggenbach and Soto, 1992; Powell and Cumming, 2010). Elements that remain in solution throughout the evolution of a geothermal system or are precipitated from the fluid in a predictable pattern as cooling occurs are considered to be conservative and allow for the evaluation of the source of hydrothermal fluids. This provides a useful tool for evaluating the evolution of the geothermal fluids.

Giggenbach and Soto (1992) describe the use of the Li-Cl-B ternary diagram for tracing the origins of hydrothermal fluids (Fig. 3.10). Li is an alkali element not affected by absorption processes and together with Cl provides a useful indicator of fluids contaminated from the dissolution of mafic to intermediate volcanic rocks (Giggenbach and Soto, 1992). As the solution cools, Li will be incorporated into the lattice of precipitating quartz, thereby reducing the concentration of aqueous Li (Giggenbach and Soto, 1992). However, the ability of Li to be taken up in quartz decreases with temperature; therefore, most Li will be taken in by quartz at intermediate temperatures (Giggenbach and Soto, 1992). So, using the Li-Cl-B ternary, it becomes apparent that Li uptake in quartz follows a predictable path and can therefore be used to delineate multiple sources of geothermal fluids, and to a first order assess the maturity of the thermal fluid (e.g., Giggenbach and Soto, 1992; Powell and Cumming, 2010).

Boron is highly volatile and prefers to be segregated into the vapor phase. If a fluid is rich in B with respect to Cl, the water has most likely been heated by steam from another geothermal fluid. If the water is high in SO_4^{2-} and the B/Cl ratio is above 0.02, then the fluid is fairly young in terms of when it was infused with B. Conversely, if the ratio is less than 0.02, but was still heated by steam from another fluid, then this can be evidence that the fluid sampled has undergone boiling, possibly due to a magmatic heat source, which over time has reduced the B/Cl ratio (Giggenbach and Soto, 1992).

Another useful tool for diagnosing the origin of thermal waters is the F-Cl-B diagram (Fig. 3.11). Fluorine is another element considered to be conservative in geothermal systems. As such, fluorine is useful in delineating multiple sources of water (Powell and Cumming, 2010).

Stable isotopes of water are another useful tool in which the origin of waters can be determined (Banerjee et al., 2011). Values in δD and $\delta^{18}O$ vary with latitude, season, age, and temperature (McSween et al., 2003). Trends in δD and $\delta^{18}O$ have been elucidated in the Basin and Range and show that aquifers in the Great Basin contain both current and Pleistocene age waters (Smith et al. 1992, 2002). Stable isotopes were used in the Paisley resource to help determine the source of water, so a discussion of trends in the Great Basin is important to be able to compare and contrast. A brief introduction to stable isotope theory and standard practices used is in Appendix A.

Craig (1961) determined that there is a relationship between δD and $\delta^{18}O$ values in meteoric water. This relationship is expressed by the global meteoric water line on a graph of δD versus $\delta^{18}O$ and is defined by the equation (Craig, 1961):

$$\delta D = 8\delta^{18}O + 10$$

This relationship can also be seen in Figure 3.11. Meteoric water always displays negative δD and $\delta^{18}O$ values.

The use of stable isotopes has been widespread in the evaluation of the origin of thermal waters (e.g. Taylor, 1974; Criss and Taylor, 1986; Giggenbach and Soto, 1992; Smith et al., 1992, 2002; Krahmer, 1995). A couple of general trends have emerged from the application of stable isotopes. The stable isotope values of water coming from geothermal systems that are being recharged by meteoric water do not plot on the meteoric water line. The relative values of δD do not change but the $\delta^{18}O$ values plot directly to the right of the meteoric water line, relative to meteoric water at that same location, suggesting enrichment of ^{18}O. This shift has been referred to as the "oxygen isotope shift" and is a result of water-rock interaction (Zhiyuan et al., 2010), and can be

seen in Figure 3.12. Rocks in which thermal waters interact are enriched in ^{18}O and have $+\delta^{18}O$ values. Values of δD are not affected because little if any exchange of hydrogen atoms is occurring between the fluid and rock. The other trend shows that some isotopic values reported from current geothermal systems have a misleading minimal shift in $\delta^{18}O$ and a more negative δD value than current meteoric water at the same location. Upon closer inspection, it has been determined by Fournier and Thompson (1980) that this may in fact be a signature of Pleistocene age waters that have undergone the same ^{18}O enrichment due to fluid-rock interactions. For example, if one extrapolates back to the meteoric water line from the current measured isotopic values of the thermal water, then the δD and $\delta^{18}O$ values will be more negative than current precipitation values at the same location, consistent with the fact that Pleistocene climatic conditions were generally cooler than the modern climate.

Summary

Geothermal systems found in extensional provinces within the western U.S. have been characterized as Basin and Range type. These systems are dominated by areas of anomalously high heat flow associated with late-Miocene-Quaternary magmatism, extension, transtension, and thinning of the upper crust. These processes have served to raise the geothermal gradient on both a regional and local scale. Along with high heat flow, extension since the mid-Miocene has created crustal scale faults that allow for deep circulation of meteoric water. In the western Northern Basin and Range, the Walker Lane Belt overlaps the Basin and Range creating an area of high deformation rates associated with the northward translation of the Sierra Nevada Crustal Block. This movement has created a transtensional stress regime manifested by dextral strike-slip

faults coexisting with Basin and Range normal faults. The intersection of these structures creates highly fractured pathways, which allow rapid infiltration of meteoric fluids to become heated by elevated geothermal gradients.

The types of fluids in geothermal reservoirs can be evaluated by aqueous geochemical methods. Major and minor element analyses can show what type of water is present, the temperature of this water, and the history of the water.

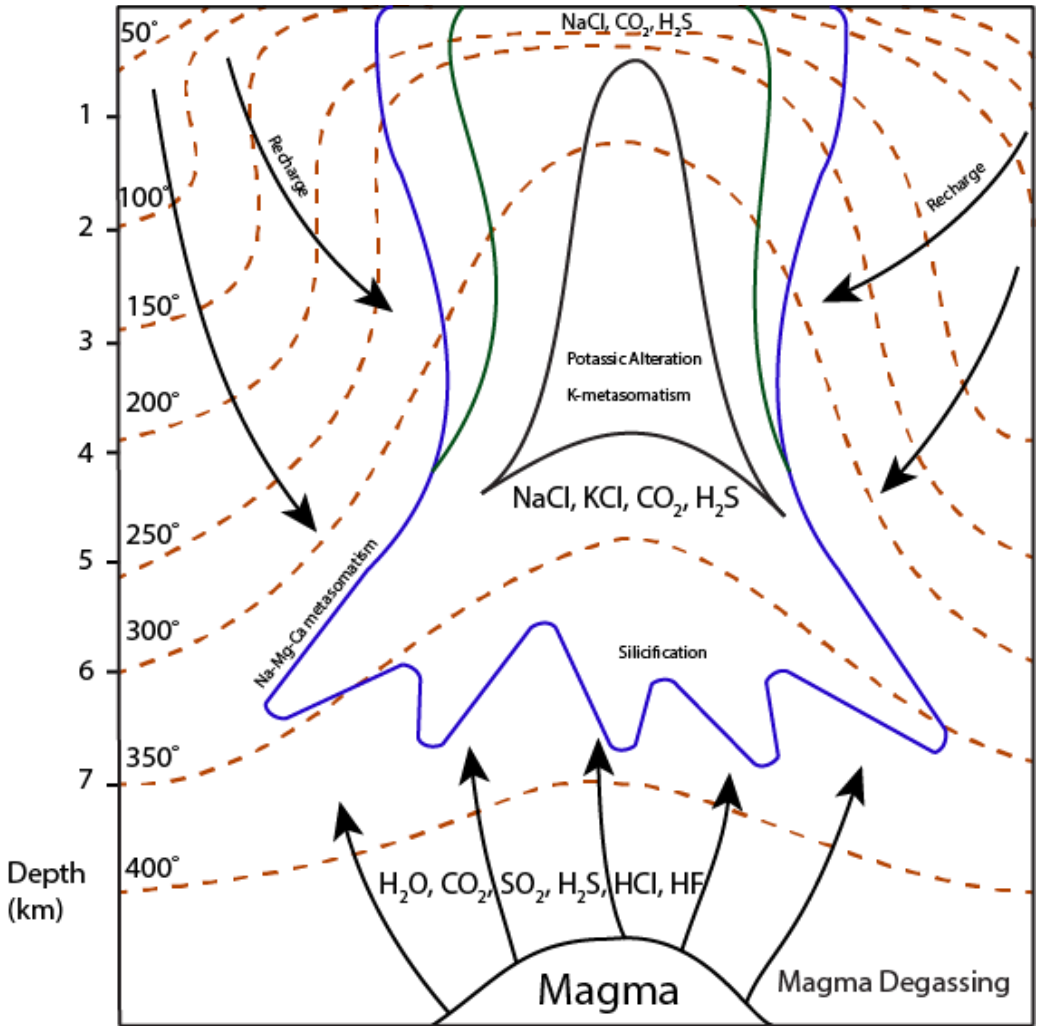

Figure 3.1. Hypothetical thermal plume caused by a shallow degassing magma body. Zone outlined in blue is the Na-Mg-Ca metasomatism zone. Recharge is through percolating meteoric groundwater. Modified from Giggenbach (1988).

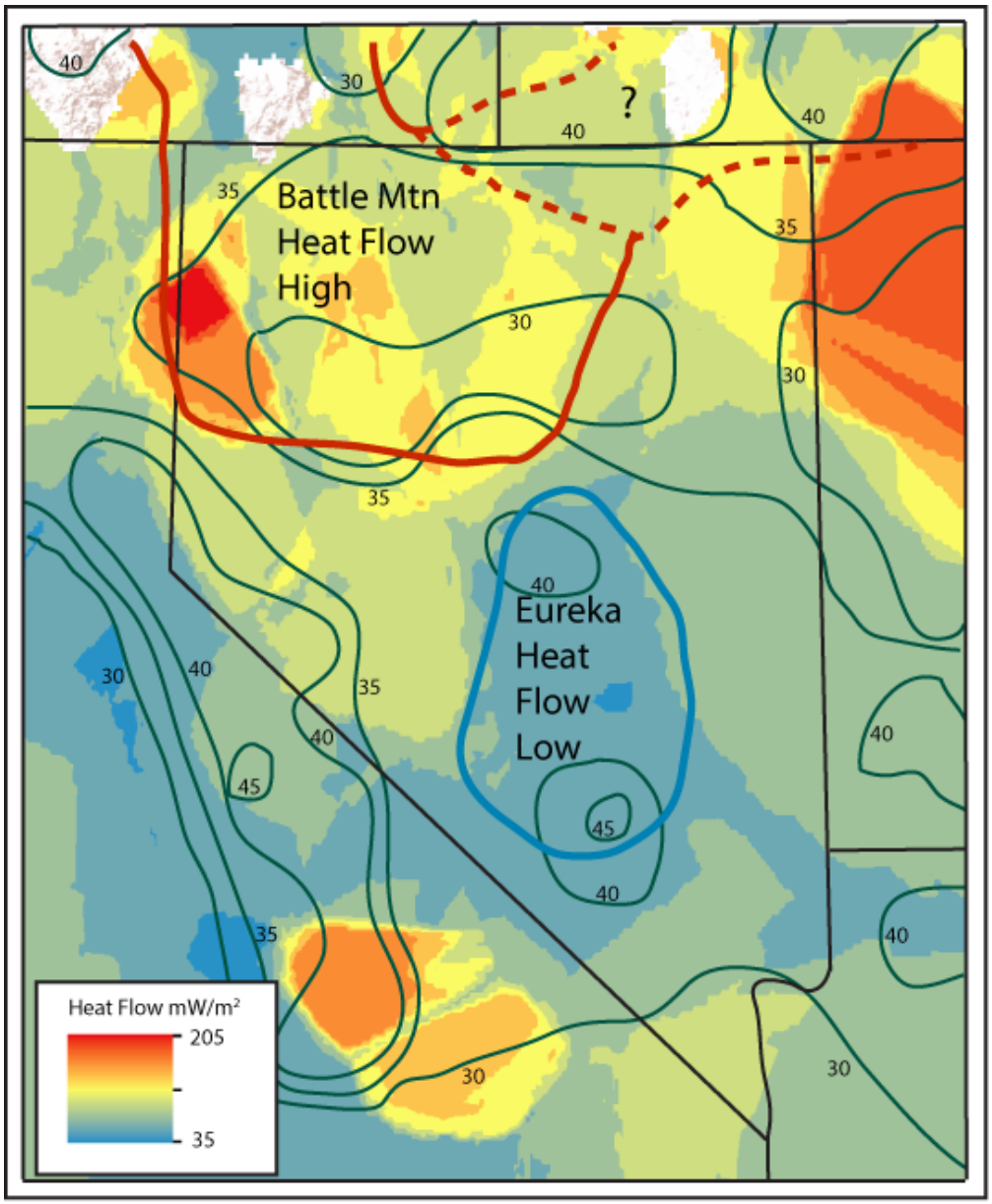

Figure 3.2. Map of Nevada showing heat flow anomalies identified by Sass et al. (1971). Green lines represent crustal thickness. Background heat flow data from the Global Heat Flow Database held at the University of North Dakota. See text for discussion. Heat flow zones modified from Blackwell (1983). Crustal thickness data modified from Gilbert (2012).

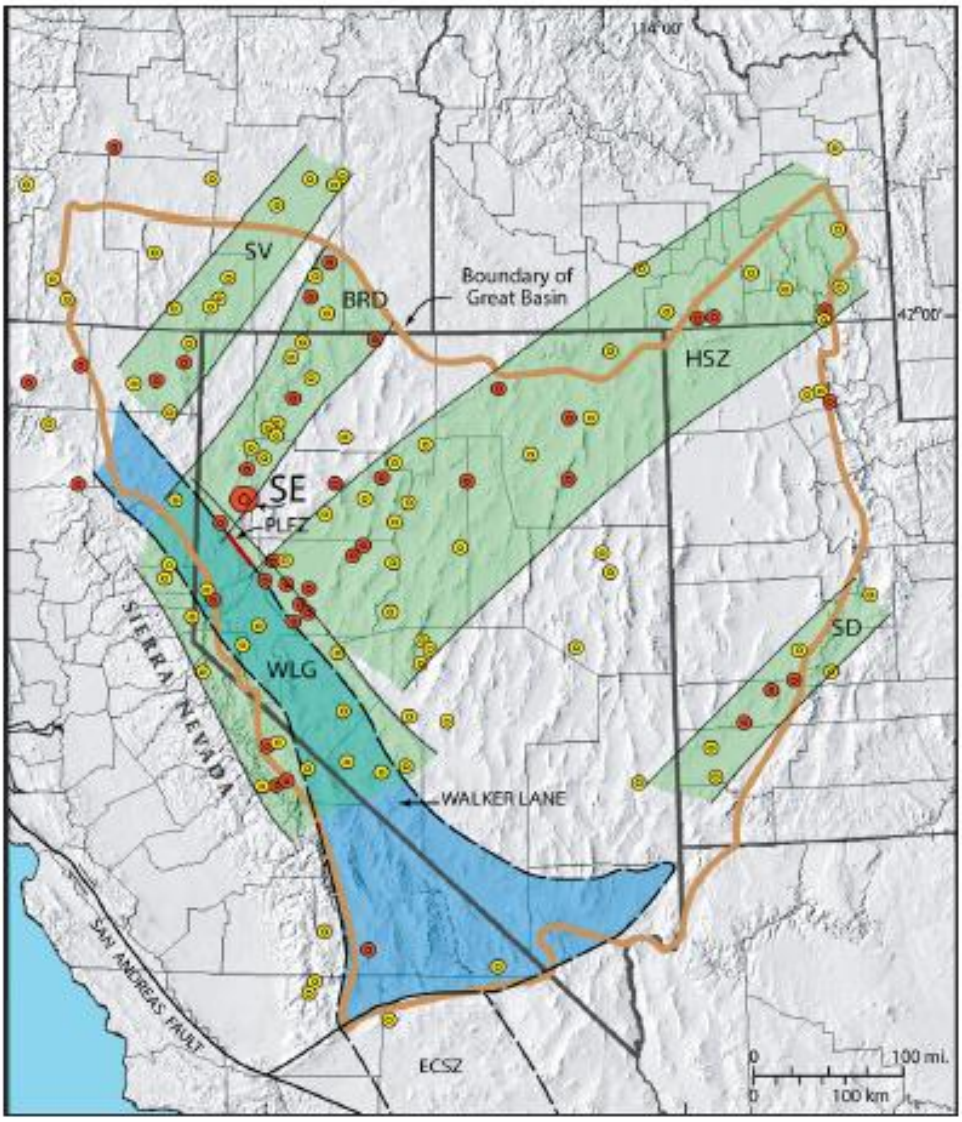

Figure 3.3. Map of the western United States showing distribution of medium to high temperature geothermal systems in the Great Basin. Geothermal systems tend to be distributed in SW-NE trending belts, which is normal to extension direction. SV- Surprise Valley; BRD- Black Rock Desert; HSZ- Humbodlt Structural Zone; WLG- Walker Lane; SD- Sevier Desert. Taken from Faulds et al. (2010).

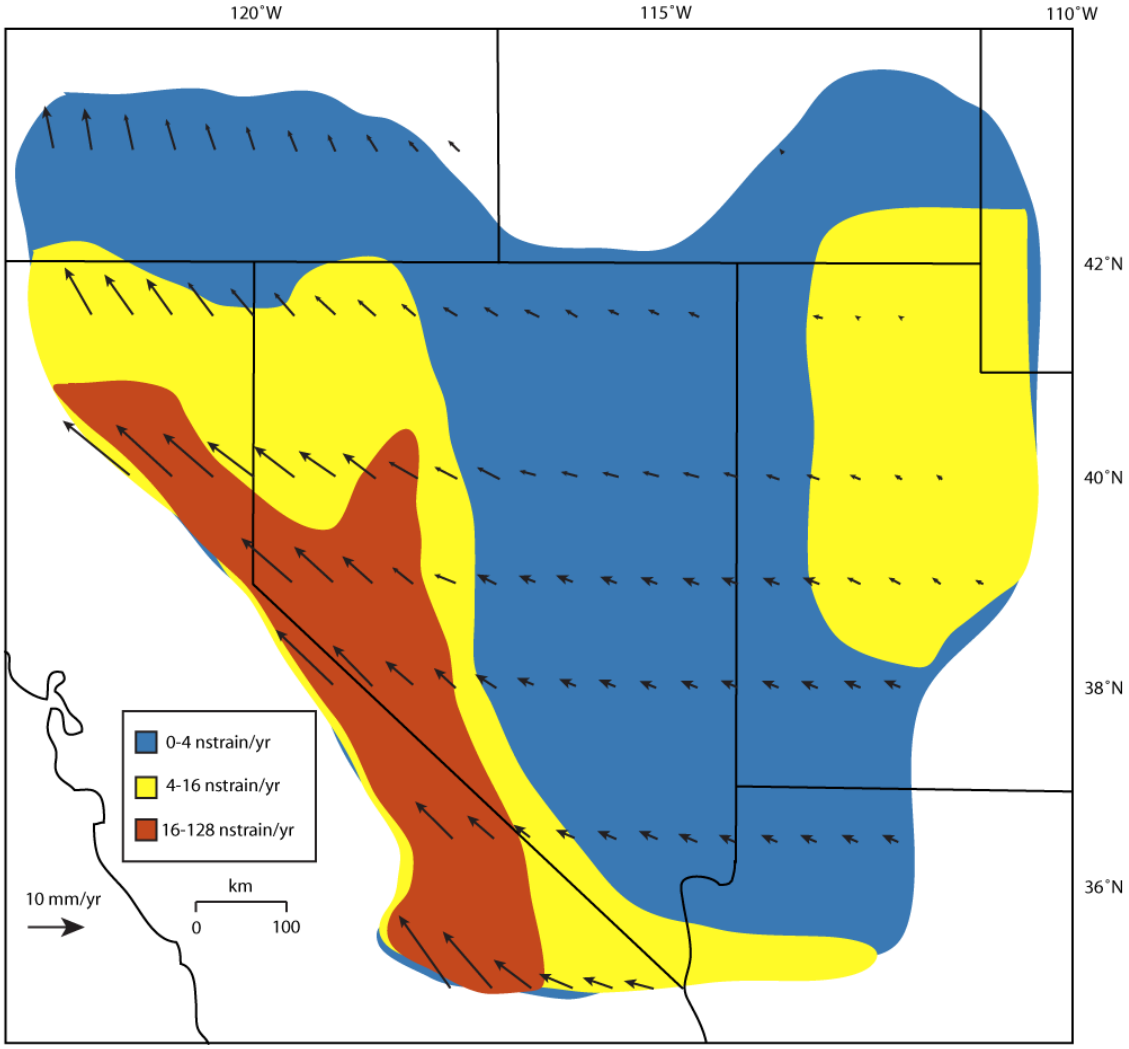

Fig. 3.4. Map showing distribution of strain across the western United States. Strain is calculated as the second invariant from GPS velocities. Note westward increase magnitude and change in direction of GPS velocities. Reader is referred to Bennett et al. (2003) and Hammond and Thatcher (2005) for alternate interpretations of GPS fields of the western United States. Modified from Kreemer et al. (2009).

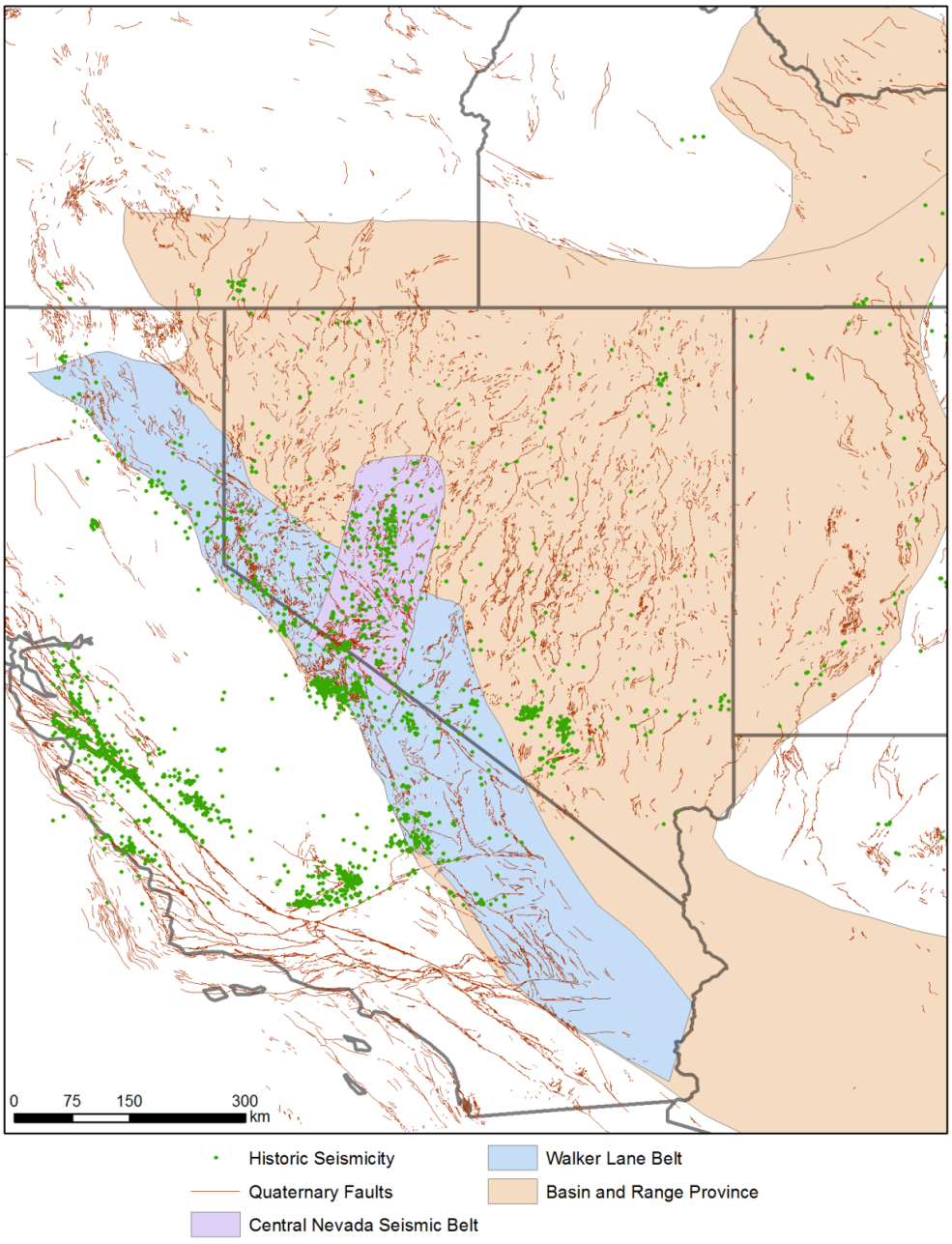

Fig. 3.5. Map showing historic seismicity (> magntidue 4, green dots) and Quaternary faults (red lines) of the western United States. Seismicity in the western Great Basin is concentrated in the Walker Lane Belt and the Central Nevada Seismic Belt. Recent faulting and active seismicity are good regional scale geothermal resource exploration targets. Fault data from USGS, seismic data from Advanced National Seismic System (USGS).

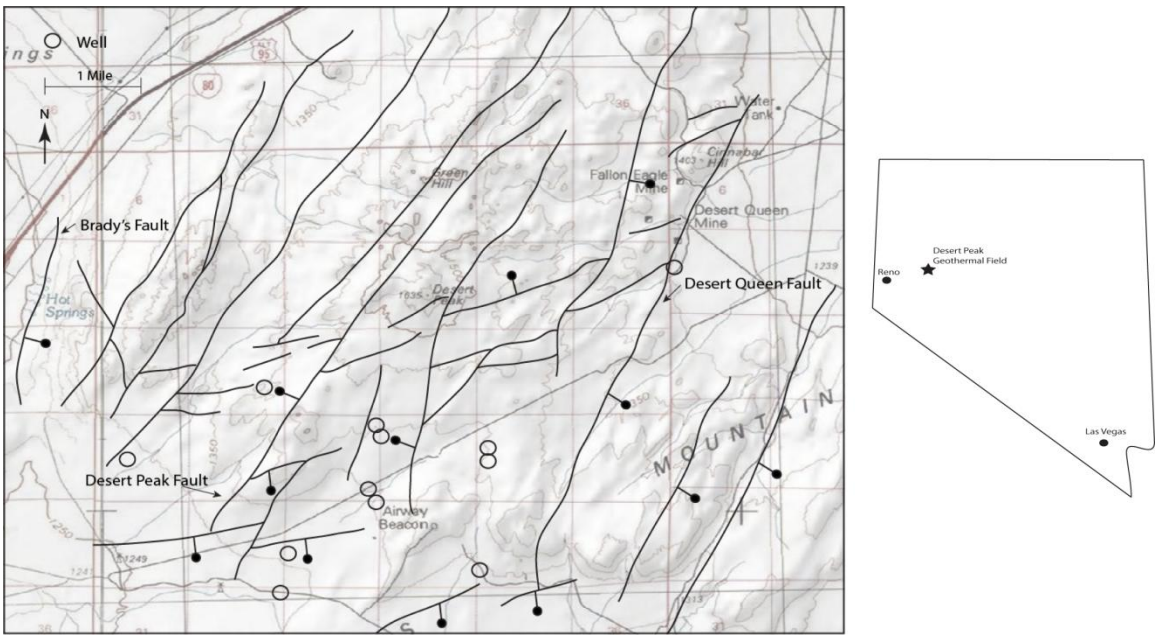

Figure 3.6. Structure map of the Brady's, Desert Queen, and Desert Peak geothermal systems. Note prominent en echelon character to normal faults, also important are fault terminations at multiple fault intersections. Bar and ball on downthrown side of faults. Circles represent wellbores drilled for either production or for stratigraphic controls. Modified from Benoit et al. (1983).

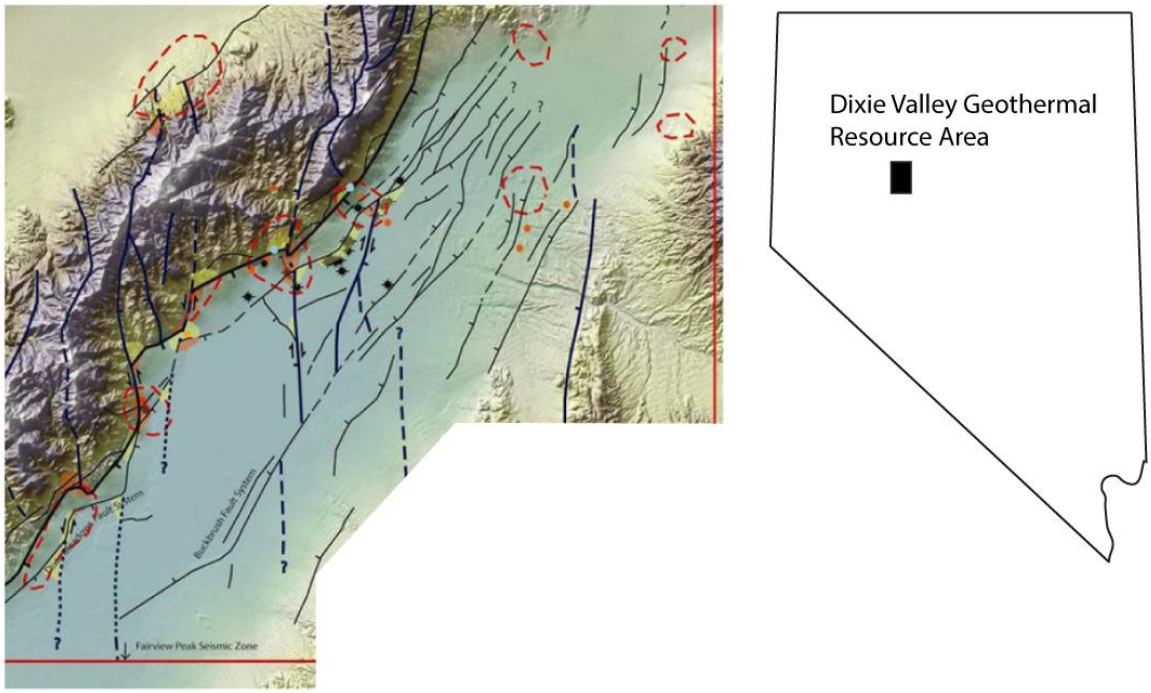

Fig. 3.7. Structural map showing rhombohedral fault patterns at Dixie Valley. Also important to this map is the older, north trending normal faults created from an earlier episode of extension. See text Waibel (2011) for further discussion. Map modified from Iovenitti et al. (2011) and Waibel (2011).

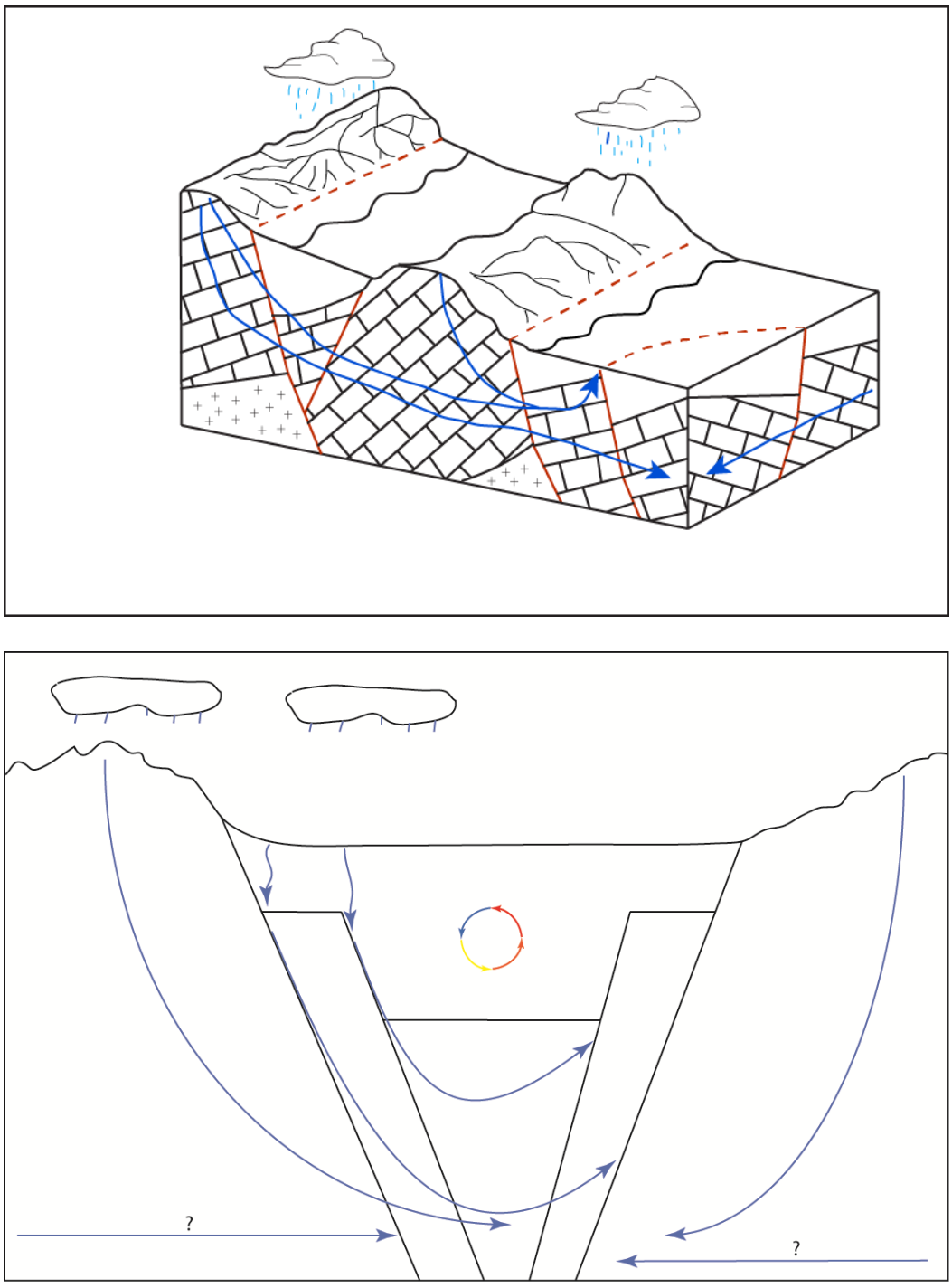

Figure 3.8. Conceptual model of topographic (a) and convective (b) groundwater flow in the Great Basin. See text for further discussion. Modified from Gillespie et al. (2012).

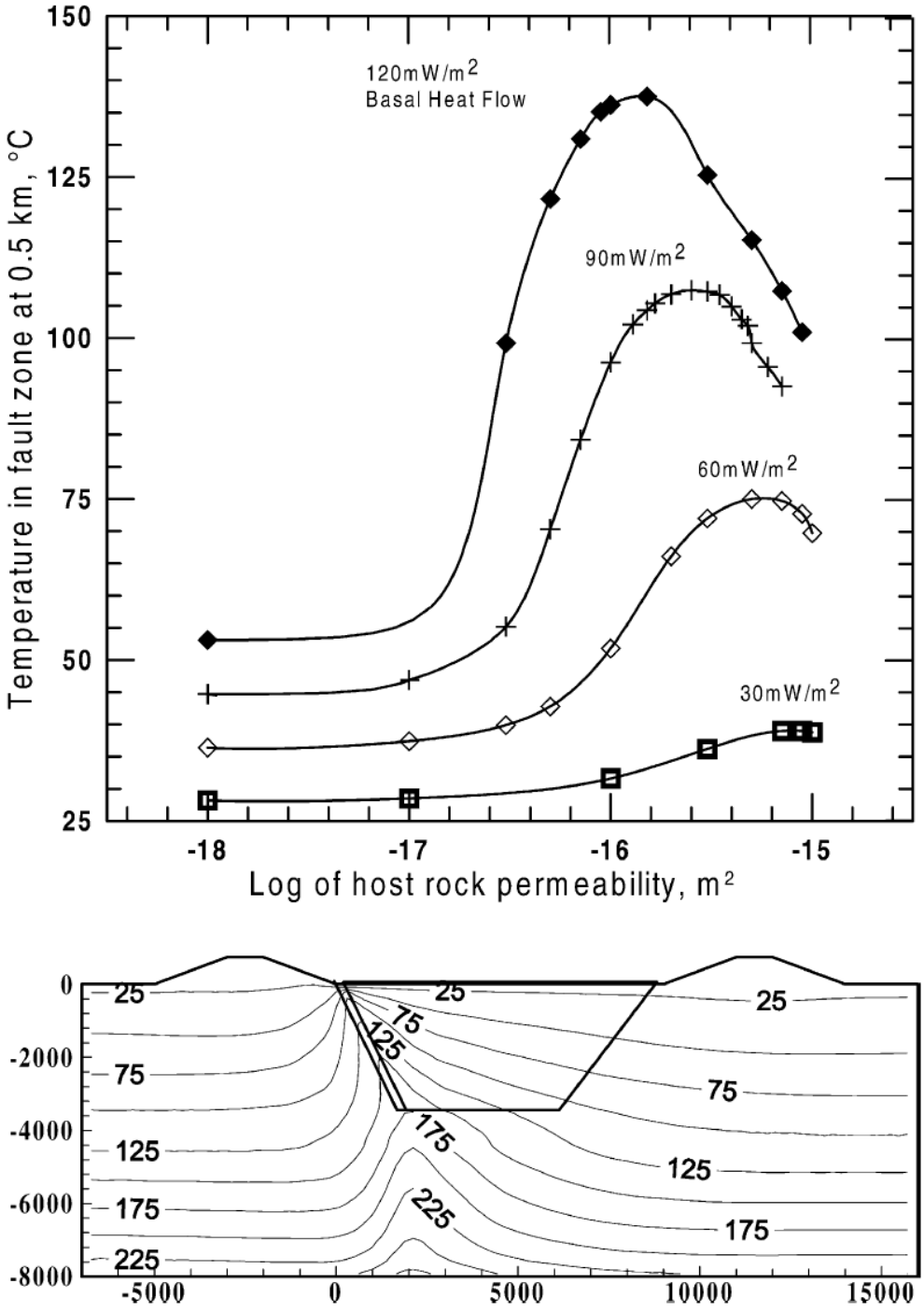

Figure 3.9. Result of numerical modeling of heat flow and temperature within a fault zone in the Basin and Range. Temperatures in the fault depend on background heat flow. Temperatures in fault are hotter than ambient temperatures if thermal water is flowing up the fault, this is represented by the isotherms in the lower figure. Taken from McKenna and Blackwell (2004).

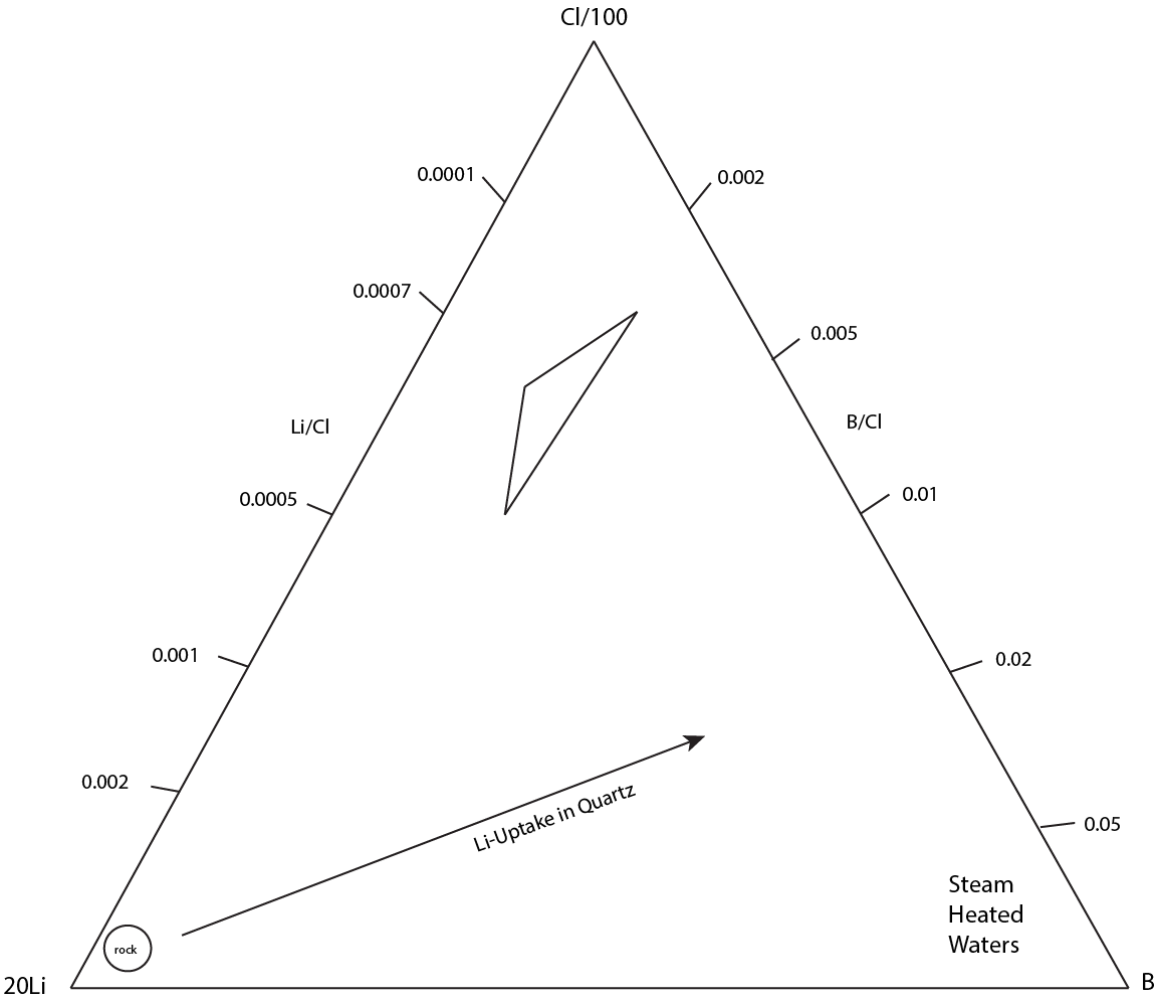

Figure 3.10. Li-Cl-B ternary plot. This diagram is useful for assessing the potential of a magmatically heated geothermal system based on the B/Cl ratio. See text for discussion on Li behavior in geothermal waters. Triangle in upper part of diagram represents mature volcanic waters.

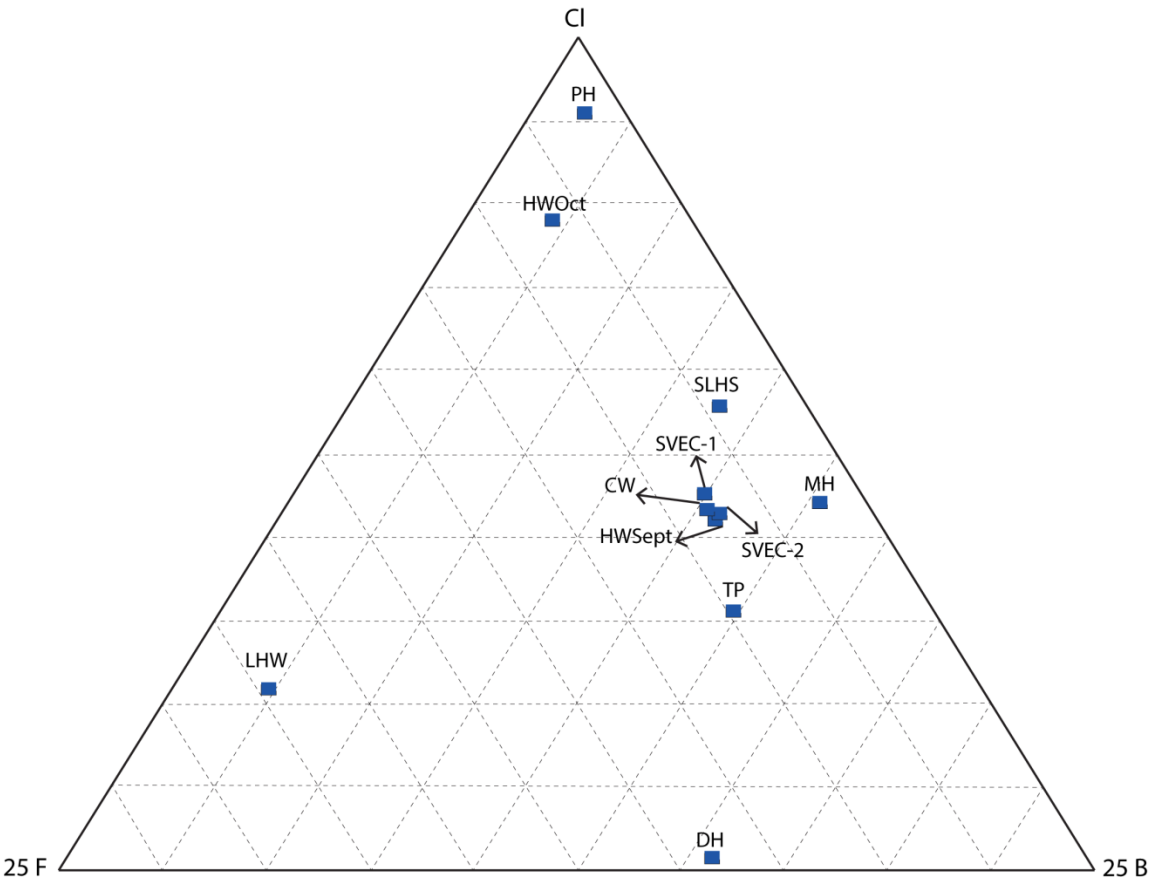

Figure 3.11. F-Cl-B ternary plot used to distinguish multiple sources of thermal waters. Data in this figure from this study. Samples were plotted in spreadsheet by Powell and Cumming (2010). Fluorine and Boron come from magmatic degassing or dissolution of igneous rocks. Chlorine most likely comes from dissolution of all rock types. See Table 1 for nomenclature.

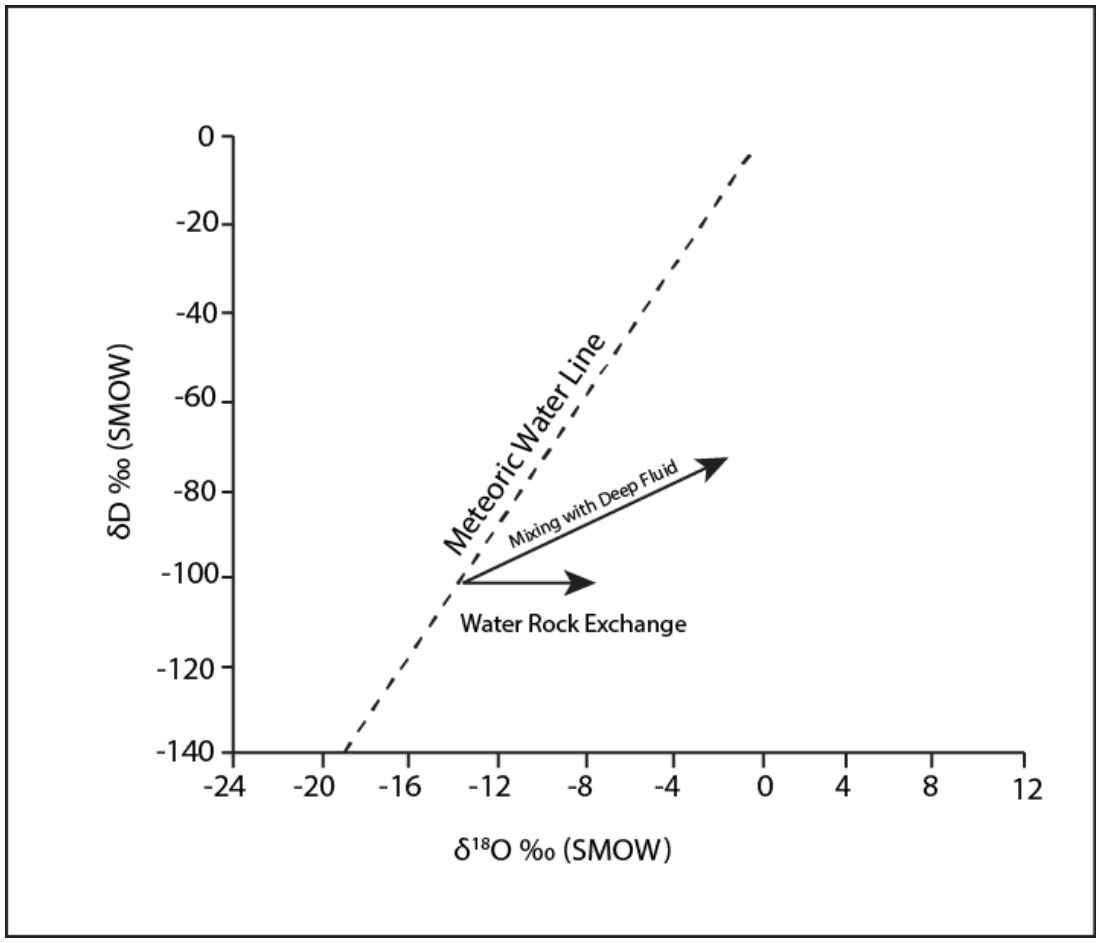

Figure 3.12. Plot of δD vs $\delta^{18}O$. Water rock interaction causes exchange of ^{18}O between fluid and rock, which cause a shift immediately to right of the meteoric water line. If fluid mixes with connate water, the samples will move up and to the right of the meteoric water line. Modified from Banerjee et al. (2011).

References Cited

Arehart, G.B., Coolbaugh, M.F., Poulson, S.R. 2007. Geochemical Characterization of Geothermal Systems in the Great Basin: Implications for Exploration, Exploitation, and Environmental Issues. Geothermal Resources Council Transactions. 5 p.

Armannsson, H., Fridriksson, T. 2009. Application of Geochemical Methods in Geothermal Exploration. Short Course on Surface Exploration for Geothermal Resources. UNU-GTP and LaGeo, in Ahuachapan and Santa Tecla, El Salvador, 2009. 12 p.

Atwater, T., Stock, J. 1998. Pacific-North America Plate Tectonics of the Neogene Southwestern United States: An Update. International Geology Review. v. 40, no. 5. p. 375-402. DOI: 10.1080/00206819809465216.

Banerjee, A., Person, M., Hofstra, A., Sweetkind, D., Cohen, D., Sabin, A., Unruh, J., Zyvoloski, G., Gable, C.W., Crossey, L., Karlstrom, K. 2011. Deep Permeable Fault-Controlled Helium Transport and Limited Mantle Flux in two Extensional Geothermal Systems in the Great Basin, United States. Geology. v. 39, no.3. p. 195-198. DOI: 10.1130/G31557.1.

Barker, B.J., Gulati, M.S., Bryan, M.A., Riedel, K.L. 1992. Geysers Reservoir Performance. *In* Monograph on the Geysers Geothermal Field. Stone, C. (ed). Geothermal Resources Council Special Report 17. Davis, California. p. 167-177.

Bennett, R.A., Wernicke, B.P., Niemi, N.A., Fridrich, A.M. 2003. Contemporary strain rates in the northern Basin and Range province from GPS data. Tectonics. v. 22, no. 2. DOI: 10.1029/2001TC001355.

Bennett, S. 2011. Geothermal Potential of Transtensional Plate Boundaries. Geothermal Resources Council Transactions. v. 35. p. 703-708.

Benoit, W.R., Hiner, J.E., Forest, R.T. 1983. Discovery and Geology of the Desert Peak Geothermal Field: A Case History. Nevada Bureau of Mines and Geology Bulletin 97. Reno, NV. 82 p.

Bestland, E.A., Hammond, P.E., Blackwell, D.S., Kays, M.A., Retallack, G.J., Stimac, J. 1999. Geologic Framework of the Clarno Unit, John Day Fossil Beds National Monument, Central Oregon. Oregon Geology. v. 61, no. 1. p. 3-19.

Blackwell, D.D., Smith, R.P., Waibel, A., Richards, M.C., Stepp, P. 2009. Why Basin and Range Systems are Hard to Find II: Structural Model of the Producing Geothermal System in Dixie Valley, Nevada. Geothermal Resources Council Transactions. v. 33. p. 441-446.

Blackwell, D.D. 1971. The Thermal Structure of the Continental Crust. *In* The Structure and Physical Properties of the Earth's Crust. Heacock, J.G. (ed). Geophysical Monograph 14. p. 169-184.

Blackwell, D.D. 1978. Heat Flow and Energy Loss in the Western United States. *In* Cenozoic Tectonics and Regional Geophysics of the Western Cordillera. Robert B. Smith and Gordon P. Eaton (eds). Geological Society of America Memoir 152. Denver, CO. p. 175-207.

Blackwell, D.D. 1983. Heat Flow in the Northern Basin and Range Province. The Role of Heat in the Development of Energy and Mineral Resources in the Northern Basin and Range Province. Geothermal Resources Council Special Report 13. p. 81-93.

Blackwell, D.D., Richards, M. 2004. Geothermal Map of North America. American Association of Petroleum Geologists. 1 sheet. 1:6 500 000 scale.

Brott, C.A., Blackwell, D.D., Mitchel, J.C. 1978. Tectonic Implications of the Heat Flow of the Western Snake River Plain, Idaho. Geological Society of America Bulletin. v. 89. p. 1697-1707.

Brott, C.A., Blackwell, D.D., Ziagos, J.P. 1981. Thermal and Tectonic Implications of Heat Flow in the Eastern Snake River Plain, Idaho. Journal of Geophysical Research. v. 86, no. B12. p. 11709-11734.

Cashman, P.H., Faulds, J.E., Hinz, N.H. 2012. Regional Variations in Structural Controls on Geothermal Systems in the Great Basin. Geothermal Resources Council Transactions. v. 36. p. 25-30.

Casteel, J., Trazona, R., Melosh, G., Niggeman, K., Fairbank, B. 2010. A Preliminary Conceptual Model for the Blue Mountain Geothermal System, Humboldt County, Nevada. Proceedings, World Geothermal Congress. Bali, Indonesia. 6 p.

Chiasson, A. 2004. Electric Power Generation in the Roosevelt Hot Springs Area- The Blundell Geothermal Power Plant. Geo-Heat Center Bulletin. p. 16-20.

Coolbaugh, M.F., Arehart, G.B., Faulds, J.E., Garside, L.J. 2005. Geothermal Systems in the Great Basin, Western United States: Modern Analogues to the Roles of Magmatism, Structure, and Regional Tectonics in the Formation of Gold Deposits. *In* Geological Society of Nevada Symposium 2005: Window to the World. Rhoden, H.N., Steininger, R.C., Vikre, P.G. (eds). Reno, NV. p. 1063-1081.

Craig, H. 1961. Isotopic Variations in Meteoric Waters. Science. v. 133, no. 3465. p. 1702-1703.

Criss, R.E., Taylor, H.P. 1986. Meteoric-Hydrothermal Systems. *In* Stable Isotopes in High Temperature Geological Processes. Valley, J.W., Taylor, H.P., O'Neil, J.R. (eds). Mineralogical Society of America. Reviews in Mineralogy Vol. 16. p. 373-424.

Dickinson, W.R., Snyder, W.S. 1979. Geometry of Subducted Slabs Related to San Andreas Transform. The Journal of Geology. v. 87, no. 6. p. 609-627.

Dickinson, W.R. 2006. Geotectonic Evolution of the Great Basin. Geosphere. v. 2, no. 7. p. 353-368. DOI: 10.1130/GES00054.1.

Donath, F.A. 1962. Analysis of Basin-Range Structure, South-Central Oregon. Geological Society of America Bulletin. v. 73. p. 1-16. DOI: 10.1130/0016-7606(1962)73[1:AOBSSO]2.0.CO;2.

du Bray, E.A., John, D.A. 2011. Petrologic, Tectonic, and Metallogenic Evolution of the Ancestral Cascades Magmatic Arc, Washington, Oregon, and northern California. Geosphere. v. 7, no. 5. p. 1102-1133. DOI: 10.1130/GES00669.1.

Duebendorfer, E.M., Black, R.A. 1992. Kinematic Role of Transverse Structures in Continental Extension: An Example from the Las Vegas Shear Zone, Nevada. Geology. v. 20. p. 1107-1110. DOI: 10.1130/0091-7613(1992)020<1107:KROTSI>2.3.CO;2.

Ellis, A.J., Mahon, W.J. 1977. Chemistry and Geothermal Systems. Energy Science and Engineering: Resources, Technology, Management, An International Series. Denton, J. (ed). Academic Press. New York, New York. 392 p.

Fairley, J.P., Hinds, J.J. 2004. Rapid Transport Pathways for Geothermal Fluids in an Active Great Basin Fault Zone. Geology. v. 32. p. 825-828. DOI: 10.1130/G20617.1.

Faulds, J.E., Varga, R.J. 1998. The Role of Accommodation Zones and Transfer Zones in the Regional Segmentation of Extended Terranes. *In* Accommodation and Transfer Zones: The Regional Segmentation of the Basin and Range Province. Faulds, J.E., Stewart, J.H. (eds). Geological Society of America Special Paper 323. Boulder, CO.

Faulds, J.E., Garside, L.J., Oppliger, G.L. 2003. Structural Analysis of the Desert Peak-Brady Geothermal Fields, Northwest Nevada: Implications for Understanding Linkages between Northeast-Trending Structures and Geothermal Reservoirs in the Humboldt Structural Zone. Geothermal Resources Council Transactions. v. 27. p. 859-864.

Faulds, J.E., Henry, C.D., Hinz, N.H. 2005. Kinematics of the Northern Walker Lane: An Incipient Transform Fault Along the Pacific-North American Plate Boundary. Geology. v. 33, no. 6. p. 505-508. DOI: 10.1130/G21274.1.

Faulds, J.E., Coolbaugh, M.F., Vice, G.S., Edwards, M.L. 2006. Characterizing Structural Controls of Geothermal Fields in the Northwestern Great Basin: A Progress Report. Geothermal Resources Council Transactions. v. 30. p. 69-76.

Faulds, J.E., Coolbaugh, M.F., Benoit, D., Oppliger, G., Perkins, M., Moeck, I., Drakos, P. 2010. Structural Controls of Geothermal Activity in the Northern Hot Springs Mountains, Western Nevada: The Tale of Three Geothermal Systems (Brady's, Desert Peak, and Desert Queen). Geothermal Resources Council Transactions. v. 34. p. 675-684.

Ferguson, G., Grasby, S.E., Hindle, R. 2009. What do Aqueous Geothermometers Really Tell Us? Geofluids. v. 9. p. 39-48. DOI: 10.1111/j.1468-8123.2008.00237.x.

Fournier, R.O., Truesdell, A.H. 1973. An Empirical Na-K-Ca Geothermometer for Natural Waters. Geochimica et Cosmochimica Acta. v. 37, no. 5. p. 1255-1276.

Fournier, R.O., Thompson, J.M. 1980. The Recharge Area for the Coso, California, Geothermal System Deduced from δD and $\delta^{18}O$ in Thermal and Non-Thermal Waters in the Region. United States Geological Survey Open-File Report 80-454. Menlo Park, CA. 25 p.

Fournier, R.O. 1989. Lectures on Geochemical Interpretation of Hydrothermal Waters. United Nations University Geothermal Training Programme. Report 10. Reykjavik, Iceland. 73 p.

Fournier, R.O. 1992. Water Geothermometers applied to Geothermal Energy. *In* Application of Geochemistry in Geothermal Reservoir Development: Series of Technical Guides on the Use of Geothermal Energy. D'Amore, F. (ed). Rome, Italy. p. 37-70.

Geothermal Energy Association. 2012. Annual Geothermal Power Production and Development Report: April 2012. Washington D.C. www.geo-energy.org.

Giggenbach, W.F., Soto, R.C. 1992. Isotopic and Chemical Composition of Water and Steam Discharge from Volcanic-Magmatic-Hydrothermal Systems of the Guanacaste Geothermal Province, Costa Rica. Applied Geochemistry. v. 7. p. 309-332.

Giggenbach, W.F. 1988. Geothermal Solute Equilibria, Derivation of Na-K-Mg-Ca Geoindicators. Geochimica et Cosmochimica Acta. v. 52. p. 2749-2765.

Gilbert, H. 2012. Crustal Structure and Signatures of Recent Tectonism as Influenced by Ancient Terranes in the Western United States. Geosphere. v. 8, no. 1. p. 141-157. DOI: 10.1130/GES00720.1.

Gillespie, J., Nelson, S.T., Mayo, A.L., Tingy, D.G. 2012. Why Conceptual Groundwater Flow Models Matter: A Trans-Boundary Example from the Arid Great Basin, Western USA. Hydrogeology Journal. v. 20. p. 1133-1147. DOI: 10.1007/s10040-012-0848-0.

Hammond, W.C., Thatcher, W. 2005. Northwest Basin and Range Tectonic Deformation Observed with the Global Positioning System, 1999-2003. Journal of Geophysical Research. v. 110. DOI: 10.1029/2005JB003678.

Hantelmann, J.J. 2006. The Geothermal Potential of Crump Geyser in Warner Valley, Lake County, Oregon. Geothermal Resources Council Transactions. v. 30. p. 77-82.

Harril, J.R., Prudic, D.E. 1998. Aquifer Systems in the Great Basin Region of Nevada, Utah, and Adjacent States- A Summary Report. United States Geological Survey Professional Paper 1409-A. p. A1-A66.

Hinz, N.H., Faulds, J.E., Bell, J.W., Oldow, J.S. 2010. Structural Controls of Three Blind Geothermal Resources at the Hawthorne Ammunition Depot, West-Central Nevada. Geothermal Resources Council Transactions. v. 34. p. 785-790.

Humphreys, E.D. 1995. Post-Laramide Removal of the Farallon Slab, Western United States. Geology. v. 23. p. 987-990. DOI: 10.1130/0091-7613(1995)023<0987:PLROTF>2.3.CO;2.

Iovenitti, J.L., Blackwell, D.D., Sainsbury, J.S., Tibuleac, I.M., Waibel, A.F., Cladouhos, T.T., Karlin, R., Kennedy, B.M., Isaaks, E., Wannamaker, P.E., Clyne, M.T., Callahan, O.C. 2011. EGS Exploration Methodology Development Using the Dixie Valley Geothermal District as a Calibration Site, A Progress Report. Geothermal Resources Council Transactions. v. 35. 12 p.

Johnson, C.M. 1991. Large-Scale Crust Formation and Lithosphere Modification Beneath Middle to Late Cenozoic Calderas and Volcanic Fields, Western North America. Journal of Geophysical Research. v. 96, no. B8. p. 13485-13507.

Kennedy, M.B., van Soest, M.C. 2007. Flow of Mantle Fluids Through the Ductile Lower Crust: Helium Isotope Trends. Science. v. 318. p. 1433-1436. DOI: 10.1126/science.1147537.

Krahmer, M.S. 1995. The Geology and Hydrochemistry of the Geothermal System Near Stanley, Idaho. Master's Thesis. Washington State University. Pullman, WA. 159 p.

Kreemer, C., Blewitt, G., Hammond, W.C. 2009. Geodetic Constraints on Contemporary Deformation in the Northern Walker lane: 2. Velocity and Strain

Rate Tensor Analysis. *In* Late Cenozoic Structure and Evolution of the Great Basin-Sierra Nevada Transition. Oldow, J.S., Cashman, P.H. (eds). Geological Society of America Special Paper 447. p. 17-31. DOI: 10.1130/2009.2447(02).

Lachenbruch, A.H. 1979. Heat Flow in the Basin and Range Province and Thermal Effects of Tectonic Extension. Pageoph. v. 117, no. 1978/1979. p. 34-50.

Lee, J., Garwood, J., Stockli, D.F., Gosse, J. 2009. Quaternary Faulting in Queen Valley, California –Nevada: Implications for Kinematics of Fault-Slip Transfer in the Eastern California Shear Zone-Walker Lane Belt. Geological Society of America Bulletin. v. 121, no. 3/4. p. 599-614. DOI: 10.1130/B26352.1.

Lipman, P.W., Prostka, H.J., Christiansen, R.L. 1972. Cenozoic Volcanism and Plate-Tectonic Evolution of the Western United States. I- Early and Middle Cenozoic. Philosophical Transactions of the Royal Society of London. Series A, Mathematical and Physical Sciences. v. 271, no. 1213, A Discussion on Volcanism and the Structure of the Earth. p. 217-248.

Liu, M. 2001. Cenozoic Extension and Magmatism in the North American Cordillera: The Role of Gravitational Collapse. Tectonophysics. v. 342. p. 407-433.

Lopez, D.L., Smith, L. 1995. Fluid Flow in Fault Zones: Analysis of the Interplay of Convective Circulation and Topographically Driven Groundwater Flow. Water Resources Research. v. 31, no. 6. p. 1489-1503.

McBirney, A.R., White, C.M. 1982. The Cascade Province. *In* Andesites: Orogenic Andesites and Related Rocks. Thorpe, R.S. (ed). John Wiley and Sons New York. 724 p.

McKenna, J.R., Blackwell, D.D. 2004. Numerical Modeling of Transient Basin and Range Extensional Geothermal Systems. Geothermics. v. 33. p. 457-476. DOI: 10.1016/j.geothermics.2003.10.001.

McSween, H.Y., Richardson, S.M., Uhle, M.E. 2003. Geochemistry: Pathways and Processes. 2nd Edition. Columbia University Press, New York, New York. 363 p.

Moore, J.N., Norman, D.I., Kennedy, M.B. 2001. Fluid Inclusion Gas Compositions from an Active Magmatic-Hydrothermal System: A Case Study of the Geysers Geothermal Field, USA. Chemical Geology. v. 173. p. 3-30.

Nicholson, K. 1993. Geothermal Fluids: Chemistry and Exploration Techniques. Springer-Verlag. New York, New York. 263 p.

Oldow, J.S. 2003. Active Transtensional Boundary Zone Between the Western Great Basin and Sierra Nevada Block, Western U.S. Cordillera. Geology. v. 31, no. 12. p. 1033-1036.

Oldow, J.S., Geissman, J.W., Stockli, D.F. 2008 Evolution and Strain Reorganization within Late Neogene Structural Stepovers Linking the Central Walker Lane and Northern Eastern California Shear Zone, Western Great Basin. International Geology Review. v. 50, no. 3. p. 270-290. DOI: 10.2747/0020-6814.50.3.270.

Person, M., Banerjee, A., Hofstra, A., Sweetkind, D., Gao, Y. 2008. Hydrologic Models of Modern and Fossil Geothermal Systems in the Great Basin: Genetic Implications for Epithermal Au-Ag and Carlin-Type Gold Deposits. Geosphere. v. 4, no. 5. p. 888-917. DOI: 1130/GES00150.1.

Powell, T., Cumming, W. 2010. Spreadsheets for Geothermal Water and Gas Geochemistry. Proceedings, Thirty-Fifth Workshop on Geothermal Reservoir Engineering. Stanford University, Stanford, California. 10 p.

Reed, M.J., Mariner, R.H. 1991. Quality Control of Chemical and Isotopic Analyses of Geothermal Water Samples. Proceedings, Sixteenth Workshop on Geothermal Reservoir Engineering. Stanford University, Stanford, California. 5 p.

Ross, H.P., Moore, J.N., Christiensen, O.D. 1982. The Cove Fort-Sulphurdale Known Geothermal Resource Area: A Geologic and Geophysical Case Study. 50th Annual International SEG Meeting, Houston, TX. 49 p.

Sass, J.H., Lachenbruch, A.H. 1978. Heat Flow and Conduction-Dominated Thermal Regimes. *In* Assessment of Geothermal Resources of the United States. Muffler, L.P. (ed). United States Geological Survey Circular 790. p. 8-11.

Sass, J.H., Lachenbruch, A.H., Munroe, R.J., Greene, G.W., Moses, Jr, T.H. 1971. Heat Flow in the Western United States. Journal of Geophysical Research. v. 76, no. 26. p. 6376-6413.

Schmitt, A.K., Grove, M., Harrison, M.T., Lovera, O., Hulen, J., Walters, M. 2003a. The Geysers-Cobb Mountain Magma System, California (Part 2): Timescales of Pluton Emplacement and Implications for its Thermal History. Geochimica et Cosmochimica Acta. v. 67, no. 18. p. 3443-3458. DOI: 10.1016/S0016-7037(02)00126-1.

Schmitt, A.K., Grove, M., Harrison, M.T., Lovera, O., Hulen, J., Walters, M. 2003b. The Geysers-Cobb Mountain Magma System, California (Part 1): U-Pb Zircon Ages of the Volcanic Rocks, Conditions of Zircon Crystallization and Magam Residence Times. Geochimica et Cosmochimica Acta. v. 67, no. 18. p. 3423-3442. DOI: 10.1016/S0016-7037(03)00140-6.

Sladek, C., Arehart, G.B., Benoit, W.R. 2004. Geochemistry of the Lake City Geothermal System, California, USA. Geothermal Resources Council Transactions. v. 28. p. 363-368.

Smith, R.L., Shaw, H.R. 1978. Igneous-Related Geothermal Systems. *In* Assessment of Geothermal Resources of the United States. Muffler, J.P. (ed). United States Geological Survey Circular 790. p. 8-11.

Smith, G.I., Friedman, I., Gleason, J.D., Warden, A. 1992. Stable Isotope Composition of Waters in Southeastern California: 2. Groundwaters and Their Relation to Modern Precipitation. Journal of Geophysical Research. v. 97, no. D5. p. 5813-5823.

Smith, G.I., Friedman, I., Veronda, G., Johnson, C.A. 2002. Stable Isotope Compositions of Waters in the Great Basin, United States 3. Comparisons of Groundwaters with Modern Precipitation. Journal of Geophysical Research. v. 107, no. D19. DOI: 10.1029/2001JD000567.

Smith, R.P., Wisian, K.W., Blackwell, D.D. 2001. Geologic and Geophysical Evidence for Intra-Basin and Footwall Faulting at Dixie Valley, Nevada. Geothermal Resources Council Transactions. v. 25. 8 p.

Snyder, W.S., Dickinson, W.R., Silberman, M.L. 1976. Tectonic Implications of Space-Time Patterns of Cenozoic Magmatism in the Western United States. Earth and Planetary Science Letters. v. 32. p. 91-106.

Stewart, J.H. 1978. Basin-Range Structure in Western North America: A Review. *In* Cenozoic Tectonics and Regional Geophysics of the Western Cordillera. Smith, R.B., Eaton, G.P. (eds). Geological Society of America Memoir 152. p. 1-31.

Stewart, J.H. 1980. Regional Tilt Patterns of Late Cenozoic Basin and Range Fault Blocks, Western United States. Geological Society of America Bulletin. v. 91, no. 8. p. 460-464. DOI: 10.1130/0016-7606(1980)91<460:RTPOLC>2.0.CO;2.

Stewart, J.H. 1988. Tectonics of the Walker Lane Belt, Western Great Basin: Mesozoic and Cenozoic Deformation in a Zone of Shear. *In* Metamorphism and Crustal Evolution of the Western United States. Ernst, W.G. (ed). Prentice Hall, Englewood Cliffs, New Jersey. p. 683-713.

Swanberg, C.A., Blackwell, D.D. 1973. Areal Distribution and Geophysical Significance of Heat Generation in the Idaho Batholith and Adjacent Intrusions in Eastern Oregon and Western Montana. Geological Society of America Bulletin. v. 84. p. 1261-1282.

Sweetkind, D.S., Knochenmus, L.A., Ponce, D.A., Wallace, A.R., Scheirer, D.S., Watt, J.T., Plume, R.W. 2007. Hydrogeologic Framework. *In* Water Resources of the

Basin and Range Carbonate Aquifer System, White Pine County, Nevada, and Adjacent Areas in Nevada and Utah. Welch, A.H., Bright, D.J. (eds). United States Geological Survey Open-File Report 2007-1156. p. 13-36.

Taylor, H.P. 1974. The Application of Oxygen and Hyrogen Isotope Studies to Problems of Hydrothermal Alteration and Ore Depositon. Economic Geology. v. 69. p. 843-883.

Thakur, M., Blackwell, D.D., Erkan, K. 2012. The Regional Thermal Regime in Dixie Valley, Nevada, USA. Geothermal Resources Council Transactions. v. 36. p. 59-68.

Trench, D., Meigs, A., Grunder, A. 2012. Termination of the Northwestern Basin and Range Province into a Clockwise Rotating Region of Transtension and Volcanism, Southeast Oregon. Journal of Structural Geology. v. 39. p. 52-65. DOI: 10.1016/j.jsg.2012.03.007.

Waibel, A. 2011. Structural Controls on the Location of Geothermal Cells in and Adjacent to Dixie Valley, Nevada. Geothermal Resources Council Transactions. v. 35. p. 1045-1052.

Walker, G.W., MacLeod, N.S. 1991. Geologic Map of Oregon. United States Geological Survey. 1:500 000 scale. 2 sheets.

Wells, R.E., Simpson, R.W. 2001. Northward Migration of the Cascadia Forearc in the Northwestern US and Implications for Subduction Deformation. Earth Planets Space. v. 53. p. 275-283.

Wernicke, B., Axen, G.J., Snow, J.K. 1988. Basin and Range Extensional Tectonics at the Latitude of Las Vegas, Nevada. Geological Society of America Bulletin. v. 100. p. 1738-1757.

Wesnousky, S.G. 2005. The San Andreas and Walker Lane Fault Systems, Western North America: Transpression, Transtension, Cumulative Slip and the Structural Evolution of a Major Transform Plate Boundary. Journal of Structural Geology. v. 27. p. 1505-1512.

Wesnousky, S.G., Barron, A.D., Briggs, R.W., Caskey, J., Kumar, S., Owen, L. 2005. Paleoseismic Transect Across the Northern Great Basin. Journal of Geophysical Research. B05408. v. 110. DOI: 10.1029/2004JB003283.

White, D.E. 1970. Geochemistry Applied to the Discovery, Evaluation, and Exploitation of Geothermal Energy Resources. Geothermics, Special Issue 2. no. 1. p. 58-80.

Williams, C.F., Reed, M.J., Mariner, R.H. 2008. A Review of Method Applied by the U.S. Geological Survey in the Assessment of Identified Geothermal Resources.

USGS Open-File Report 2008-1296. Reston, VA. 27 p. http://pubs.usgs.gov/of/2008/1296/.

Williams, C.F., Sass, J.H., Grubb, F.V. 1997. Thermal Signature of Subsurface Fluid Flow Near the Dixie Valley Geothermal Field, Nevada. Proceedings, Twenty-Second Workshop on Geothermal Reservoir Engineering. Stanford University, Stanford, California.

Wisian, K.W., Blackwell, D.D. 2004. Numerical Modeling of Basin and range Geothermal Systems. Geothermics. v. 33. p. 713-741. DOI: 10.1016/j.geothermics.2004.01.002.

Wisian, K.W., Blackwell, D.D., Richards, M. 1999. Heat Flow in the Western United States and Extensional Geothermal Systems. Proceedings, Twenty-Fourth Workshop on Geothermal Reservoir Engineering. Stanford University, Stanford, California. 8 p.

Zehner, R.E., Coolbaugh, M.F., Shevenell, L. 2006. Regional Groundwater Trends in the Great Basin: Implications for Geothermal Exploration. Geothermal Resources Council Transactions. v. 30. p. 117-124.

Zhiyuan, M., Yu, J., Su, Y., Xie, J., Jia, X., Hu, Y. 2010. $\delta^{18}O$ Shifts of Geothermal Waters in the Central of Weihi Basin, NW China. Environment Earth Science. v. 59. p. 995-1008.

Zoback, M.L., Anderson, R.E., Thompson, G.A. 1981. Cainozoic Evolution of the State of Stress and Style of Tectonism of the Basin and Range Province of the Western United States. Philosophical Transactions of the Royal Society of London. Series A, Mathematical and Physical Sciences. v. 300, no. 1454, Extensional Tectonics Associated with Convergent Plate Boundaries. p. 407-434.

CHAPTER FOUR: CHARACTERIZATION OF THE GEOTHERMAL SYSTEM NEAR PAISLEY, OREGON

Introduction

The tectonic and magmatic framework of southeast Oregon is one that is supportive of high geothermal potential. However, few detailed studies of geothermal systems in this part of the Basin and Range have been conducted. Young bimodal magmatism and faulting associated with the High Lava Plains coupled with the encroachment of the Basin and Range tectonic province and potentially the Walker Lane have created the heat source and secondary permeability necessary for geothermal systems in southeast Oregon. The relative contribution of these geologic provinces on the overall regional framework is less well understood. In this study, the geothermal system near Paisley, Oregon has been characterized by a detailed regional heat flow study, geologic mapping, aqueous geochemical analysis, a gravity survey, and by X-ray diffraction analysis of secondary alteration minerals. These studies help to characterize the Paisley geothermal system within the framework created from previous (Chapters Two and Three) discussions of magmatic and Basin and Range-type geothermal systems.

Paisley lies at the intersection of the northwest boundary of the Basin and Range tectonic province, southern High Lava Plains, and the Cascades (Fig. 2.1). The oldest of these provinces is the Cascades, which have been volcanically active since mid-Eocene (~45 Ma). Around 5 Ma, a major shift in style of volcanism and local normal faulting is

generally defined by the transition from the older volcanism of Western Cascades to the modern High Cascades. Close to this time, the encroachment of Basin and Range-style faulting began in southeast Oregon and has persisted until present times (e.g., Scarberry et al., 2010). Bimodal magmatism and associated normal to strike-slip faulting characteristic of the High Lava Plains began in southeast Oregon around 6-8 Ma. The Walker Lane Belt in the western Great Basin is associated with areas of high geothermal potential, related to the formation of complex structural patterns between Basin and Range and overprinted Walker Lane structures. Though the Walker Lane may not have a direct effect on the Paisley geothermal system, it serves as an analogue for similar types of structural features found in southeastern Oregon.

Work in the Paisley area has mostly focused on local structures and Miocene-Recent volcanism. The faulting east of Summer Lake has been the focus (Figs. 1.1 and 4.11) of many studies (e.g., Donath, 1962; Donath and Kuo, 1962; Travis, 1977; Crider, 2001). Donath (1962) concluded that the complex faulting there is the result of N-S directed compression in the Miocene, but Crider (2001) concluded that it is instead related to oblique extension. Trench et al. (2012) state that clockwise rotation of southeast Oregon created normal and strike-slip faults that are analogous to structures at oceanic spreading centers. This model may work work well for the major normal faults of southeast Oregon (i.e., Steens Mountain, Hart Mountain, Poker Jim, and Abert Rim) but does not adequately explain the Winter Ridge or Paisley Mountain faults. Given the Miocene-Recent geologic setting of Paisley, it is believed by some that the oblique rifting model of Crider (2001) works best.

Regional stratigraphy has been studied by several workers (e.g. Walker, 1963; Peterson and McIntyre, 1970; MacLeod et al., 1976; Walker, 1977; Diggles et al., 1990, Walker and MacLeod, 1991) and stratigraphy in the Paisley Hills has been correlated with this regional stratigraphy (e.g., Appling, 1950; Muntzert and Field, 1969; Muntzert, 1969, this study).

Regional Stratigraphy

A geologic map of the Paisley area was compiled at 1:48 000 scale for this thesis (Plate 1). Rock types present in the Paisley area are primarily volcanic and range in age from early-Eocene (?) to Holocene. A general shift in volcanism took pace around the Eocence-Oligocene boundary from intermediate rock types to chiefly bimodal basalts and rhyolites. Basaltic and rhyolitic volcanism persisted into the Miocene and ends with the eruption of Miocene-Pliocene basalts.

Dacite Flows (Tdf)

Eocene dacite flows mapped in the Paisley Hills by Appling (1950) and Muntzert (1969) are the oldest rocks exposed in the field area. This unit was assigned a pre-early Oligocene age by Muntzert (1969) based on stratigraphic relationships. It has been estimated that these rocks are 750-900 meters thick (Appling, 1950; Muntzert, 1969). These dacites are reported to be aphyric to slightly porphyritic with plagioclase being the dominant mineral. Individual flows show flow banding and are brecciated near the top. Chlorite and sericite are reported to be the dominant alteration minerals in this unit, reflecting the widespread hydrothermal alteration in the area.

Andesitic Volcanic Breccia (Tvb)

A thick sequence of volcanic breccias interpreted as having been deposited by lahars is exposed in the Coglan Buttes and comprises the second oldest map unit in the field area. The Coglan Buttes Lahar unit is comprised mostly of lahars but also contains some interstratified basalt, andesite, and minor volcanic sediments. An Eocene age has been assigned to this unit, based on plant and vertebrate fossils (Peterson and McIntyre, 1970). These rocks are not exposed in the northern and southern Coglan Buttes due to decreased offset along the range bounding fault.

The Coglan Buttes lahars are generally tan to light gray in color and occur in massive flows ranging from 5-15 meters thick (Fig. 4.1). The lahars are matrix supported with clasts up to 3 meters in diameter. Clasts within the lahars are angular to subrounded and consist of andesite, vesicular basalt, and non-volcanic lithic fragments. The andesite clasts are dark gray and show signs of hydrothermal alteration as evidenced by a white zeolite mineral. In the map area of the Coglan Buttes, these flows are tilted about 15°-20° to the northeast because of normal faulting.

Interstratified with these lahars are basalt lava flows and minor volcanic sedimentary beds (Muntzert, 1969). A plagioclase phyric basalt that lies at the base of the Coglan Buttes is traceable below the 1500 meter contour on the geologic map and is included in unit Tvb because it is underlain by a porphyritic andesite lava flow near 715460E 4722919N (UTM Zone 10N). This basalt unit contains abundant plagioclase and is brecciated and vesiculated near the top. This basalt transitions into the lahar units above and is interpreted to be part of the same volcanic sequence; therefore, there was no justification for them to be split into separate units. However, these basalt flows offer a

possible glimpse into local volcanism that was occurring in the fore-arc, whereas the andesitic volcanoes were producing the lahars and are far travelled.

Abundant layered tephras and breccias mapped by Appling (1950), Muntzert (1969), and White and Robinson (1992) in the Paisley Hills south of Paisley are now correlated to the Coglan Buttes section. One of the most prominent rock types they describe are lava flows with autobrecciated textures and debris flows. These types of breccias form as a result of differential cooling between the top and bottom of a lava flow from the central part, which cools slower. At mile marker 3 on Country Road 2-08, southwest of Paisley, an outcrop of an autobrecciated basalt flow interstratified with debris flows and lahars similar to those described by White and Robinson (1992) can be found (Fig. 4.2).

An X-ray diffraction analysis of a basalt flow located near mile marker 3 on County Highway 2-08 southwest of Paisley (location #1 on geologic map) shows that olivine and plagioclase are the dominant phenocrysts. As expected, the olivine is Mg-rich and the plagioclase is Ca-rich. The matrix in this basalt has been determined to contain cristobalite by X-ray diffraction. In thin section, plagioclase phenocrysts typically show albite twinning and iddingsite occurs as an alteration product on the rims of olivine.

The age of unit Tvb in the Paisley Hills is problematic. Two ages are possible, Oligocene or late-Eocene, depending on regional correlations. Muntzert (1969) correlated andesitic flows and breccias in the Paisley Hills with the andesite flows of the Cedarville Series of northern California, implying an early-Oligocene age for the Paisley Hills andesites (~32 Ma, Duffield and McKee, 1986). The Coglan Buttes section was not

taken into consideration by either Appling (1950) or Muntzert (1969). Here the units in the Paisley Hills are correlated with the andesitic lahars and minor basalt flows of the Coglan Buttes based upon their similar lithologies and stratigraphic positions. Walker and MacLeod (1991) mapped both the Paisley Hills and Coglan Buttes sections as Tca and describe them as Clarno Formation equivalents of mid-Eocene age. Therefore, it is believed by the author that Muntzert (1969) misinterprets the age of the andesite flows in the Paisley Hills because of significant horizontal and vertical changes of lithology within this section. This misinterpretation is further supported by evidence from Walker and MacLeod (1991). They found that overlying the andesites in the Coglan Buttes section exists a 200 m thick sequence of tuffaceous sedimentary rocks, silicic ash-flow tuffs, and minor basalt flows, which they correlated to the post-Clarno, John Day Formation of central Oregon. Another line of evidence is that these rocks underlie basalts correlative to the mid-Miocene (~14 Ma) Saddle Mountain Basalt (Walker and MacLeod, 1991). It is possible that the Saddle Mountain age basalt was not found by Muntzert (1969) in the Paisley Hills and therefore accounts for why he misinterpreted the age of the andesite flows.

Rhyolitic Ash Flows, Tuffaceous Sedimentary Rocks, and Minor Basalt Flows (Taf)

In the southern Coglan Buttes (location #2 on geologic map), a ~130 meter thick section of ash flows, tuffaceous sedimentary rocks, and minor basalt flows lie on top of unit Tvb. At the base of the section, a 50 meter package of fine-grained, gray to tan mudstone lies on top of unit Tvb. This unit has been correlated with tuffaceous sedimentary units in the Paisley Hills of Muntzert (1969). These tuffaceous sediments consist of mudstones and breccias. These sediments are reported to be nearly 750 meters

thick and the most widely exposed rock type in the Paisley Hills (Muntzert, 1969). Towards the top, this unit becomes dominated by basalt and rhyolitic ash-flows. About 50 meters from the base, a 20 meter thick dark gray green basaltic andesite flow occurs, which is more vesiculated towards the top, suggesting this was a subaerial flow. Overlying this basalt is a 44 meter thick succession of ignimbrite deposits. The lowermost ignimbrite is a white to light gray, unwelded ash flow approximately 20 meters thick. This unit contains sanidine and quartz crystal fragments, with nearly 15% lithic fragments and white flattened pumice clasts (Fig. 4.3). The next ignimbrite is a medium gray, slightly welded ash flow nearly 4 meters thick. This unit contains abundant sanidine crystals and minor lithic fragments and forms a prominent cliff; it is easily traceable for nearly 4 kilometers north along the 1485 meter contour. The uppermost ignimbrite is another white, unwelded ash flow. This unit is approximately 20 meters thick and contains abundant lithic fragments and is nearly devoid of any visible crystals. These lithic fragments consist of angular to subrounded vesicular basalt and pink and white pumice ranging in size from 1 mm to 1.5 cm (Fig. 4.4). Overlying the uppermost ignimbrite is another basalt flow approximately 20 meters thick. This basalt is dark gray and porphyritic, with plagioclase being the most abundant phenocryst.

The nature of the contact between Taf and Tvb is uncertain. Walker (1963) reports mammalian fossils from tuffaceous sedimentary rocks in the southern Coglan Buttes that are Arikareean in age (a North American mammalian stage from 30.6 Ma to 20.8 Ma; see Figure 1 in Albright et al., 2008), but a later map by Peterson and McIntyre (1970) reports unit Taf (their Ttf) as late-Miocene early-Pliocene in age. They incorrectly inferred the stratigraphic position from whence the fossils reported by Walker

(1963) came, which made them interpret these rocks as younger than they actually are. Here it is inferred that the map published by Walker and MacLeod (1991) correctly reports the age of this unit as early-Oligoene-early-mid-Miocene (~33.6 Ma-15.5 Ma), based on lithologic similarities and the presence of Saddle Mountain equivalent basalt stratigraphically above this unit. The upper age constraint for Taf in the Paisley Hills, where quartz monzonite and granodiorite intrude Taf, are dated at 33.6 ± 1.5 Ma (K/Ar) (Muntzert, 1969). But if the basalts in the Paisley Hills that overlie Taf are not Saddle Mountain equivalent basalts and are instead basalts derived from local vents, then it is possible that this unit is indeed late-Miocene-Pliocene. Radiometric dating and geochemical fingerprinting of the laterally continuous slightly welded ignimbrite described above would allow for a more robust correlation of unit Taf.

Intermediate to Felsic Intrusives (Ti)

Muntzert (1969) describes plutonic rocks of dioritic, granodioritic and quartz monzonitic composition exposed on the east side of the Paisley Hills. The diorite is porphyritic and contains plagioclase phenocrysts up to 5 mm in length. The second most abundant plutonic rock is granodiorite. These rocks are also pophyritic and contain abundant plagioclase crystals. The quartz monzonite intrusives contain an equal amount of plagioclase and orthoclase feldspars. Quartz in these rocks occurs as micrographic intergrowths. Hornblende and biotite are the major mafic minerals in the quartz monzonite intrusive rocks. All three of these rock types have been hydrothermally altered as evidenced by chlorite, sericite, and other alteration minerals (Muntzert, 1969). These rocks have been dated by the K/Ar method on both biotite and hornblende grains, and have an average date of 33.1 ±1 Ma (Muntzert, 1969). The timing of emplacement

for the intrusive rocks in the Paisley Hills correlates with volcanism in the Western Cascades (Lux, 1982; Verplanck and Duncan, 1987; du Bray and John, 2011). Muntzert (1969) speculated that these rocks are indeed part of the Western Cascades but are generally higher in K_2O and Al_2O_3 but lower in Na_2O, CaO, MgO, and FeO than most dioritic intusive rocks of the Western Cascades, which he relates to different magma sources. Perhaps this could also be due to the fact that these rocks rose through less mafic crustal rocks (i.e. Western Cascade magmas rose through mafic accreted rocks of the Columbia Embayment). Either way, this unit provides robust age constraints for units in this area.

Saddle Mountain Basalt Equivalents (Tsm)

In both the western and easternmost parts of the field area, a ~20 meter thick basalt lies unconformably over unit Taf, therefore making it younger than 20 Ma. North of the field area for this study, this same basalt underlies late-Miocene early-Pliocene ash-flow tuffs (6 Ma-10 Ma, K/Ar) and sedimentary rocks, as reported by Walker and MacLeod (1991). Therefore, based on these field relationships, the age of this unit can be narrowed to be between 20 Ma and 10 Ma. Walker and MacLeod (1991) have assigned this basalt unit to be correlative to the Saddle Mountain basalt member of the Columbia River Basalt Group. This assignment is at best tenuous and radiometric dating remains the only way to ascertain its exact age and stratigraphic correlation to regional units.

Mafic Intrusives (Tmi)

Southeastern Oregon is host to several dike swarms of Miocene-Pliocene age. Several dikes were found by the author and are reported in the field area from other

workers. The dikes mapped in the Coglan Hills are much larger than those found in the Paisley Hills and are vitrophyric, possibly owing to rapid cooling upon entering water bearing sediments, though no peperitic textures were observed. It is difficult to identify minerals in unit Tmi, however, some plagioclase grains can be seen. The dikes in the Coglans have a northeasterly trend and crosscut units Taf and presumably unit Tvb but do not crosscut what is interpreted to be Saddle Mountain Basalt (Fig. 4.5). This relationship constrains their age to older than the assigned mid- Miocene (~16 Ma) of the Saddle Mountain Basalt. Alternatively, because they do not crosscut the Saddle Mountain basalts they could be local feeder dikes to this member.

In the Paisley Hills similar cross cutting relationships of the basaltic dikes to the surrounding stratigraphy are observed. However, they differ in their general direction of strike, changing from NE-SW in the Coglan Hills to NW-SE in the Paisley Hills. In Figure 4.5 it can be seen that a basaltic dike cuts unit Tvb. It was more difficult to determine the relative ages of these basalt dikes in the Paisley Hills than it was in the Coglan Hills. Nevertheless, one explanation for the emplacement of these dikes is that they are also feeder dikes to the Saddle Mountain Basalts located in the Paisley Hills (Plate 1). Another explanation is that they could be feeder dikes to Pliocene mafic volcanic centers. This interpretation stems from the fact that these dikes trend northwest, parallel to the strike of major normal faults in the area and are thus likely related to the onset of extension in the Pliocene. However, no substantial evidence was found to support the latter conclusion; therefore, they are interpreted to be a part of the same event which emplaced dikes in the Coglan Hills.

Rhyolite Lava Flows and Domes (Tsv)

Several rhyolite lava flows (Tsv) were mapped in the western part of the field area. They are pale red to gray in color and often form prominent outcrops. Two features make these rocks easily identifiable in the field, they are heavily fractured and often exhibit flow banding (Fig. 4.6). Fractures in these rocks are often at a high angle to the flow banding and were used to help distinguish them from other rock types in the field. The matrix in these rocks is often a pinkish gray color with white plagioclase phenocrysts coalescing into layers to create the flow banding. Muntzert (1969) also mapped several of these rhyolite lava flows in the Paisley Hills and describes the same flow banding texture. Lava flows mapped by the author often display minor amounts of alteration, which is in accordance with flows mapped by Muntzert (1969).

One flow associated with unit Tsv was analyzed by petrographic and X-ray diffraction methods to determine mineralogy and texture. Under the microscope alkali feldspar, most likely anorthoclase was identified. The temperature was probably not great enough within the magma chamber in which this flow originated to produce sanidine, the K rich end-member in the anorthoclase-sanidine solid solution system. This feldspar also exhibits Carlsbad twinning, which is not seen in sanidine. The identification of this mineral was substantiated by X-ray diffraction where two peaks at 21.88 2θ and 27.68 2θ match well with peaks created by pure anorthoclase. Most of the feldspar grains are fractured and partially replaced by an unidentified grey mineral. The fractures seen in the feldspars could be the result of fracturing during flow, during cooling, or perhaps from crystal inversion, during changing to a lower temperature polymorph. Biotite was also identified in thin section by its brown color and strong

pleochroism in plane polarized light. A large peak at 8.82 2θ confirms that this is biotite. The groundmass in this rock is amorphous as indicated by its lack of any observable optical properties and lack peaks in its X-ray diffraction pattern.

A rhyolite dome located at 709400E 4714824N in UTM Zone 10N is locally known as Tucker Hill. Another rhyolite dome is located at 695184E 4717741N UTM Zone 10N and is known locally as McComb Butte. These domes have been dated by MacLeod et al. (1976; K/Ar) at 7.42 ± 0.19 Ma and 7.71 ± 0.09 Ma, respectively. Muntzert (1969) describes rhyolite flows in the Paisley Hills exhibiting radial fracture patterns, suggesting a local source for flows in the area. This is also supported by the fact that rhyolite flows are highly viscous and will not travel far from their source. This could be substantiated by detailed geochemical work on the flows and on local vents to determine their relationship. These domes have been interpreted to be part of the Newberry Trend, a belt of rhyolitic volcanic centers trending from southeastern Oregon to Newberry Crater complex (MacLeod et al., 1976; Jordan et al., 2004).

Volcaniclastic Sedimentary Rocks (Tvs)

In the northwestern part of the map area, a ~5 meter thick, poorly consolidated unit consisting of arkosic and volcaniclastic sandstone is present. This unit is dominated by interbedded red and white colored units averaging about 50 cm in thickness. Some of the red layers occur as lenses within the white layers. This unit exhibits cut and fill structures suggestive of floodplain deposits in some areas (Fig. 4.7). The clasts in these units are well-sorted and are generally angular to subangular. Clast size ranges from fine to coarse. The red color is interpreted to be due to the alteration of feldspars. The white beds in this unit are interpreted to be more clay-rich, a result of weathering of volcanic

glass. This unit has been mapped by Badger and Watters (2004) in the fault scarp of the Winter Rim Fault, ~3 km to the northwest, where it dips westward 5°-10°. In the Paisley area, this unit is nearly horizontal but is cut by several small displacement normal faults (Fig. 4.7). This unit has been assigned mid-Miocene age by Walker and MacLeod (1991) based on plentiful vertebrate and plant fossils. It is possible that this unit is younger immediately adjacent to the Paisley area as several clasts of perlite were found in the cut and fill structures. This perlite is interpreted to have come from local rhyolite volcanic centers, which have been dated at 7-8 Ma, making it late-Miocene in age (Peterson and McIntyre, 1970; MacLeod et al., 1976). The total thickness of this unit is unknown and therefore this age could be a minimum and could represent the upper part of the unit; therefore, a mid-late-Miocene age is assigned for this unit.

Mafic Volcanic Rocks (Tmv)

A mafic volcanic center has been mapped directly southwest of Paisley, Oregon (location #3 on geologic map). This unit is contains a variety of mafic volcanic and volcaniclastic rocks produced at a Strombolian type volcano. Lava flows, scoria, fine lapilli, and basaltic ash are the main deposits of this unit. Lava flows are highly vesicular and amygdaloidal with zeolites often filling the vesicles. In hand specimen, the zeolites are commonly pistachio green and white and are translucent to transparent, and they display both botryoidal and fibrous textures. Most of the zeolites are soft and can be scratched with the fingernail. Plagioclase is the dominant phenocryst with minor olivine. If olivine is present, it has been altered to iddingsite, as evidenced by its red color. Most lava flows have autobrecciated tops and bottoms with a well-defined central core containing variable degrees of columnar jointing. Basalts higher in the section typically

show spheroidal weathering, creating onion like weathering patterns and in places are palagonitic, suggesting interaction with external water at the time of deposition (Fig. 4.8).

Fine lapilli stone is also a dominant rock type in this unit. This rock is typically light purple and contains virtually no crystals. The small grain size is due to a greater degree of fragmentation contemporaneous with its eruption. At the location 698683E 4728651N UTM Zone 10N, there are abundant rocks of this type with heavy calcite mineralization. Euhedral calcite grains within the matrix as well as vein calcite are present. This mineralization is evidence of hydrothermal fluids having circulated through these rocks. Quartz veins are also dominant in this area.

This unit is considered to be of Mio-Pliocene age due to its stratigraphic position. However, given its proximity to a major range-bounding fault (i.e., the Paisley Hills fault; Plate 1), it could be strictly Pliocene. If the latter is true, then this unit could reflect an episode of Pliocene extension and associated basaltic magmatism. The difficult nature of the contacts between this unit and units both above and below, coupled with poor exposure, has led to a tenuous age determination for unit Tmv.

Fluvial and Lacustrine Sediments (Qfl)

Ancient Lake Chewaucan (Fig. 1) had it highstand at a present elevation of 1378 meters around 16.8 ka and was nearly 114 m deep at this time (Negrini and Davis, 1992; Licciardi, 2001; Badger and Watters, 2004). Wave-cut terraces are present in Summer Lake Basin, representing shorelines of the lake during its regression into its current location. A large and complex fluvio-lucustrine fan delta system was formed near Paisley where the present-day Chewaucan River flows into the Upper Chewaucan Marsh of the greater Summer Lake Basin.

Course sand, gravels, and conglomerates are dominant in this fan delta near the range front and grade laterally into fine sands and silts stepping away from the range-front. Gravel and sand-sized clasts in this unit consist of quartz grains, lithics of basalt and vesicular basalt, and are typically well-rounded. Silt-sized particles are typically quartz.

Regional Structure

The Neogene structural history of the Paisley area is complex and the structural architecture has a profound impact on the transport of fluids in geothermal systems; therefore, understanding the regional structural framework is essential to characterizing and understanding the Paisley resource. Prior to work done in this study, the role of fault intersections, en echelon faults, and transfer zones in the development of the Paisley geothermal system was unevaluated, but is shown here to be important. These types of structures have been identified in the western Great Basin and shown to be extremely important in controlling thermal fluid flow (e.g., Faulds et al., 2006).

Folding

According to Peterson and McIntyre (1970), rocks of pre-Pliocene age have been folded into low amplitude anticlines and synclines. In the Paisley area, an anticlinal axis trending northwest has been identified by Peterson and McIntyre (1970) in a line connecting Silver Lake, Summer Lake, and Goose Lake, Oregon. Evidence for this in the rocks mapped in the Paisley Hills is that they are dipping ~45° to the northeast because they lie east of the fold axis defined above and because rocks west of the fold axis dip to the west. In support of their idea, they cite Walker et al. (1967) and state that the folding

is apparent in Walker's cross section. However, given the shallow dips reported in the tilted units, the apparent "folding" could possibly be explained by changes in normal fault dip direction (see Walker et al., 1967). Hence, it is unclear if the apparent folding of these rocks is related to young tectonic stresses or due to an earlier regional compressive event, or perhaps even by the emplacement of localized volcanic centers. The emplacement of the volcanic centers has been dated by the K/Ar method at 33.6 ± 1.5 Ma (Muntzert, 1969). Muntzert (1969) interpreted the tilting of units Tvb and Taf in the Paisley Hills with the emplacement of plutonic quartz monzonite, diorite, and granodiorite. However, this does not explain the tilting of units younger than these intrusives. Subsequent tilting in the Paisley Hills and in the Coglan Buttes is interpreted to be related to rotations associated with normal faulting.

The tilting of these rocks may have played an important role in the development of the Paisley geothermal system. Because the topographically high areas lie SW of Paisley and the beds dip to the NE, water could enter the ground in these high places and flow along boundaries of, or within, these dipping beds. This will be elaborated upon in the Conceptual Model and Conclusions section.

Faults

Two main orientations of normal faults occur in the Summer Lake area. The highest frequency of these faults trend northwest (~307°) and have less offset relative to the northeast trending (~30°) set of faults (Fig. 4.9). Donath (1962) first documented the two orientations of faults in the area east of Summer Lake. The NW striking faults are interpreted to be part of the Brothers Fault Zone, a series of en echelon normal faults that form the northern boundary of the Basin and Range Province (Lawrence, 1976; Trench et

al., 2012). Northeast striking faults such as Abert Rim, Slide Mountain, and Winter Ridge are most likely caused by northwestward migration of Basin and Range-related stress into southeast Oregon (Scarberry et al., 2010). It is interesting to note, however, that the axial trend of the Summer Lake graben is roughly parallel to that of a southern arm of northwest migrating silicic volcanic centers of Pliocene age, which is roughly coeval with the initiation of these faults (Walker and MacLeod, 1991; Pezzopane and Weldon, 1993; Scarberry et al., 2010). The close temporal association between these two entities suggests that they could be related.

Initiation of Faulting

The age of initiation of the NE striking normal faults in southeast Oregon was around 10-7 Ma, constrained by $^{40}Ar/^{39}Ar$ dating and cross-cutting relationships (Scarberry et al., 2010). This is much younger than the age of normal fault initiaition in the central Basin and Range province, which began around 17-14 Ma (Colgan et al., 2006; Egger and Miller, 2011). The only exception in southeast Oregon is the Steens Mountain Fault, which intiated at ~16.6 Ma (Scarberry et al., 2010). Winter Ridge (Fig. 1.1) is one of these major normal faults that initiated in the latest Miocene (~$\leq$6.6 Ma) (Walker and MacLeod, 1991; Jordan et al., 2004; Scarberry et al., 2010).

The initiation of NW striking faults in the area east of Summer Lake is less well-constrained than faults with similar orientations in the westernmost Northern Basin and Range. They are here thought to be slightly younger and coeval with the Basin and Range faults of southeastern Oregon. The faults that constitute the Brothers Fault Zone allowed magma to be emplaced at the base of the crust (e.g., Jordan et al., 2004). If the same northwest younging of silicic volcanic centers of the Newberry Trend is then

related to the initiation of faulting associated with that volcanism, then the faults would have initiated around 7.42 ± 0.19 Ma (K/Ar age of Tucker Hill) in the area mapped near Paisley (MacLeod et al., 1976). This is consistent with the 7.5-7 Ma $^{40}Ar/^{39}Ar$ dates published by Scarberry et al. (2010) for the initiation of the NE-striking Abert Rim fault ~40 miles east of Paisley.

Quaternary faulting has also been identified in Summer Lake Basin. Latest Pleistocene faults offset lacustrine sediments of ancient Lake Chewaucan at the Slide Mountain fault (Silvio Pezzopane, personal communication, 2012). A north-trending, west-dipping normal fault offsets Pleistocene fluvio-lucustrine sediments by about 3 meters located near UTM 10N 700287 4729817. The strike of this fault is oriented parallel to the range front normal fault near Paisley but dips in the opposite direction, making it antithetic to the main range bounding fault.

The Paisley Transfer Zone

A transfer zone connecting two en echelon normal faults on the western side of Summer Lake Basin just north of Paisley is controlling regional thermal fluid flow (Figs. 1.1 and 4.10), and this is referred to here as the Paisley Transfer Zone. The en echelon normal faults are active in the Quaternary and display dip-slip displacement (Pezzopane and Weldon, 1993; Badger and Watters, 2004). It is interesting to note that transfer zones typically consist of a strike-slip fault that acts to accommodate strain between to en echelon normal faults; however, in the Paisley Transfer zone, the transfer fault is a normal fault, despite the fact that it separates two en echelon normal faults. This begs the question on how accurate the motion has been constrained on the early motions of the Winter Ridge and Paisley Hills faults. They undoubtedly have dip-slip motion because

they create large topographic features, but reconciling how a dip-slip fault accommodates strain between two en echelon normal faults is difficult. Perhaps, this transfer fault is younger than the Winter Ridge and Paisley Hills faults that were once one linear structure, and is now the result of a change to oblique motion in NW-trending faults across central Oregon (Pezzopane and Weldon, 1993). Another hypothesis is that relative rates of motion are different on the Winter Ridge and Paisley Hills faults, thus creating a transfer fault to accommodate this differential motion.

Regional Heat Flow

Areas of active crustal extension are typically associated with an elevated geothermal gradient and associated high heat flow. It was discussed in the previous chapter how heat flow can be used as a tool to guide exploration for geothermal resources. Based on measurements taken from regional and two local boreholes, Figure 4.11 shows the distribution of heat flow in southern Oregon, northern Nevada, and northern California (Global Heat Flow Database of the International Heat Flow Commission, University of North Dakota). Heat flow measurements range from 45 mW/m^2–388 mW/m^2. A large area of high heat flow averaging 235.9 mW/m^2–273.97 mW/m^2 is located in Warner Valley and extends northward into Summer Lake Basin and eventually terminates in Christmas Valley.

High heat flow in Warner Valley, Summer Lake Basin, and Christmas Valley is attributed to both active extension and young basaltic volcanism (Walker and MacLeod, 1991; Pezzopane and Weldon, 1993; Eggar and Miller, 2011). This map shows that the area immediately adjacent to Paisley is a zone of high heat flow. Also, the heat flow anomaly shown in Figure 4.11 lies near the edge of the Basin and Range Province, which

highlights the importance of both high regional heat flow coupled with the architecture of regional faults, for the potential of geothermal resources in southeast Oregon, and specifically Paisley.

Aqueous Geochemistry

The chemistry and isotopic compositions of thermal fluids can fingerprint their origins and also help determine reservoir conditions. For the Paisley geothermal resource, several local wells, springs, and a local river were sampled. The application of aqueous geochemistry and stable isotopes of water was aimed at fingerprinting the source, potential age, and conditions within the reservoir. This was done by using standard practices in geothermal exploration to assess their relevance to the Paisley resource.

Major and Minor Elemental Analysis

It was discussed in Chapter Three how the analysis of major and trace elements of thermal fluids can be used to delineate origin, mixing, and predict the thermal state within the reservoir. Table 1 shows the results of the chemical analysis performed on water from wells and springs, and on local meteoric water sources for the Paisley system. In general, the wells sampled are slightly alkaline with pH values ranging from 7.4-9.25. These same waters are high in Na and HCO_3. Colahan Hot Well, Corky's Well, Summer Lake Hot Springs, Calf Pen Well, and Trailer Park Well (Fig 4.12) are all low in Mg, suggesting minimal mixing with meteoric water.

The thermal waters in Paisley do not display a signature of magmatic contribution. This is illustrated by a $Cl\text{-}SO_4\text{-}HCO_3$ diagram (Fig. 4.13), which shows the

type of waters present, potential mixing, and suitability for use in geothermometry (Giggenbach, 1992). Two types of water are identifiable from this diagram, SO_4 and HCO_3 dominated waters. From this diagram, the samples in the SO_4 domain are classified as acid sulphate and include Colahan Hot Well, Corky's Well, SVEC-1, and SVEC-2; however, the pH of these samples are all slightly alkaline. This suggests that SO_4 dissolved in these fluids is not of magmatic origin but rather from a salt despite the fact that this diagram was created with the assumption that all SO_4 in the geothermal system is of magmatic origin (Giggenbach, 1988). If these fluids were heated by volcanic gases, the oxidation of these gases (i.e., H_2S and SO_4) and the condensing CO_2 steam would create a pH near 2.8 (Nicholson, 1993). However, the pH of the fluids range from about 7-8; therefore, the high SO_4 concentrations are interpreted to have come from elsewhere. It is worth noting that fluvial and lacustrine sediments (Qfl, Plate 1) lie stratigraphically above the thermal reservoir in which these fluids are derived. If recharge to the thermal aquifer happens from downward percolating water through these sediments, this water would become more saturated with evaporate derived SO_4. It is therefore possible that some of the aqueous SO_4 is a result of the dissolution of gypsum and other evaporates contained in these sediments. Caution is taken in using this type of water for geothermometry as the dissolved constituents are not the result of water rock reactions taking place in the reservoir but instead reflect reactions happening in near-surface environments. The classic interpretation of acid sulphate waters is that the oxidation of the volcanic gases H_2S and SO_4 create highly acidic waters, which get mixed into groundwater, thereby indicating that the thermal reservoir in which the steam is derived lies underneath the shallow waters (Nicholson, 1993). This hypothesis is null

since it has been interpreted that the SO_4 in the Paisley thermal wells comes from percolation of meteoric water to the thermal aquifer.

Samples residing in the HCO_3 domain of Figure 4.13 are classified simply as HCO_3-dominated waters. Most of the samples in this domain are wells drilled for irrigation purposes and are not hot. Exceptions to this are Little Hot Well and Summer Lake Hot Springs. It is interpreted that the cool, HCO_3-rich waters are examples of local groundwater, residing in shallow aquifers consisting of fluvio-lacustrine sediments. The hot samples that reside in HCO_3 corner of Figure 4.13 are therefore the result of mixing between shallow groundwater and thermal water. As such, they are not useful indicators of the thermal conditions in the subsurface (Nicholson, 1993).

The Na-K-Mg diagram is used to assess mixing trends between thermal and nonthermal waters and to calculate the coupled Na/K and K/Mg geothermometers (Appendix A). Na and K in this system comes from the dissolution of feldspars in the subsurface, where their concentrations are a function of the water's temperature, pH, and residence time within the reservoir. Mg solubility rapidly decreases with increasing temperature; therefore, the concentration of Mg in thermal waters is used as a proxy for mixing with non-thermal meteoric water. The composition of alkaline lakes of southern Oregon and California taken from Hantelmann (2006) and Drever (1982) are also plotted in this diagram for comparison between regional lakes and waters sampled in the Paisley area. It can be seen on Figure 4.14 that there is a clear mixing trend between thermal waters and groundwaters from wells in Paisley. A line drawn from the compositions of Summer Lake water to the Mg corner of the diagram defines a mixing line of meteoric water to Summer Lake water. Most of the thermal waters from the Paisley geothermal

system lie on this line. It can also be seen that most of the samples measured that lie along the mixing line in Figure 4.14 lie in the partial equilibration sector. This is interpreted to be because of the mixing, which is occurring between thermal and nonthermal waters (i.e., local groundwater). A maximum temperature of 160 °C is read from this diagram and is determined by the combination of the Na/K and K/Mg geothermometers. The results of this diagram coincide well with the results from the analysis of the Cl-SO_4-HCO_3 diagram.

The Li-Cl-B ternary diagram was also constructed to help assess the source of these waters (Fig. 4.15). Boron in geothermal waters is typically used to evaluate the possibility of boiling caused by adiabatic cooling. The source of B and Cl is volcanic gas and high B/Cl ratios are associated with younger systems because of B's high volatility, which leads to it being expelled from the thermal water early in the formation of the volcanic geothermal system (Giggenbach and Soto, 1992). The ratio of B/Cl can therefore be used to determine the amount of boiling and age of the thermal system. Lithium is dissolved from mafic rocks by thermal waters and will be taken up into secondary quartz upon precipitation out of the thermal water. The amount of lithium present is therefore a function of how much quartz has been precipitated from solution. Figure 4.15 is important for the geothermal system near Paisley because it demonstrates that due to low B/Cl ratios, this system shows no definitive association with a magmatic heat source.

The F-Cl-B ternary diagram (Fig. 4.16) provides information to help delineate possible sources of water. This diagram assumes that F is from volcanic rocks, and behaves as a conservative element (not readily taken up by precipitating solids), thereby

making it a useful tracer for geothermal fluids. Figure 4.16 shows that most samples cluster in the same area of the diagram, suggesting that there is only one source of thermal fluid, at least for the samples that were collected. It is suspected by the author that there are several geothermal aquifers in Summer Lake Basin and the samples plotted in Figure 4.16 only represent one, but most likely two such aquifers or sources. The Summer Lake Hot Springs waters lie outside the cluster of points representing the Colahan Hot Well, Corky's Well, SVEC-1, and SVEC-2 wells. This suggests, based on their F concentrations, these reservoirs are of different origin or are not connected hydrologically. The large deviation of the HWOct point is anomalous and is regarded as a bad data point because of mixing with other water. This deviation could also be the result of contamination during the sampling process.

Other constituents such as As and NH_4 were also measured for fluids in the Paisley area. High concentrations of As in thermal fluids is typically interpreted to be the result of a magmatic heat source (Nicholson, 1993; Arehart et al., 2007). The concentrations of As in the Paisley waters are low, ranging from 0.004-0.6 mg/kg. These low values suggest that the Paisley geothermal system is not directly heated by a magmatic source, but rather is typical of Basin and Range-type geothermal systems where heat is derived from the overall high geothermal gradient. This interpretation also agrees with the fact that these are not acid-sulphate waters per se, if they were they would be highly corrosive due to the low pH and would undoubtedly leach more As from the host rock. Though these values are low relative to magmatic geothermal systems, the concentrations are high enough that they warrant careful consideration when dealing with the effluent waters created during operation of the geothermal power plant (i.e. they

cannot be introduced into the local groundwater as the concentrations are too high for human consumption).

Ammonia (NH_3) typically occurs in geothermal systems as the dissolved ion ammonium, NH_4^+ (Nicholson, 1993). This element is also typical of geothermal systems heated by a magmatic source. The concentrations of NH_4 in the Paisley waters range from 0.2-1.8 mg/kg. The concentrations are low enough in these waters to rule out the possibility of a magmatically heated system.

Geothermometry

Reservoir temperatures have been calculated using standard methodology based on both cation and silica geothermometers. Table 2 and Table 3 shows the results of the geothermometry calculations. The measured temperature at the bottom of SVEC-1 was 110 °C. The cation geothermometers have temperatures that range from 95 °C-166 °C. The calculated temperatures are in approximate agreement with the measured temperature in well SVEC-1, suggesting that they are accurately predicting the maximum temperature possible within the reservoir. For most of the thermal wells and springs measured, the K/Mg geothermometer is consistently lower than the Na/K geothermometer of Giggechbach, which suggest rapid ascent to the surface. If these two geothermometers are in agreement, then the sampled water has had time to come into equilibrium, as the Na/K system takes longer to become equilibrated than does the K/Mg system; therefore, the degree of separation between the two calculated temperatures can be used as a gauge to how quickly the water rose. It appears the water in the Paisley system rises rapidly enough to cause a difference in reported temperatures between these two systems.

It was recommended by Giggenbach (1992) that the cation geothermometers be used with caution in acid-sulphate waters, but several authors have found that the predicted subsurface temperatures agree well with other geothermometers despite not being alkali-chloride waters (e.g., Sladek et al., 2004; Hantelmann, 2006; Garcher and Arehart, 2008). Problems with the cation geothermometers arise when the fluid source for a particular geothermal system is meteoric and must flow through sedimentary rocks (e.g., the Basin and Range-type systems). Many of these Basin and Range basins contain various aqueous salts in their lacustrine sediments precipitated as evaporites. Thus, waters that are in reservoirs of this rock type, or circulate though such sediments will likely display increased amounts of dissolved constituents such as Ca, Na, K, and SO_4, thereby introducing error in the cation geothermometers.

The silica geothermometers report reservoir temperatures that range from 116 °C-161 °C. The amorphous silica geothermometer reports a range of temperatures from 21 °C-38 °C for the Colahan Hot Well, which is clearly not accurate. This latter result is because the equation derived for this geothermometer was created for high temperatures and large errors occur below about 140 °C (Garcher and Arehart, 2008). At temperatures below 140 °C, the chalcedony geothermometer most accurately predicts subsurface temperatures (Fournier, 1992). The range in calculated temperatures from the chalcedony geothermometer is 116 °C-136 °C for the Colahan Hot Well and wells SVEC-1 and SVEC-2. These values are feasible, considering a measured well temperature of 110 °C. It is believed that the silica geothermometer works for the Paisley geothermal system, despite being categorized as acid sulphate waters, because the presence of SO_4 is not the result of volcanic processes but rather from the dissolution of

salts during the downward percolation of meteoric waters to the thermal aquifer. This works because the silica geothermometer was developed for near neutral waters, which is the case for most thermal waters measured in Paisley. The slight alkalinity in the aqueous solution could be the result of CO_2 steam loss during boiling, which would also allow for the dissolution of more silica during ascent and may account for the maximum temperatures reported from the silica geothermometer.

Stable Isotope Analysis

Stable isotopes have been used extensively to help predict the source of water in geothermal systems. Water of meteoric source has a predictable isotopic value, often denoted on plots of δD vs $\delta^{18}O$ as the Global Meteoric Water Line (Craig, 1961). Though the heat source in magmatic and Basin and Range-type geothermal systems differ, both are recharged by meteoric source water. However, if fluids derived from the degassing of a shallow magmatic body mix with meteoric waters, they tend to follow a mixing line up and to the right (Fig. 4.17) of local meteoric samples, often referred to as the andesitic water mixing trend (Powell and Cumming, 2010). Alternatively, if the geothermal system is of Basin and Range type (i.e., not heated by an igneous body), samples typically plot to the right of the meteoric water line, evidence of fluid rock interaction.

It was hypothesized by the author that the thermal water in the Paisley geothermal system is of local meteoric origin. To help assess the source and reservoir residence time of the Paisley thermal water, samples collected from the Chewaucan River, wells SVEC-1 and SVEC-2, were analyzed for the isotopic composition of hydrogen and oxygen to compare to those values for the thermal wells. Figure 4.17 shows the isotope data plotted

as δD vs $\delta^{18}O$ along with the global meteoric water line. As expected, the Chewaucan River plots directly on the meteoric water line, however, none of the thermal samples plot on the meteoric water line.

In geothermal systems being fed by modern meteoric water, the $\delta^{18}O$ value becomes less negative due to the enrichment of ^{18}O from water-rock interactions (e.g., Taylor, 1974; Criss and Taylor, 1986; Giggenbach and Soto, 1992; Smith et al., 1992; Krahmer, 1995; Smith et al., 2002; Sladek et al., 2004). The enrichment of ^{18}O results in a shift directly to the right relative to the meteoric water line from local meteoric samples plotted on that line.

This leads to a second possible interpretation where the enrichment in water in both D and ^{18}O could be produced by evaporation of groundwater near the surface and would manifest itself on a diagram similar to Figure 4.17 in a shift up and to the right from the meteoric value of water from that same location. This shift is similar to the one produced from meteoric water mixing with volcanic waters (i.e., the andesitic water mixing trend).

A third hypothesis for the shift in δD values is that the recharge to the aquifer comes from water originating at higher elevations; but again, this would require a depletion of both D and ^{18}O. Therefore, the shift in isotopic composition of the Paisley thermal waters cannot be accounted for by this process.

A fourth possibility for the Paisley thermal waters is that they are old, Pleistocene waters. This is hypothesis is preferred by the author. It has been shown by Smith et al. (2002) that the isotopic composition of meteoric water from the Pleistocene of the Great Basin is lighter, evidenced by more negative δD and $\delta^{18}O$ relative to current meteoric

waters. If the points representing the thermal samples on Figure 4.17 are extrapolated back to the meteoric water line about a horizontal line (i.e. depleting ^{18}O), then values of δD and $\delta^{18}O$ of -120‰ and -16.5‰, respectively, are obtained. This corresponds to a change in δD values from -106‰ to -120‰ and a change in $\delta^{18}O$ from -14.2‰ (average) to -16.5‰. This is a change in δD values of about 14‰, consistent with the results of Smith et al. (2002), suggesting that the Paisley water may be Pleistocene age waters, and thus this is a "fossil" geothermal system.

The results of this analysis also have implications for the length of time geothermal systems are active. Geothermal systems typically last on the order of 1,000 to 10,000 years but can last as long as 10^6 years (Rybach, 1981; Nicholson, 1993; Coolbaugh et al., 2005; Person et al., 2008). Basin and Range-type geothermal systems owe their longevity to continued seismicity and the fact that faults can be active for millions of years (Coolbaugh et al., 2005). Evidence that the water in the Paisley geothermal system is Pleistocene comes from its stable isotope composition. It also reflects water-rock interaction by the enrichment of ^{18}O, which if enough time is spent in the reservoir, will move towards isotopic equilibrium with the host rock, the rate of which is dependent on the temperature of the system. A higher temperature system would allow the fluid and host rock to reach equilibrium faster because partitioning of isotopes between two materials is almost entirely temperature dependent (McSween et al., 2003). However, it is not possible to determine residence time with stable isotopes alone but can be used to a first order to say that the water has or has not spent a significant amount of time within the reservoir.

Gravity Survey

In order to assess the subsurface structure, a gravity survey was conducted over the Paisley site. A gravitational anomaly may be produced when a major range bounding fault juxtaposes less dense basin fill in the hanging wall (i.e., unconsolidated sediments) against more dense bedrock in the footwall. The goal of this survey was to identify such a fault in the Paisley, Oregon area, and the results of this survey confirm that there is a major structure at the Paisley Hills front.

Regional Gravity

The regional gravity of southeast Oregon suggests that there is a major transition of structural architecture between the Basin and Range and the Cascades to the west, evidenced by changes from northwest-oriented linear anomalies of the Basin and Range to north-south oriented anomalies of the Cascades (Veen, 1981). This change in orientation is related to the trends of major structural features and to north-south oriented structures of the Cascades, respectively (Fig. 4.18). A regional gravity survey northeast of Summer Lake by Cox (2011) of High Lava Plains suggests that the crustal structure of this area is similar to that of the Basin and Range of northern Nevada, i.e., the silicic volcanism of the Newberry Trend has not modified the upper crust in a significant way, contrary to that of its mirror image, the hot spot trend of the Eastern Snake River Plain. This is important to geothermal resources of southeast Oregon because it suggests that this volcanism may have little influence on upper crustal fluids (i.e., those that are important to geothermal systems).

A few gravity studies have been conducted near Summer Lake to try and delineate structures buried by sediments in the basin. Muntzert (1969) noted that there is

a closed gravity anomaly in the Paisley Hills, possibly suggesting a buried magma body. Travis (1977) conducted a gravity survey in the area near Summer Lake to determine basin depth and east of Summer Lake to determine possible origin of arcuate-shaped faults. He discovered that the basin could be as deep as 2 km but did not have the gravity station density required to model the arcuate shaped faults at the north end of Summer Lake Basin. Blank (1973) also determined a depth of Summer Lake near 2 km based on a gravity survey.

Results

The equations and MATLAB© script used here to reduce the raw gravity data can be found in Appendix B. The methodology of the survey was given in Chapter One. The range in gravity values for the Simple Bouguer Anomaly is from -9.8088e5 to -9.8079e5 mgals. The range in gravity values for the Complete Bouguer Anomaly range from -9.8085e5 to -9.8065e5 mgals. It is important to note that these values are not typical of other gravity surveys because no measurement was taken at an absolute base station; therefore, this survey is not tied into the global gravity network. Figure 4.19a and b are plots of the Simple and Complete Bouguer Anomaly produced directly from the MATLAB© script that was written for this study. The results show a well-defined gravity contrast trending in a northeast to southwest direction. This contrast would suggest that there are materials of different densities immediately adjacent to each other. One way to explain this is that a fault juxtaposes these two materials of different densities. This is where the range front fault has been interpreted to be based on geologic mapping and the gravity data confirms the existence and position of this fault.

Figure 4.19c and d are the Simple and Complete Bouguer Anomaly overlain on aerial imagery near Paisley. The wells sampled for this study are shown with the fault identified by the gravity survey and by geologic mapping. These figures are much more intuitive and perhaps show much more detail in the subsurface distribution of density. There is still a nicely defined density contrast in the southwest part of the survey, which as mentioned previously is the signature of a fault. It is interesting to note what is happening in the northeast corner of Figure 4.19d, where a gravity high is located. It is difficult to interpret if this high represents a flaw in the terrain correction process or whether it is a real geologic phenomenon.

Lithologic Well Logs

Samples of well cuttings were collected from wells SVEC-1 and SVEC-2 during drilling to establish the subsurface stratigraphy. These samples were then cleaned, dried, and catalogued in the laboratory. Samples were cleaned with water under a 200 mesh sieve. After cleaning, descriptions were made using a binocular microscope with 20x magnification. Figure 4.20 shows the lithologic logs for both wells.

The upper 400 feet of well SVEC-1 consists of mostly brown sand, gravel, and cobbles. The clasts are dominantly basalt in composition but range from quartz, feldspar, and lithic fragments of basalt. From about 400 to 540 feet, the average grain size decreases to sand, silt, and clay. Several interstratified ash layers are also present. These ash layers are also abundant in clay, most likely created from alteration of volcanic glass. In the interval from 540 feet to 680 feet, the average clast size coarsens to gravel and boulders.

Bedrock is encountered at ~680 feet, which is evidenced by a fractured basalt unit. Basalt lava flows, interpreted from trachytic textures, are the dominant rock types in the interval from 680-710 feet and from 795-905 feet. Along with basalt lava flows, red cinders with high degrees of calcification occur at various depths between the interval of 800-850 feet. These cinders are vesicular to amygdaloidal and are typically 1-2 mm in size and slightly rounded. The amygdules contain white, cream, pale yellow, and light green translucent minerals, most likely zeolites formed either during initial cooling or from the later action of hydrothermal fluids. The basaltic units are all highly altered and contain euhedral quartz, calcite, and pyrite. Abundant red cinders are found with varying amounts of alteration is present in the interval from 995-1030 feet. Most of the units below 1030 feet to total depth (1182 feet) are altered ash beds with varying amounts of lithic fragments and degrees of alteration. Pyrite is an abundant secondary mineral that is often seen with and inside of quartz grains and also as small cubic grains.

Petrographic and X-ray diffraction analyses were conducted on samples at depths of 895, 995, 1095, and 1197 feet from well SVEC-1. At all depths, basalt was the dominant rock type. Minerals within the basalt are sub to anhedral in a microcrystalline groundmass. The dominant feldspar is plagioclase but due to alteration and associated optical degradation, exact composition was impossible to ascertain by optical methods but X-ray diffraction analysis revealed that andesine was the abundant plagioclase minerals. Albite was also identified but probably represents an alteration product, not a primary mineral in basalt. Zonation in plagioclase was also observed with the most abundant being at 1095 feet. Some basalt grains exhibit trachytic texture evidenced by layering of plagioclase feldspar phenocrysts. Remnants of olivine phenocrysts are

present but have been altered to iddingsite. The amount of alteration increases with depth where samples at 1197 feet are weathered to the degree that original rock types could not be determined. Along with the increase in alteration of primary volcanics comes an increase in alteration minerals such as quartz and calcite. Calcite grains as large as 2 mm were identified and can be seen to grow at the expense of the matrix of basalt grains. X-ray diffraction analysis on all samples reveals that the dominant zeolite minerals in all samples are phillipsite, sodalite, heulandite, analcime, and clinoptilolite; all of which are Na-K-Ca rich tectosilicates. The implications of the presence of these will be discussed later. Major clay minerals include smectite, illite, and montmorillonite.

Similar to SVEC-1, well SVEC-2 is dominated by Plio-Pleistocene sediments deposited in a fluvio-lacustrine environment. The upper ~500 feet consists of rounded sand and silt grains of dominantly basaltic composition. Below 500 feet, the well encounters bedrock of mostly basaltic andesite and basaltic composition. Most of these basalts are olivine and plagioclase phyric with phenocrysts typically <1 mm in length. Plagioclase phenocrysts exhibit trachytic textures. Opaque minerals constitute almost 15% of basalt grains and are most likely magnetite. All samples show some degree of alteration, becoming more altered at greater depths. They are also generally more altered than samples from SVEC-1. Alteration minerals include both euhedral and amorphous quartz, rhombic calcite, and a preponderance of zeolite minerals. Similar to well SVEC-1, SVEC-2 contains abundant zeolite minerals including heulandite, phillipsite, sodalite, laumontite, and stilbite identified from x-ray diffraction analysis.

Alteration Mineral Assemblage

X-ray diffraction analyses were performed on samples from wells SVEC-1 and SVEC-2 for alteration mineral assemblages. Samples used for X-ray diffraction analysis were not washed in order to preserve the clay content within them because under the sieve, the clay fraction is lost and it was deemed important to have that clay fraction for x-ray studies. The purpose was to focus on zeolites and to assess their implications for reservoir temperatures from mineral stability diagrams. This also provides an independent check of the geothermometers described above. Preparation for analysis included washing, drying, and creating a powder. A powder is created because this increases the potential for random orientation among mineral grains, thereby increasing the confidence that a mineral is present in the sample based on its diffraction pattern. The powder was created using a mortar and pestle. This was done because using a Shatterbox could have potentially introduced strain on mineral grains thereby deforming the crystal lattice and ultimately altering their x-ray diffraction pattern. All samples were analyzed with CuKα as the source of radiation at 40mA and 40kV. The 2θ range was from 5 to 40 with a 2θ step size of 0.02.

Many studies have been done on the natural occurrences and chemical properties of zeolite minerals (e.g., Kristmannsdottir and Tomasson, 1976; Benning et al., 2000; Chipera and Apps, 2001). Zeolites typically develop in the vesicles of basalt flows from the introduction of meteoric water at or near the surface on which they were erupted. Zeolites can also develop as the product of hydrothermal alteration of basalt or rhyolitic glass by neutral to alkaline waters in low-medium temperature (<300°C), low pressure environments (Chipera and Apps, 2001). A study by Kristmannsdottir and Tomasson

(1976) discussed how zeolite minerals in boreholes in a geothermal field in Iceland change with depth and increasing temperature. They discovered that in general a trend in the type of zeolites occurs such that chabazite makes up the lowest temperature zones and laumontite constitutes the higher temperature zones at 75 °C and 180 °C, respectively (Kristmannsdottir and Tomasson, 1976). The host rock in the Iceland reservoir is dominantly tholeiitic basalt, but according to Chipera and Apps (2001), a similar pattern and mineral assemblage can be seen in rocks of basaltic to basaltic andesitic compositions. The study here was done to assess if this type of zonation occurs in the Paisley geothermal system.

Ph, temperature, rock composition, and fluid composition are all factors that contribute to the type of zeolite that is precipitated from solution. In terms of rock composition, glass that is more mafic will tend to produce the aluminous zeolites analcime, heulandite, phillipsite, and natrolite (Chipera and Apps, 2001). The dominant variable controlling zeolite precipitation and composition is temperature; therefore, if the temperature of formation of a zeolite mineral is taken to be the temperature of the fluid in which it precipitated from, then the type of zeolite mineral can be used to independently estimate the temperature of the fluid. Figure 4.21 shows which zeolite minerals are stable at certain temperature ranges and how a zeolite package could be useful in estimating reservoir temperatures. Also, since zeolites form at low temperatures, the rate of reaction in forming these minerals is slow and suggests that conditions within the reservoir are stable enough to produce said minerals.

Several different zeolite minerals were identified by X-ray diffraction analysis. Peaks were picked manually and also with the aid of computer software and an X-ray

diffraction pattern database (PDFMaint). Mineral matches were fit with corresponding peaks and correct d-spacings. It is noted that zeolites are a fairly difficult mineral to exactly match to standard peaks because natural zeolites are not chemically homogenous and also entrain variable amounts of water, thereby affecting the d-spacings and the diffraction pattern. The majority of zeolite minerals identified have their most intense peaks around 9.83-9.88 2θ and 23-25 2θ. Zeolite minerals with this 2θ range include heulandite, phillipsite, clinoptilolite, analcime, wairakite, stilbite, mordenite(?), laumontite(?) and sodalite(?). All of these minerals have varying ratios of Na, K, and Ca cations and varying ratios of Si to Al, but all are formed from hydrothermal alteration.

Clay minerals belonging to the smectite group such as nontronite, montmorillonite, hectorite(?), and bentonite(?) were also identified. Montmorillonite, hectorite, and bentonite are hydrothermal alteration products of volcanic glass that is felsic in composition, whereas nontronite is the product of hydrothermal alteration of mafic glass. These minerals were also used to help constrain reservoir temperatures but, as can be seen in Figure 4.21, the smectite group has a large range in temperatures of formation, and is therefore not useful by itself as a constraint on reservoir temperatures. Other minerals such as calcite and low quartz were identified but again they have a wide range in temperatures of formation and are not particularly useful by themselves.

Based on the mineralogic temperature ranges of Figure 4.21, it has been determined the alteration mineral assemblage of the Paisely geothermal wells appear to have formed from 25 °C to 170 °C, where the lower end represents smectite stability and the upper end reflects the stability of stilbite. However, since phillipsite was identified in almost every sample a better estimate for the low end temperature is 58 °C.

Every mineral identified by X-ray diffraction lies within the range of 58 °C to 170 °C. These temperatures agree well with the temperatures calculated with the geothermometers described above, which reports a temperature range of 95 °C to 166 °C. However, if the full ranges of zeolite temperature stabilities are considered, reservoir temperature could reach as high as 300 °C, but it is assumed that at this temperature, higher temperature minerals such as epidote, prehnite, and actinolite would have been identified. Therefore, since those minerals are not present, minerals such as wairakite and laumontite are most likely in the beginning stages of formation.

Geothermal System Conceptual Model and Conclusions

Several datasets have been integrated to create a conceptual model for the Paisley geothermal system at Paisley, Oregon. The model has been created mostly from the results of detailed geologic mapping, aqueous geochemistry, stable isotopes, regional heat flow, and analysis of alteration mineral assemblages (Fig. 4.22). The result of a ~2.5 km^2 gravity survey was also used to constrain the geometry of the range bounding fault controlling thermal fluid upflow. This range bounding fault is part of the Paisley Transfer Zone, which through complex fault interactions, has created the necessary permeability for this fluid flow (Fig. 4.10). The Paisley geothermal system is similar in many ways to those classified as extensional geothermal systems (i.e., Basin and Range type), with minimal to no influence from active magmatic systems.

Several different rock types occur in the Paisley area and represent a complex geologic history from the late-Eocene (?) to present. The reservoir for the thermal fluids is several basalt flows and scoriaceous basalt cinders at depths ~300-400 meters, determined by lithologic logs from the Colahan Hot Well, and wells SVEC-1 and SVEC-

2 (Fig. 4.20). Zeolitic alteration of the basalt suggests that these fluids have spent a significant amount of time in the reservoir. The presence of phillipsite and stilbite indicate possible reservoir temperature of 58 °C to 170 °C (Fig. 4.21; Chipera and Apps, 2001).

Upward fluid flow of the system is facilitated along a northwest trending normal fault that separates the Paisley Hills from Summer Lake Basin. This fault dips approximately 65° to the northeast based on well log and gravity data. The depth of Plio-Pleistocene Summer Lake basin is estimated to be 2 km based on geophysical surveys (Donath and Kuo, 1962; Blank, 1973; Travis, 1977). A sedimentary basin with this thickness requires faults that penetrate the crust at least several kilometers. Another northwest trending fault that offsets Pleistocene fluvial and lacustrine sediments of ancient Lake Chewaucan is evidence that faulting in Summer Lake Basin has continued at least into the Pleistocene. A major range bounding fault separates the eastern margin of Summer Lake Basin at the base of the Coglan Hills; therefore, making Summer Lake Basin a graben by definition. It is interesting to note that most of the rocks in the Coglan Hills are unaltered to only slightly altered, suggesting that for at least as long as that fault has been active, no significant thermal fluid has risen from depth on the eastern side of the graben. The apparent localization of the hydrothermal system seems to be controlled by faults bounding the western edge of the basin. Recent faulting coupled with high heat flow from extension is most likely the heat source for the fluids in the geothermal system at Paisley.

Aqueous geochemistry has shown that the thermal and nonthermal fluids in the Paisley area are classified as acid-sulphate or bicarbonate waters, respectively. From this

data, temperatures have been calculated for water in the thermal reservoir based on both cation and silica geothermometers. The total range in temperatures based on both systems is from 95 °C-166 °C, which agrees very well with temperatures determined by looking at alteration minerals.

The source of the sulphate in the thermal fluids is from dissolution of evaporated minerals as meteoric water percolates through the lacustrine sediments into the aquifer as opposed to a magmatic source of SO_4, which would account for the near neutral to alkaline pH of the thermal fluids. Other factors, such as low As content and low B/Cl ratios, support the idea that these fluids are not of magmatic origin and are not being heated by a magmatic source.

Stable isotope analysis on current meteoric and thermal wells demonstrates that the thermal waters are isotopically distinct from those of current meteoric water. It is believed the water from the thermal wells is of Pleistocene age determined by their lighter isotopic composition than that of current meteoric water sampled from the same location. This implies then that recharge to the thermal aquifer is happening geologically slowly. Meteoric water infiltrates the subsurface in high elevations southwest of Paisley, driven by topographic flow-hydraulic head. As water flows through the subsurface, it becomes heated by the elevated regional geothermal gradient and starts to interact and exchange ^{18}O atoms with the host rock, accounting for the oxygen isotope shift (Fig. 4.17). Simultaneously, water from the Chewaucan River percolates through fluvio-lacustrine sediments in the basin and is the source of non-magmatic SO_4.

It is likely that a finite amount of water exists within the reservoir, or at least circulation of meteoric water to that reservoir takes several hundred to thousands of

years. This has obvious implications for the exploitation of this resource. Injection back to the thermal aquifer must happen in order to make this resource sustainable but not at a rate that will decrease the enthalpy of the system.

Implications for Geothermal Resources in Southeast Oregon

The geothermal system near Paisley has served as a case study for Basin and Range-type geothermal systems in southeast Oregon. The majority of magmatism associated with the High Lava Plains lies to the north of Basin and Range structures in southeast Oregon (Fig. 4.23). Therefore, the role of this magmatism appears to be minimal on geothermal system in the Oregon Basin and Range. However, careful examination of a system's thermal water and detailed geologic mapping near the system are the only ways to determine which type of geothermal system it is.

Regardless of heat source, the role of structural preparation is extremely important for the concentration of fluid flow in rapid transport pathways. In the Paisley system, a structural transfer zone has created the necessary permeability to allow for concentrated thermal upwelling. Similar structures can be found in Southeast Oregon (Fig. 4.23). The geologic setting of southeast Oregon offers many opportunities for geothermal resources.

Figure 4.1. Picture of andesitic lahar flows representing the bulk of unit Tvb. Red clipboard measures 9" x 12". This particular flow was taken in the Coglan Hills east of Paisley.

Figure 4.2. Example of auto-brecciated lava flows in unit Tvb. This picture was taken near mile marker 3 on Country Road 20-08 southwest of Paisley.

Figure 4.3. Unwelded ash flow tuff in unit Taf. Note the abundance of flattened white pumice clasts, a typical settling structure created by ignimbrites. This picture was taken in the southern Coglan Hills.

Figure 4.4. Ash-flow tuff containing abundant lithic fragments that sit stratigraphically higher than the slightly welded unit described in text. This flow lies within unit Taf and the picture was taken in the southern Coglan Hills.

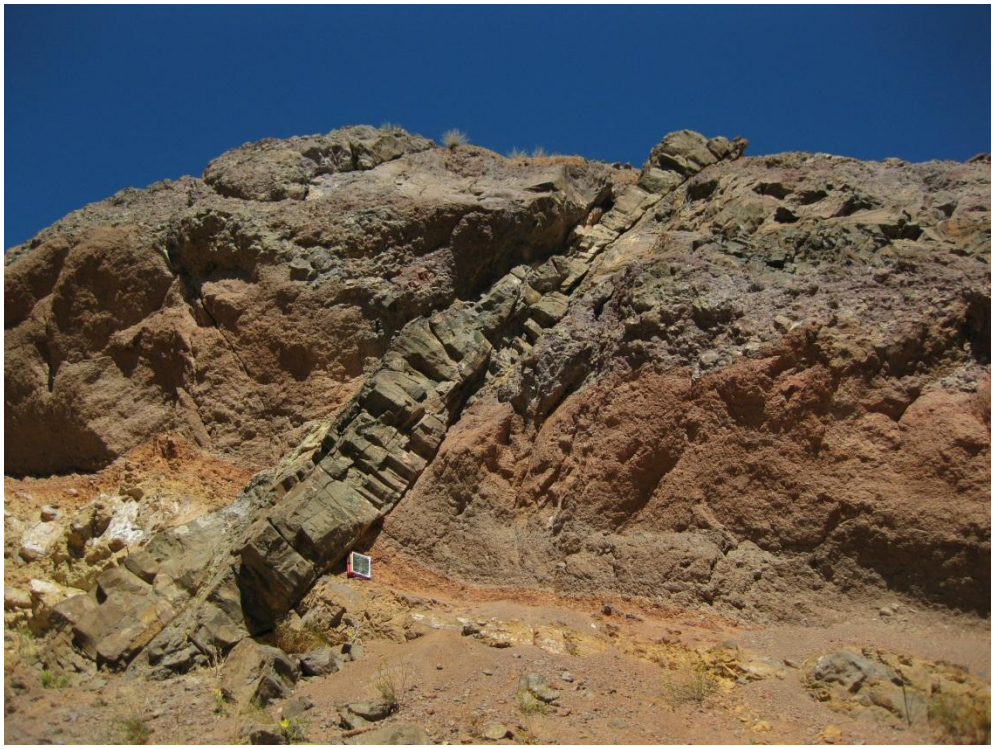

Figure 4.5. Pictures representing mafic intrusive unit Tmi. These dikes crosscut units Tvb and Taf but terminate against unit Tsm, possibly indicating that these were feeder dikes to local basalt flows. Picture on left was taken in the southern Coglan Hills, whereas the picture on the right was taken near mile marker 3 on County Highway 20-08 southwest of Paisley.

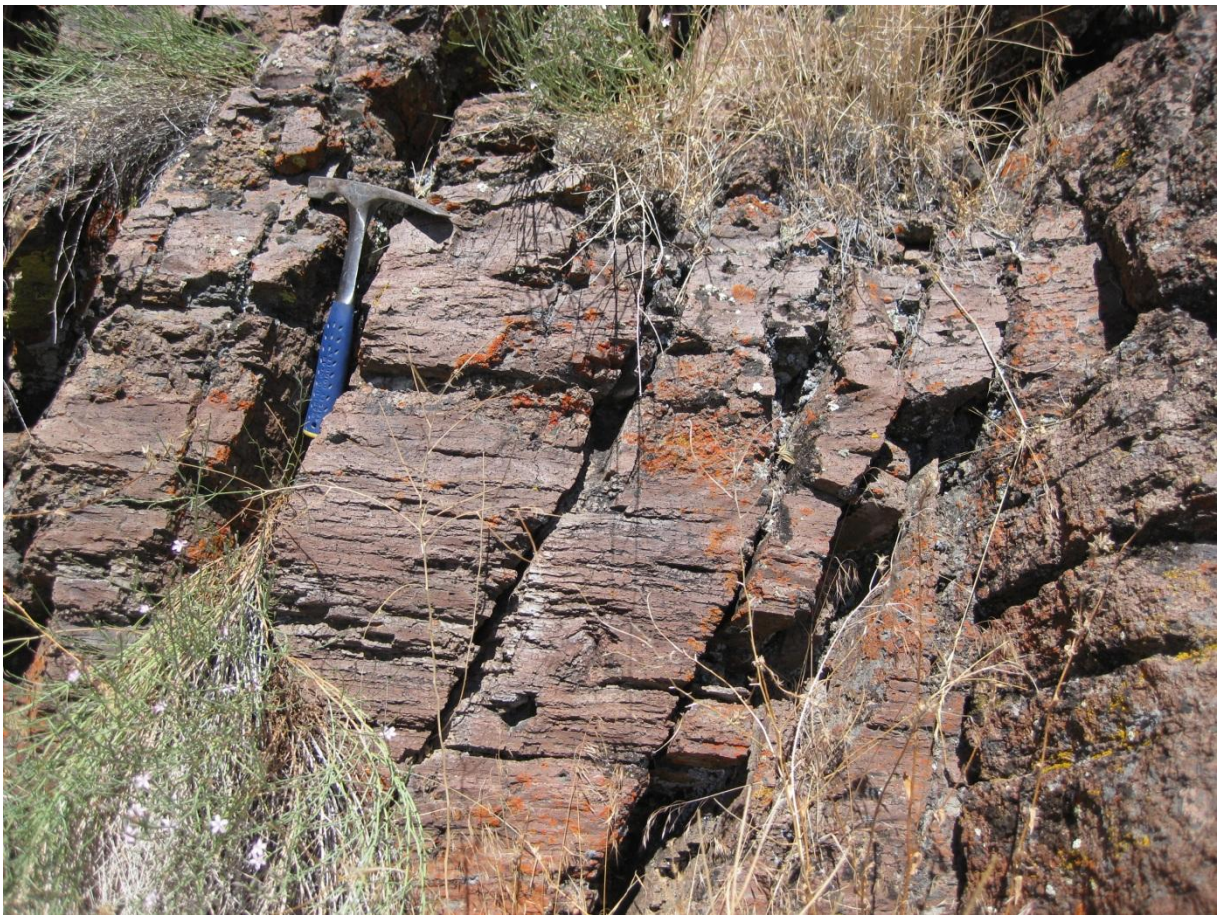

Figure 4.6. Flow banding in unit Tsv. Note jointing at regular angles to flow banding, a feature used to help distinguish this unit from others in the field. Picture taken in the Paisley Hills southwest of Paisley.

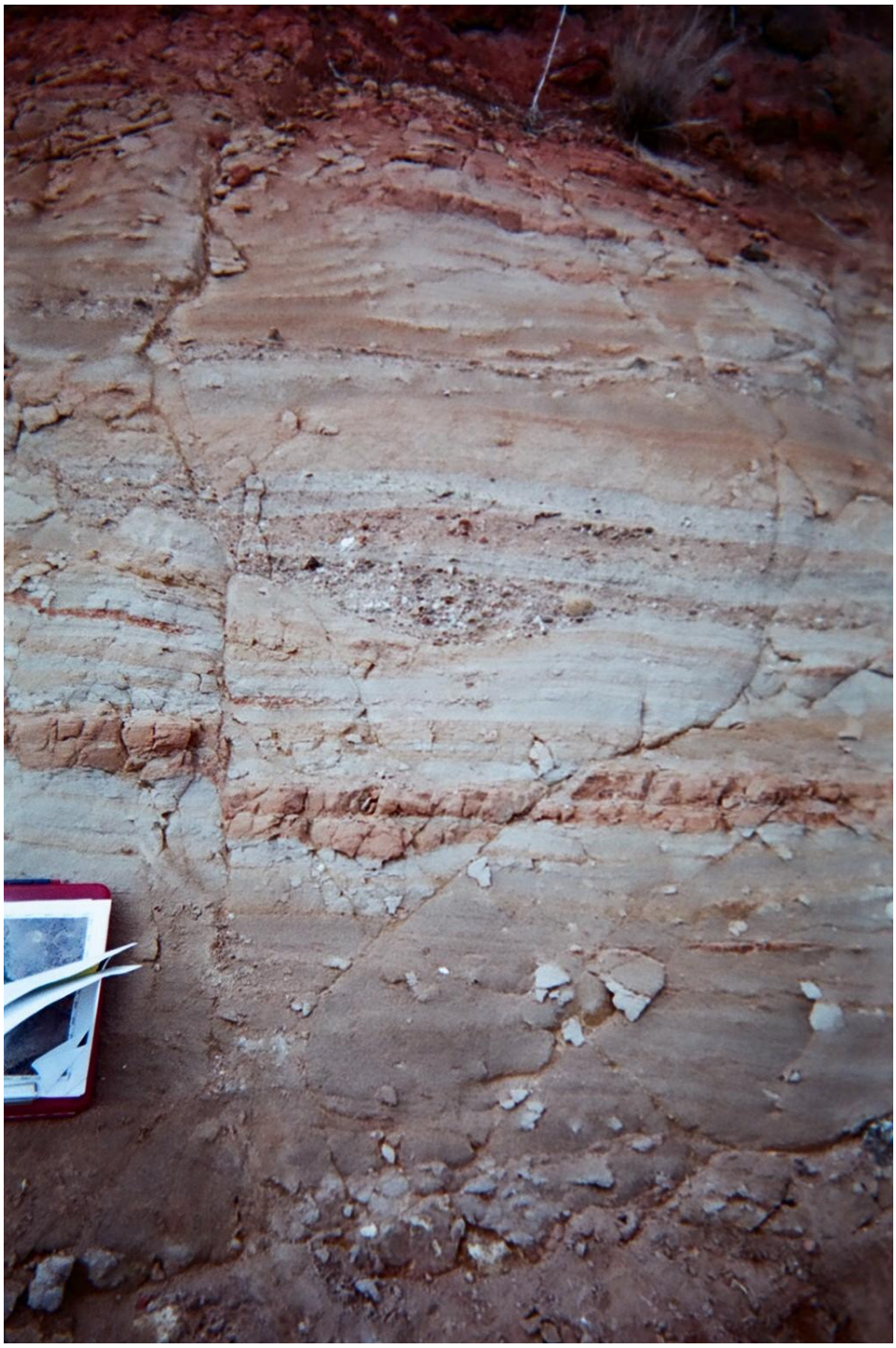

Figure 4.7. Picture of volcaniclastic sedimentary rocks constituting unit Tvs. Note in center of picture a cut and fill structure containing pebble-sized material. Some clasts in this structure are rounded perlite material often associated with unit Tsv, suggesting this unit is younger or at least contemporaneous to unit Tsv. Numerous small-offset normal faults occur throughout this unit as well. Picture taken on the "high road" southwest of Paisley.

Figure 4.8. Spheroidal weathering of a basalt in unit Tmv.

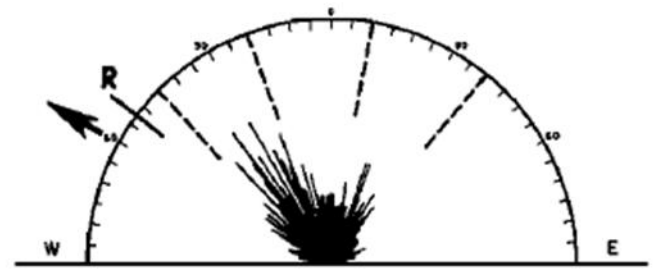

a: Summer Lake [from Donath, 1962]

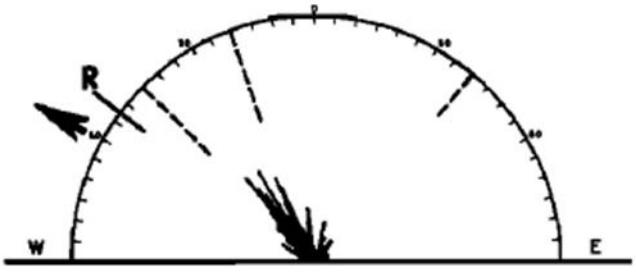

b: Southern Summer Lake

Figure 4.9. Diagrams showing strike of faults in and adjacent to Summer Lake, Oregon. The dominant strike direction in this area is ~307°. The lengths of the lines are proportional to the amount of faults with that particular strike, where the radius equals 18 fault segments. Modified from Donath (1962) and Pezzopane and Weldon (1993).

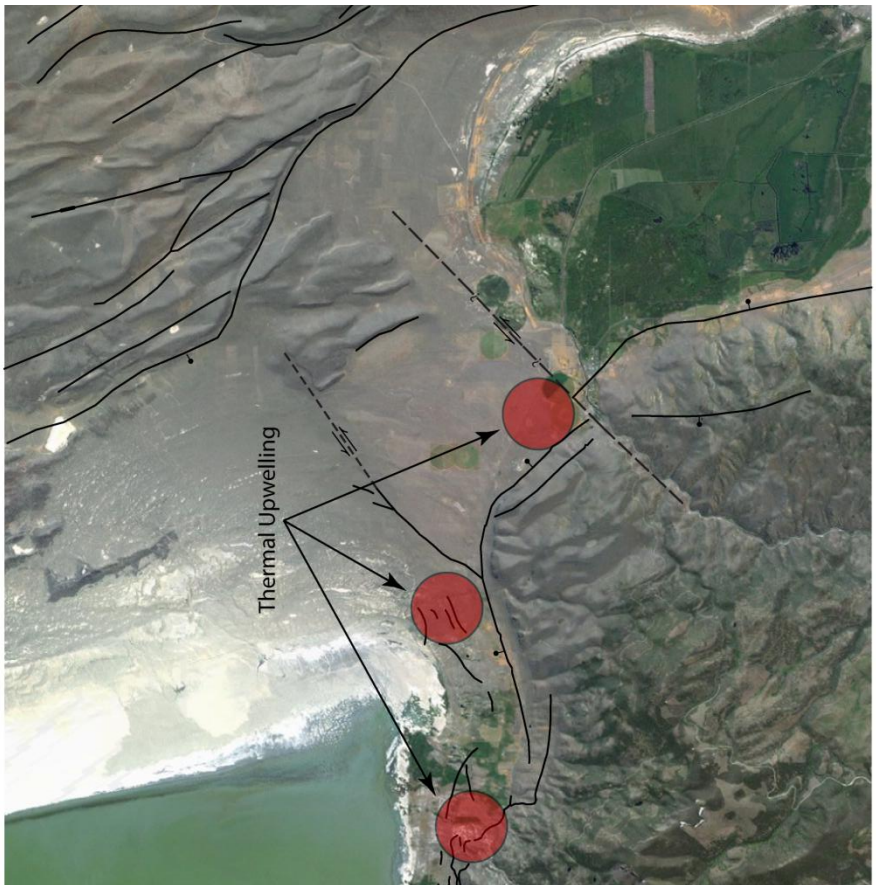

Figure. 4.10. Map showing the Paisley Transfer Zone. Faults shown in this figure come from the results of this study, from the Quaternary fault database from the USGS (Pezzopane and Weldon, 1993), and from the Oregon geology layer available from the USGS after Walker and McLeod (1991). Red circles are zones where thermal water has been located. From left to right, the red circles are: The Colahan Hot Springs, Summer Lake Hot Springs, and the Paisley geothermal system. Line A-A' is the cross-section line for Figure 4.21.

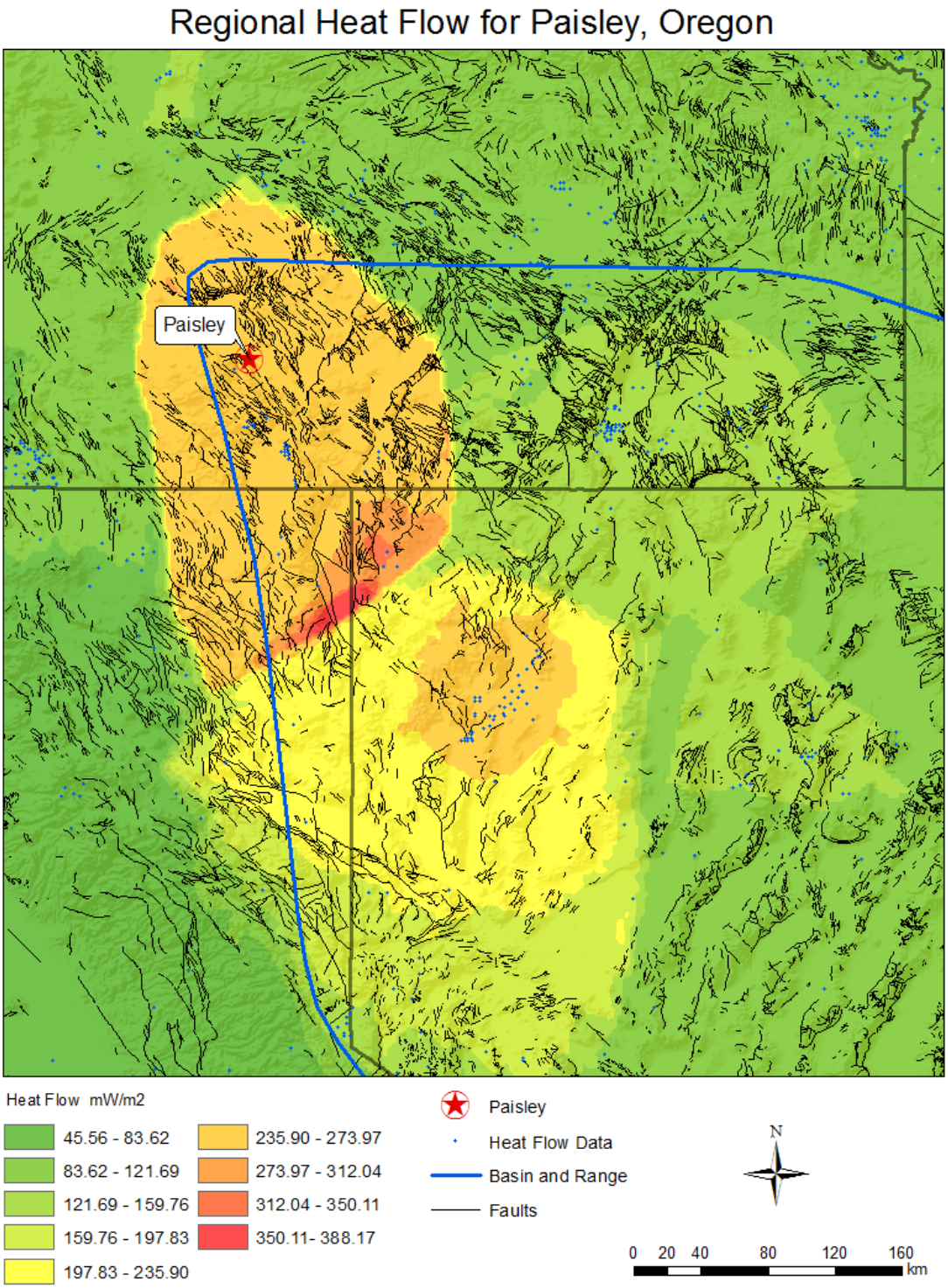

Figure 4.11. Regional heat flow map for Paisley, Oregon. Blue dots represent data from the Global Heat Flow Database held at the University of North Dakota and mostly comes from borehole temperature measurements. Heat flow layer was calculated by creating a raster interpolation using the Spherical Kriging method.

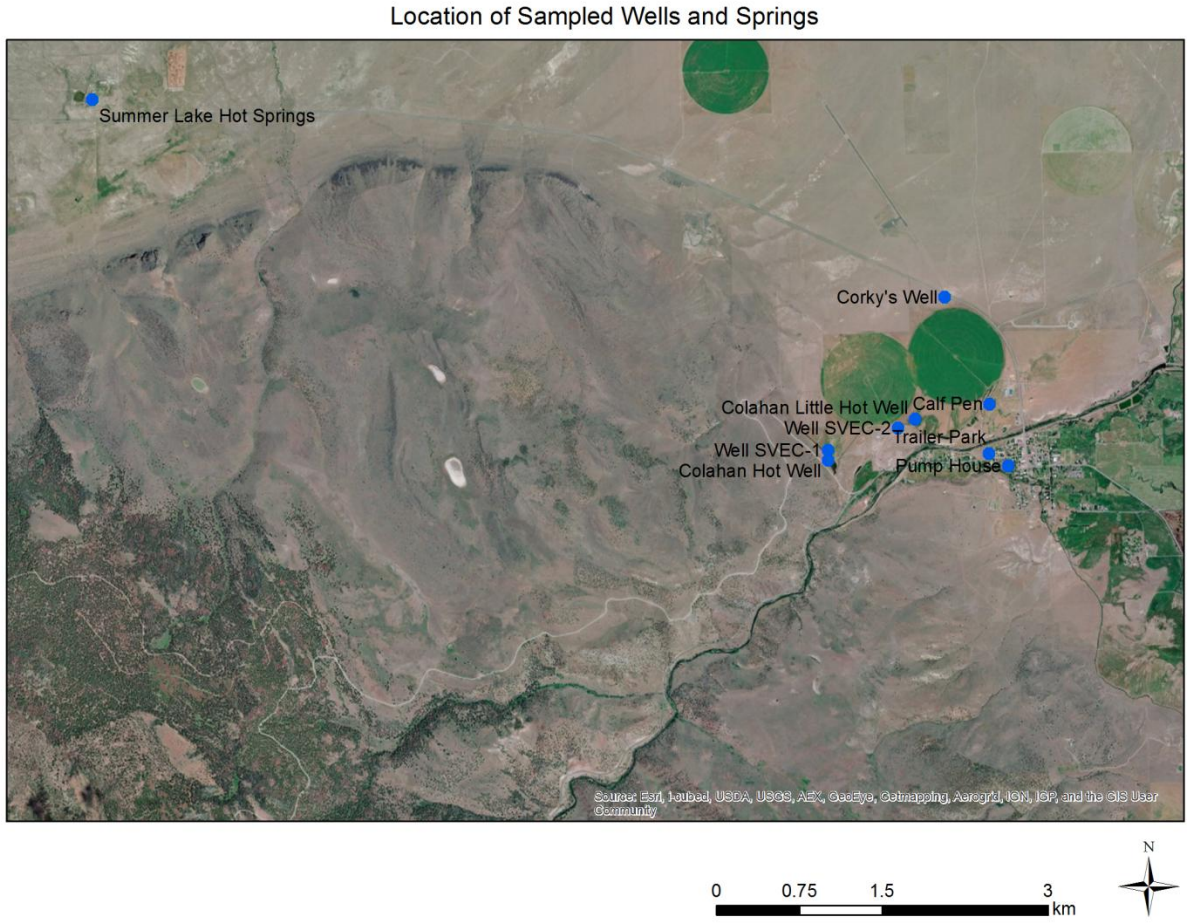

Figure 4.12. Location map of wells and springs sampled for aqueous geochemistry.

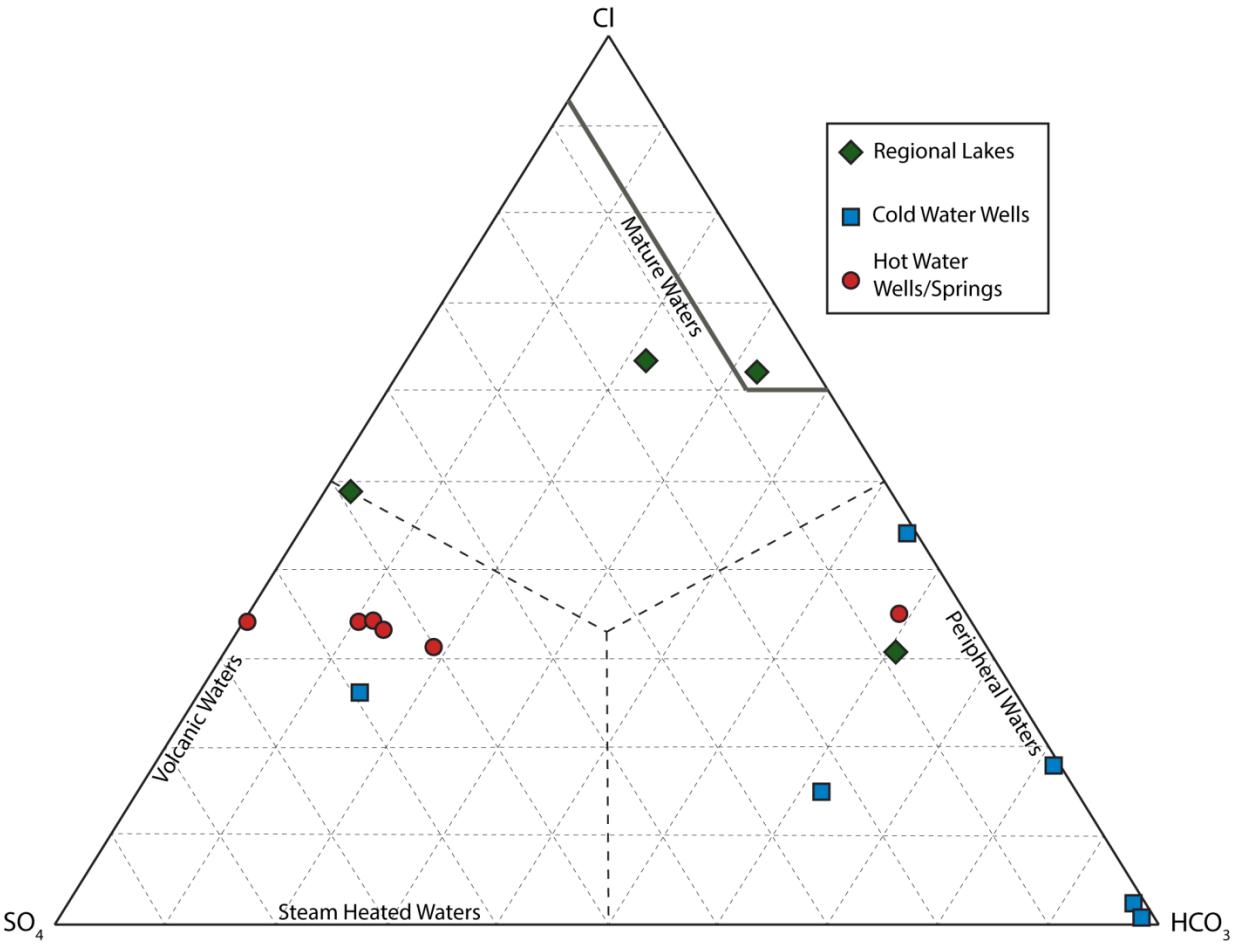

Figure 4.13. SO_4-Cl-HCO_3 ternary diagram. Used to help determine suitability of water samples to be used in geothermometry and to potentially discover any mixing trends. It appears all of the thermal samples lie in the SO_4 corner, classifying them as acid-sulphate waters. Green diamonds represent regional lakes in which chemistry data was taken from Drever (1982) and Hantelmann (2006).

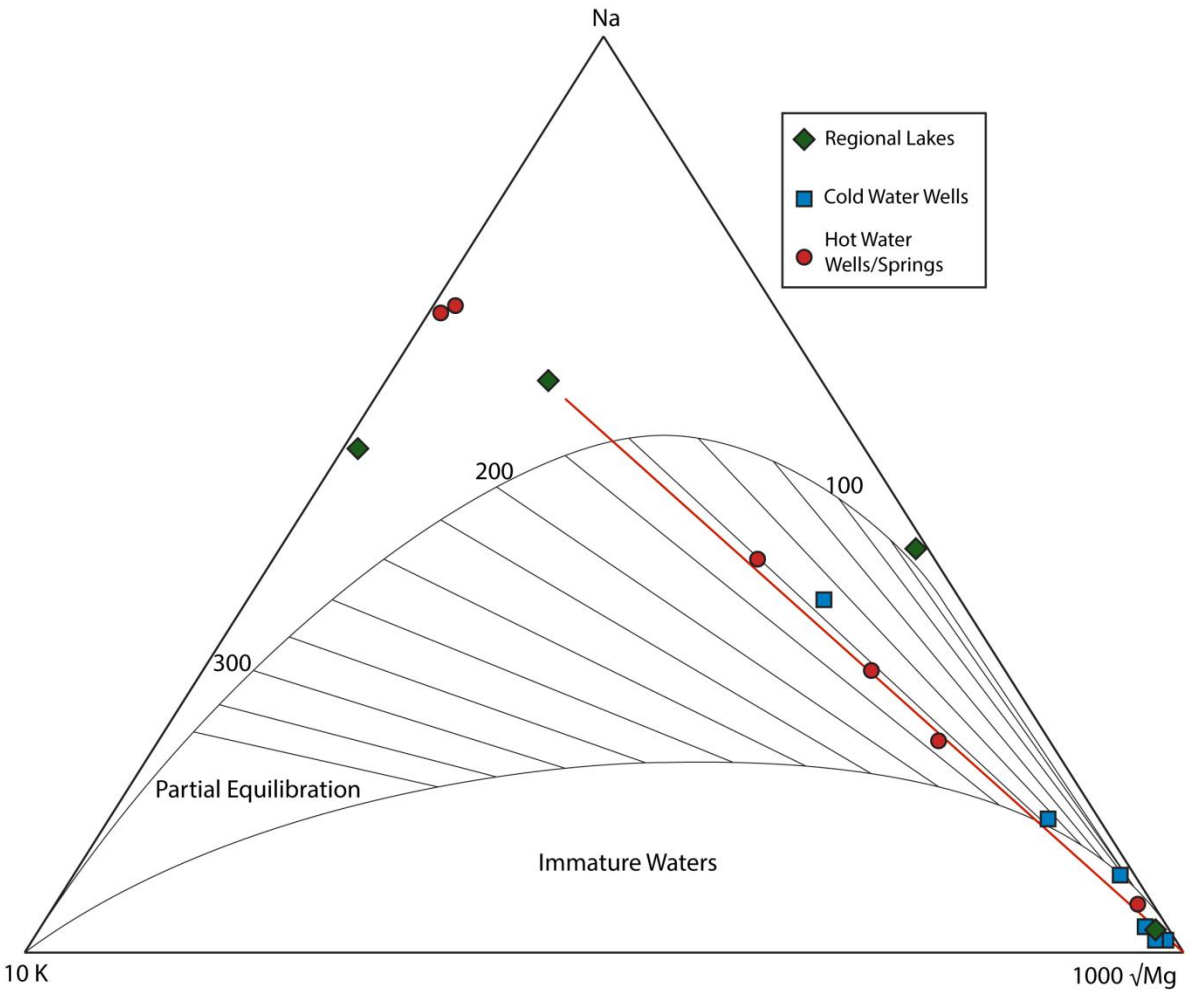

Figure 4.14. Na-K-Mg ternary diagram used to determine mixing with meteroic water and also used to determine the K-Na-Mg geothermometer. It can be seen that a well-defined mixing trend occurs starting from the Mg corner along a line toward the point SL (Summer Lake). All of the thermal wells lie along this line. Also, from this line, the K-Na-Mg geothermometer temperature is 170 °C.

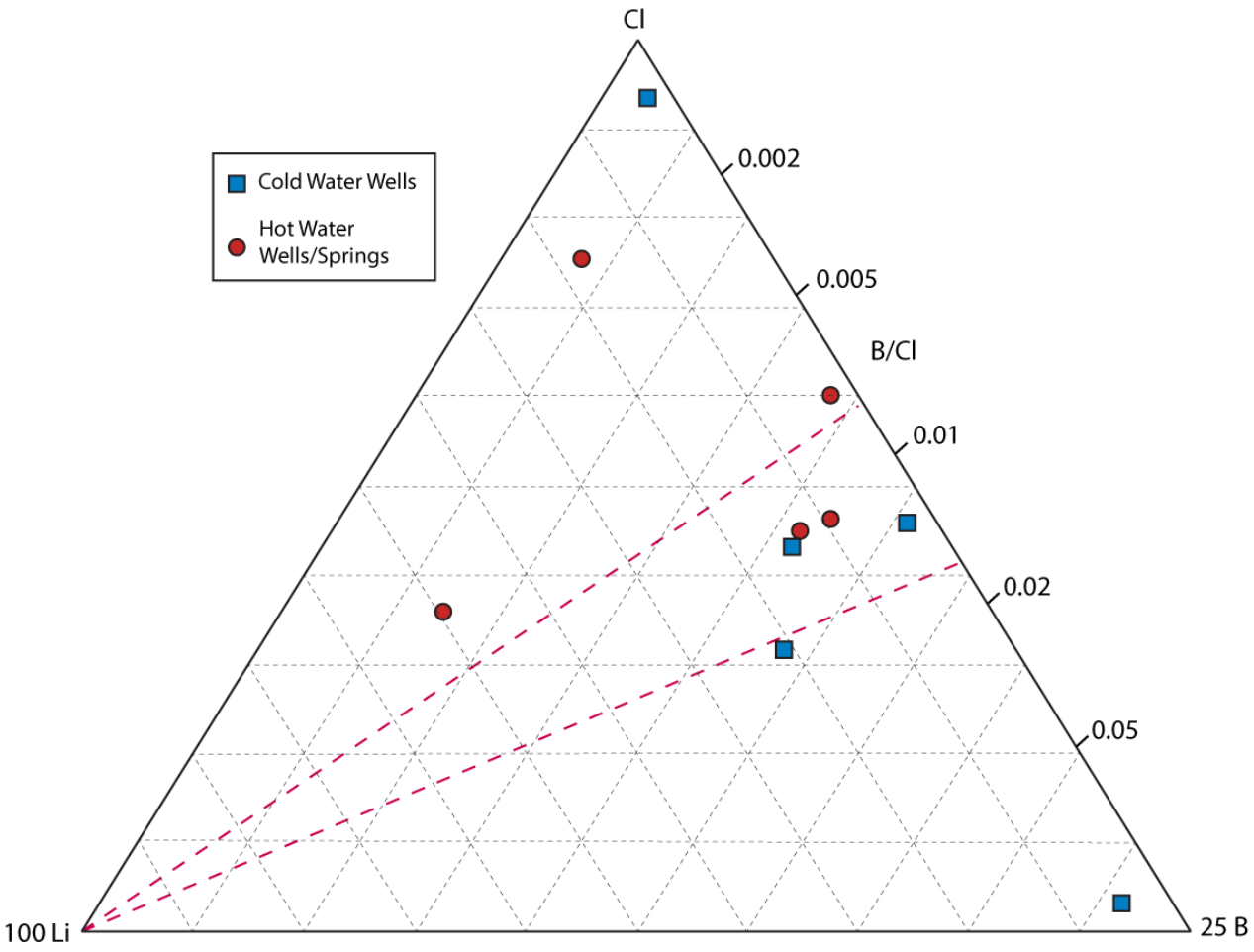

Figure 4.15. Li-Cl-B ternary diagram for thermal and non-thermal waters in the Paisley area. The samples show a low to moderate B/Cl ratio, suggesting a non-magmatic source. Also, Li loss is representing Li uptake into the quartz lattice.

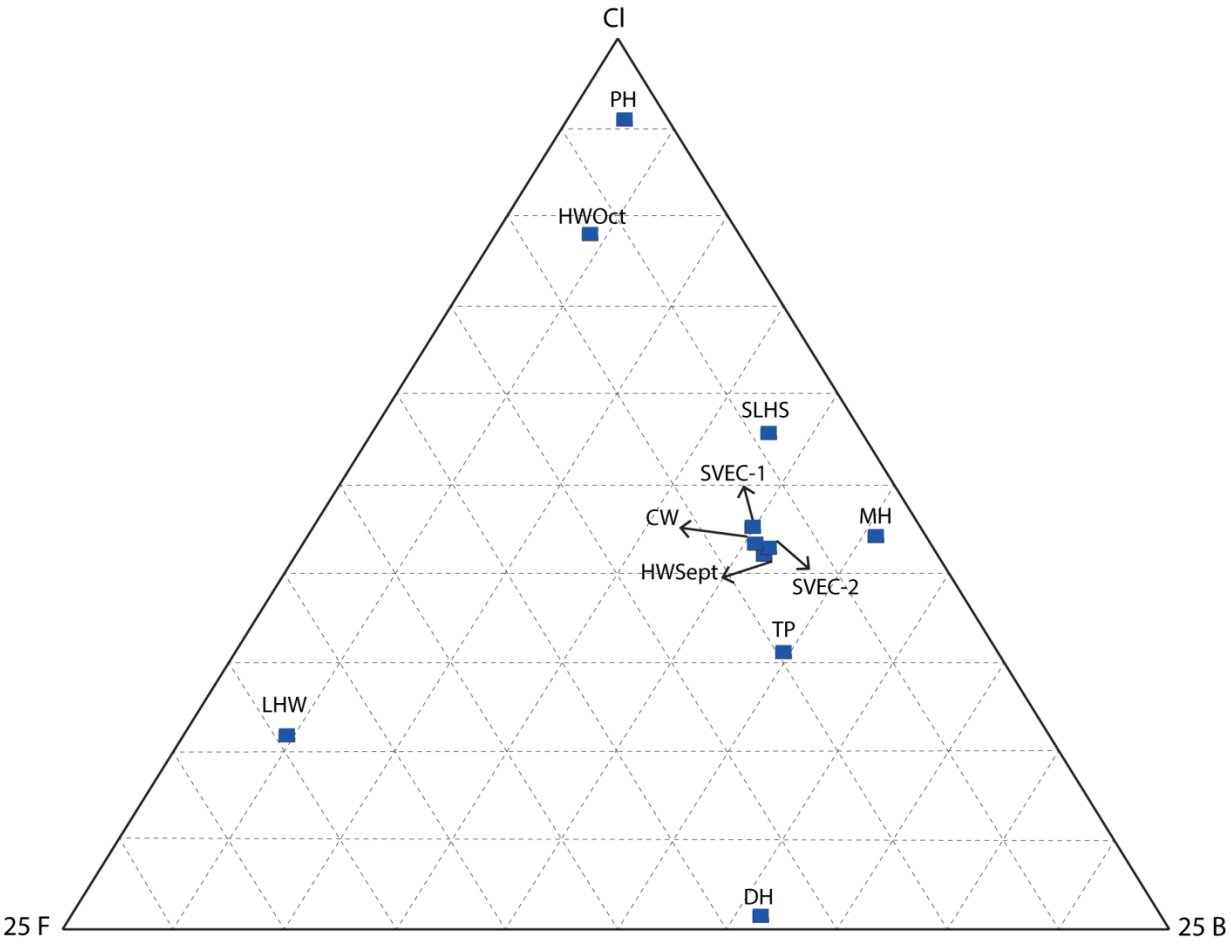

Figure 4.16. F-Cl-B ternary diagram used to distinguish fluids from different sources, typically based on its F content. Based on this, it appears that all of the thermal water is from the same source region. However, point HWOct and LHW deviate from the other points; this is interpreted to be errors in measurements.

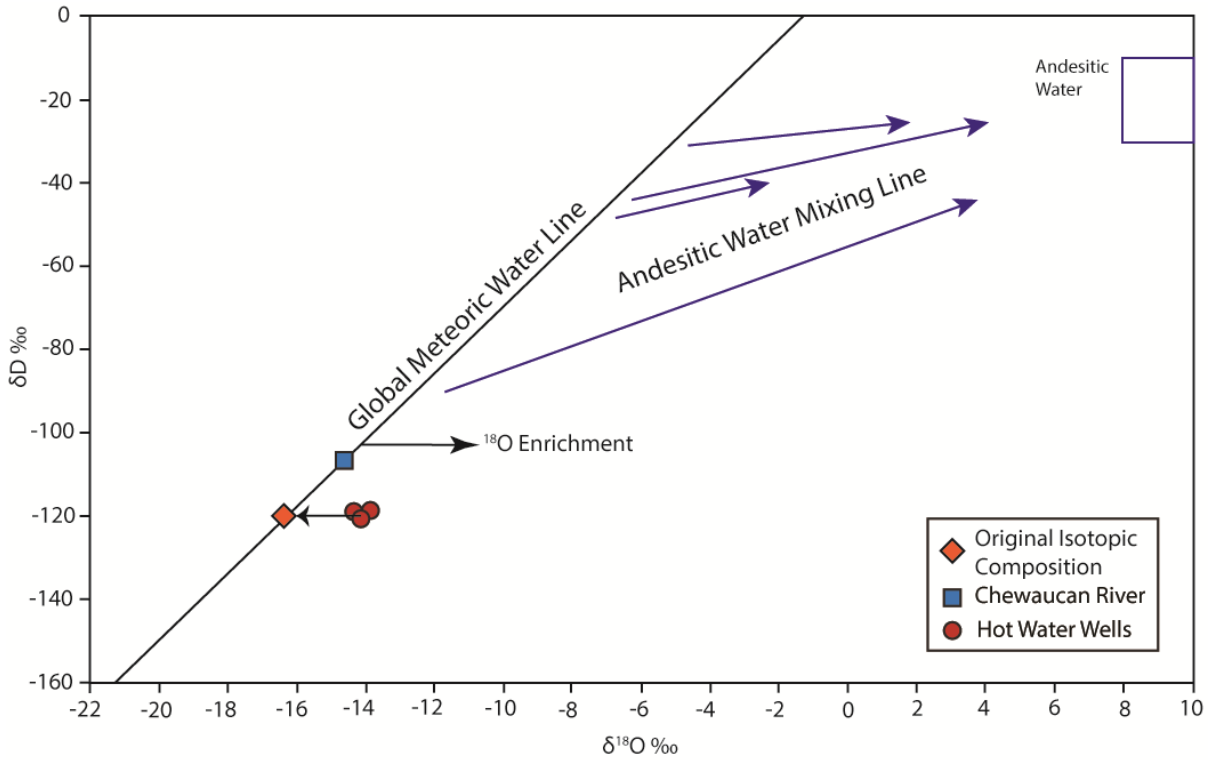

Figure 4.17. Plot of δD vs $\delta^{18}O$ with the meteoric water line. See text for detailed discussion. Cluster of points represents samples taken from thermal wells and point on meteoric water line is that from the Chewaucan River. Modified from Powell and Cumming (2010).

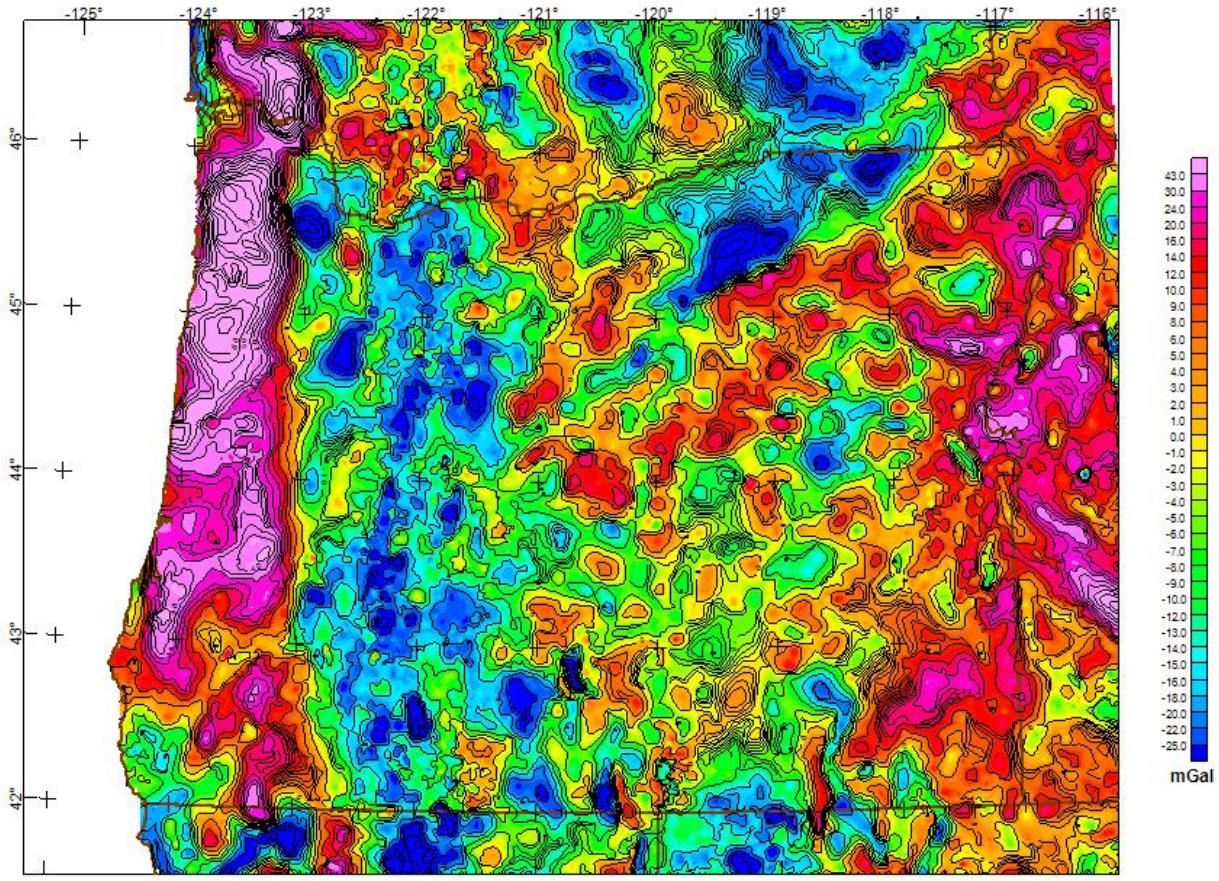

Figure 4.18. Isostatic gravity map for the state of Oregon. One major feature to notice is the change in anomaly orientations at the Cascades from northwest oriented to north-sound oriented. Also, note that Summer Lake Basin is a large gravity low, suggesting it is a deep sedimentary basin (~2 km). Taken from Roberts et al. (2008).

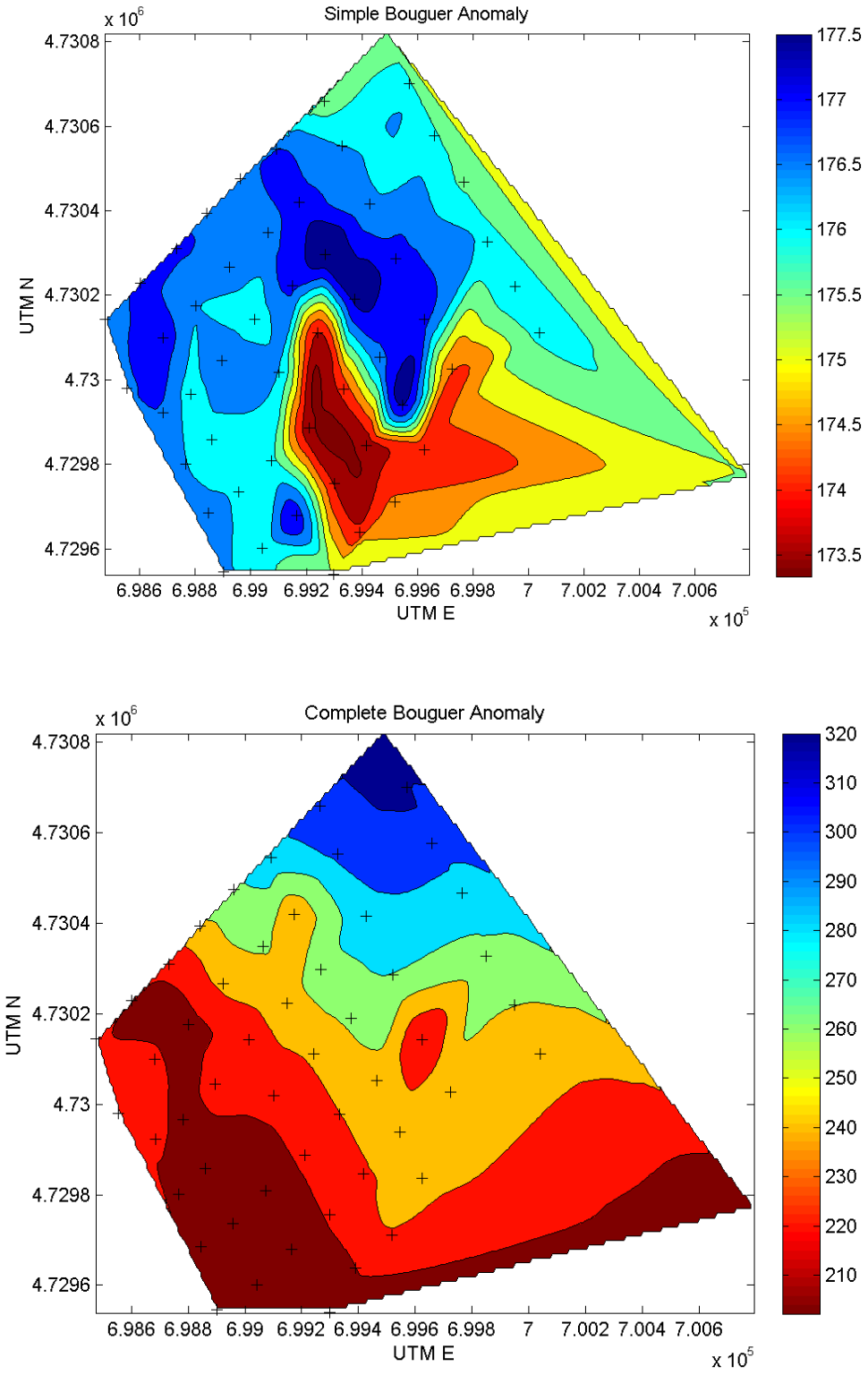

Figure 4.19 a and b. Figures showing results of the gravity data reduction process. These are the raw images returned from the MATLAB script that was created for this study.

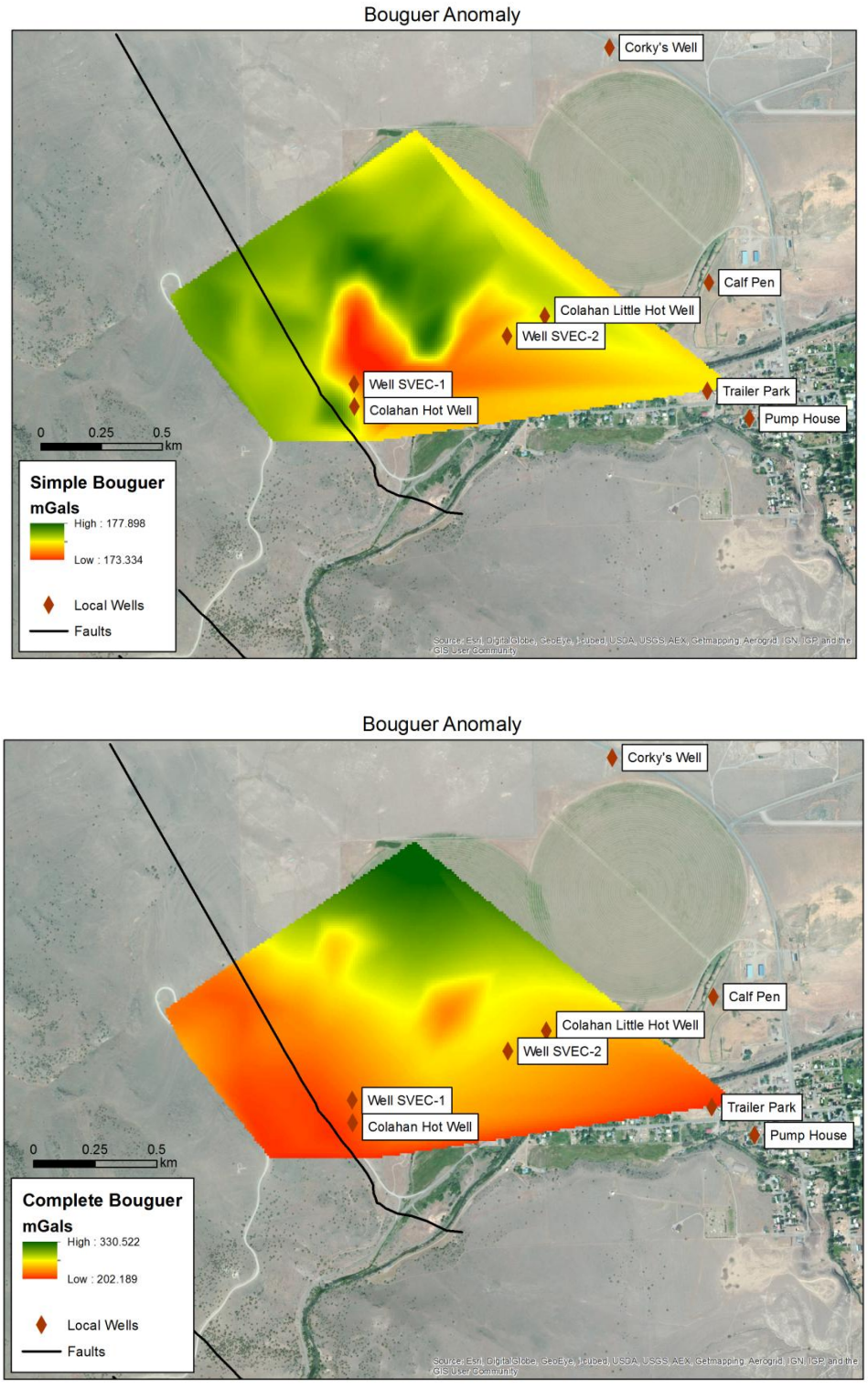

Figure 4.19 c and d. Maps showing both Simple (a) and Complete Bouguer (b) Anomalies overlayed on the Paisley site. Red diamonds are locations of wells sampled for aqueous geochemistry. Black line represents fault identified with the gravity survey and by geologic mapping. See text for further discussion.

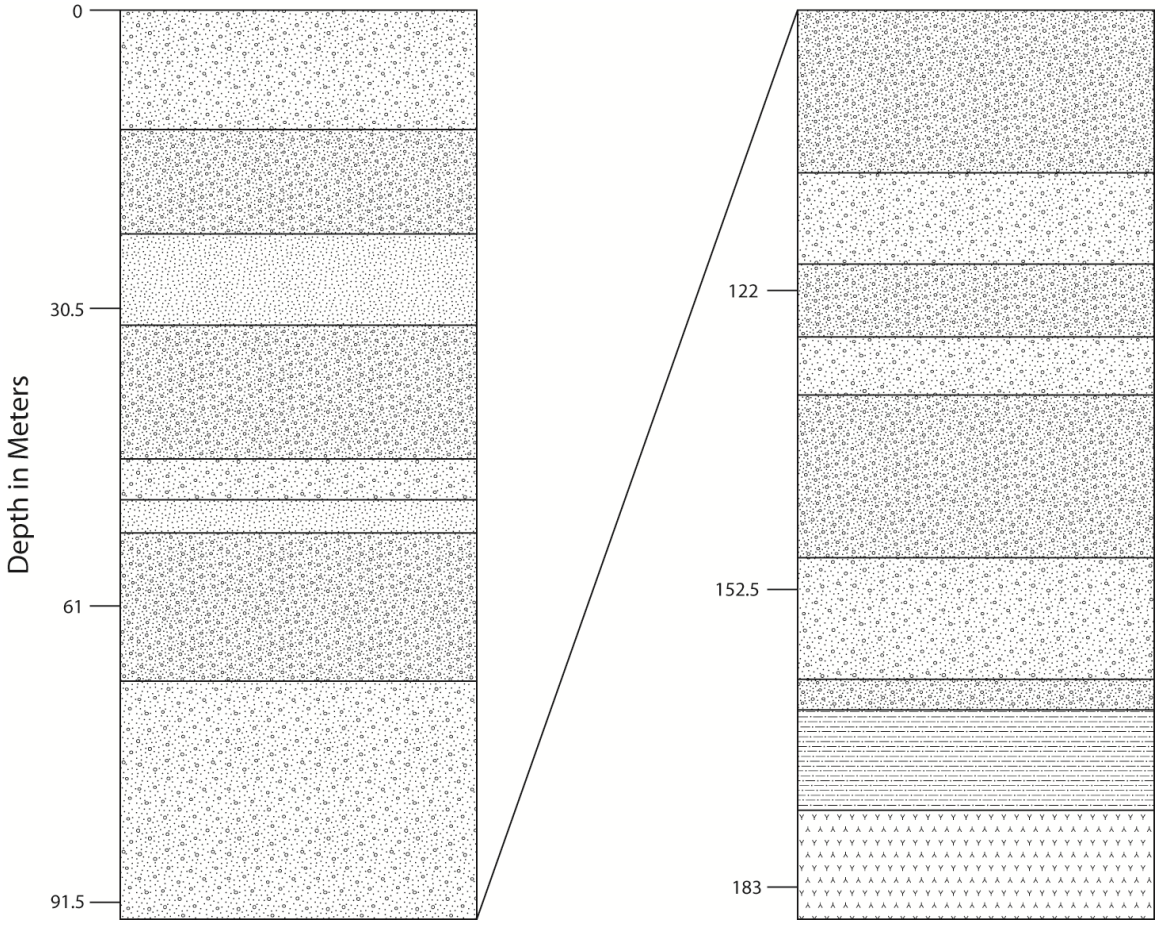
Depth in Meters
0
30.5
61
91.5
122
152.5
183

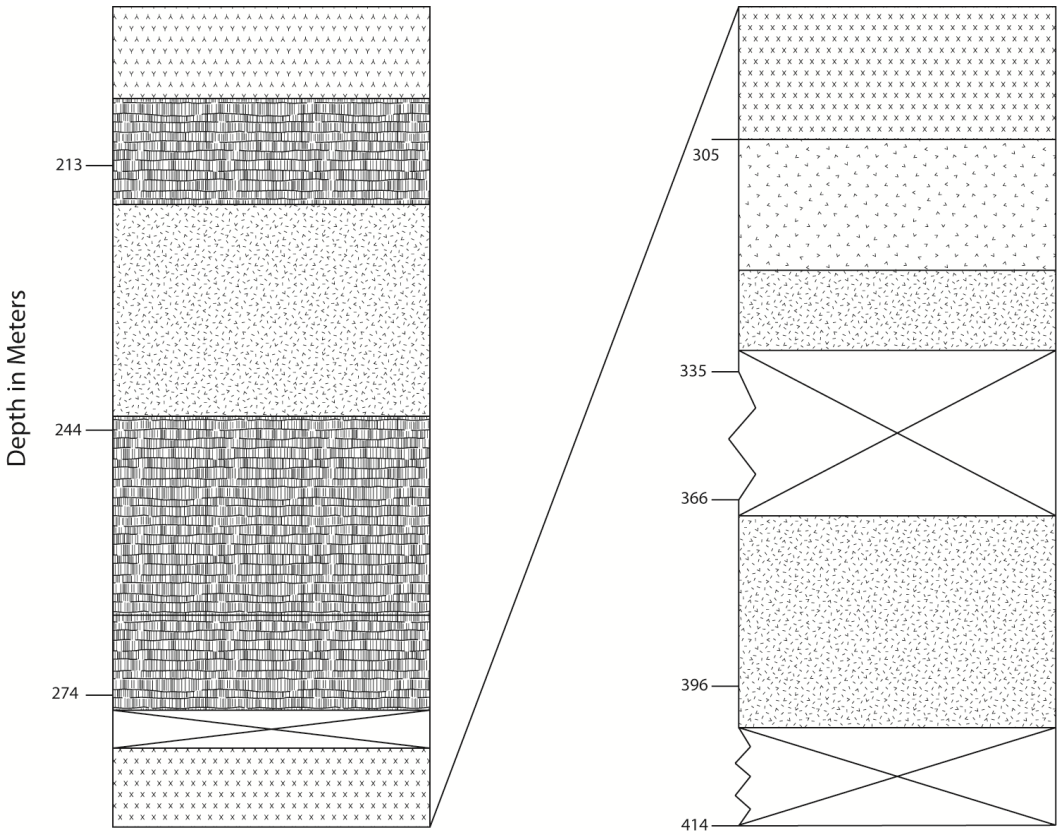
Depth in Meters
213
244
274
305
335
366
396
414

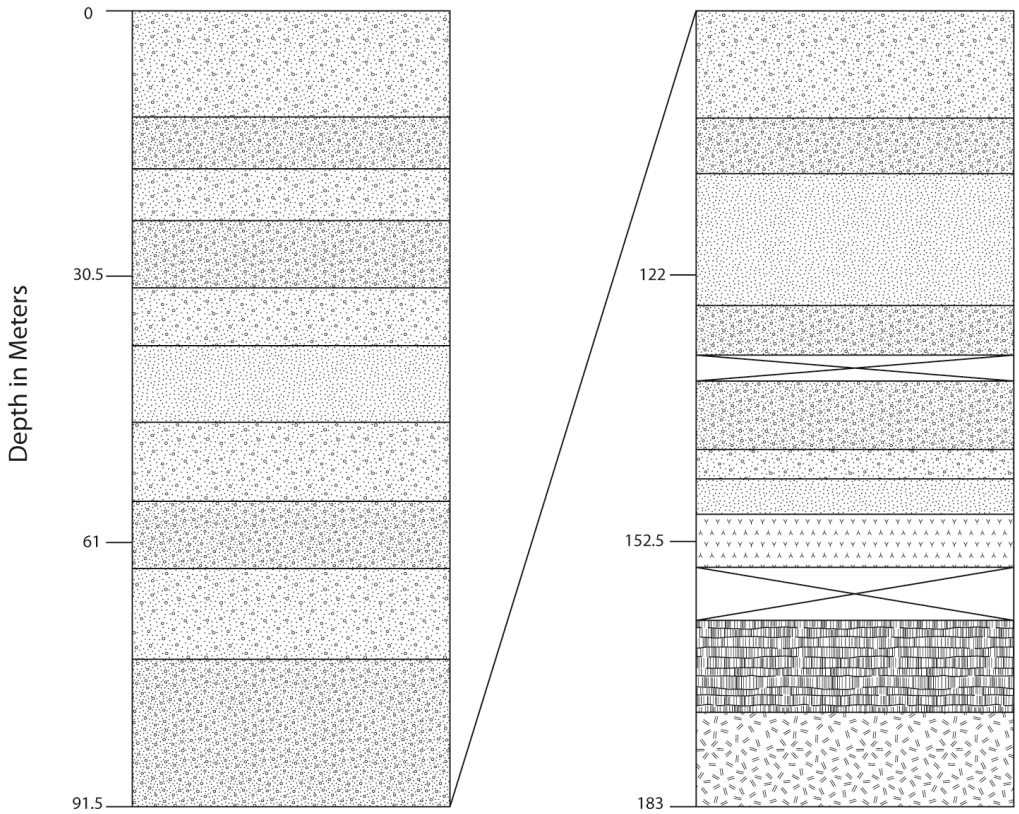
Depth in Meters
0
30.5
61
91.5
122
152.5
183

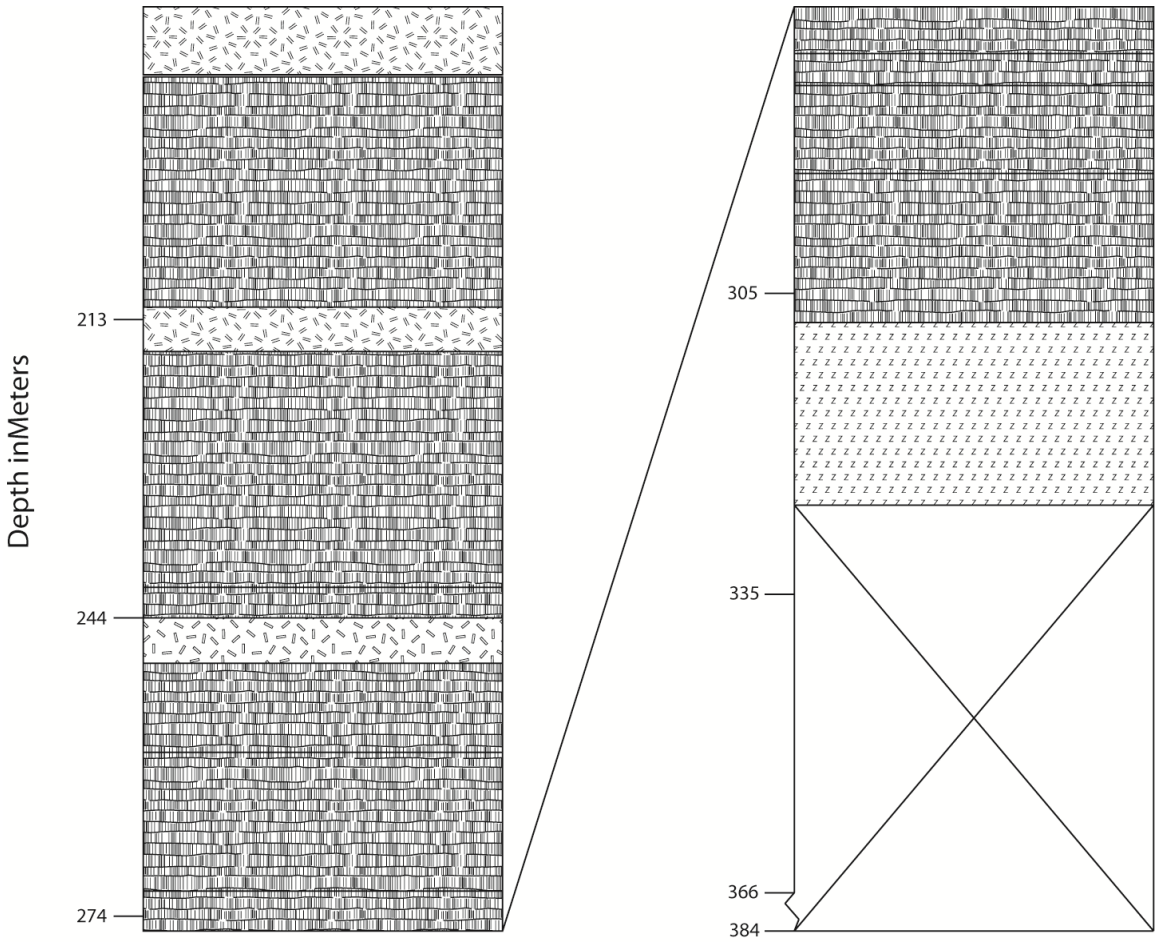

Figure 4.20. Lithologic logs for wells SVEC-1 and SVEC-2 created from well cuttings sampled in 1.5 meter intervals.

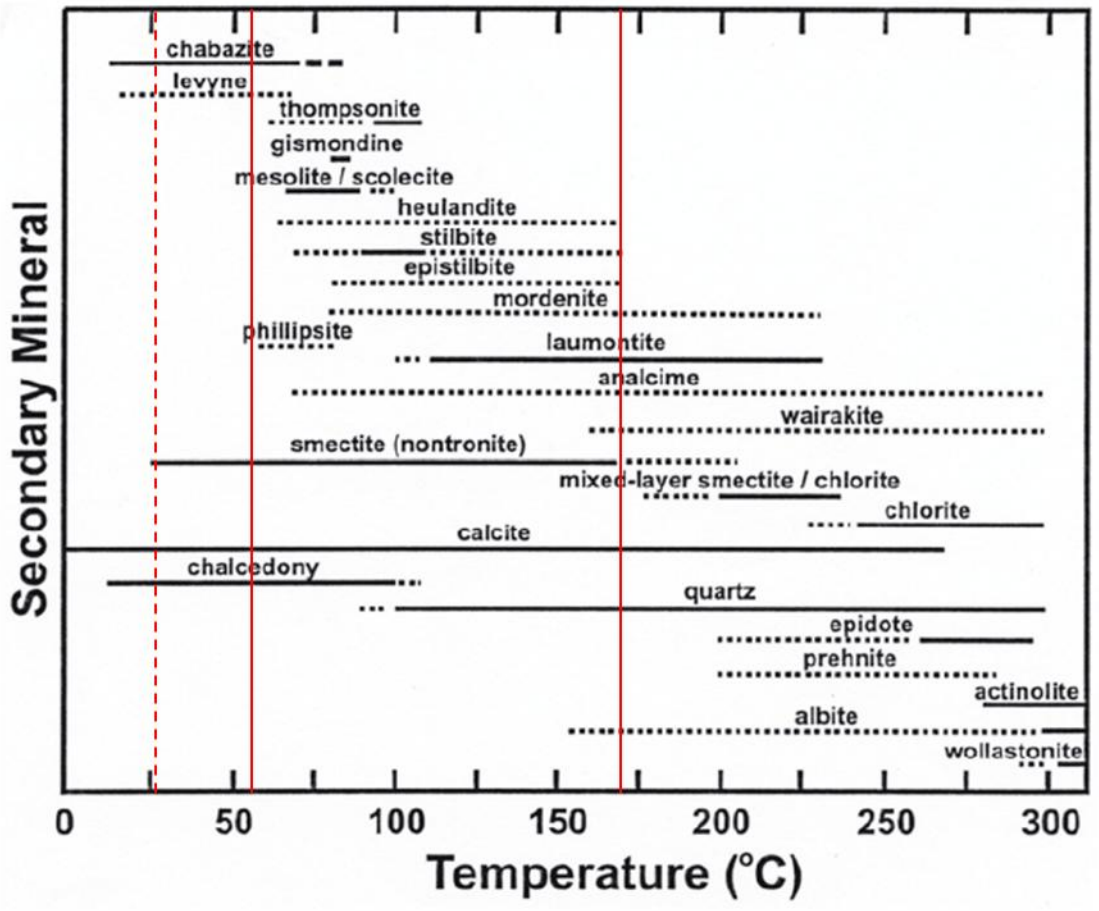

Figure 4.21. Diagram showing progression of stable zeolite minerals with increasing temperature. Dashed line represents absolute minimum temperatures based on minerals identified by x-ray diffraction in cuttings from wells SVEC-1 and SVEC-2. Upper solid line represents maximum temperature-based minerals identified by the same methods. Figure modified from Chipera and Apps (2001).

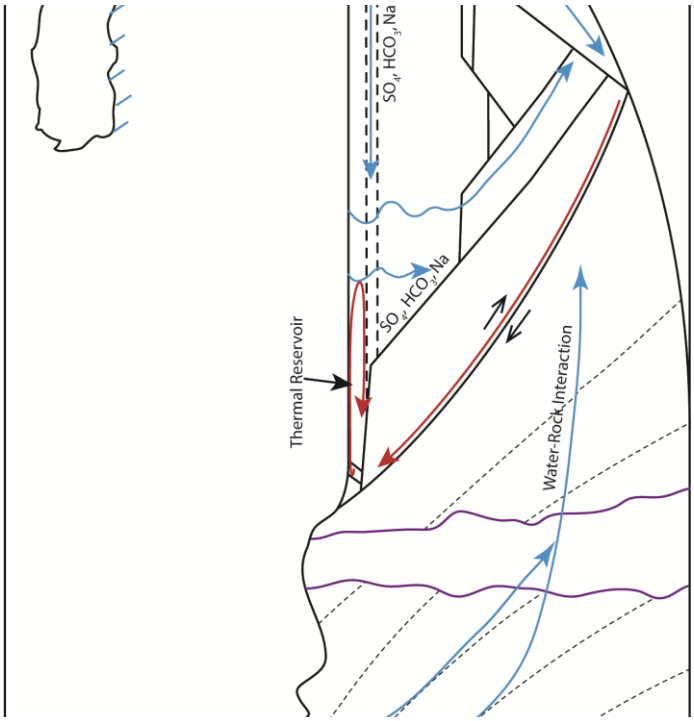

Figure 4.22. Conceptual Model for the Paisley geothermal system, line of section can be found on Figure 4.10. Meteroic water infiltrates the ground at high elevations, becomes heated by the high regional heat flow, and interacts with rocks to create the oxygen isotope shift in Figure 4.17. Water percolating through fluvio-lacustrine sediments in Summer Lake Basin account for high concentrations of non-magmatic SO_4. See text for further discussion.

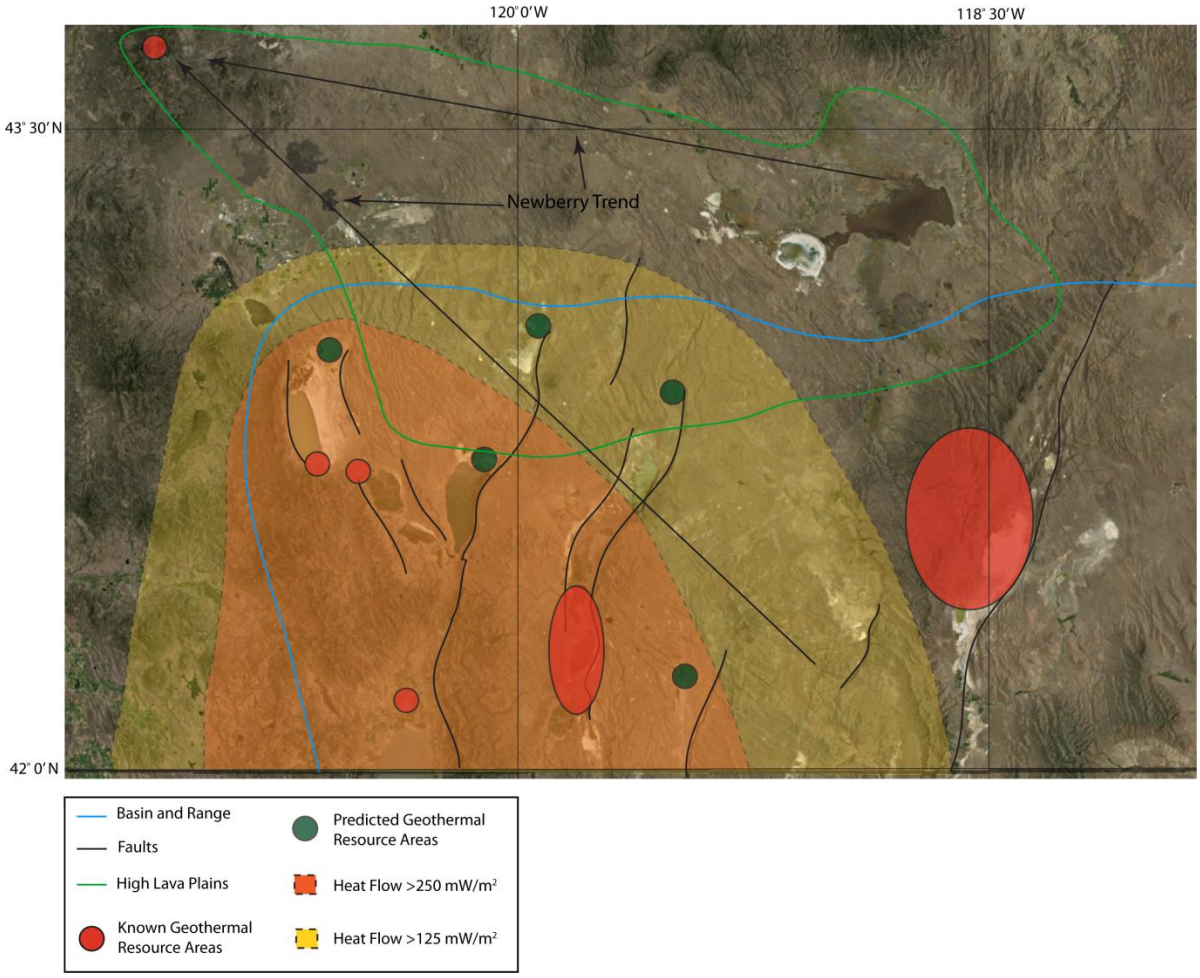

Figure 4.23. Geothermal resources of southeast Oregon. Known Geothermal Resource Areas from Geothermal Resources Layer provided by DOGAMI. Areas of highest heat flow lie within the boundary of the Basin and Range Province. Predicted geothermal resource areas were chosen based on the structural framework and high heat flow. See text for further discussion.

Sample Name	Latitude	Longitude	pH	Li	Na	K	Ca	Mg	SiO2	B	Cl
Colahan Hot Well	42.69385	-120.56773	8.29	0.436	314	10.9	27.1	0.138	148	8.55	221
Colahan Hot Well	42.69385	-120.56773			289	11.1	30.3	0.5	140		180
Colahan Hot Well	42.69385	-120.56773	7.6	0.357	240	8.73	25.7	0.795	109	0.633	158
Colahan Little Hot Well	42.697	-120.55435	8.24	0.2	57.8	3.77	20.3	2.74	27.6	0.234	14.5
Corky's Well	42.70688	-120.55435	7.75	0.527	326	9.34	47	0.258	92.5	7.04	187
Summer Lake Hot Springs	42.72495	-120.64793	8.8	0.105	438	5.97	1.44	0.02	83.9	8.63	340
Douglas House	NA	NA	7.64	0.02	8.46	3.42	12	5.01	20.7	1.8	1.39
Calf Pen	42.69807	-120.54969	8.26	0.153	132	3.75	11.7	0.403	52.9	1.8	45.8
Trailer Park	42.69405	-120.54993	9.25	0.02	48.4	0.732	2.64	0.2	26.2	0.189	3.08
Chewaucan River	NA	NA			6.8	2.5	7.6	1.9	29		0.5
Pump House	42.69299	-120.54785	7.39	0.02	66.3	7.23	30.4	17.7	46.7	0.241	122
Main House	NA	NA	7.4	0.02	37.8	4.82	28.4	18.2	49.5	1.8	40.5
Colahan Hot Well	42.69385	-120.56773									
Colahan Hot Well	42.69385	-120.56773									
Colahan Hot Well	42.69385	-120.56773									
Chewaucan River	NA	NA									
Well SVEC-1	42.69468	-120.56771	8.5		311	10.9	29.5		142	8.07	232
Well SVEC-2	42.69631	-120.55994	7.7		272	10	27.6		128	8.67	217
Summer Lake, OR	42.809	-120.747	NA		6567	264		1	103		3039
Alkali Valley, OR	NA	NA	10.1		117000	8850		10	542		45700
Abert Lake, OR	42.631	-120.229	9.8		119000	3890		10	645		115000
Surprise Valley, CA	NA	NA	9.2		4090	11	11	31	36		4110

Sample Name	B/Cl	F	SO4	HCO3	CO3	NH4	NH4/B	As	Fe	Cond µml	δ18O	δD
Colahan Hot Well	0.03868778	2.88	368	95.9	2	0.27	0.031579	0.669				
Colahan Hot Well			346									
Colahan Hot Well	0.00400633	1.11	253	93.7	2	0.4511	0.712638	0.343		1360		
Colahan Little Hot Well	0.01613793	1.69	22.6	173	2	0.5	2.136752	0.004		395		
Corky's Well	0.03764706	2.3	420	102	2	0.5971	0.084815	0.549		1830		
Summer Lake Hot Springs	0.02538235	1.84	48.8	556	2	1.842	0.213441	0.0064		2070		
Douglas House	1.29496403	1	0.462	83.5	2	0.451	0.250556	0.004		166		
Calf Pen	0.03930131	0.636	73	198	2	0.5	0.277778	0.163		696		
Trailer Park	0.06136364	0.073	1.39	136	2	0.5	2.645503	0.0067		227		
Chewaucan River			4.5	44	0							
Pump House	0.00197541	0.218	1.79	155	2	0.5	2.074689	0.004		565		
Main House	0.04444444	0.161	0.321	205	2	0.5	0.277778	0.0047		480		
Colahan Hot Well	0.02988292										-14.27	-120.41
Colahan Hot Well											-14.34	-119.68
Colahan Hot Well											-14.3	-120.11
Chewaucan River											-14.655	-106.674
Well SVEC-1	0.03478448	3.2	391	76.8	0			0.01	0.26	1750	-13.8915	-118.038
Well SVEC-2	0.03995392	2.86	349	80.6				0.539		1560	-14.1159	-119.724
Summer Lake, OR			695	5916								
Alkali Valley, OR			46300	2510	91400							
Abert Lake, OR			9230	60000	60300							
Surprise Valley, CA			900	1410	664							

Table 1. Name, location, and chemistry of all wells and springs sampled in the Paisley area.

Sample Name	Amorphous Silica	Chalcedony conductive	Quartz Conductive	Quartz Adiabatic
Colahan Hot Well	38	136	161	152
Colahan Hot Well	35	133	157	149
Colahan Hot Well	21	116	142	137
Colahan Little Hot Well	-36	44	76	80
Corky's Well	13	106	133	129
Summer Lake Hot Springs	8	100	128	125
Douglas House	-45	33	65	70
Calf Pen	-12	75	105	105
Trailer Park	-37	42	74	78
Chewaucan River	-34	47	79	82
Pump House	-17	68	99	100
Main House	-14	71	102	102
Colahan Hot Well				
Colahan Hot Well				
Colahan Hot Well				
ChewyRiver				
SVEC-1	36	134	158	150
SVEC-2	30	126	152	145
Summer Lake, OR	18	112	139	134
Alkali Valley, OR	136	254	267	231
Abert Lake, OR	154	276	293	244
Surprise Valley, CA	-26	56	88	90

Table 2. Temperatures (°C) calculated from silica geothermometers for all wells and springs sampled in the Paisley area.

Sample Name	Na-K-Ca	Na-K-Ca Mg Corrected	Na/K Fournier	Na/K Truesdell	Na/K Giggenbach	K/Mg Giggenbach
Colahan Hot Well	136	136.2	140.4	96.2	160	127
Colahan Hot Well	106	106.5	146.7	103.3	166	108
Colahan Hot Well	99	99.3	143.3	99.4	163	95
Colahan Little Hot Well	61	30.3	182.9	145.7	200	60
Corky's Well	91	90.9	129.0	83.3	149	113
Summer Lake Hot Springs	122	121.9	90.3	41.1	111	139
Douglas House	50	-101.9	375.5	411.0	375	52
Calf Pen	81	81.2	128.6	82.8	149	82
Trailer Park	52	51.6	95.3	46.4	116	53
Chewaucan River	48	-24.1	361.5	389.1	363	55
Pump House	74	-169.2	224.5	197.0	239	54
Main House	58	-180.8	238.7	215.3	252	45
Colahan Hot Well						
Colahan Hot Well						
Colahan Hot Well						
ChewyRiver						
SVEC-1	107	107.4	141.0	96.8	161	
SVEC-2	104	104.1	144.0	100.2	163	
Summer Lake, OR			149.6	106.6	169	211
Alkali Valley, OR			194.2	159.3	211	352
Abert Lake, OR			136.8	92.0	156	294
Surprise Valley, CA	77	-335.1	27.1	-23.5	49	57

Table 3. Temperatures (°C) calculated from cation geothermometers for all wells and springs sampled in the Paisley area.

References Cited

Albright, B.L., Woodburne, M.O., Fremd, T.J., Swisher III, C.C., MacFadden, B.J., Scott, G.R. 2008. Revised Chronostratigraphy and Biostratigraphy of the John Day Formation (Turtle Cove and Kimberly Members), Oregon, with Implications for Updated Calibration of the Arikareean North American Land Mammal Age. The Journal of Geology. v. 116. p. 211-237. DOI: 10.1086/587650.

Appling., R.N. 1950. Economic Geology of the Brattain mining area, Paisley, Oregon. Master's Thesis. University of Oregon. Eugene, Oregon. 74 p.

Arehart, G.B., Coolbaugh, M.F., Poulson, S.R. 2007. Geochemical Characterization of Geothermal Systems in the Great Basin: Implications for Exploration, Exploitation, and Environmental Issues. Geothermal Resources Council Transactions. 5 p.

Badger, T.C., Watters, R.J. 2004. Gigantic Seismogenic Landslides of Summer Lake Basin, South-Central Oregon. Gelogical Society of America Bulletin. v. 116, no. 5/6. p. 687-697. DOI: 10.1130B25333.1.

Benning, L.G., Wilkin, R.T., Barnes, H.L. 2000. Solubility and Stability of Zeolites in Aqueous Solution: II. Calcic Clinoptilolite and Mordenite. American Mineralogist. v. 85. p. 495-508.

Blank., H.R. 1973. Geothermal Investigations in Eastern Oregon: A report on work carried out on behalf of Eugene Water and Electric Board. 49 p.

Chipera, S.J., Apps, J.A. 2001. Geochemical Stability of Natural Zeolites. Reviews in Mineralogy and Geochemistry. p. 117-161. DOI: 10.2138/mag.2001.45.3.

Colgan, J.P., Dumitru, T.A., McWilliams, M., Miller, E.L. 2006. Timing of Cenozoic Volcanism and Basin and Range extension in the northwestern Nevada: New constraints from the northern Pine Forest Range. Geological Society of America Bulletin. v. 118, no. 1/2. p. 126-239. DOI: 10.1130/B25681.1.

Coolbaugh, M.F., Arehart, G.B., Faulds, J.E., Garside, L.J. 2005. Geothermal Systems in the Great Basin, Western United States: Modern Analogues to the Roles of Magmatism, Structure, and Regional Tectonics in the Formation of Gold Deposits. *In* Geological Society of Nevada Symposium 2005: Window to the World. Rhoden, H.N., Steininger, R.C., Vikre, P.G. (eds). Reno, NV. p. 1063-1081.

Cox, C.M. 2011. A Controlled-Source Seismic and Gravity Study of the High Lava Plains (HLP). Master's Thesis. University of Oklahoma, Norman, Oklahoma. 110 p.

Craig, H. 1961. Isotopic Variations in Meteoric Waters. Science. v. 133, no. 3465. p. 1702-1703.

Crider, J.G. 2001. Oblique Slip and the Geometry of Normal –Fault Linkage: Mechanics and a Case Study from the Basin and Range in Oregon. Journal of Structural Geology. v. 23. p. 1997-2009.

Criss, R.E., Taylor, H.P. 1986. Meteoric-Hydrothermal Systems. *In* Stable Isotopes in High Temperature Geological Processes. Valley, J.W., Taylor, H.P., O'Neil, J.R. (eds). Mineralogical Society of America. Reviews in Mineralogy Vol. 16. p. 373-424.

Diggles, M.F., King, H.D., Gettings, M.E., Conrad, J.E., Sawatzky, D.L., Soreghan, G.S., Peters, T.J., Willet, S.L. 1990. Mineral Resources of the Diablo Mountian Wilderness Study Area, Lake County, Oregon. United States Geological Survey Bulletin 1738-D. Mineral Resources of Wilderness Study Areas: South-Central Oregon. 22 p.

Donath, F.A. 1962. Analysis of Basin-Range Structure, South-Central Oregon. Geological Society of America Bulletin. v. 73. p. 1-16. DOI: 10.1130/0016-7606(1962)73[1:AOBSSO]2.0.CO;2.

Donath, F.A., Kuo, J.T. 1962. Seismic-Refraction Study of Block Faulting, South-Central Oregon. Geological Society of America Bulletin. v. 73. p. 429-434. DOI: 10.1130/0016-7606(1962)73[429:SSOBFS]2.0.CO;2.
1986

Drever, J.I. 1982. Evaporation and Saline Waters in the Geochemistry of Natural Waters. Prentice-Hall, Inc., Englewood Cliffs, New Jersey. p. 200-228.

du Bray, E.A., John, D.A. 2011. Petrologic, Tectonic, and Metallogenic Evolution of the Ancestral Cascades Magmatic Arc, Washington, Oregon, and northern California. Geosphere. v. 7, no. 5. p. 1102-1133. DOI: 10.1130/GES00669.1.

Duffield, W.A., McKee, E.H. 1986. Geochronology, Structure, and Basin-Range Tectonism of the Warner Range, Northeastern California. Geological Society of America Bulletin. v. 97, no. 2. p. 142-146. DOI: 10.1130/0016-7606(1986)97<142:GSABTO>2.0.CO;2.

Egger, A.E., Miller, E.L. 2011. Evolution of the Northwest Margin of the Basin and Range: The Geology and Extensional History of the Warner Range and Environs, Northeastern California. Geosphere. v. 7. p. 756-773. DOI: 10.1130/GES00620.1.

Faulds, J.E., Coolbaugh, M.F., Vice, G.S., Edwards, M.L. 2006. Characterizing Structural Controls of Geothermal Fields in the Northwestern Great Basin: A Progress Report. Geothermal Resources Council Transactions. v. 30. p. 69-76.

Fournier, R.O. 1992. Water Geothermometers applied to Geothermal Energy. *In* Application of Geochemistry in Geothermal Reservoir Development: Series of Technical Guides on the Use of Geothermal Energy. D'Amore, F. (ed). Rome, Italy. p. 37-70.

Garcher, L., Arehart, G. 2008. Origin and Characterization of Geothermal Waters at Desert Queen, Nevada. Geothermal Resources Council Transactions. v. 32. p. 147-152.

Giggenbach, W.F., Soto, R.C. 1992. Isotopic and Chemical Composition of Water and Steam Discharge from Volcanic-Magmatic-Hydrothermal Systems of the Guanacaste Geothermal Province, Costa Rica. Applied Geochemistry. v. 7. p. 309-332.

Giggenbach, W.F. 1988. Geothermal Solute Equilibria, Derivation of Na-K-Mg-Ca Geoindicators. Geochimica et Cosmochimica Acta. v. 52. p. 2749-2765.

Giggenbach, W.F. 1992. Chemical Techniques in Geothermal Exploration. *In* Application of Geochemistry in Geothermal Reservoir Development: Series of Technical Guides on the Use of Geothermal Energy. D'Amore, F. (ed). Rome, Italy. p. 119-144.

Hantelmann, J.J. 2006. The Geothermal Potential of Crump Geyser in Warner Valley, Lake County, Oregon. Geothermal Resources Council Transactions. v. 30. p. 77-82.

Jordan, B.T., Grunder, A.L., Duncan, R.A., Deino, A.L. 2004. Geochronology of Age-Progressive Volcanism of the Oregon High Lava Plains: Implications for the Plume Interpretation of Yellowstone. Journal of Geophysical Research. v. 109. DOI: 10.1029/2003JB002776.

Krahmer, M.S. 1995. The Geology and Hydrochemistry of the Geothermal System Near Stanley, Idaho. Master's Thesis. Washington State University. Pullman, WA. 159 p.

Kristmannsdottir, H., Tomasson, J. 1976. Zeolite Zones in Geothermal Areas in Iceland. *In* Natural Zeolites: Occurrence, Properties, Use, A Selection of Papers Presented at Zeolite, 76, an International Conference on the Occurrence, Properties, and Utilization of Natural Zeolites, Tuscan, Arizona, June 1976. Sand, L.B., Mumpton, F.A. (eds). Pergamon Press Ltd., Oxford, England. p. 277-284.

Lawrence, R.D. 1976. Strike-Slip Faulting Terminates the Basin and Range Province in Oregon. Geological Society of America Bulletin. v. 87, no. 6. p. 846-850. DOI: 10.1130/0016-7606(1976)87<846:SFTTBA>2.0.CO;2.

Licciardi, J.M. 2001. Chronology of the latest Pleistocene Lake Level Fluctuations in the Pluvial Lake Chewaucan Basin, Oregon, USA. Journal of Quaternary Science. v. 16, no. 6. p. 545-553. DOI: 10.1002/jqs.619.

Lux, D.R. 1982. K-Ar and $^{40}Ar/^{39}Ar$ ages of mid-Tertiary Volcanic Rocks from the Western Cascade Range, Oregon. Isochorn/West. v. 33. p. 27-32.

MacLeod, N.S., Walker, G.W., McKee, E.H. 1976. Geothermal Significance of Eastward Increase in Age of Upper Cenozoic Rhyolitic Domes in Southeastern Oregon. Proceedings, Second United Nations Symposium on the Development and Use of Geothermal Resources, San Fransisco, 1975. v. 1. 10 p.

McSween, H.Y., Richardson, S.M., Uhle, M.E. 2003. Geochemistry: Pathways and Processes. 2nd Edition. Columbia University Press, New York, New York. 363 p.

Muntzert, J.K. 1969. Geology and Mineral Deposits of the Brattain District, Lake County, Oregon. Master's Thesis. Oregon State University. 70 p.

Muntzert, J.K., Field, C.W. 1969. Geology and Mineral Deposits of the Brattain District, Lake County, Oregon. Geological Society of America Abstracts. p. 616-617.

Negrini, R.M., Davis, J.O. 1992. Dating Late Pleistocene Pluvial Events and Tephras by Correlating Paleomagnetic Secular Variation Records from the Western Great Basin. Quaternary Research. v. 38. p. 46-59.

Nicholson, K. 1993. Geothermal Fluids: Chemistry and Exploration Techniques. Springer-Verlag. New York, New York. 263 p.

Person, M., Banerjee, A., Hofstra, A., Sweetkind, D., Gao, Y. 2008. Hydrologic Models of Modern and Fossil Geothermal Systems in the Great Basin: Genetic Implications for Epithermal Au-Ag and Carlin-Type Gold Deposits. Geosphere. v. 4, no. 5. p. 888-917. DOI: 1130/GES00150.1.

Peterson, N.V., McIntyre, J.R. 1970. The Reconnaissance Geology and Mineral Resources of Eastern Klamath County and Western Lake County, Oregon. Oregon Department of Geology and Mineral Industries Bulletin 66. 70 p.

Pezzopane, S.K., Weldon, R.J. 1993. Tectonic Role of Active Faulting in Central Oregon. Tectonics. v. 12, no. 5. p. 1140-1169.

Powell, T., Cumming, W. 2010. Spreadsheets for Geothermal Water and Gas Geochemistry. Proceedings, Thirty-Fifth Workshop on Geothermal Reservoir Engineering. Stanford University, Stanford, California. 10 p.

Roberts, C.W., Kucks, R.P., Hill, P.L. 2008. Oregon Magnetic and Gravity Maps and Data- A Website for Distribution of Data. United States Geological Survey Data Series 355. Accessed February 5, 2013. http://pubs.usgs.gov/ds/355/index.html.

Rybach, L. 1981. Geothermal Systems, Conductive Heat Flow, Geothermal Anomalies. *In* Geothermal Systems: Principles and Case Histories. Rybach, L., Muffler, L.P. (eds). Wiley, Chichester. p. 3-36.

Scarberry, K.C., Meigs, A.J., Grunder, A.L. 2010. Faulting in a Propagating Continental Rift: Insight from the late Miocene Structural Development of the Abert Rim Fault, Southern Oregon, USA. Tectonophysics. v. 488. p. 71-86. DOI: 10.1016/j.tecto.2009.09.025.

Sladek, C., Arehart, G.B., Benoit, W.R. 2004. Geochemistry of the Lake City Geothermal System, California, USA. Geothermal Resources Council Transactions. v. 28. p. 363-368.

Smith, G.I., Friedman, I., Gleason, J.D., Warden, A. 1992. Stable Isotope Composition of Waters in Southeastern California: 2. Groundwaters and Their Relation to Modern Precipitation. Journal of Geophysical Research. v. 97, no. D5. p. 5813-5823.

Smith, G.I., Friedman, I., Veronda, G., Johnson, C.A. 2002. Stable Isotope Compositions of Waters in the Great Basin, United States 3. Comparisons of Groundwaters with Modern Precipitation. Journal of Geophysical Research. v. 107, no. D19. DOI: 10.1029/2001JD000567.

Taylor, H.P. 1974. The Application of Oxygen and Hyrogen Isotope Studies to Problems of Hydrothermal Alteration and Ore Depositon. Economic Geology. v. 69. p. 843-883.

Travis, P.L. 1977. Geology of the Area near the North End of Summer Lake, Lake County, Oregon. Master's Thesis. University of Oregon. Corvallis, OR. 95 p.

Trench, D., Meigs, A., Grunder, A. 2012. Termination of the Northwestern Basin and Range Province into a Clockwise Rotating Region of Transtension and Volcanism, Southeast Oregon. Journal of Structural Geology. v. 39. p. 52-65. DOI: 10.1016/j.jsg.2012.03.007.

Veen, C.A. 1981. Gravity Anomalies and Their Structural Implications for the Southern Oregon Cascade Mountains and Adjoining Basin and Range Province. Master's Thesis. Oregon State University, Corvallis, Oregon. 86 p.

Verplanck, E.P., Duncan, R.A. 1987. Temporal Variations in Plate Convergence and Eruption Rates in the Western Cascades, Oregon. Tectonics. v. 6, no. 2. p. 197-209.

Walker, G. 1963. Reconnaissance Geologic Map of the Eastern Half of the Klamath Falls (AMS) Quadrangle, Lake and Klamath Counties, Oregon. United States Geological Survey Miscellaneous Field Studies Map MF-260. 1:250 000 scale. 1 sheet. Reston, VA.

Walker, G., Peterson, N., Greene, R. 1967. Reconnaissance Geologic Map of the East Half of the Crescent Quadrangle, Lake, Deschutes, and Crook Counties, Oregon. United States Geological Survey Miscellaneous Geologic Investigations Map I-493. 1:250 000 scale. 1 Sheet. Reston, VA.

Walker, G. 1977. Geologic Map of Oregon east of the 121st Meridian. United States Geological Survey Miscellaneous Investigation Series Map I-902. 1:500 000 scale. 2 sheets. Reston, VA.

Walker, G.W., MacLeod, N.S. 1991. Geologic Map of Oregon. United States Geological Survey. 1:500 000 scale. 2 sheets.

White, J., Robinson, P.T. 1992. Intra-arc Sedimentation in a Low-Lying Marginal Arc, Eocene Clarno Formation, Central Oregon. Sedimentary Geology. v. 80. p. 89-114.

APPENDIX A

Derivation of Cation and Silica Geothermometers and Stable Isotope Theory

The Na/K Geothermometer

The Na/K geothermometer is based on the premise that the concentrations of these chemical constituents in the fluid is reliant on the ionic exchange between albite and microcline feldspars from the host rock as albite alters to microcline, given by Fournier (1989):

$$NaAlSi_3O_8 + K^+ = KAlSi_3O_8 + Na^+$$

Where the equilibrium constant, K_{eq}, equals:

$$K_{eq} = [KAlSi_3O_8][Na^+]/[NaAlSi_3O_8][K^+]$$

Where the square brackets refer to the activities of the enclosed species. If the activities of albite and microcline are considered to be equal and the activities of Na and K are taken to be equivalent to their molal concentrations, then the equation simplifies to

$$K_{eq} = Na^+/K^+$$

It has been found that the change in K_{eq} with respect to temperature is given by an integrated form of the van't Hoff equation (Fournier, 1989):

$$\log K_{eq} = (\Delta H°/2.303RT) + C$$

Where $\Delta H°$ is the enthalpy of reaction, T is temperature in kelvins, R is the gas constant, and C is a constant of integration. $\Delta H°$ changes little with temperature in the range of 0-300°C, and therefore a graph of $\log K_{eq}$ vs 1000/T results in a straight line (Fournier, 1989, 1992).

The equation above describing the aqueous solution constituents is for end-member compositions of these two fluid-mineral systems, and such a simple system is unlikely in nature. Other constituents such as Ca in plagioclase and K, Mg, Li, Ca, and

Na in clay minerals affect the solid solutions playing a role in chemical reactions with the water and therefore introduce inconsistencies in the Na/K geothermometer (Fournier, 1989).

The Na-K-Ca-Mg Geothermometer

An attempt to account for the activities of solid solutions led Fournier and Truesdell (1973) to empirically derive the Na-K-Ca geothermometer. This was necessitated by the fact that several different curves can arise when log Na/K is plotted versus reciprocal temperature, reflecting the dependency of the Na/K concentration on the minerals controlling the reaction (Fournier and Truesdell, 1973). Plus, Ca in natural systems is dependent on the temperature, pH, and partial pressure of CO_2 of a Ca bearing carbonate (aqueous), usually calcite, and of Ca bearing feldspars (Fournier and Truesdell, 1973). The general equation describing these reactions is given by Fournier and Truesdell (1973):

$$\log (Na/K) + \beta \log[\sqrt{(Ca)}/Na]$$

where β is 1/3 for fluids equilibrating above 100°C and β is 4/3 for fluids equilibrating below 100°C. The values obtained from the equation above plotted against reciprocal temperature produces a straight line. For this geothermometer to work, assumptions are made such that there is abundant silica, Al is fixed to the solid components and that H^+ ions participating in hydrolysis cancel on either side of the equation (Fournier and Truesdell, 1973). The assumption that Al is fixed to the solid components only holds true with near neutral pH waters.

An additional correction to the Na-K-Ca geothermometer was proposed by Fournier and Potter (1979) to account for the concentration of Mg in thermal waters. The concentration of Mg^{2+} decreases with increasing temperature; therefore, one must subtract the temperature affect that Mg^{2+} concentration has from the calculated Na-K-Ca geothermometer (Founrier and Potter, 1979). The magnitude of this correction was determined empirically and is typically given by the equation (Fournier and Potter, 1979):

$$\Delta t_{Mg} = 10.66 - 4.7415R + 325.87(\log R)^2 - 1.032 \times 10^5(\log R)^2/T - 1.968 \times 10^7(\log R)^2/T^2 + 1.605 \times 10^7(\log R)^3/T^2$$

where Δt_{Mg} is the temperature in °C that must be subtracted from the Na-K-Ca calculated temperature and where:

$$T = \text{The calculated Na-K-Ca temperature in °C}$$

$$R = [Mg/(K + Ca + Mg)] \times 100$$

The equation above is for use when $5<R<50$, above $R = 50$ the water has become equilibrated with the host rock (Fournier and Potter, 1979).

Giggenbach (1992) describes how to select the correct geothermometer by first plotting on a ternary diagram the relative abundances of the anions Cl^-, HCO_3^-, and SO_4^{2-}. This is necessary because in order for most cation geothermometers to be accurate they must be measured from a water that is near neutral in pH and has Cl^- has the major anion. This diagram is useful for indicating which water samples are useful for cation geothermometry and is not intended to provide further information regarding specific thermodynamic properties of the fluid (Giggenbach, 1992). The diagram is separated

into three divisions, the uppermost corner is that of mature Cl rich water, the bottom left corner is the SO_4^{2-} division, representing waters heated at high temperature by volcanic HCl steam or at low temperatures by H_2S steam, and the HCO_3 corner in the bottom-right proxies for waters that have interacted with fluids saturated with CO_2 (Giggenbach, 1992). Reliable temperatures from the cation geothermometers can only be calculated from waters that reside in the hatched area of the upper-right hand corner within the Cl field because this type of water was used to derive the equations used in calculating temperature.

The Na-K-Mg Geothermometer

The Na/K and K/Mg geothermometers are used in conjunction to form the Na-K-Mg geothermometer. Unlike the Na/K geothermometer the K/Mg geothermometer is the result of the reaction of K-mica with chlorite and silica to produce K-feldspar and Mg^{2+} ions (Giggenbach, 1992). The equation to calculate the temperature with the K/Mg geothermometer is given by (Giggenbach, 1992):

$$T_{km} = 4410/(14.0 - L_{km}) - 273.15$$

Where $L_{km} = \log(c_K/c_{Mg})$, c in mg/kg. The evaluation of these two geothermometers separately will generally give different temperatures because the rate in which these systems come into equilibrium with the host rock at a given temperature differ. The Na-K system tends to be slower to reach equilibrium than the K-Mg system; therefore, temperatures calculated by the Na-K system are generally higher than those calculated from the K-Mg system (Giggenbach, 1992). The Na-K-Mg system is generally plotted on a ternary diagram, first provided by Giggenbach (1988). The diagram is separated into three main areas: An area of immature waters, partially

equilibrated waters, and an area of fully equilibrated waters. Other uses for this diagram are to approximate the amount of mixing with meteoric waters and to qualitatively predict the speed in which thermal waters ascended to near surface environments. For example, if the K/Mg geothermometer is much lower than the Na/K geothermometer, this could suggest that there was rapid ascent to the surface, given that the K-Mg system equilibrates much faster than the Na-K system. Also, as stated above, the concentration of Mg^{2+} decreases with increasing temperature, implying that meteoric waters are enriched with Mg^{2+} with respect to thermal waters.

An example of how this diagram shows mixing is provided here: If water samples from deep wells and samples from surface springs lie along a line starting at full or partial equilibrium for the deep well samples and they progress towards the Mg corner for shallow wells and springs, this is strong evidence that the shallower wells and springs are mixing with Mg-rich meteoric waters. If the same line points towards the Mg corner, the other end of the line will point towards the full equilibrium line. From this end, one will be able to predict a reservoir temperature for these fluids by reading the temperature on the full equilibrium line.

Silica Geothermometers

The original observation that the concentration of silica is related to temperature was made by Morey et al. (1962). Fournier and Rowe (1966) and Mahon (1966) were successful at deriving equations that could be used to calculate reservoir temperature based on silica concentrations but were only valid between temperatures of 120° to 330°C. These equations allowed for the evaluation of reservoir temperatures during adiabatic cooling, conductive cooling, and conductive cooling with a one stage steam loss

at 100°C. Morey et al. (1962) also noted that if the log of silica concentration was plotted against the reciprocal of temperature, the data would plot along a straight line between the 20°-250°C. Fournier and Potter (1982) expanded the silica geothermometers to be used for temperatures in the range of 0°-250°C. They fit their experimental data with data from natural systems and noticed it was in good agreement. In geothermal systems above 180°C, quartz is the mineral controlling silica solubility, whereas in systems below 140°C, chalcedony has been found to be the mineral controlling silica solubility (Krahmer, 1995). The four main silica geothermometers are listed below, from Henley et al. (1984):

Quartz- No steam loss (cond. cooling): $t(°C) = [1309/(5.19 – \log S)] – 273.15$

Quartz- Max steam loss (adiab. cooling): $t(°C) = [1522/(5.75 – \log S)] – 273.15$

Chalcedony: $t(°C) = [1032/(4.69 – \log S)] – 273.15$

Amorphous Silica: $t(°C) = [731/(4.52 – \log S)] – 273.15$

Where S = SiO_2 concentration in mg/kg.

Stable Isotopes

Isotopes of elements are measured using mass spectrometry and are reported to a standard. The standard used in this discussion is that of the Vienna Standard Mean Oceanic Water or V-SMOW. A sample is measured for both heavy and light isotope composition and is reported as a ratio with the rare isotope in the numerator and the common isotope in the denominator. Subtracted from this ratio is the ratio of the rare to common isotope value of the standard, the difference is then divided by the ratio of the standard multiplied by one thousand, has units of per mil, and is reported in delta

notation. For example, for the isotopic value of $^{18}O/^{16}O$ for waters reported with respect to V-SMOW, the proper notation would be:

$$\delta^{18}O = [\{(^{18}O/^{16}O)_{sample} - (^{18}O/^{16}O)_{V\text{-}SMOW}\}/(^{18}O/^{16}O)_{V\text{-}SMOW}] \times 1000‰$$

Therefore, the $\delta^{18}O$ value for V-SMOW would be 0‰.

Isotopic values of water are a result of the fractionation process. For example, as water is evaporated from the oceans, the resultant vapor will be depleted in ^{18}O relative to the water in which it evaporated from. If this water vapor condenses to form a cloud, then the water droplet formed will be enriched in ^{18}O with respect to the vapor in which it formed, though being depleted with respect to the ocean water in which it started. The final $\delta^{18}O$ value obtained is a function of the temperature, elevation and latitude in which the droplet formed. Deuterium is the rarer and heavier of the hydrogen isotopes found in water; therefore, δD is the isotope used for hydrogen notation.

References Cited

Fournier, R.O. 1989. Lectures on Geochemical Interpretation of Hydrothermal Waters. United Nations University Geothermal Training Programme. Report 10. Reykjavik, Iceland. 73 p.

Fournier, R.O. 1992. Water Geothermometers applied to Geothermal Energy. *In* Application of Geochemistry in Geothermal Reservoir Development: Series of Technical Guides on the Use of Geothermal Energy. D'Amore, F. (ed). Rome, Italy. p. 37-70.

Fournier, R.O., Potter, R.W. 1979. Magnesium correction to the Na-K-Ca chemical geothermometer. Geochimica et Cosmochimica Acta. v. 42. p. 1543-1550.

Fournier, R.O., Potter, R.W. 1982. A revised and expanded silica (quartz) geothermometer. Geothermal Resources Council Bulletin, November 1982. p. 3-12.

Fournier, R.O., Rowe, J.J. 1966. Estimation of Underground Temperatures from the Silica Content of Water from Hot Springs and Wet-Steam Wells. American Journal of Science. v. 264. p. 685-697.

Fournier, R.O., Truesdell, A.H. 1973. An empirical Na-K-Ca geothermometer for natural waters. Geochimica et Cosmochimica Acta. v. 87. p. 1255-1275.

Giggenbach, W.F. 1988. Geothermal solute equilibria. Derivation of Na-K-Mg-Ca geoindicators. Geochimica et Cosmochimica Acta. v. 52. p. 2749-2765.

Giggenbach, W.F. 1992. Chemical Techniques in Geothermal Exploration. *In* Application of Geochemistry in Geothermal Reservoir Development: Series of Technical Guides on the Use of Geothermal Energy. D'Amore, F. (ed). Rome, Italy. p. 119-142.

Henley, R.W., Truesdell, A.H., Barton Jr, P.B. 1984. *In* Fluid-Mineral Equilibria in Hydrothermal Systems. Reviews in Economic Geology. Robertson, James (ed). v. 1. El Paso, TX. 267 p.

Krahmer, M.S. 1995. The Geology and Hydrochemistry of the Geothermal System Near Stanley, Idaho. Master's Thesis. Washington State University. Pullman, WA. 159 p.

Mahon, W.A. 1966. Silica in Hot Water Discharged from Drillholes at Wairakei, New Zealand. New Zealand Journal of Science. v. 9. p. 135-144.

Morey, G.W., Fournier, R.O., Rowe, J.J. 1962. The solubility of Quartz in Water in the Temperature Interval from 29° to 300°C. Geochimica et Cosmochimica Acta. v. 26, no. 10. p. 1029-1043.

APPENDIX B

MATLAB© Script for Gravity Data Reduction

The instrument used in the Paisley study was a Worden gravimeter, which uses a quartz spring suspended in a sealed vacuum to make its measurements. These instruments measure the gravitational field in units of milligals (mgals). Gravity has SI units of m/s^2. 1 gal has units of cm/s^2, therefore a milligal has units of $cm/s^2 \times 10^{-3}$. The accepted theoretical value for gravity on earth is 9.8 m/s^2, in milligals, one would report this value as 980,000 mgals.

For a gravity survey, four things need to be measured in the field: the elevation of the gravity station, the latitude and longitude of the gravity station, the gravity reading at the gravity station, and the time at which the gravity measurement was taken. This information is necessary to compute the several different corrections that produce the Complete Bouguer Anomaly. The Complete Bouguer Anomaly essentially shows the variations of density in the subsurface.

The first correction made in this gravity survey was the theoretical value for gravity at each station. This was done using the geodetic reference system formula of 1967 or GRS67 described in Burger et al. (2006):

$$g_n = 978031.85 * (1 + 0.005278895 \times (\sin^2 \varphi) + 0.000023462 * (\sin^4 \varphi))$$

where ϕ is the latitude of the gravity station and the result of this equation has units of mgals.

The next correction is called the free air correction. This correction is made because the measured observed gravity will decrease with increasing distance from the center of the Earth (Burger et al., 2006).

$$g_{fa} = -0.3086 - 0.00023 * (\cos 2\varphi) + 0.00000002 * z$$

where ϕ is the latitude of the gravity station and z is the elevation of the gravity station. The free air correction also has units of mgals.

The next correction applied is the Bouguer Slab correction; this correction accounts for the mass that is in between the gravity station's elevation and the reference ellipsoid. The density used in the equation is usually assigned a value of 2.67 g/cm^3 but a site-specific average density can also be used (Burger et al., 2006).

$$g_{sc} = 0.04193 * \rho * z$$

where ρ is density and z is elevation of the gravity station. Like the previous two corrections, the Bouguer Slab has units of mgals.

The final correction made is the Terrain Correction, which takes into account the terrain of the surrounding area. The measured gravity of a point can be affected by topographic highs or lows several kilometers away (Burger et al., 2006). This correction is the most complex of all the corrections. The method employed in this survey was that adopted by Burger et al. (2006) after Hammer (1939). From each survey location, a ring is created with an inner and outer radius; the lengths of these radii have been determined by Hammer (1939) (Burger et al., 2006). Each ring is then broken down into sectors, with the outer rings having more sectors than the inner rings (Burger et al., 2006). "The absolute value of the difference between the gravity station and the average elevation of a sector is then computed" (Burger et al., 2006). Once this is computed, then the equation (Burger et al., 2006):

$$g_{ring} = 0.11 * (R_o - R_i + ((R_i^2 + z^2)\text{^}(1/2)) - ((R_o^2 + z^2)\text{^}(1/2)))$$

is used, where R_o is the outer radius, R_i is the inner radius, and z is the computed absolute difference (Burger et al., 2006). A total of 68 sectors are created, defining 8 rings. The innermost ring has 4 sectors, the next two have 6 sectors, the next two have 8 sectors, and the outermost three rings have 12 sectors (Burger et al., 2006). Because of this, the value of g_{ring} will have to be divided by the number of sectors that are contained within a particular ring. After dividing by the number of sectors, the final step is to sum all 68 sectors to get the terrain correction value for a gravity survey point. When this value is added to the Simple Bouguer Anomaly, the Complete Bouguer Anomaly has then been determined.

The Algorithm

A code was written in MATLAB© with the methods for data reduction following that of Burger et al. (2006) and the script can be found in Appendix B. The algorithm was written to streamline the data reduction process, which in large surveys can be very time consuming to do by hand; therefore, this code was intended to be as generic as possible so that it could be used without having to manually change the size and names of the input variables from one survey to the next.

The following is a list that contains the general procedure of the algorithm:

1. Create .mat file that contains:
    a. Station ID
    b. Latitude and Longitude of gravity stations
    c. Elevation of gravity stations
    d. Observed gravity values for each station

e. UTM's for each station

f. Duration since first measurement for each gravity station

g. Drift values

i. Currently these have to be determined from outside sources

2. A Digital Elevation Model

a. Used for the terrain correction calculation

3. Set up empty containers for variables.

4. Define variables for the terrain correction process.

5. Outer most for loop (i) that:

a. Sets up x and y dimensions of survey

b. Determines radius R that each pixel in the DEM lies from current (ith) survey point

c. Sets up variable Theta that sweeps 2pi radians around each survey point

d. Determines the absolute value of the difference between the elevation of a survey point and the elevation of a sector

e. Calculates the gravity effect for each sector, then sums the sectors

f. The sum of the sectors is added to the Simple Bouguer Anomaly to produce the Complete Bouguer Anomaly

g. Calculates all the corrections necessary to determine the Complete Bouguer Anomaly

6. Nested for loop (j) that is using the inner radius of a ring to produce an equal amount of sectors based on the vector NSector
7. Doubly nested for loop (k) that is determining the average elevation of each sector
8. Create Figures

MATLAB Script

```
clear all;
close all;

load('PaisleyGravitySurvey.mat');

% VARIABLES

Nsurvey = size(PaisleyGravitySurvey,1); % Creates dummy variable
that has the number of survey points of gravity survey
Gobs = PaisleyGravitySurvey(:,5); % Observed Gravity in mGals
lat = PaisleyGravitySurvey(:,3); % Latitude in degrees
elev = PaisleyGravitySurvey(:,4); % Elevation in meters
rho = 2.5; % Density g/cm^3
Datum = PaisleyGravitySurvey(1,4);
zd = zeros(size(PaisleyGravitySurvey(:,1))); % Creates a
container for change in elevations to be stored in wrt datum
(=elevation of base station)
LAT=lat(1);  % Use station 1 as base latitude
y = PaisleyGravitySurvey(:,7);
ybase= PaisleyGravitySurvey(1,7); % Datum for latitude correction
Dgds = (0.811/1000) * sind(LAT*2.0); % mGal/meter latitude
effect, + as move toward pole for current hemisphere
Ds = zeros(size(PaisleyGravitySurvey(:,1))); % Creates a
container for Ds
StationID = PaisleyGravitySurvey(:,1); % Station ID Number
Dur = PaisleyGravitySurvey(:,8); % Duration Since First
Observation (hours)
Drift = PaisleyGravitySurvey(:,9); % Drift accounts for meter and
tidal variations in gravity readings (assuming base stations are
reoccupied every 2-3 hours)
Gcba = zeros(size(PaisleyGravitySurvey(:,1))); % Creates a
container for Complete Bouguer Anomaly
Gba = zeros(size(PaisleyGravitySurvey(:,1))); % Creates a
container for Simple Bouguer Anomaly values
Gn = zeros(size(PaisleyGravitySurvey(:,1))); % Creates a
container for Theoretical Gravity Values
Gfa = zeros(size(PaisleyGravitySurvey(:,1))); % Creates a
container for Free Air Anomaly Values
Gbs = zeros(size(PaisleyGravitySurvey(:,1))); % Creates a
container for Bouguer Slab
```

```
      % TERRAIN CORRECTION VARIABLES

      ZoneIR = [2 16.64 53.34 170.08 390.14 894.89 1529.49 2614.57]; %
Defines inner radius for 8 zones
      ZoneOR = [16.64 53.34 170.08 390.14 894.89 1529.49 2614.57
4453.74]; % Defines outer radius for 8 zones
      NSector = [4 6 6 8 8 12 12 12]; % Defines number of sectors for
each zone
      NZ = sum(NSector); % Total number of sectors
      Elevsec = zeros(NZ,Nsurvey); % Creates a container for sector
elevations
      ZoneIR_long = zeros(NZ,1); % Creates container with length of NZ
      ZoneOR_long = zeros(NZ,1); % Creates container with length of NZ
      Zavg = zeros(NZ,1); % Creates container to store computed average
elevations per sector
      Gterr = zeros(NZ,Nsurvey); % Create a container for terrain
correction values
      Gtotal = zeros(NZ,Nsurvey); % Creates a container for sector
correction in mGals
      [A,R] = geotiffread('repr45_2.tif'); % Reads in the DEM
      A(A<0) = nan; % Gets rid of any no data/bad data points
      EastingLimits = R.XLimWorld; % Defines easting limits for DEM
      NorthingLimits = R.YLimWorld; % Defines northing limits for DEM
      nrows = size(A,1); % Creates vector with the size of A, which is
the same size as the DEM
      ncols = size(A,2); % Creates vector with the size of A, which is
the same size as the DEM
      x_dem = linspace(EastingLimits(1),EastingLimits(2),ncols); %
Creates a vector of ncols between limits for x dimension
      y_dem = linspace(NorthingLimits(1),NorthingLimits(2),nrows); %
Creates a vector of nrows between limits for y dimension
      [X_dem,Y_dem] = meshgrid(x_dem,y_dem); % Grids the rows and
columns of x_dem and y_dem
      gg = waitbar(0,'Please Wait, Computing Gravity Values');

      for i=1:Nsurvey % Length of Survey
          waitbar(i/Nsurvey); % Shows progress on waitbar
          x_surv = PaisleyGravitySurvey(i,6); % Defines Easting
coordinate in UTM's for a station
          y_surv = PaisleyGravitySurvey(i,7); % Defines Northing
coordinate in UTM's for a station

          Dx_surv = X_dem - x_surv; % Creates matrix with delta x
distances from survey point to pixel point
          Dy_surv = Y_dem - y_surv; % Creates matrix with delta y
distances from survey point to pixel point

          R = sqrt(Dx_surv.^2 + Dy_surv.^2); % Computes radius

          Theta = zeros(nrows,ncols); % Defines the size of Theta
          Theta(Dx_surv>=0) = pi/2 +
atan(Dy_surv(Dx_surv>=0)./Dx_surv(Dx_surv>=0));
          Theta(Dx_surv<0) = 3*pi/2 +
atan(Dy_surv(Dx_surv<0)./Dx_surv(Dx_surv<0));

          z_counter = 1; % Counts the number of iterations
```

```
          for j=1:length(ZoneIR)

              DeltaTheta = 2*pi/NSector(j);
              ThetaL = 0;
              ThetaU = ThetaL + DeltaTheta;

              for k=1:NSector(j)


if(isempty(A((R>ZoneIR(j))&(R<=ZoneOR(j))&(Theta>=ThetaL)&(Theta<ThetaU
))))  % If there's no elevation value in pixel, use station elevation
                        SecAvgZ = elev(i);
                    else
                        SecAvgZ =
nanmean(A((R>ZoneIR(j))&(R<=ZoneOR(j))&(Theta>=ThetaL)&(Theta<ThetaU)))
; % Computes mean elevation value of all pixels that lie in radius R
from theta lower to theta upper
                    end

                    Zavg(z_counter) = SecAvgZ;

                    ThetaL = ThetaU;
                    ThetaU = ThetaL + DeltaTheta;

                    ZoneIR_long(z_counter) = ZoneIR(j);
                    ZoneOR_long(z_counter) = ZoneOR(j);

                    z_counter = z_counter + 1;

              end % Closes k=1:NSector(j)


          end % Closes j=1:length(ZoneIR)

          % COMPUTE TERRAIN CORRECTION FACTOR

          Elevsec(:,i) = abs(Zavg - elev(i)); % Computes the absolute
value of the difference in elevation between a sector and a survey
point
          Gterr(:,i) = 0.11*(ZoneOR_long - ZoneIR_long +
(((ZoneIR_long.^2) + (Elevsec(:,i).^2)).^(1/2)) - (((ZoneOR_long.^2) +
(Elevsec(:,i).^2)).^(1/2))); % Computes the gravitational attraction in
mGals of the change in elevation of Elevsec
          if i==4
              Gterr(1:4,:) = Gterr(1:4,:)./4; % Divides rows 1 thru 4
by 4
          elseif i==16
              Gterr(5:16,:) = Gterr(5:16,:)./6; % Divides rows 5 thru
16 by 6
          elseif i==32
              Gterr(17:32,:) = Gterr(17:32,:)./8; % Divides rows 17
thru 32 by 8
          elseif i==68
```

```
            Gterr(33:68,:) = Gterr(33:68,:)./12; % Divides rows 33
thru 68 by 12
        end

        Gtotal = sum(Gterr(:,i)); % Sums each column in Gterr, which
is the total terrain correction value for any given survey point

        % CALCULATIONS

        Gobs(i) = Gobs(i) + Drift(i); % Computes the effect of Drift
in mGals
        Ds(i) = y(i) - ybase;
        Gn(i) = (Dgds * Ds(i)) * -1;
        %Gn(i) = 978031.85*(1 + 0.005278895*(sind (lat(i)).^2) +
0.000023462*(sind (lat(i)).^4)); % mGals, Computes Normal Gravity, Or
Theoretical Gravity at any Latitude
        % Gn(i) =
978032.67714*((1+(0.0019318513869*(sind(lat(i).^2)).^2))/(1-
(0.00669437999013.^2)*(sind(lat(i))).^2))
        zd(i) = elev(i) - Datum;
        Gfa(i) = 0.3086 * zd(i); %- (0.00023*cosd(2*lat(i))*111*1000)
+ (0.00000002*elev(i)); % mGals, 111 = km/degree of latitude, 1000
converts km tom, computes the free air correction
        % Gfawrong(i) = -0.3086 * zd(i);
        Gbs(i) = -0.04193 * rho * zd(i); % mGals, Bouguer Slab
Correction
        % Gbawrong(i) = (Gobs(i) + Gn(i) + Gfawrong(i) + Gbs(i));
        Gba(i) = (Gobs(i) + Gn(i) + Gfa(i) + Gbs(i)); % Simple
Bouguer Anomaly
        Gcba(i) = Gba(i) + Gtotal; % Complete Bouguer Anomaly

    end % closes for i=1:Nsurvey
    close(gg); % Closes waitbar command
    % FIGURES

    % SIMPLE BOUGUER ANOMALY

    X = PaisleyGravitySurvey(:,6); % Defines X axis values
    Y = PaisleyGravitySurvey(:,7); % Defines Y axis values
    rangeX = (floor(min(X))):10:(ceil(max(X))); % Defines range for x
axis
    rangeY = (floor(min(Y))):10:(ceil(max(Y))); % Defines range for y
axis
    [Xm Ym] = meshgrid(rangeX,rangeY); % Grids the ranges for x and y
    SB = griddata(X,Y,Gba,Xm,Ym,'cubic');
    % SB = TriScatteredInterp(X,Y,Gba); % Interpolates the value of
Gba for X and Y in between the ranges of Xm and Ym with the cubic
method SB = Simple Bouguer
    figure % Creates Figure
    contourf(Xm,Ym,SB); % Creates contours for interpolated values
from SB
    cm = flipud(jet); % Reversed colormap on figure so that less
negative values, ie gravity lows, are shown in cooler colors
    colormap(cm);
    hold on; % Allows overlay to happen
    plot(X,Y,'k+'); % Creates Plot
```

```
      xlabel('UTM E');
      ylabel('UTM N');
      title('Simple Bouguer Anomaly');

      % COMPLETE BOUGUER ANOMALY

      X = PaisleyGravitySurvey(:,6); % Defines X axis values
      Y = PaisleyGravitySurvey(:,7); % Defines Y axis values
      rangeX = (floor(min(X))):10:(ceil(max(X))); % Defines range for x
axis
      rangeY = (floor(min(Y))):10:(ceil(max(Y))); % Defines range for y
axis
      [Xm Ym] = meshgrid(rangeX,rangeY); % Grids the ranges for x and y
      CB = griddata(X,Y,Gcba,Xm,Ym,'cubic');
      % SB = TriScatteredInterp(X,Y,Gba); % Interpolates the value of
Gba for X and Y in between the ranges of Xm and Ym with the cubic
method SB = Simple Bouguer
      figure (2) % Creates Figure
      contourf(Xm,Ym,CB); % Creates contours for interpolated values
from SB
      cm = flipud(jet); % Reversed colormap on figure so that less
negative values, ie gravity lows, are shown in cooler colors
      colormap(cm);
      hold on; % Allows overlay to happen
      plot(X,Y,'k+'); % Creates Plot
      xlabel('UTM E');
      ylabel('UTM N');
      title('Complete Bouguer Anomaly');

      figure (3)
      imagesc(Gterr)
      xlabel('Gravity Stations');
      ylabel('Sector Number');
      title('Terrain Correction Values Per Sector');

      figure (4)
      imagesc(Elevsec)
      xlabel('Gravity Stations');
      ylabel('Sector Number');
      title('Absolute Value of the Difference of the Sector Elevation
from the Station Elevation');
```

References Cited

Burger, R.H., Sheehan, A.F., Jones, C.H. 2006. Introduction to Applied Geophysics: Exploring the Shallow Subsurface. W.W. Norton & Company. 600 p.

Hammer, S. 1939. Terrain Corrections for gravimeter stations. Geophysics. v. 4, p. 184-194.

APPENDIX C

Geologic Map of the Paisley Hills and Coglan Buttes Areas, Paisley, Oregon

See physical copy of thesis for full map.